Mathematical Modelling and Identifiability Applied to Positron Emission Tomography Data

Roger Gunn BSc

Department of Engineering
University of Warwick
Coventry

MRC Cyclotron Unit
Hammersmith Hospital
London

Thesis submitted to the University of Warwick for the degree of Doctor of Philosophy

April 1996

Contents

List of Figures

List of Tables

Acknowledgements

There are many people I wish to thank for their help. The major thanks must go to my two supervisors. Firstly Dr Vin Cunningham for his great support, for sharing his expertise, and for many interesting discussions. Secondly to Dr Mike Chappell for his encouragement and advice. I am greatly indebted to others for advice Dr Suren Rajeswaran thesis advisor, to Dr Andrea Malizia for his help. I am very thankful to all the clinicians who provided me with excellent data, especially Dr Paula Wells. To Prof Terry Jones for his enthusiasm and support. To Dr Julian Matthews for his helpful comments. I would like to thank the staff at the MRC Cyclotron Unit, especially Peter Bloomfield, Len, Dr Terry Spinks, Saffye Osman, Dr Adriaan Lammertsma, Chris Rhodes, Heather Boyd, John Ashburner, and Dr Paul Grasby. To my brother Steve for sharing the great PhD experience with me and many interesting discussions. To Kim for all her love and support, especially in the last few months. To mum and dad for their continual encouragement and support. I would also like to acknowledge MATLAB and MATHEMATICA for making programming a much simpler experience. My PhD work was supported by an MRC PhD studentship.

Declaration

The content of this thesis is solely the work of the author. Some of this work has been presented at international conferences, as indicated in the bibliography.

Summary

Positron emission tomography (PET) is an *in vivo* tracer kinetic technique. This thesis is concerned with the analysis of data derived from PET studies in humans. There are two related themes in the thesis. Firstly, the derivation of mathematical models with particular reference to the modelling of radiolabelled metabolite formation in plasma and tissue. Secondly, the identifiability of model structures is examined, and a method for the reparameterisation of unidentifiable models is derived. Compartmental models describing the accumulation of radiolabelled metabolites in plasma following the intravenous administration of [^{11}C]flumazenil and [^{11}C]diprenorphine are presented. A theorem is presented which gives conditions for a unique solution to the spectral analysis approach (a kinetic modelling technique used in PET which is based on the *a priori* definition of a large set of basis functions). Mathematical techniques are presented for the analysis of expired $^{11}CO_2$, a major labelled metabolite in many PET studies. This range of analytical and modelling techniques is then applied to the analysis of [^{11}C]thymidine scans. [^{11}C]Thymidine is a PET tracer being developed for the measure of tumour proliferation in cancer patients. The techniques developed in the thesis allow for the removal of the confounding labelled metabolite signals from both plasma and tissue data.

Chapter 1

Introduction

This thesis will consider the mathematical modelling of biomedical systems in the field of positron emission tomography (PET). PET is an *in vivo* tracer technique which allows the measurement of tissue functions in humans and as such is a unique clinical research tool. The method employs radiolabelled compounds to study the kinetics of selected biochemical and pharmacological functions. The technique relies on the quantitative modelling of the kinetic behaviour of the injected tracer and therefore a substantial part of PET research considers mathematical models and their application. Important topics include model formulation, model selection, identifiability and parameter estimation techniques. PET relies heavily on mathematical methods, not just for modelling but also for tomographic reconstruction, image analysis and image realignment. For quantification of tissue function (with tracer kinetic modelling) input and output data are a prerequisite. These data are obtained by blood sampling from the PET tomograph respectively. These data allow for the creation of plasma and tissue time courses of the concentration of tracer. A major problem in PET is the metabolism of the injected tracer. Consequently, the measured data is usually contaminated by the presence of labelled metabolites. Techniques for the correction of the plasma and tissue data are essential such that accurate model parameters can be estimated. This

thesis is concerned with the development of mathematical models for both plasma and tissue data and their application to PET.

The three inter-related themes to this thesis will be identifiability analysis, tracer kinetic modelling and metabolite contamination of the data. An outline of the thesis is illustrated in Figure (1.1). Following the two introductory Chapters (2 and

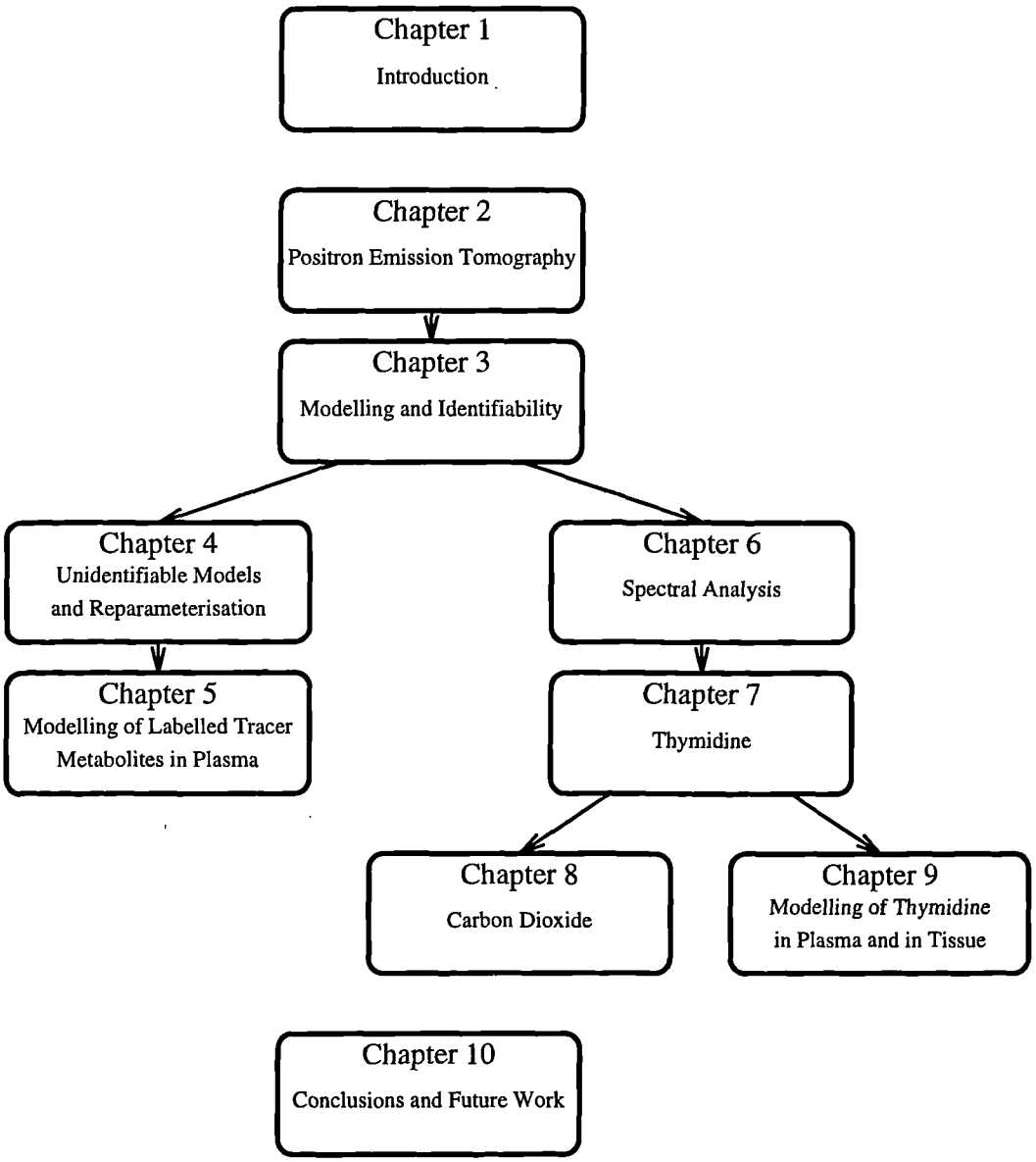

Figure 1.1: Thesis Structure

3) on PET and modelling Chapter 4 considers identifiability and unidentifiable systems. The process of identifiability allows for the theoretical investigation of model structures to determine whether they are robust when utilised for parameter estimation from input output data. A method for reparameterising unidentifiable systems is investigated and this is applied to a model for the metabolite correction of plasma input functions in Chapter 5. The theme of tracer kinetic modelling is apparent throughout the thesis, a review of available techniques is presented in Chapter 3 and one method (spectral analysis) is examined in detail in Chapter 6 with particular reference to the uniqueness of the solution. Applications of compartmental modelling and spectral analysis as tools for the investigation of tracer kinetics are considered in Chapters 5, 8 and 9. The theme of metabolite correction via the application of mathematical mddels will be considered in Chapters 5, 8 and 9 with reference to the tracers [^{11}C]flumazenil, [^{11}C]diprenorphine and [^{11}C]thymidine. A conclusion will be presented in Chapter 10 together with future work arising from this thesis.

Chapter 2

Positron Emission Tomography

2.1 Overview

PET is a unique tool for studying pharmacokinetic, physiological and biochemical processes *in vivo* in humans. The ability of PET to acquire non-invasive functional images makes it an unprecedented tool for the study of neurology, cardiology, and oncology. Its principle roles include the *in vivo* measurement of blood flow, metabolism and receptor concentrations [1]. PET has been used widely by neurologists with respect to brain mapping of cognitive function [2] and the study of neurological diseases such as Parkinson's disease [3], epilepsy and Alzheimer's [4]. Cardiologists use PET to measure myocardial blood flow, metabolism and receptor concentrations [5] [6]. Oncologists are now increasingly using PET to investigate the biochemistry of cancers and their response to anti-cancer agents and other forms of therapy [7] [8] [9]. Psychiatrists use PET to study the neuroreceptor systems in brain disorders such as depression and schizophrenia [10]. The technique is making use of an increasing variety of radiolabelled tracers. The fundamental mechanism of PET is the emission of a positron from an unstable nucleus and the consequent annihilation with a nearby electron. This annihilation produces two almost collinear gamma rays of 511keV each which can be detected in coincidence on either side of the active volume. The localisation of the an-

nihilation allows the tracers spatio-temporal distribution to be determined. In addition, the detection of the two gamma photons as opposed to single photons as in conventional nuclear medicine facilitates the determination of absolute tracer concentrations [11]. This enables functional parameters to be accurately derived and increases detection sensitivity.

2.2 Tracers

The use of positron emitters that are isotopes of commonly occurring elements facilitates the use of many different tracer compounds of biological significance [12]. A tracer should not disturb the underlying biological system, that is the amount of non-radioactive material is required to be small. The compounds are administered in minute quantities and this radiation dose corresponds to approximately one year's normal background radiation. The tracers are produced by chemical reactions involving one of the several common isotopes. Isotopes that are frequently used as positron emitters are listed with their physical half-lives in Table (2.1). The short half-lives of the isotopes reduces the dose of radiation to the subject and allow for repeat studies to be performed.

Radionuclide	**Half-Life (mins)**
^{11}Carbon	20.4
^{13}Nitrogen	9.96
^{15}Oxygen	2.05
^{18}Fluorine	109.7

Table 2.1: Half-lives of commonly used isotopes

These radioisotopes are produced with a particle accelerator (a cyclotron). The

cyclotron produces the isotopes by accelerating a beam of charged atomic particles (protons, alpha particles or deutrons) under the influence of electric and magnetic fields. The beam irradiates a target (solid, liquid or gas) causing a nuclear reaction to take place, producing the raw radioisotope. The short physical half-lives of positron emitting tracers necessitates the presence of an on-site cyclotron (or nearby - i.e. $\sim$ 1-2 hours journey for ^{18}F is reasonable) for their production. The radioisotope then undergoes chemical synthesis producing the required compound incorporating a positron emitting label. High initial yields of positron emitters and fast subsequent synthesis produce tracers with high specific activity. The specific activity of a compound is defined to be the ratio of radioactivity to mass of the compound. This must be high to ensure that the concentrations of the unlabelled compound do not interfere pharmacologically with the *in vivo* measurement of the radioligand kinetics [13]. In essence, a high specific activity compound meets the criterion for an ideal tracer.

2.3 Physical Principles

Positron emission involves the decay of certain proton-rich nuclides by the emission of a positron, a positively charged electron, to leave an extra neutron and one less proton [14]. The total kinetic energy released by this process is shared between the positron and a neutrally charged particle, a neutrino. The competing decay scheme for nuclides having an extra proton is capture of an inner shell electron.

$$\begin{aligned} p &\rightarrow n + \beta^+ + v \quad \text{(Positron Emission)} \\ p + e &\rightarrow n + v \quad \text{(Electron Capture)} \end{aligned} \tag{2.1}$$

On emission, the positron loses kinetic energy via collisions with electrons from surrounding atoms until its energy is about a few electron volts, at which point its

collision with an electron results in annihilation of the electron pair and conversion of their total mass to energy (via Einstein's equation the energy released is $E = 2m_0c^2$). Conservation of energy yields two photons each of energy 511keV which are emitted in close to opposite directions, the small non-collinearity arising from possible non-zero momentum on annihilation.

An emitted positron travels a short distance (up to a few mm in tissue) until it annihilates with a stationary electron and this introduces a spatial blur in the distribution of the compound. This and the non-collinearity define the intrinsic maximum resolution that one can achieve with a PET system.

2.4 Detection of Gamma Rays

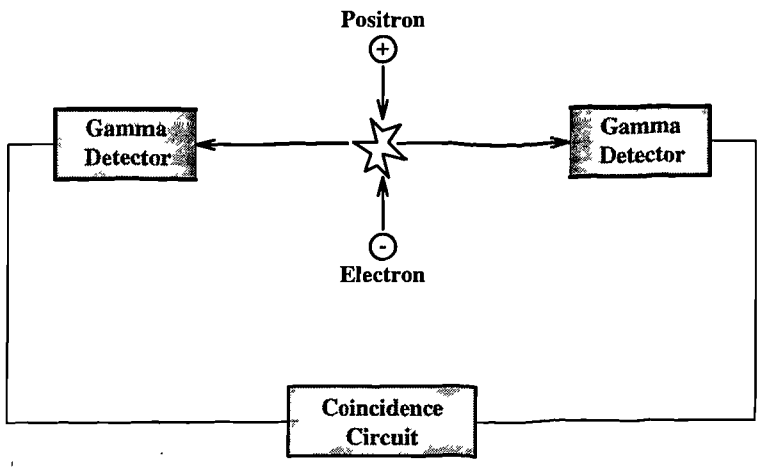

Figure 2.1: Scheme of basic PET principle

The principle behind the gamma ray detection involves the use of scintillation crystals [11]. When a gamma ray interacts with a crystal, such as bismuth germanate (BGO), the motion energy is converted into light which is then transformed into an amplified electrical pulse by a photo multiplier tube (PMT) attached to the rear of the crystal. The PMTs are wired up to electronic hardware that allows for rapid recording of the detected events. Using a pair of gamma detectors, the

occurrence of an annihilation can be ascertained (Figure (2.1)). By connecting a pair of gamma detectors in a coincidence circuit the occurrence of single nuclear disintegrations can be accounted for. The coincidence unit behaves similarly to a logical AND gate, if both input pulses are registered within a small time window (coincidence window < 20 ns) then a coincidence count or event is recorded.

2.5 PET Camera

A commercial PET tomograph [15] [16] usually consists of multiple crystal PMT modules, or detector blocks arranged in rings surrounding the subject which are connected up to detect coincidences, as in Figure (2.2). The tomograph localises

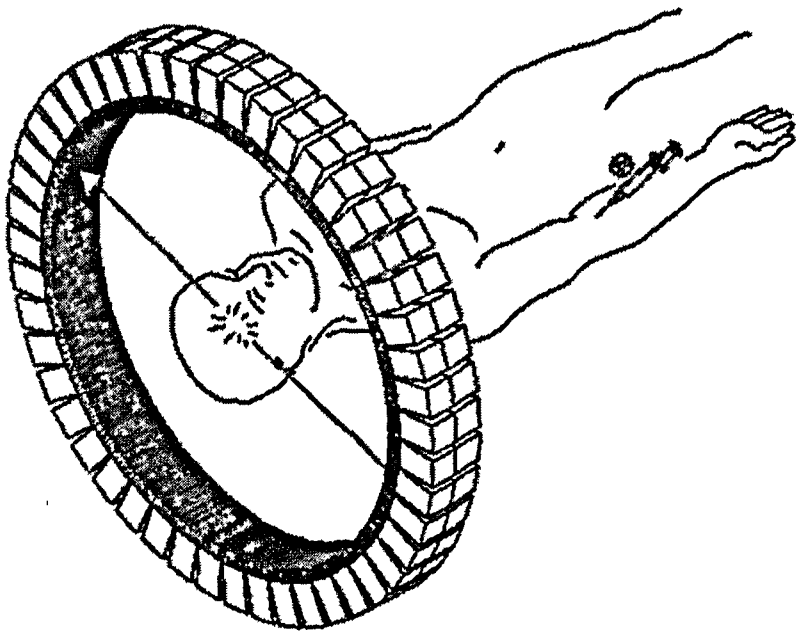

Figure 2.2: PET tomograph

disintegrations by means of electronic collimation. When two gamma rays are detected within the coincidence time window an event is recorded. The spatial position of the disintegration can be localised to a straight line joining the two

coincident detectors, termed a line of response (LOR). During a PET scan events are recorded between the currently many millions of detector pairs which represent line integrals or projections at different angles around the subject. The raw data set is termed a sinogram (a matrix of angle vs. projection LOR). Using tomographic reconstruction techniques an image of the tracer distribution can be obtained (localisation is effected by the intersection of many LOR's passing through a particular source location). There are two favoured reconstruction techniques; Filtered back projection [17] and iterative reconstruction [18]. The spatial resolution is primarily determined by the dimensions of the detector elements and can be as high as 3mm for modern scanners. The temporal resolution or frame rate that can be used is limited by the radioactivity in the field of view and the decay of the radionuclide.

2.6 Sinogram

Each disintegration event is recorded by coincidence processing hardware and stored in a 2-D matrix, or sinogram [14], as in Figure (2.3). A sinogram is an

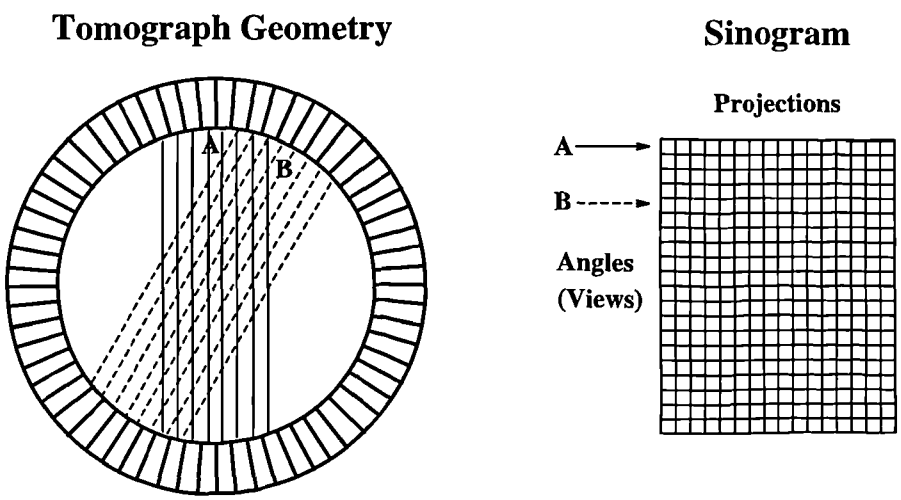

Figure 2.3: Composition of a sinogram

array that consists of the coincidence LOR's reformatted into sets of parallel projections at different angles or views. The value in each element of the sinogram is the number of counts for each LOR, i.e. a line integral.

2.7 Mispositioning of Events

There are three types of coincidence events recorded, see Figure (2.4); i) a true event, from an annihilation lying within the detection channel, ii) a random event, two uncorrelated photons from separate annihilations detected within the coincidence time window, iii) a scattered event, when one or both gamma ray interact with an atomic electron in the medium the direction of the gamma ray changes as a result of losing some energy (by the principle of conservation of momentum) [14].

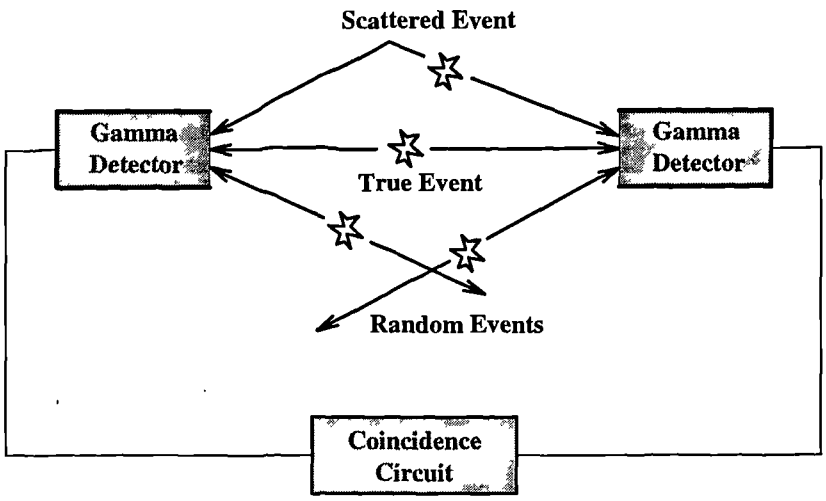

Figure 2.4: Possible coincidence detections

The raw counts measured by a PET camera are defined by the following equation;

$$C_{measured} = C_{true} + C_{random} + C_{scatter} \tag{2.2}$$

So to obtain the true counts the measured signal must be corrected for randoms

and scatter.

Randoms are normally measured by delaying the signal on one of the detector pairs so that just randoms are recorded, i.e. all the true coincidences have been removed from the signal. Alternatively one can use $C_{random} = 2\tau N_i N_j$ where 2τ is the length of the coincidence time window and N_i and N_j are the singles count rates from the two coincident detectors. However, the width of the time window needs to be known very accurately for such a technique to be used.

The counts in a detector channel must be corrected for counts lost due to scatter out of the LOR and in addition for photons absorbed by the medium.

The following equation defines the number of photons lost due to the traversal through a medium.

$$I = I_0 e^{-\mu x} \tag{2.3}$$

where I = number of photons after traversal, I_0 = number of photons before traversal, x = the total thickness of the medium, μ = the attenuation coefficient of the medium.

Unlike single photon emitters the detection of the two photons in PET means the attenuation is not dependent on the depth of the source in the medium and only depends on the thickness of the medium. This greatly simplifies the process of attenuation correction. A transmission scan is acquired with the patient in the scanner, and involves the measurement of attenuation by utilising an external long-lived positron emitting source (normally ^{68}Ge). A blank scan is similarly acquired but without the patient in the scanner. The ratio of blank scan to transmission scan is then used as the attenuation correction. There are various methods for scatter correction such as convolution subtraction or the dual energy window approach [19] [20].The accurate correction for attenuation and scatter is essential for the production of quantitative functional images.

2.8 2D and 3D Acquisition

Data can be collected in two different geometries; In 2-D, events within narrow axial acceptance angles are recorded, these being restricted by the presence of inter-ring lead or tungsten septa which are used to remove scatter and randoms. In 3-D, septa are removed and any detector ring can be in coincidence with any other ring (unlimited acceptance angle) [21]. 3-D mode is more sensitive (more events are recorded per activity) and this allows for a reduction in the amount of radioactivity administered to a subject. The reduction in dose is becoming increasingly important as the advisory boards are lowering the allowable doses of activity.

2.9 Resolution of PET

The data collected from the scanner is a temporal and spatial distribution of the tracers' concentration. For each measured time frame of data a discretised volume of the tracers concentration is obtained. The maximal spatial resolution of any PET system is limited, this results from a positron travelling up to a few mm before annihilating with an electron and also non-collinearity (the bigger the detector ring the bigger the blur due to this) [11]. However in practise the size of the detector elements is the limiting factor, although modern technology means that PET cameras are now approaching their maximal spatial resolution.

2.10 Quantification

Studies are performed where the activity concentration in a test cylinder or phantom, can be determined by placing samples of the activity in a calibrated sodium iodide well counter [11]. This enables accurate factors to be obtained which produce cross calibration between the PET camera and the well counter, i.e.

Counts/voxel $\leftrightarrow$ μCi/ml. The BGO blood detection system (see below) is also calibrated with the same well counter (counts/ml $\leftrightarrow$ μCi/ml), and this facilitates the calculation of a linear factor which calibrates the PET data to the blood data. To achieve quantitative measures of tissue function it is necessary to acquire several associated measurements. In addition to normalisation (for detector inefficiencies and geometrical effects) and calibration data for the scanner the following measures are required;

- Spatio-temporal measure of concentration of tracer in tissue
- Attenuation data
- Concentration of the label in blood
- Distribution of label between plasma and whole blood
- Metabolite measurements of the parent tracer in plasma

During a PET scan, aliquots of blood are drawn from the subject and counted in the well counter which enables a direct quantification of the activity in the PET images.

2.11 Blood Sampling

To acquire quantitative information from the tissue of interest it is essential to know the temporal concentration of the compound in plasma. The most robust method of acquiring these data involves utilising continuous on-line blood sampling throughout the scan [22]. The subject's radial artery is cannulated and a pump is used to withdraw blood at a constant rate through a BGO detector block which continuously measures the activity in the blood, see Figure (2.5). Discrete samples of blood are taken for calibration, plasma to whole blood calculations and

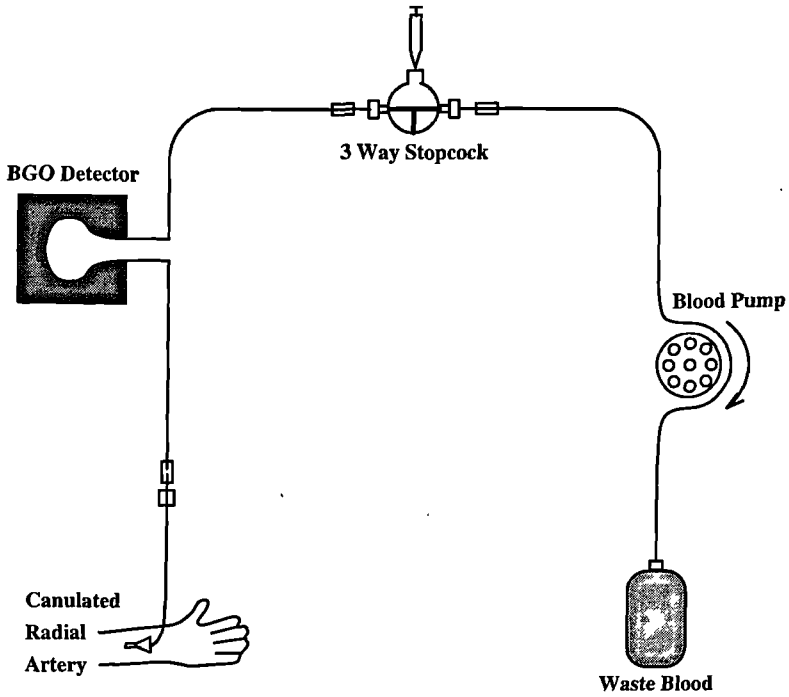

Figure 2.5: Blood sampling system

for metabolite analysis. The tubing passes through the BGO detector block in the shape of a hairpin, this maximises the volume of blood which can be detected, increasing sensitivity.

Both 1022keV "sum" coincidences and 511keV "singles" events are recorded giving extra sensitivity (heavy lead shielding of the equipment is employed to minimise background counts). The continuous sampling contains a series of "blips" in the data due to the flushing of the line with saline which ensures that the blood does not clot in the tubing. The background count rate needs to be removed from the data. The true background count rate is related to the activity surrounding the detector and theoretically this will depend on the activity in the subject, however with suitable lead shielding this problem can be minimised.

2.12 Tracer Metabolism

One of the most challenging problems in PET results from any metabolism of the injected compound. Metabolism refers to the degradation of the parent compound into various smaller component parts. As a consequence of the parents positron label some of it's associated metabolites will have an inherent label as well [13]. These metabolites which also produce annihilation events confound the signal of the compound of interest. When metabolism of a compound occurs mathematical models of the metabolism are necessary to account for the contribution of metabolites.

2.13 Metabolite Analysis

To ascertain the contribution of metabolites to the plasma input function discrete plasma samples are analysed for their parent and metabolite composition. Various methods for the analysis of samples exist of which the two most common are High Pressure Liquid Chromotography (HPLC) and Thin Layer Chromotography (TLC) [23] [24].

2.14 Summary

This chapter has explained the principles and methodology in obtaining quantitative tracer concentrations in tissues of interest and plasma. The next chapter considers how these data may be transformed using mathematical models to provide physiological "functional" parameters.

Chapter 3

Modelling and Identifiability

3.1 Overview

This chapter reviews the topics of modelling and identifiability which form the two main aspects of this thesis. The two topics are intrinsically linked. A model defines some form or structure with which parameters are associated. Parameter values are obtained so that the model output matches the measured data as closely as possible. Identifiability refers to the process of assessing whether it is possible to obtain unique values for these parameters from experimental data.

3.2 Modelling

Mathematical modelling techniques are applied to PET data in order to produce relevant functional parameters of the body's physiology, biochemistry and pharmacology. The raw data often gives little insight into the parameters of interest and this is why it is necessary to use tracer modelling techniques so as to extract a more comprehensive description of the underlying physiological processes. Hence, rather than just recording the integrated radioactivity counts, it is possible to derive various important functional parameters such as the distribution volume (VD), blood flow, concentrations of binding sites, binding affinities and

mean residence times, etc [25].

3.2.1 Introduction

The information obtained from a PET scan is a temporal and spatial measure of the tracer concentration in the tissue of interest. A simultaneous measure of the tracer concentration in plasma can be obtained and the acquisition of both plasma and tissue time courses allows for the investigation of plasma to tissue transfer of the compound, as in Figure (3.1). The frame durations for which

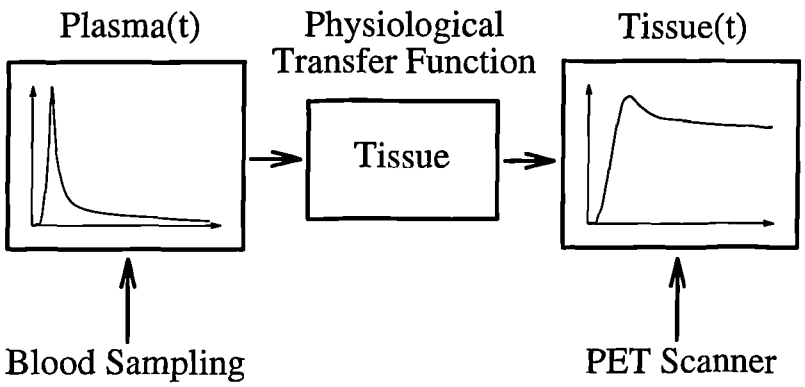

$$\text{Tissue(t)} = \text{Physiological Model} \otimes \text{Plasma(t)}$$

Figure 3.1: Modelling scheme

tissue data are collected are variable and a typical protocol would consist of short, initial time frames (typically 5-60 secs) to characterise the fast, initial stages of the distribution of the tracer in tissue and longer, later time frames (typically 5-15 mins) to capture the uptake or washout from the tissue. The protocol for data acquisition should consider the important parameters to be estimated and tailor the experimental design to maximise the accurate estimation of these parameters [26] [27].

3.2.2 Tissue Data

The kinetic data obtained from a PET camera can be either analyzed at the single pixel level (i.e. at the order of the spatial resolution of the camera - e.g. 6mm x 6mm x 6mm [15]) or on the basis of a so called region of interest (ROI) which is taken to mean a larger region defined by the user (e.g. 50 mm x 50 mm x 30 mm). There are advantages to analysis at both levels with a trade-off having to be made between statistical noise and resolution. Pixel by pixel analysis gives detailed spatial information, that may be obscured at the ROI level. This allows for the generation of "functional" or "parametric images", where each pixel in the image contains the parameter value at that spatial location (it should always be emphasised that image "pixels" are not statistically independent - i.e. anything with dimensions < resolution of the camera). However, the data are noisy at the pixel level compared to the low noise properties of ROI-generated curves, and the noise levels determine the number of viable parameters that are numerically identifiable.

An ROI is drawn on a reference image which is usually the integral of the dynamic image sequence. The reference image is chosen such that it maximises the delineation of the structures of interest. The ROI is then applied to the dynamic image sequence and all pixel values within the ROI are averaged for each time frame resulting in a complete time activity curve for the ROI.

3.2.3 Plasma Data

The simultaneous measure of continuous on-line blood radioactivity, the plasma to blood partition, and metabolite analysis of plasma assays allow for the generation of a plasma metabolite-corrected input function. This provides a continuous measure of the parent compound's concentration in plasma and this process is described in more detail in Chapter 5.

3.3 Modelling Techniques

Typically in PET we are concerned with single-input single-output (SISO) systems and the system identification problem. There are various different modelling approaches which can be used to examine the data, ranging from data-led techniques to ones incorporating more *a priori* assumptions, or model-led techniques (Figure (3.2)). The more data-led techniques minimise *a priori* assumptions and instead

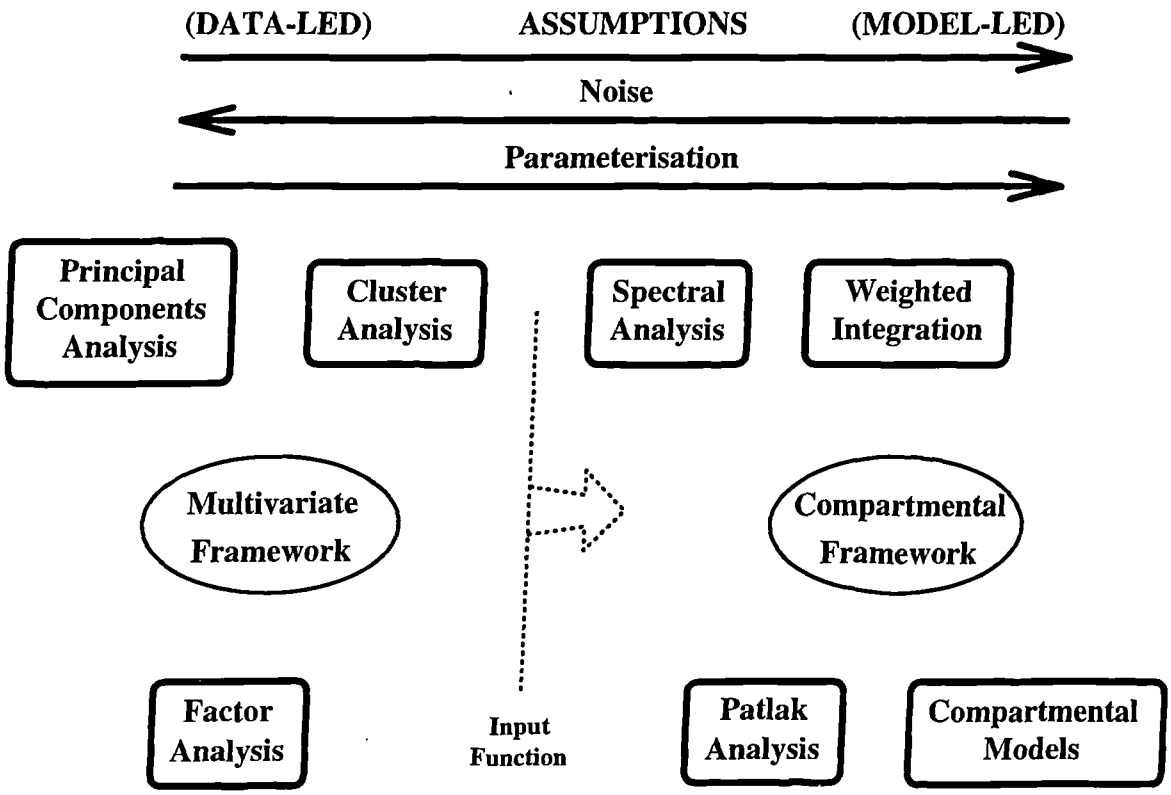

Figure 3.2: Spectrum of modelling techniques

interrogate the measured data to ascertain the characteristics of the system. An example of this is principal components analysis (PCA) [28] which considers the variance-covariance structure of the tissue data. The model-led (or constrained) techniques utilise knowledge of the underlying system and involve an increased degree of parameterisation. This corresponds with a loss in the number of degrees

of freedom in the system which makes them increasingly susceptible to noise. A model-led technique is exemplified by compartmental analysis and may not be robust at the pixel level if the model is too complex.

With an increase in model structure, the problems of theoretical and numerical identifiability become more important. The data-led techniques dictate what can be identified from the data themselves, whereas the structures of the more model-led techniques require investigation in order to validate their applicability. Data-led techniques often fail to fully characterise the parameters of interest, however they are extensively used as first pass analyses with new tracers when little is known about the tracer's behaviour. Their important advantage here is that they make few *a priori* assumptions.

Model-led techniques, such as compartmental analysis, are far more involved with processes such as model selection, identifiability, and model validation is required. Compartmental analyses normally requires a metabolite-corrected plasma input function to give truly quantitative parameter estimates. If compartmental techniques are successful they provide a greater understanding of the system.

Data-led techniques lend themselves to noise reduction, whereas more structured models can be more easily related to physiologically interpretable parameters.

3.3.1 Multivariate Based Techniques

Principal Components Analysis

PCA [28] is a technique which extracts the key temporal components from a dynamic data set. The method is based on an orthonormal transformation of the standard coordinate axes. The method is frequently used to obtain components for the purpose of factor analysis, see below. The number of significant components can be assessed by choosing components whose eigenvalues account for a significant proportion of the variance (typically 70-90%). The method is limited to

extracting the fundamental components and any small pockets of distinctly different behaviour may be ignored. The method of principal components examines the variance-covariance structure of the data via a linear combination of the original data. Interpretation of the factors is the difficult and involved part of the process. The factors obtained often need to be transformed to produce intelligible physiological factors. This is normally performed by a rotation of the factors which constrains them to be positive (physiologically plausible) [29]). These factors may then be used as part of a factor analysis [30] .

Factor Analysis

Factor analysis is performed by fitting a linear combination of temporal components to the tracer time course. The distinct temporal components can be obtained from time activity curves derived from ROI's, by PCA, or other kinetic techniques such as cluster analysis. Factor analysis has recently been applied to cardiac PET data [31] [32].

Cluster Analysis

Cluster analysis is a data-led technique. It attempts to identify clusters of pixels in feature space (the n-dimensional time activity curves are treated as points in n-dimensional space) by fitting a small number of multi-normal distributions which encompass most of the data. The probability of a pixel lying within each of these clusters may be calculated and this gives the weightings for the contribution of each identified shape. Cluster analysis has a potential as a segmentation technique and relies on distinct temporal shapes existing in the data [33].

3.3.2 Compartmental Based Techniques

With the acquisition of an input function, modelling techniques which propagate from a compartmental framework can be applied. These methods address the general modelling problem in PET, that of system identification which involves identifying a tissue response function from measured input (plasma) and output (tissue) data.

Spectral Analysis

Spectral analysis was first applied to PET data by Cunningham and Jones [34], and is a technique which lies in between data-led and model-led techniques. It assumes that the tissue impulse response function can be constructed from a sum of nonnegative exponential terms. By taking a discrete spectrum of possible exponentials (β_i), which are pre-chosen and fixed, from the fastest (blood effects) to the slowest (decay of the isotope), the problem can be linearised, i.e.

$$PETobs(t_k) = C_p(t) \otimes \sum_{i=1}^{n} \alpha_i e^{-\beta_i t_k} \tag{3.1}$$

given $k \in \{1, 2, ..., N\}$ and the non-negativity constraint $\alpha_i \geq 0$ and where,

$$\begin{aligned} PETobs(t) &: \text{Tissue time course} \\ C_p(t) &: \text{Plasma time course} \end{aligned}$$

The problem is then solved using a nonnegative least squares algorithm. By definition of the impulse response the method is able to characterise both irreversible and reversible systems with many compartments. Spectral Analysis has been used at the pixel level to produce functional images [35]. This thesis deals with a particular aspect of the method (the uniqueness of the solution) that was originally perceived as a problem [36]. Chapter 6 presents a novel proof which gives conditions for a unique solution.

Patlak Analysis

Patlak or graphical approaches [37] [38] [39] were first used by Rutland [40] and developed in a more theoretical framework by Patlak , and can be used to measure the irreversible uptake rate of a tracer. The basic method involves a transformation of the tissue and plasma data.

$$\frac{PETobs(t)}{C_p(t)} = K_i \frac{\int_0^t C_p(\tau)d\tau}{C_p(t)} + V_0 + V_p \tag{3.2}$$

where

$PETobs(t)$	:	Tissue time course
$C_p(t)$	:	Plasma time course
K_i	:	Irreversible uptake rate constant
V_p	:	Volume of plasma in sampled tissue region
V_0	:	Volume of distribution

This relationship approaches linearity after a certain amount of time when the exchangeable compartments approach a pseudo-equilibrium. The irreversible uptake rate, K_i, can then be measured by fitting a straight line to the data after this time. The advantage of this method is that the number of intermediate reversible compartments is unimportant and just the overall uptake rate constant from plasma into the irreversible compartment is obtained. Logan extended the graphical approach to consider reversible systems [39].

Weighted Integration

Weighted integration is a technique that was originally developed in PET for analysis of blood flow and can be applied at the pixel level [41] [42]. The method requires two or more weighted count rate integrals, depending on the number of parameters that are to be estimated. The particular advantage of this technique

is that it can be used during data acquisition, thus providing a reduction in the size of acquired data sets. The weighted count rate integrals are defined as

$$I_i = \int_0^T w_i(t) C_{PETobs}(t) dt \ \ (i = 1, \ldots, n) \tag{3.3}$$

where

$PETobs(t)$	:	Tissue time course
$w_i(t)$	:	Weighting functions
T	:	Time at the end of the scan
n	:	Number of distinct integrals

The weighting functions w_i must be distinct and typical functions include unity, exponential decay and time [43]. Equation (3.3) can also be defined in terms of the model parameters,

$$I_i = (1 - V_b) \int_0^T w_i(t).C_p(t) \otimes IR(t) dt + V_b w_i(t) C_{wb}(t) \ \ (i = 1, \ldots, n) \tag{3.4}$$

where

$IR(t)$	:	Impulse response function
$C_p(t)$	:	Plasma time course
$C_{wb}(t)$	:	Whole blood time course
V_b	:	Blood volume

The parameter values are then obtained by setting (3.3) and (3.4) equal to each other and then solving for the parameter values. Weighted integration has been used to calculate [^{11}C]flumazenil binding parameters, B_{max}(receptor concentration) and K_D(equilibrium dissociation constant), using a single compartment model and a dual study, steady-state protocol [44]. The method can be extended to consider the two compartment (3 parameter) model for [^{18}F]fluorodeoxyglucose (FDG) producing effective images of K_i, which represents the irreversible uptake of FDG and is proportional to the tissues utilisation rate of glucose [43].

Linear Compartmental Systems

A system is defined as a complex entity consisting of interacting parts [45]. In compartmental modelling a complex system is constructed from a series of interacting compartments. Each individual compartment obeys a simple set of rules and these compartments are combined to form a complex system which describes the whole biological process. General systems theory has its origins in the 1940's. A description of compartmental analysis in medicine and biology can be found in Jacquez [46] . The processes which will be examined will all contain some form of input to the system and some form of output. Compartmental modelling is a technique involving a simplification of the underlying physiological processes, instead taking into account the principal dynamic elements.

Each compartment is considered as a homogeneous well mixed entity with its own distribution volume. The distribution volume is defined by the ratio at equilibrium of the concentration of tracer in tissue divided by the concentration in plasma, and has units of (ml plasma)(ml tissue)$^{-1}$. Compartments can be spatially distinct or they can denote the same physical space occupied by different chemical species. The term linear refers to the fact that the rate at which material is transferred between compartments is linear, that is proportional to the amount of material in the compartment and hence the transfer rates are called rate constants.

Initially the model may be constructed in terms of interacting compartments which convey the appropriate biological processes. The compartmental system is then transcribed into the appropriate system of ordinary linear differential equations. In compartmental modelling, one derives a set of equations which are obtained from the theory of conservation of mass. A set of first order ordinary linear differential equations are obtained.

In the limit, at equilibrium or steady-state, the quantities and concentrations of the tracer in the compartments remains unchanged.

There are certain assumptions which a linear compartmental system imposes:-

- the tracer mixes uniformly in each compartment
- the tracer mixes instantaneously in each compartment
- the rate constants between compartments are constant
- the amount of tracer must be very small compared to the system it is to measure.

The Laplace transform [47] provides a very effective and established method for solving a set of ordinary linear differential equations.

Nonlinear Compartmental Systems

The rate constants for compartmental systems are not always constant (the rate may depend on time or a system variable), producing nonlinear compartmental models. Nonlinear models are more complicated to solve with a general analytical solution rarely available (Laplace transforms only apply to linear systems) and numerical methods are normally required. An example of a nonlinear compartmental model in PET is a saturable ligand binding model with the injection of a low SA labelled ligand such as flumazenil [48].

3.4 Identifiability

Structural identifiability refers to the theoretical process of ascertaining whether a model is well defined when fitting to experimental data. Theoretical structural identifiability analysis is the process of examining the model in the case of perfect data and determining whether model parameters can be obtained. Many models have parameters which cannot be determined given perfect data [49] [50], so it is very important to establish whether a model is robust before fitting to

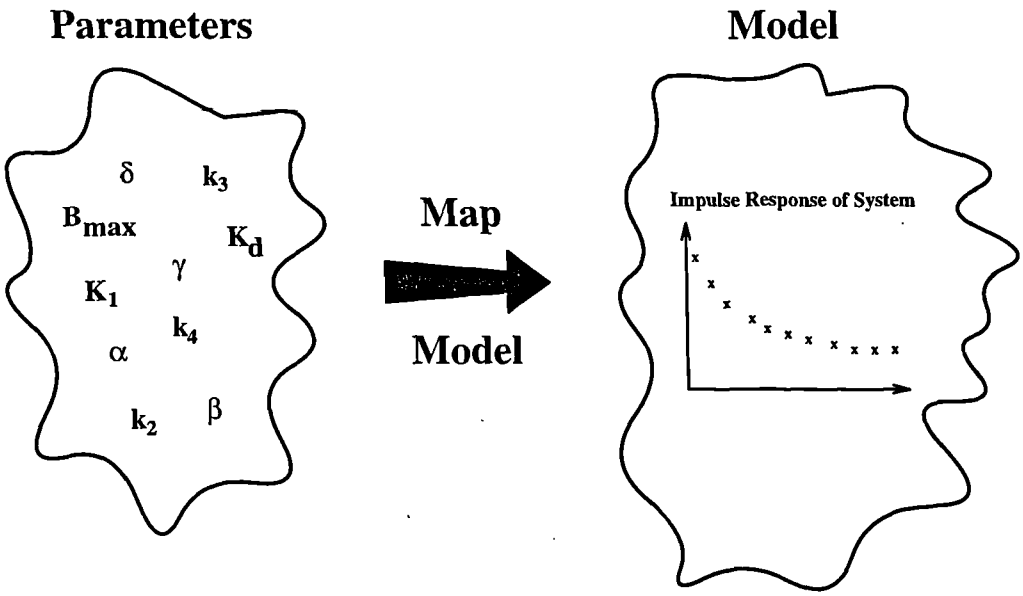

Figure 3.3: Identifiability

any data. An experiment is declared uniquely (globally) identifiable if all the parameter values are uniquely determined from noiseless input-output data. It is locally identifiable if a finite discrete set of parameter values are determined and unidentifiable if an infinite number of possible parameter sets exist.

The method of structural identifiability is directly applicable to compartmental models, and has been used extensively to examine the viability of compartmental systems [51] [52] [53] [54]. The methods available examine the properties of the mapping of the parameters onto the system response. This mapping is defined by the chosen model.

The scheme of structural identifiability is described in Figure (3.3). By postulating a model, a map, M, is defined which maps from the parameter space,P, onto the system response space,IR.

$$M : P \longrightarrow IR \tag{3.5}$$

If the mapping M is injective, i.e.

$$if\ p_1 \neq p_2\ implies\ M(p_1) \neq M(p_2) \tag{3.6}$$

then the model is globally (uniquely) identifiable. Essentially this means that given two distinct system responses they are parameterised by different parameter sets. A criterion for an ideal model would be that all the required parameters are uniquely (globally) identifiable. However, in cases where the model is only locally identifiable, it is possible to work out the finite number of parameter sets which give rise to the system data. It may then be possible to discard some of these parameter sets due to additional constraints that are known about the various parameters or the system as a whole. Care can be taken to start fitting routines in the neighbourhood of the required solution.

3.4.1 Introduction to Identifiability

Structural identifiability analysis is a technique which should be applied to model structures to determine whether the unknown, independent, model parameters can be deduced if perfect input-output data is available. The identifiability problem is fundamentally concerned with the uniqueness of solutions of a certain class of mathematical models. Bellman and Åström in 1970 [55] were the first to put identifiability analysis into a rigorous framework and they coined the term "structural identifiability". The expression "deterministic identifiability" is sometimes used to avoid problems with the term structural when the identifiability properties of the system are influenced by the type of input. When the model is deterministic and the data are noise-free, the problem is generally a nonlinear algebraic one. However, the solution to this problem is generally both nontrivial and nonunique. With the addition of noise to the data the problem becomes extremely complicated and is referred to as a problem of "numerical identifiability". One method of analyzing numerical identifiability is to examine the standard deviation of each

parameter estimate [56]. Another example of numerical identifiability is ensuring that the number of measurements exceeds the number of parameters to be estimated.

3.4.2 The Laplace Transform Approach

By employing the Laplace transform to differential equations generated by a particular model this enables the process of identifiability of the system parameters to be undertaken. For (SISO) linear systems the identifiability analysis is performed by examining the transfer function, $TF(s)$, of the system. The system variables are defined in the following manner,

$$Y(s) = TF(s)U(s) \tag{3.7}$$

where Y defines the observation and U defines the input.

For linear compartmental systems the transfer function is a quotient of polynomials in s. Interrogation of the coefficients in the transfer function allows the identifiability properties of the parameter vector to be established. Given perfect data one would be able to measure the values of the coefficients in the measurable transfer function, $Y(s)/U(s)$, and so these values can be considered as measured constants. The investigation of the identifiability of the system is concluded by examining the solution of a system of generally nonlinear equations. These equations are determined from the coefficients in the numerator and denominator of the transfer function which are equal to measured arbitrary constants.

Establishing the system of nonlinear equations is straightforward, but the problem with this method is that the solution is often difficult to determine when more than a few equations exist, due to the nonlinearity. However the use of symbolic manipulation packages [57], such as MATHEMATICA, often simplify this process. The Laplace transform approach for identifiability analysis has been applied to

many linear systems [58] [59] [60] [61] [62].

3.4.3 The Taylor Series Approach

This method involves expressing the observation, $Y(t)$, as a Taylor series about some known time point, say $t = 0^+$ for an impulse response, with the successive coefficients being constructed from the unknown model parameters [53] [51], i.e.

$$Y_i(t) = Y_i(0^+) + t\dot{Y}_i(0^+) + \frac{t^2}{2!}\ddot{Y}_i(0^+) + \dots \tag{3.8}$$

The successive derivatives are measurable, given perfect data, and unique and contain information about the unknown parameters which are to be identified. Chapter 4 describes the Taylor series method in more depth and goes on to introduce a novel method for the reparameterisation of unidentifiable systems.

The principal advantage of the Taylor series method is its applicability to nonlinear and time varying systems as well as linear systems. It suffers from the same problems as the Laplace transform method in that the algebraic equations constructed are often difficult to solve for all but the simplest of systems. Once again the use of a symbolic manipulation package becomes invaluable. A drawback in the method is that no upper bound exists on the number of coefficients that need to be calculated for nonlinear models. For linear systems an upper bound can be obtained by utilising the Cayley-Hamilton Theorem which declares that there are, at most, $2n$-1 independent equations required in this set [63]. It is important to note that this is a necessary but not sufficient condition for identifiability.

3.4.4 The Similarity Transform Approach

The similarity transform, or exhaustive modelling, approach [52] [54] [64] proceeds by generating all output indistinguishable models which are compatible with the assumptions of the model. The method is most easily defined in terms of matrix

notation. The system can described by

$$\dot{\mathbf{x}}(t,\mathbf{p}) = A(\mathbf{p})\mathbf{x}(t,\mathbf{p}) + B(\mathbf{p})\mathbf{u}(t) \tag{3.9}$$

with

$$\mathbf{x}(0,\mathbf{p}) = \mathbf{x_0} \tag{3.10}$$

$$\mathbf{y}(t,\mathbf{p}) = C(\mathbf{p})\mathbf{x}(t,\mathbf{p}) \tag{3.11}$$

with $t \in [0,T], \mathbf{x}(t,\mathbf{p}) \in \Re^n, \mathbf{y}(t,\mathbf{p}) \in \Re^m, \mathbf{p} \in \Omega \subset \Re^q$, and $u(t) \in U[0,T]$. A is the system matrix (n x n), B is the input matrix (n x no_inputs), and C is the output matrix (m x n).

All equivalent models must have corresponding matrices A', B', C' related to A, B, C by a similarity transform.

$$\begin{aligned} A' &= TAT^{-1} \\ B' &= TB \\ C' &= CT^{-1} \end{aligned} \tag{3.12}$$

A necessary condition for applicability of the similarity transform approach is that the model is both structurally controllable and also structurally observable. If these conditions are met, then the method is employed by applying (3.12) and known constraints on A, B, C to determine the unknown elements of T [65]. The identifiability properties are then determined by the dimension of the set of possible matrices, T. If T=I the system is uniquely (globally) identifiable, if there is a finite set of possible matrices, T, the system is locally identifiable and when the set has infinite dimension the system is unidentifiable. Examples of the similarity transform approach as applied to linear systems are given by Chapman and Godfrey [66]. The similarity transform approach may also be applied to nonlinear models [52] [64].

3.4.5 Other Identifiability Techniques

The Volterra series approach [67] extends the Laplace transform method to consider nonlinear systems. Ljung and Glad have presented a differential groups approach [68]. The method examines for global structural identifiability by considering whether the model can be rearranged as a linear regression. Both of these methods are extremely difficult to apply for all but the simplest systems, due to the complex algebraic equations generated.

3.4.6 Summary

This chapter has briefly reviewed some modelling approaches applicable to PET and has presented various methods for performing identifiability analysis. The choice of which method makes the identfiability analysis simplest is not straightforward and a certain amount of trial and error is normally required [54] [64]. In the next chapter, novel work is presented which considers what can be done when a system is unidentifiable. The system is reparameterised in terms of a reduced parameter set, which guarantees the system to be locally identifiable.

3.4.5 Other Identifiability Techniques

The Volterra series approach [67] extends the Laplace transform method to consider nonlinear systems. Ljung and Glad have presented a differential groups approach [68]. The method examines for global structural identifiability by considering whether the model can be rearranged as a linear regression. Both of these methods are extremely difficult to apply for all but the simplest systems, due to the complex algebraic equations generated.

3.4.6 Summary

This chapter has briefly reviewed some modelling approaches applicable to PET and has presented various methods for performing identifiability analysis. The choice of which method makes the identfiability analysis simplest is not straightforward and a certain amount of trial and error is normally required [54] [64]. In the next chapter, novel work is presented which considers what can be done when a system is unidentifiable. The system is reparameterised in terms of a reduced parameter set, which guarantees the system to be locally identifiable.

Chapter 4

Unidentifiable Models and Reparameterisation

4.1 Overview

This chapter considers a novel method of locally reparameterising unidentifiable systems. This reparameterisation reduces a system to its minimal form (in the sense of the number of parameters in the reparameterisation) and ensures that all the parameters are (at least) locally identifiable. The chapter presents a theorem which gives conditions for the existence of a reparameterisation. A theorem is also presented which shows how a reparameterisation may be calculated. In the second part of the chapter examples of four unidentifiable systems are given for illustrative purposes. The examples consist of two standard PET compartmental models (a reference region model and a nonlinear ligand binding model) and two other examples (a linear system and a nonlinear batch reactor model). This method of reparameterisation is applied to a metabolism model in Chapter 5.

4.2 Introduction

The determination of the structural identifiability of system parameters is an important procedure since it is a necessary prerequisite for experimental design. Over

recent years a large amount of work has centred on the development of analytical methods and approaches for the determination of the identifiability of system parameters both for linear and nonlinear models (see for example [51] [52] [53] [54] [68] [64] [69] [70]). An important question is 'what can be done with unidentifiable parameters and systems ?'. Aside from obvious model simplification or redesign of the experiment considered, little has been conjectured theoretically except for the ideas presented in [71] [72] [73] [74]. Milanese and Sorrentino [71] consider a method for analysing unidentifiable linear models which involves classifying the parameters as identifiable or having some degree of freedom. This is achieved by looking at the coefficients yielded by the transfer function. Rothenburg [72] considers how the rank of the system's Jacobian matrix can be utilised in assessing the identifiability of the system parameters. Cobelli and Toffolo [73] consider how parameter bounds can be derived for linear systems by using constraints implicit in a compartmental structure. Walter and Lecourtier [74] use the exhaustive modelling approach to obtain the whole set of output indistinguishable linear compartmental models.

In this chapter, a method is presented which offers criteria for the existence of a locally identifiable reparameterised version of an unidentifiable system. A method for determining the reparameterisation using identifiable parameter combinations and a state space transformation is introduced. This reparameterised system is essentially a reduction of the original system to its minimal locally identifiable form (with respect to the parameterisation). The Taylor series approach [53] and Pohjanpalo's Jacobian rank test [75] are employed which means that the approach is applicable to both linear and nonlinear systems and also systems with specified inputs.

4.3 Background Theory

4.3.1 General System

Consider a system of the form

$$\begin{aligned} \dot{x}(t) &= f(x, u, \theta, t,) \\ y(t) &= g(x, \theta, t) \\ x(0) &= x_0(\theta) \end{aligned} \tag{4.1}$$

where $x \in \Re^n$, $y \in \Re^m$, $u \in U$ (an appropriate space of input functions: usually piecewise continuous functions on an interval $U[0,T]$ which have infinitely many derivatives with respect to t) and $\theta \in \Omega_p \subset \Re^p$ where Ω_p is the feasible parameter region and θ is a p-dimensional parameter vector. The functions f and g are assumed to be analytic in each component.

4.3.2 Structural Identifiability

The identifiability of system (4.1) is examined at some parameter value $\theta \in \Omega_p$ in the experiments specified by $(x_0, U[0,T])$, where the initial conditions x_0 are well defined once θ is selected [64]. The notation $\theta \sim \tilde{\theta}$ denotes that the parameter values $\theta, \tilde{\theta} \in \Omega_p$ are indistinguishable in the experiments $(x_0, U[0,T])$. System (4.1) is defined to be globally identifiable at $\theta \in \Omega_p$ if $\theta \sim \tilde{\theta}, \tilde{\theta} \in \Omega_p$, implies $\theta = \tilde{\theta}$, and it is defined as locally identifiable if there exists an open neighbourhood Ω_n of θ in Ω_p such that $\theta \sim \tilde{\theta}$ for $\theta \in \Omega_n$ implies $\theta = \tilde{\theta}$. These definitions can be extended generically so that (4.1) is globally (locally) structurally identifiable if it is globally (locally) identifiable at all $\theta \in \Omega_p$, except (at most) the points of a subset of zero measure in Ω_p. Furthermore (4.1) is unidentifiable if the system is neither locally or globally identifiable.

4.3.3 Taylor Series Approach

The Taylor series approach [53] examines for the structural identifiability of a parameterised system assuming that y and its derivatives, evaluated at some $t = t_0$, are available and perfect (noiseless), i.e.

$$\begin{bmatrix} y_1^{(0)}(t_0) \\ \vdots \\ y_m^{(0)}(t_0) \end{bmatrix}, \begin{bmatrix} y_1^{(1)}(t_0) \\ \vdots \\ y_m^{(1)}(t_0) \end{bmatrix}, \begin{bmatrix} y_1^{(2)}(t_0) \\ \vdots \\ y_m^{(2)}(t_0) \end{bmatrix}, \ldots, \begin{bmatrix} y_1^{(n)}(t_0) \\ \vdots \\ y_m^{(n)}(t_0) \end{bmatrix}, \ldots$$

These are essentially measurable constants (and in particular are independent of θ). Denote these coefficients by

$$\begin{bmatrix} y_1^{(0)} \\ \vdots \\ y_m^{(0)} \end{bmatrix}, \begin{bmatrix} y_1^{(1)} \\ \vdots \\ y_m^{(1)} \end{bmatrix}, \begin{bmatrix} y_1^{(2)} \\ \vdots \\ y_m^{(2)} \end{bmatrix}, \ldots, \begin{bmatrix} y_1^{(n)} \\ \vdots \\ y_m^{(n)} \end{bmatrix}, \ldots$$

Then the Taylor series approach involves comparing

$$y_i^{(0)} = g_i^{(0)}(\theta), y_i^{(1)} = g_i^{(1)}(\theta), y_i^{(2)} = g_i^{(2)}(\theta), \ldots, y_i^{(n)} = g_i^{(n)}(\theta), \ldots$$

$$for\ i = 1, \ldots, m$$

in order to solve for θ. The number of solutions for θ defines the identifiability structure of the system.

4.3.4 Pohjanpalo's Rank Test

For some $\theta^0 \in \Omega_p$, consider the infinite Jacobian matrix of derivatives of the Taylor series coefficients of y with respect to the parameter vector θ, i.e.

$$G\left(\theta^0\right) = \begin{bmatrix} \frac{\partial g^{(0)}\left(\theta^0\right)}{\partial \theta_1} & \cdots & \frac{\partial g^{(0)}\left(\theta^0\right)}{\partial \theta_p} \\ \frac{\partial g^{(1)}\left(\theta^0\right)}{\partial \theta_1} & \cdots & \frac{\partial g^{(1)}\left(\theta^0\right)}{\partial \theta_p} \\ \vdots & & \vdots \\ \frac{\partial g^{(k)}\left(\theta^0\right)}{\partial \theta_1} & \cdots & \frac{\partial g^{(k)}\left(\theta^0\right)}{\partial \theta_p} \\ \vdots & & \vdots \end{bmatrix} \tag{4.2}$$

Pohjanpalo's result [75] states that the parameters $\theta = (\theta_1, \theta_2, ..., \theta_p)$ are locally identifiable if and only if $G(\theta^0)$ has rank p. This follows from the rank theorems provided by Rothenburg [72].

In order to extend the result of Pohjanpalo to consider unidentifiable systems the Implicit function theorem, and a corollary of the Rank theorem are required [76].

Theorem 1 *(Implicit Function Theorem [76]). Let $A \subset \Re^n \times \Re^m$ be an open set and let $F : A \longrightarrow \Re^m$ be a function of class C^r (that is F has r continuous derivatives where r is a positive integer). Suppose $(x_0, y_0) \in A$ and $F(x_0, y_0) = 0$. Form the determinant of the submatrix given by*

$$\Delta = \begin{vmatrix} \frac{\partial F_1}{\partial y_1} & \cdots & \frac{\partial F_1}{\partial y_m} \\ \vdots & & \vdots \\ \frac{\partial F_m}{\partial y_1} & \cdots & \frac{\partial F_m}{\partial y_m} \end{vmatrix} \tag{4.3}$$

evaluated at (x_0, y_0), where $F = (F_1, \ldots, F_m)$. Suppose that $\Delta \neq 0$. Then there is an open neighbourhood $U \subset \Re^n$ of x_0 and a neighbourhood V of y_0 in $\Re^m$ and a unique function $f : U \longrightarrow V$ such that

$$F(x, f(x)) = 0 \tag{4.4}$$

for all $x \in U$. Furthermore, f is of class C^r.

A corollary of the Rank theorem is also required.

Corollary 1 *[76] Let $G : A \subset \Re^p \longrightarrow \Re^N$ (where A is open in $\Re^n$) be a function of class C^r such that $DG(\theta)$ has rank q for all θ in a neighbourhood of $\theta^0 \in A$. Then there is an open set $U_1 \subset \Re^p$, an open set $U_2 \subset \Re^p$ with $\theta^0 \in U_2$, an open set V_1 around $G(\theta^0)$, an open set $V_2 \subset \Re^N$, and functions $h : U_1 \longrightarrow U_2$ and $f : V_1 \longrightarrow V_2$ of class C^r with inverses of class C^r such that $f \circ G \circ h(\theta_1, \ldots, \theta_p) = (\theta_1, \ldots, \theta_q, 0, \ldots, 0)$.*

4.4 Existence of a Reparameterisation

Theorem 2 *Given a function $Y(\theta_1, \ldots, \theta_p, t)$ whose Taylor series expansion gives rise to the coefficients $g_1(\theta), \ldots, g_p(\theta)$ where $g_i : A \subset \Re^p \longrightarrow \Re$ for $i = 1, \ldots, p$. Define $G = (g_1, \ldots, g_p)$. Suppose that the Jacobian matrix $DG(\theta)$ with respect to θ has rank $q(< p)$ for all θ in a neighbourhood of $\theta^0 \in A$ then the function Y may be locally reparameterised in terms of a set of q of the Taylor series coefficients,*

$$\{\phi_1 = g_{j_1}, \ldots, \phi_q = g_{j_q}\} \tag{4.5}$$

i.e.

$$G(\theta_1, \ldots, \theta_p) = \hat{G}(\phi_1, \ldots, \phi_q) \tag{4.6}$$

Furthermore the reparameterised system is locally identifiable.

Proof : If $DG(\theta^0)$ has rank q for some $q < p$ then by Corollary 1 there exists an open set $U_1 \subset \Re^p$, an open set $U_2 \subset \Re^p$ with $\theta^0 \in U_2$, an open set V_1 around

$G(\theta^0)$, an open set $V_2 \subset \Re^p$, and functions $h : U_1 \longrightarrow U_2$ and $f : V_1 \longrightarrow V_2$ of class C^r with inverses of class C^r such that

$$f \circ G \circ h(\theta_1, \ldots, \theta_p) = (\theta_1, \ldots, \theta_q, 0, \ldots, 0). \tag{4.7}$$

Let $M : \Re^p \longrightarrow \Re^{p-q}$ be the last $p-q$ components of f, hence,

$$\begin{aligned} M_1(g_1, \ldots, g_p) &= 0 \\ \vdots \quad & \quad \vdots \\ M_{p-q}(g_1, \ldots, g_p) &= 0 \end{aligned} \tag{4.8}$$

Since f is invertible, the Jacobian matrix DM with respect to $\{g_1, \ldots, g_p\}$ must have rank equal to $p-q$ where

$$DM = \begin{bmatrix} \dfrac{\partial M_1(\theta^0)}{\partial g_1} & \cdots & \dfrac{\partial M_1(\theta^0)}{\partial g_p} \\ \vdots & & \vdots \\ \dfrac{\partial M_{p-q}(\theta^0)}{\partial g_1} & \cdots & \dfrac{\partial M_{p-q}(\theta^0)}{\partial g_p} \end{bmatrix}. \tag{4.9}$$

Now by the definition of the rank being the number of linearly independent rows or columns of a matrix there exists a partitioning of $G = \{g_1, \ldots, g_p\}$ into two sets A and B where $A = \{g_{i_1}, \ldots, g_{i_{p-q}}\} \subset G$, $B = \{g_{i_{p-q+1}}, \ldots, g_{i_p}\} \subset G$, $A \cap B = \{0\}$ and $A \cup B = G$ such that the determinant, Δ, is

$$\Delta = \begin{vmatrix} \dfrac{\partial M_1(\theta^0)}{\partial g_{i_1}} & \cdots & \dfrac{\partial M_1(\theta^0)}{\partial g_{i_{p-q}}} \\ \vdots & & \vdots \\ \dfrac{\partial M_{p-q}(\theta^0)}{\partial g_{i_1}} & \cdots & \dfrac{\partial M_{p-q}(\theta^0)}{\partial g_{i_{p-q}}} \end{vmatrix} \neq 0. \tag{4.10}$$

Now by invoking the implicit function theorem it follows that we can locally solve

$$\begin{aligned} M_1(g_1, \ldots, g_p) &= 0 \\ \vdots & \quad \vdots \\ M_{N-q}(g_1, \ldots, g_p) &= 0 \end{aligned} \tag{4.11}$$

for

$$\begin{aligned} g_{i_1} &= L_1(g_{i_{p-q+1}}, \ldots, g_{i_p}) \\ \vdots & \quad \vdots \\ g_{i_{p-q}} &= L_{p-q}(g_{i_{p-q+1}}, \ldots, g_{i_p}). \end{aligned} \tag{4.12}$$

where $L : \Re^q \longrightarrow \Re^{p-q}$. Now

$$G(\theta_1, \ldots, \theta_p) = (g_1, \ldots, g_p) \tag{4.13}$$

and from equation (4.12) this can be represented as

$$\begin{aligned} G(\theta_1, \ldots, \theta_p) &= \hat{G}(g_{i_{p-q+1}}, \ldots, g_{i_p}) \\ &= \hat{G}(\phi_1, \ldots, \phi_q) \end{aligned} \tag{4.14}$$

where $\{\phi_1 = g_{i_{p-q+1}}, \ldots, \phi_q = g_{i_p}\}$.

Finally by application of Pohjanpalo's rank test the parameters $\{\phi_1, \ldots, \phi_q\}$ are (at least) locally identifiable.

□

Remark : The reparameterisation deriving from the implicit function theorem is only guaranteed in a neighbourhood of θ^0. The theory also applies to the Nth order Taylor expansion of the function Y.

As an extension to Theorem 2 let us consider the conditions on ϕ for a reparameterisation to exist, i.e what are the "new" parameters $(\phi_1, \ldots, \phi_q)$ with which the system can be reparameterised.

Theorem 3 *Given*

$$G(\theta_1, \ldots, \theta_p) = \hat{G}(\phi_1, \ldots, \phi_q) \tag{4.15}$$

as in Theorem 2 where $q < p$ such that rank $(DG(\theta^0)) = q$ and let the kernel, N_G, of $(DG(\theta^0))$ be given by,

$$N_G = \{\theta \in \Re^p | DG(\theta^0).\theta = 0\}. \tag{4.16}$$

Now given

$$\Phi(\theta_1, \ldots, \theta_p) : \Omega_p \subset \Re^p \longrightarrow \Omega_q \subset \Re^q \tag{4.17}$$

Suppose that

$$< D\Phi(\theta^0), N_G > = 0 \tag{4.18}$$

where $<,>$ is the Euclidean inner product on $\Re^p$, and that

$$rank(D\Phi(\theta^0)) = q \tag{4.19}$$

then there exists a $\hat{G}$ such that

$$G(\theta_1, \ldots, \theta_p) = \hat{G}(\phi_1, \ldots, \phi_q) \tag{4.20}$$

Furthermore if (4.18) and (4.19) are not met then no such $\hat{G}$ exists. (i.e. the function ,G , can be reparameterised in terms of the parameter set $(\phi_1, \cdots, \phi_q)$ if and only if conditions (4.18) and (4.19) are true).

Proof : If

$$G(\theta_1, \ldots, \theta_p) = \hat{G}(\phi_1, \ldots, \phi_q), \tag{4.21}$$

then

$$DG(\theta) = D\hat{G}(\Phi(\theta)).D\Phi(\theta) \tag{4.22}$$

Given

$$\begin{aligned} DG(\theta).N_G &= 0, \\ D\Phi(\theta).N_G &= 0, \\ rank(D\Phi(\theta)) &= q, \end{aligned} \tag{4.23}$$

let M_G be the q dimensional complement of N_G such that $M_G \cap N_G = \{0\}$ and $M_G \oplus N_G = \Omega_p$. Then

$$DG(\theta).N_G = D\hat{G}(\Phi(\theta)).D\Phi(\theta).N_G \tag{4.24}$$

which implies that

$$0 = D\hat{G}(\Phi(\theta)).0 \tag{4.25}$$

and this is satisfied for all $\hat{G}$. But $\hat{G}$ must also satisfy

$$DG(\theta).M_G = D\hat{G}(\Phi(\theta)).D\Phi(\theta).M_G. \tag{4.26}$$

Now $D\Phi(\theta).M_G$ is a qxq matrix with rank q and therefore has an inverse such that

$$DG(\theta).M_G(D\Phi(\theta).M_G)^{-1} = D\hat{G}(\Phi(\theta)). \tag{4.27}$$

Hence there exists a function $\hat{G}$ such that (4.22) is satisfied. Furthermore it is trivial to show that if $N_G \neq N_\Phi$ (where $N_\Phi = \{\theta \in \Re^p | D\Phi(\theta^0).\theta = 0\}$) then (4.22) is false and no $\hat{G}$ exists. Choose $D\Phi(\theta).N_\Phi = 0$ which implies that $DG(\theta).N_\Phi \neq 0$ and hence

$$DG(\theta).N_\Phi = D\hat{G}(\Phi(\theta)).D\Phi(\theta).N_\Phi \tag{4.28}$$

which implies

$$DG(\theta).N_\Phi = 0 \tag{4.29}$$

and the desired result is achieved by contradiction.

□

4.4.1 Reparameterisation

This section briefly describes the methodology for reparameterising an unidentifiable system. Firstly the nullspace,N_G, of the Jacobian matrix G is calculated and it is spanned by

$$N_G = [\underline{n}_1, \ldots, \underline{n}_{p-q}] \tag{4.30}$$

where the vectors $\underline{n}_i$ for $i = 1, \ldots, p-q$ are p dimensional. The locally identifiable parameters for the reparameterisation may be calculated from the conditions given in Theorem 3, i.e. the new parameters $\Phi = (\phi_1, \ldots, \phi_q)$ must satisfy,

$$< [\frac{\partial \phi_i}{\partial \theta_1}, \ldots, \frac{\partial \phi_i}{\partial \theta_p}]^T, [\underline{n}_1, \ldots, \underline{n}_{p-q}] > = 0. \tag{4.31}$$

for $i = 1, \ldots, q$. This produces a partial differential equation whose solution yields the required functions ϕ_i. For the case $p - q = 1$ the partial differential equation is given by

$$\frac{\partial \phi_i}{\partial \theta_1} n_{1_1} + \ldots + \frac{\partial \phi_i}{\partial \theta_p} n_{1_p} = 0 \tag{4.32}$$

Once q solutions have been found such that rank $(D\Phi)$ =q then by Theorem 3 there exists a reparameterisation of the system involving just these q parameters.

The final stage involves finding a state space transformation of the original differential equations such that the system may be reparameterised in terms of the new parameter set Φ. This step is nontrivial and the choice of simple functions for Φ gives the best chance of finding a simple state space transformation.

4.5 Method of Reparameterisation

The idea behind reparameterising the system involves finding locally identifiable parameter groupings and then a state space transformation such that the transformed equations only involve these identifiable parameter groupings. Firstly, a simple way of obtaining identifiable parameter combinations from the nullspace of the Jacobian matrix is described. To illustrate the situation consider the problem geometrically for a three parameter system, see Figure (4.1). Henceforth examples will only be considered for systems where the Jacobian matrix is rank deficient by 1,(i.e $q = p - 1$) although the ideas presented here apply for higher dimensions of rank deficiency. If the system under consideration is locally identifiable (i.e. full rank Jacobian, $q = p$) then a set of experimental data will map back to a distinct point or finite number of points in parameter space. However in the case where the Jacobian is rank deficient by 1, ($q = p - 1$) the experimental data will map back to a curve in parameter space.

Let the nullspace of the corresponding Jacobian matrix G be spanned by those vectors $\underline{n} \in \Re^3$ which satisfy,

$$G\underline{n} = \underline{0} \tag{4.33}$$

For $q = p - 1$ the nullspace of the Jacobian matrix is spanned by a vector which is tangent to the solution curve at all points in parameter space. Hence the nullspace gives the local direction in which a solution for the parameters may be perturbed such that the observation y is unaffected. If the nullspace has any zero entries the corresponding parameter is identifiable because the nullspace is orthogonal to this

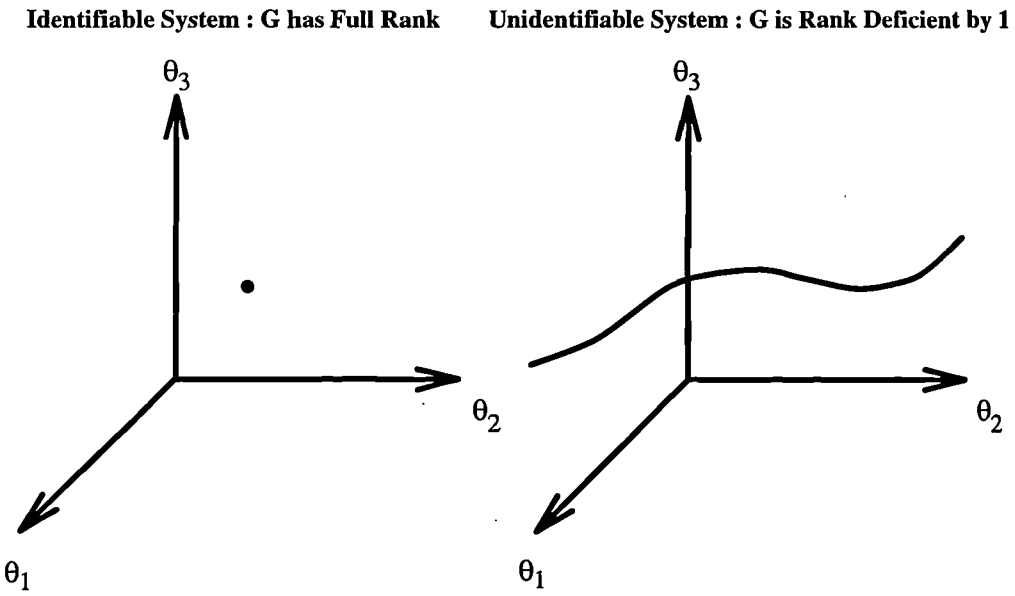

Figure 4.1: Parameter space for a three parameter system

parameter axis. However for a non-zero entry this implies that it is possible to perturb this and other parameters in a way such that the observation, y, remains unchanged.

Consider a family of functions, $\Phi(\theta_1, \theta_2, \theta_3)$ where $\phi_i : \Re^3 \longrightarrow \Re$ (i=1,2), such that the image of ϕ_i is a locally identifiable combination of the parameters. Any function ϕ_i will have a directional derivative in the direction of the nullspace equal to zero, see Figure (4.2), i.e. moving in parameter space in such a way that the observation y remains unchanged, the function ϕ_i has a constant value. To calculate the functions ϕ_i whose directional derivative in the direction of the nullspace vector $\underline{n}$ is zero requires that,

$$< D\phi_i, \underline{n} > = 0 \tag{4.34}$$

where $D\phi_i(\theta)$ is the gradient of the function ϕ_i.

For our three dimensional example the partial differential equation which provides solutions for ϕ_i is

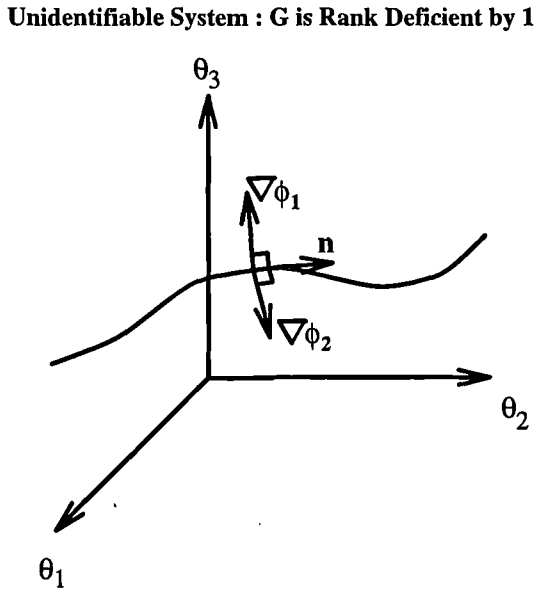

Figure 4.2: Parameter space for a three parameter system

$$\frac{\partial \phi_i}{\partial \theta_1} n_1 + \frac{\partial \phi_i}{\partial \theta_2} n_2 + \frac{\partial \phi_i}{\partial \theta_3} n_3 = 0. \tag{4.35}$$

Any new parameter defined by the image of ϕ_i which solves equation (4.35) is locally identifiable, as the directional derivative in the direction of the nullspace is zero and hence this parameter must be fixed for each distinct observation. There is no unique solution for ϕ_i to equation (4.35).

To reparameterise the system it is necessary to find a set of $q(= 2$ in this case) identifiable parameter combinations which span the manifold in parameter space describing all possible system responses. Firstly, 2 locally identifiable parameter groupings ϕ_1 and ϕ_2 are deduced from the partial differential equation in ϕ_i (equation (4.35)), such that these parameters are independent (see Theorem 3). Normally the boundary values in (4.35) are chosen to be zero and this is the case in the following illustrative examples. The final step in the reparameterisation involves finding a state space transformation which reconstructs the original set of equations such that they only involve these 2 identifiable parameter group-

ings. The new parameter groupings and the state space transformation constitute the reparameterisation of the system. By determining the identifiable parameter groupings first it facilitates the discovery of an appropriate state space transformation by inspection.

4.5.1 Summary of Reparameterisation Process

- Calculate the Taylor series

  The Taylor series of the observation is evaluated at some $t = t_0$ from the system equations and initial conditions.

- Calculate the Jacobian matrix and its associated rank

  Calculate the partial derivatives of the Taylor series coefficients (see Discussion).

- Determine the identifiable parameter combinations

  Calculate the nullspace of the Jacobian matrix G by employing row operations. Utilise the nullspace to calculate locally identifiable parameter combinations using Theorem (3).

- Determine the state space transformation

  By inspection of the system equations construct a state space transformation which converts the system into a form which is parameterised by just q locally identifiable parameter combinations which span the viable parameter space. The state space transformation must preserve the input-output map of the system.

4.6 Examples

To illustrate the methodology and results presented for minimally locally identifiable forms of parameterised systems four examples are considered. Example 1 is a standard 2-dimensional linear system in which observation is of one compartment only. Examples 2 and 3 are standard PET models for ligand binding. The reparameterisation of example 3 puts into a more rigorous context the parametrisation that has previously been applied empirically [77]. The 4th example does not relate directly to PET studies but is included as an example to demonstrate the methods full power with a non-trivial reparameterisation of a nonlinear system. For the purpose of the examples the parameters are assumed to be dimensionless, the dimensions having no effect on the reparameterisation process.

4.6.1 Example 1 : Linear System

Consider a two dimensional linear system defined by,

$$\frac{dx_1(t)}{dt} = \theta_1 x_1(t) + \theta_2 x_2(t) + u(t)$$

$$\frac{dx_2(t)}{dt} = \theta_3 x_1(t) + \theta_4 x_2(t)$$

$$\begin{aligned} y(t) &= x_2(t) \\ x_1(0) &= 0 \\ x_2(0) &= 0 \end{aligned} \tag{4.36}$$

The experiment considered is for a unit impulsive input, $u(t) = \delta(t)$, with observation of x_2 only. Thus the system can be considered to have zero input and non-zero initial conditions, i.e.

$$\begin{aligned} u(t) &= 0 \\ x_1\left(0^+\right) &= 1 \\ x_2\left(0^+\right) &= 0 \end{aligned} \tag{4.37}$$

For this system it is a straightforward procedure to generate the Taylor Series coefficients of the observation function y of which the first three non-zero coefficients are given by :-

$$y^{(1)}\left(0^+\right) = \theta_3$$

$$y^{(2)}\left(0^{+}\right) = \theta_3\left(\theta_1 + \theta_4\right)$$

$$y^{(3)}\left(0^{+}\right) = \theta_3\left(\theta_1^2 + \theta_2\theta_3 + \theta_1\theta_4 + \theta_4^2\right) \tag{4.38}$$

By taking partial derivatives of the Taylor series coefficients of y with respect to the parameter vector $\theta = (\theta_1, \theta_2, \theta_3, \theta_4)$ the following Jacobian matrix is obtained,

$$G\left(\theta^0\right) = \begin{bmatrix} 0 & 0 & 1 & 0 \\ \theta_3 & 0 & \theta_1 + \theta_4 & \theta_3 \\ \theta_3\left(2\theta_1 + \theta_4\right) & \theta_3^2 & \theta_1^2 + 2\theta_2\theta_3 + \theta_1\theta_4 + \theta_4^2 & \theta_3\left(\theta_1 + 2\theta_4\right) \end{bmatrix} \tag{4.39}$$

By a process of row reduction the matrix can be reduced to

$$G'\left(\theta^0\right) = \begin{bmatrix} 1 & 0 & 0 & 1 \\ 0 & 1 & 0 & -\frac{\theta_1}{\theta_3} + \frac{\theta_4}{\theta_3} \\ 0 & 0 & 1 & 0 \end{bmatrix} \tag{4.40}$$

It follows that the matrix,$G\left(\theta^0\right)$, has rank 3, since using Vajda's result [63] concerning structural identifiability of linear systems, we know that there are at most 3 ($2n$-1) independent equations that can be obtained from the Taylor coefficients (where n is the dimension of the state space of the system). Hence it is implicit that no more terms need to be calculated as the matrix will only ever have rank less than or equal to 3. Using Theorem 2 there is 1 $(p - q)$ redundant parameter and there exists a reparameterisation of the system in terms of just three parameters which is locally identifiable.

Reparameterisation of the System

For the Jacobian matrix $G\left(\theta^0\right)$ the nullspace is spanned by the vector,

$$\underline{n} = \left[-1,\ \frac{\theta_1 - \theta_4}{\theta_3},\ 0,\ 1\right] \tag{4.41}$$

To solve for functions ϕ whose images are identifiable combinations of the parameters consider,

$$< \left[\frac{\partial\phi}{\partial\theta_1},\ \frac{\partial\phi}{\partial\theta_2},\ \frac{\partial\phi}{\partial\theta_3},\ \frac{\partial\phi}{\partial\theta_4}\right], \left[-1,\ \frac{\theta_1 - \theta_4}{\theta_3},\ 0,\ 1\right] > = 0 \tag{4.42}$$

Hence the following partial differential equation in ϕ is obtained,

$$-\frac{\partial\phi}{\partial\theta_1} + \frac{\theta_1 - \theta_4}{\theta_3}\frac{\partial\phi}{\partial\theta_2} + \frac{\partial\phi}{\partial\theta_4} = 0 \tag{4.43}$$

Possible solutions for ϕ are,

$$\begin{aligned}
\phi_1(\theta_1, \theta_2, \theta_3, \theta_4) &= \theta_2 - \frac{\theta_1\theta_4}{\theta_3} \\
\phi_2(\theta_1, \theta_2, \theta_3, \theta_4) &= \theta_3 \\
\phi_3(\theta_1, \theta_2, \theta_3, \theta_4) &= \theta_1 + \theta_4
\end{aligned} \tag{4.44}$$

where $\Phi = \{\phi_1, \phi_2, \phi_3\}$ and rank $D\Phi = 3$.

The original system (4.36) may now be rearranged to include just these three parameter groupings as and hence may be reparameterised in terms of them. Let $x_1(t)^* = x_1(t) - \frac{\theta_1}{\theta_3}x_2(t)$

Substituting into the original pair of equations yields,

$$\begin{aligned}
\frac{dx_1(t)^*}{dt} + \frac{\theta_1}{\theta_3}\frac{dx_2(t)}{dt} &= \theta_1(x_1(t)^* + \frac{\theta_1}{\theta_3}x_2(t)) + \theta_2 x_2(t) + u\,(t) \\
\frac{dx_2(t)}{dt} &= \theta_3(x_1(t)^* + \frac{\theta_1}{\theta_3}x_2(t)) + \theta_4 x_2(t)
\end{aligned} \tag{4.45}$$

Subtracting $\frac{\theta_1}{\theta_3}$ times the second equation from the first and simplifying yields,

$$\frac{dx_1(t)^*}{dt} = (\theta_2 - \frac{\theta_1\theta_4}{\theta_3})x_2(t) + u(t)$$

$$\frac{dx_2(t)}{dt} = \theta_3 x_1(t)^* + (\theta_1 + \theta_4)x_2(t) \tag{4.46}$$

Hence a reparameterised version of system (4.36) which is a locally identifiable system is given by,

$$\frac{dx_1(t)^*}{dt} = \phi_1 x_2(t) + u(t)$$

$$\frac{dx_2(t)}{dt} = \phi_2 x_1(t)^* + \phi_3 x_2(t)$$

$$\begin{aligned} y(t) &= x_2(t) \\ x_1\left(0^+\right)^* &= 1 \\ x_2\left(0^+\right) &= 0 \end{aligned} \tag{4.47}$$

where $\phi_1 = \theta_2 - \frac{\theta_1\theta_4}{\theta_3}$, $\phi_2 = \theta_3$, and $\phi_3 = \theta_1 + \theta_4$ are locally identifiable. Note that the reparameterisation is not unique and that the parameterisation of the system has been reduced from p(=4) to q(=3) parameters.

4.6.2 Example 2 : Nonlinear Saturable Ligand Binding Model

A typical example of a ligand whose kinetics are accurately described by the model shown in Figure (4.3) is flumazenil which binds reversibly to benzodiazepine receptors [78]. Flumazenil is an ideal ligand because it has a high blood brain barrier permeability and a high specific to non-specific ratio [79].

A model for the binding kinetics of flumazenil has been described by Delforge [56] and Price [48] and derives from the pioneering work of Mintun [80]. The model is based on Mintun's receptor binding model which contains free ligand, nonspecifically bound ligand and specifically bound ligand. In this model, the free and non-specifically bound ligand are assumed to be in rapid equilibrium allowing the model's complexity to be reduced by considering the free and nonspecifically bound pools as one. The model is described by the compartmental form given in Figure (4.3), and the following nonlinear system equations can be derived:-

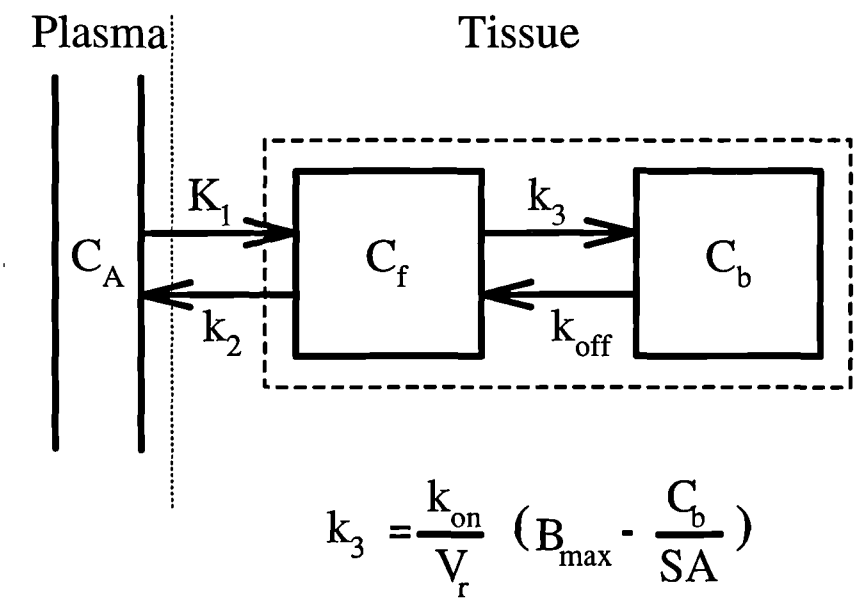

Figure 4.3: Ligand binding compartmental model

$$\frac{dC_f(t)}{dt} = K_1 C_a(t) - \left(k_2 + \frac{k_{on}B_{max}}{V_r}\right) C_f(t) + k_{off}C_b(t) + \frac{k_{on}C_f(t)C_b(t)}{V_r SA}$$

$$\frac{dC_b(t)}{dt} = \frac{k_{on}B_{max}C_f(t)}{V_r} - k_{off}C_b(t) - \frac{k_{on}C_f(t)C_b(t)}{V_r SA}$$

$$y(t) = C_f(t) + C_b(t) \tag{4.48}$$

where

K_1	is flow x extraction
k_2	is the efflux rate constant
B_{max}	is the maximum concentration of available binding sites
V_r	is the volume of reaction
k_{on}	is the apparent 2nd order association rate constant
k_{off}	is the dissociation rate constant
SA	is the specific activity of the compound

A nonlinear term is an intrinsic part of the model because the rate at which the free ligand binds to the receptors depends on the concentration of available binding sites. The rate at which the free ligand binds is defined by $k_3 = \frac{k_{on}B_a}{V_r}$ where the concentration of available binding sites,B_a, is determined by the nonlinear term $B_a = B_{max} - \frac{C_b}{SA}$. It should be noted that the constant V_r is composed of two factors; i) the volume within which the free ligand exists, and ii) the fraction of ligand which is free to bind.

The rate constants k_{on} and k_{off} in the model derive from theory first applied to pharmacological systems by Clark [81] (cited in [82]) in which he laid down the

foundations for receptor occupancy. The equations are defined as,

$$[L] + [R] \underset{k_{off}}{\overset{k_{on}}{\rightleftharpoons}} [LR] \tag{4.49}$$

where

$[L]$	is the concentration of free ligand
$[R]$	is the concentration of receptors
$[LR]$	is the concentration of bound ligand
k_{on}	is the 2nd order association rate constant
k_{off}	is the dissociation rate constant

By introducing a dose of high specific activity to the system the model can be approximated by a linear system where $k_3 = \frac{k_{on}B_{max}}{V_r}$. This results from the fact that the large value of specific activity renders the nonlinear term in the equation negligible. However when a low specific activity dose of the compound is administered the system is nonlinear. The nonlinearity derives from the large amount of cold compound available to bind to the receptors. The more available cold compound reduces the number of available binding sites. Delforge has shown that only five parameters are identifiable from this model because k_{on} and V_r always occur together in the system equations [83]. The reparameterisation process is applied to this model showing how a simple reparameterisation is obtained.

The specific activity of the compound is known prior to administration and this measured constant is removed from the following calculations without loss of generality by assuming that SA=1. The experiment is considered for a unit impulsive input, $C_a(t) = \delta(t)$, with observation of the sum of $C_f + C_b$. Hence the system can be considered as having zero input and non-zero initial conditions, i.e.

$$\begin{aligned} C_f(0^+) &= K_1 \\ C_b(0^+) &= 0 \end{aligned} \tag{4.50}$$

It is then possible to calculate the Taylor Series coefficients of the observation function $y(t)$. The first five Taylor series coefficients are :-

$$y^{(0)}\left(0^{+}\right) = K_1$$

$$y^{(1)}\left(0^{+}\right) = -\left(K_1 k_2\right)$$

$$y^{(2)}\left(0^{+}\right) = \frac{K_1 k_2}{V_r}\left(k_2 V_r + k_{on} B_{max}\right)$$

$$y^{(3)}\left(0^{+}\right) = -\frac{K_1 k_2}{V_r^{2}}\left(k_2^{2} V_r^{2} + K_1 k_{on}^{2} B_{max} + 2k_2 k_{on} V_r B_{max} + k_{on}^{2} B_{max}^{2} + k_{on} V_r B_{max} k_{off}\right)$$

$$y^{(4)}\left(0^{+}\right) = \frac{K_1 k_2}{V_r^{3}}\left(k_2^{3} V_r^{3} + K_1^{2} k_{on}^{3} B_{max} + 4K_1 k_2 k_{on}^{2} V_r B_{max} + 3k_2^{2} k_{on} V_r^{2} B_{max} + 4K_1 k_{on}^{3} B_{max}^{2} + 3k_2 k_{on}^{2} V_r B_{max}^{2} + k_{on}^{3} B_{max}^{3} + 2K_1 k_{on}^{2} V_r B_{max} k_{off} + 2k_2 k_{on} V_r^{2} B_{max} k_{off} + 2k_{on}^{2} V_r B_{max}^{2} k_{off} + k_{on} V_r^{2} B_{max} k_{off}^{2}\right) \quad (4.51)$$

The Jacobian matrix is obtained by taking partial derivatives of the Taylor series coefficients with respect to the parameter vector $\theta = (K_1, k_2, k_{on}, V_r, B_{max}, k_{off})$. The Jacobian matrix, $G(\theta^0)$, is given in Appendix A.1. By a process of row reduction, within MATHEMATICA, the Jacobian matrix can be reduced to,

$$G'\left(\theta^0\right) = \begin{bmatrix} 1 & 0 & 0 & 0 & 0 & 0 \\ 0 & 1 & 0 & 0 & 0 & 0 \\ 0 & 0 & 1 & -\frac{k_{on}}{V_r} & 0 & 0 \\ 0 & 0 & 0 & 0 & 1 & 0 \\ 0 & 0 & 0 & 0 & 0 & 1 \end{bmatrix} \quad (4.52)$$

Therefore the rank of the Jacobian matrix, $G(\theta^0)$, is at least 5. Using Theorem 2 there is 1 $(p-q)$ redundant parameter and there exists a reparameterisation of the system in terms of just five parameters which is locally identifiable.

Reparameterisation of the System

To consider what reparameterisation of the system will render the model identifiable it is necessary to calculate the nullspace of the Jacobian matrix, $G(\theta^0)$, given by 4.52. The nullspace of $G(\theta^0)$ is spanned by the vector,

$$\underline{n} = \left[0, 0, \frac{k_{on}}{V_r}, 1, 0, 0\right] \tag{4.53}$$

Applying Theorem 3 the locally identifiable parameter groupings are determined from,

$$< \left[\frac{d\phi}{dK_1}, \frac{d\phi}{dk_2}, \frac{d\phi}{dk_{on}}, \frac{d\phi}{dV_r}, \frac{d\phi}{dB_{max}}, \frac{d\phi}{dk_{off}}\right], \left[0, 0, \frac{k_{on}}{V_r}, 1, 0, 0\right] > = 0 \tag{4.54}$$

This yields a partial differential equation in $\phi(\theta)$ such that all solutions $\phi(\theta)$ satisfying this equation are locally identifiable. The partial differential equation in this case is given by,

$$\frac{k_{on}}{V_r}\frac{d\phi}{dk_{on}} + \frac{d\phi}{dV_r} = 0 \tag{4.55}$$

Solutions to (4.55) are found by inspection. The following simple locally identifiable parameter combinations are obtained,

$$\begin{aligned}
\phi_1(K_1, k_2, k_{on}, V_r, B_{max}, k_{off}) &= K_1 \\
\phi_2(K_1, k_2, k_{on}, V_r, B_{max}, k_{off}) &= k_2 \\
\phi_3(K_1, k_2, k_{on}, V_r, B_{max}, k_{off}) &= \frac{k_{on}}{V_r} \\
\phi_4(K_1, k_2, k_{on}, V_r, B_{max}, k_{off}) &= B_{max}
\end{aligned}$$

$$\phi_5(K_1, k_2, k_{on}, V_r, B_{max}, k_{off}) = k_{off} \tag{4.56}$$

where $\Phi = \{\phi_1, \phi_2, \phi_3, \phi_4, \phi_5\}$ and rank $D\Phi = 5$.

This leads us to a simple reparameterisation of the model in which the parameter combination k_{on}/V_r is introduced as a new parameter. This illustrates the method of reparameterising an unidentifiable system even though the reparameterisation for this example is simple and could have been deduced fairly easily from close inspection of the original equations. Hence the locally reparameterised version of system (4.48) which is locally identifiable is given by,

$$\begin{aligned}
\frac{dC_f(t)}{dt} &= K_1 C_a(t) - (k_2 + k^*_{on} B_{max})\, C_f(t) + k_{off} C_b(t) + k^*_{on} C_f(t) \frac{C_b(t)}{SA} \\
\frac{dC_b}{dt} &= k^*_{on} B_{max} C_f(t) - k_{off} C_b(t) - \phi C_f(t) \frac{C_b(t)}{SA} \\
y(t) &= C_f(t) + C_b(t)
\end{aligned} \tag{4.57}$$

where $k^*_{on} = \frac{k_{on}}{V_r}$.

Note that the reparameterisation is not unique and that the parameterisation of the system has been reduced from p $(= 6)$ to q $(= 5)$ parameters. Sometimes a vascular component is included in the model to take into account a blood volume component in the region of interest [84]. The inclusion of this vascular term in the observation function $y(t)$ yields the same result as before with the blood volume term being identifiable and hence no further reparameterisation is neces-

sary. Often this component is fixed using *a priori* knowledge and hence reduces the number of kinetic parameters to be estimated. Further analysis of this model with respect to numerical identifiability and different protocols is described by Delforge [84].

The parameters of interest generally are B_{max} and K_d the maximum concentration of binding sites and the equilibrium dissociation constant (or half saturation concentration, $K_d = \frac{K_{off}}{k_{on}}$), respectively. B_{max} is locally identifiable from a single experiment, given that the specific activity is suitably small and the experiment can be considered nonlinear. Hence to identify the parameter K_d it is necessary to either know V_r *a priori* or to perform an *in vitro* experiment to ascertain its value [48] [85] [83].

4.6.3 Example 3 : Reference Region Model

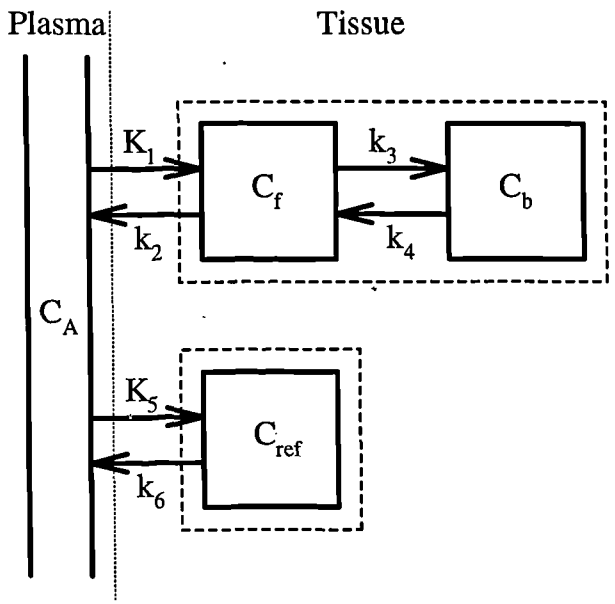

Figure 4.4: Reference region compartmental model

A reference region model described by Blomqvist [86] and Cunningham [77] provides a method of avoiding arterial blood sampling. The method relies on the fact that there exists an area in which little or no specific binding is present. A region of interest is defined on this reference region such that the kinetics of the free ligand can be obtained. The model is illustrated by the compartmental model given in Figure (4.4).

The compartmental model is described by the following set of ordinary linear differential equations,

$$\frac{dC_{ref}(t)}{dt} = K_5 C_a(t) - k_6 C_{ref}(t)$$

$$\frac{dC_f(t)}{dt} = K_1 C_a(t) - (k_2 + k_3)\, C_f(t) + k_4 C_b(t)$$

$$\frac{dC_b(t)}{dt} = k_3 C_f(t) - k_4 C_b(t)$$

$$y(t) = C_f(t) + C_b(t)$$

(4.58)

where

$C_{ref}(t)$	is the concentration of label in the reference region
$C_f(t)$	is the concentration of label in the combined free and nonspecifically bound pools
$C_b(t)$	is the concentration of label in the specifically bound pool
$C_a(t)$	is the concentration of parent ligand label in plasma
K_1	is flow x extraction
k_2	is the efflux rate constant
k_3	is the product of the association rate constant and the maximum specific binding capacity (tracer conditions only)
k_4	is the dissociation rate constant
K_5	is flow x extraction in the reference region
k_6	is the efflux rate constant for the reference region

Transformation of the system equations (4.58) allows us to remove the presence of the term $C_a(t)$. Rearrangement of the first equation gives,

$$C_a(t) = \frac{\frac{dC_{ref}(t)}{dt} + k_6 C_{ref}(t)}{K_5} \tag{4.59}$$

Substituting this equation into the second of (4.58) eliminates $C_a(t)$ yielding,

$$\frac{dC_f(t)}{dt} = \frac{K_1}{K_5}\frac{dC_{ref}(t)}{dt} + \frac{K_1 k_6}{K_5} C_{ref}(t) - (k_2 + k_3)\, C_f(t) + k_4 C_b(t)$$

$$\frac{dC_b(t)}{dt} = k_3 C_f(t) - k_4 C_b(t)$$

$$y(t) = C_f(t) + C_b(t)$$

(4.60)

$C_{ref}(t)$ may now be treated as the input for this system. The system is examined for a constant input,

$$C_{ref}(t) = \begin{cases} 0 & t < 0 \\ 1 & t > 0 \end{cases}$$

$$\frac{dC_{ref}(t)}{dt} = \delta(t). \tag{4.61}$$

This system can be considered as having zero input and non-zero initial conditions, i.e.

$$\frac{dC_f(t)}{dt} = \frac{K_1 k_6}{K_5} - (k_2 + k_3)\, C_f(t) + k_4 C_b(t)$$

$$\frac{dC_b(t)}{dt} = k_3 C_f(t) - k_4 C_b(t)$$

$$y(t) = C_f(t) + C_b(t)$$

$$C_f(0^+) = \frac{K_1}{K_5}$$

$$C_b(0^+) = 0 \tag{4.62}$$

The Taylor series of the observation function $y(t)$ expanded about $t = 0$ can now be calculated. The first five Taylor series coefficients are :-

$$y^{(0)}\left(0^+\right) = \frac{K_1}{K_5}$$

$$y^{(1)}\left(0^{+}\right) = \frac{K_1\left(k_6 - k_2\right)}{K_5}$$

$$y^{(2)}\left(0^{+}\right) = \frac{K_1 k_2\left(k_2 + k_3 - k_6\right)}{K_5}$$

$$y^{(3)}\left(0^{+}\right) = -\frac{K_1 k_2\left({k_2}^2 + 2k_2k_3 + {k_3}^2 + k_3k_4 - k_2k_6 - k_3k_6\right)}{K_5}$$

$$y^{(4)}\left(0^{+}\right) = \frac{K_1 k_2\left(k_2^3 + 3k_2^2k_3 + 3k_2k_3^2 + k_3^3 + 2k_2k_3k_4 + 2k_3^2k_4 + k_3k_4^2 - k_2^2k_6\right.}{K_5}$$
$$\frac{\left.-2k_2k_3k_6 - k_3^2k_6 - k_3k_4k_6\right)}{K_5} \tag{4.63}$$

The Jacobian matrix $G(\theta^0)$, consisting of the partial derivatives of the Taylor series coefficients with respect to the parameter vector $\theta = (K_1, k_2, k_3, k_4, K_5, k_6)$, can then be obtained. This process was performed using MATHEMATICA and the coefficients are given in Appendix A.2. A process of row reduction of the Jacobian matrix yields,

$$G'\left(\theta^0\right) = \begin{bmatrix} 1 & 0 & 0 & 0 & -\frac{K_1}{K_5} & 0 \\ 0 & 1 & 0 & 0 & 0 & 0 \\ 0 & 0 & 1 & 0 & 0 & 0 \\ 0 & 0 & 0 & 1 & 0 & 0 \\ 0 & 0 & 0 & 0 & 0 & 1 \end{bmatrix} \tag{4.64}$$

It follows that the matrix,$G(\theta^0)$, has rank 5, since using Vajda's result [63] concerning structural identifiability of linear systems, we know that there are at most 5 ($2n$-1) independent equations that can be obtained from the Taylor coefficients (where n=3 is the dimension of the state space of the system). Using Theorem 2 there is 1 $(p - q)$ redundant parameter and there exists a reparameterisation of the system in terms of just five parameters which is locally identifiable.

Reparameterisation of the System

Calculation of the nullspace of $G(\theta^0)$ yields,

$$\underline{n} = [\frac{K_1}{K_5}, 0, 0, 0, 1, 0] \tag{4.65}$$

By application of Theorem 3 the locally identifiable parameter groupings can be derived by solving for ϕ in,

$$< \left[\frac{d\phi}{dK_1}, \frac{d\phi}{dk_2}, \frac{d\phi}{dk_3}, \frac{d\phi}{dk_4}, \frac{d\phi}{dK_5}, \frac{d\phi}{dk_6}\right], \left[\frac{K_1}{K_5}, 0, 0, 0, 1, 0\right] > = 0 \tag{4.66}$$

$$\frac{K_1}{K_5}\frac{d\phi}{dK_1} + \frac{d\phi}{dK_5} = 0 \tag{4.67}$$

Solution of the differential equation yields the following simple locally identifiable parameter combinations,

$$\begin{aligned}
\phi_1(K_1, k_2, k_3, k_4, K_5, k_6) &= \frac{K_1}{K_5} \\
\phi_2(K_1, k_2, k_3, k_4, K_5, k_6) &= k_2 \\
\phi_3(K_1, k_2, k_3, k_4, K_5, k_6) &= k_3 \\
\phi_4(K_1, k_2, k_3, k_4, K_5, k_6) &= k_4 \\
\phi_5(K_1, k_2, k_3, k_4, K_5, k_6) &= k_6
\end{aligned} \tag{4.68}$$

where $\Phi = \{\phi_1, \phi_2, \phi_3, \phi_4, \phi_5\}$ and rank $D\Phi = 5$.

This leads us to a simple reparameterisation of the model in which the parameter combination $R_{influx} = \frac{K_1}{K_5}$ is readily introduced as a new parameter. Hence the reparameterised system is defined by,

$$\frac{dC_f(t)}{dt} = R_{influx}\frac{dC_{ref}(t)}{dt} + R_{influx}k_6C_{ref}(t) - (k_2 + k_3)\,C_f(t) + k_4C_b(t)$$

$$\frac{dC_b(t)}{dt} = k_3C_f(t) - k_4C_b(t)$$

$$y(t) = C_f(t) + C_b(t) \tag{4.69}$$

Note that the reparameterisation is not unique and that the parameterisation of the system has been reduced from p $(= 6)$ to q $(= 5)$ parameters.

4.6.4 Example 4 : Batch Reactor Model

A model of microbial growth in a batch reactor was introduced by Holmberg [87] and further analysed by Chappell and Godfrey [50]. The batch reactor model is defined by the equations,

$$\frac{dx_1(t)}{dt} = \frac{\theta_1 x_1(t) x_2(t)}{\theta_2 + x_2(t)} - \theta_3 x_1(t) + \theta_4 u_1(t)$$

$$\frac{dx_2(t)}{dt} = -\frac{\theta_1 x_1(t) x_2(t)}{\theta_5 (\theta_2 + x_2(t))} + \theta_6 u_2(t)$$

$$\begin{aligned} y(t) &= x_1(t) \\ x_1(0) &= 0 \\ x_2(0) &= 0 \end{aligned} \tag{4.70}$$

where

x_1	is the concentration of micro-organisms
x_2	is the concentration of growth limiting substrate
θ_1	is the maximum velocity of the reaction
θ_2	is the Michaelis-Menten constant
θ_5	is the yield coefficient
θ_3	is the decay rate coefficient
θ_4	is the initial concentration of micro-organisms
θ_6	is the initial concentration of substrate.

The experiment considered is for impulsive inputs to both compartments, $u_1(t) = \delta(t)$ and $u_2(t) = \delta(t)$, with observation of x_1. Thus the system can be considered to have zero input to both compartments and non-zero initial conditions, i.e.

$$\begin{aligned} u_1(t) &= 0 \\ u_2(t) &= 0 \\ x_1(0^+) &= \theta_4 \\ x_2(0^+) &= \theta_6 \end{aligned}$$

The first five Taylor coefficients of the observation are obtained (within MATHEMATICA).

$$y^{(0)}(0^+) = \theta_4$$

$$y^{(1)}(0^+) = -(\theta_3\theta_4) + \frac{\theta_1\theta_4\theta_6}{\theta_2+\theta_6}$$

$$y^{(2)}(0^+) = {\theta_3}^2\theta_4 + \frac{{\theta_1}^2{\theta_4}^2{\theta_6}^2}{\theta_5(\theta_2+\theta_6)^3} - \frac{{\theta_1}^2{\theta_4}^2\theta_6}{\theta_5(\theta_2+\theta_6)^2} + \frac{{\theta_1}^2\theta_4{\theta_6}^2}{(\theta_2+\theta_6)^2} - \frac{2\theta_1\theta_3\theta_4\theta_6}{\theta_2+\theta_6}$$

$$\begin{aligned} y^{(3)}(0^+) = &-\left({\theta_3}^3\theta_4\right) - \frac{{\theta_1}^3\theta_2{\theta_4}^3{\theta_6}^2}{{\theta_5}^2(\theta_2+\theta_6)^5} + \frac{2{\theta_1}^3{\theta_4}^3{\theta_6}^3}{{\theta_5}^2(\theta_2+\theta_6)^5} + \frac{{\theta_1}^3\theta_2{\theta_4}^2{\theta_6}^3}{\theta_5(\theta_2+\theta_6)^5} + \\ &\frac{{\theta_1}^3{\theta_4}^2{\theta_6}^4}{\theta_5(\theta_2+\theta_6)^5} + \frac{{\theta_1}^3\theta_2{\theta_4}^3\theta_6}{{\theta_5}^2(\theta_2+\theta_6)^4} - \frac{2{\theta_1}^3{\theta_4}^3{\theta_6}^2}{{\theta_5}^2(\theta_2+\theta_6)^4} - \frac{{\theta_1}^3\theta_2{\theta_4}^2{\theta_6}^2}{\theta_5(\theta_2+\theta_6)^4} - \\ &\frac{{\theta_1}^2\theta_2\theta_3{\theta_4}^2{\theta_6}^2}{\theta_5(\theta_2+\theta_6)^4} + \frac{2{\theta_1}^3{\theta_4}^2{\theta_6}^3}{\theta_5(\theta_2+\theta_6)^4} - \frac{{\theta_1}^2\theta_3{\theta_4}^2{\theta_6}^3}{\theta_5(\theta_2+\theta_6)^4} + \frac{{\theta_1}^2\theta_2\theta_3{\theta_4}^2\theta_6}{\theta_5(\theta_2+\theta_6)^3} - \\ &\frac{3{\theta_1}^3{\theta_4}^2{\theta_6}^2}{\theta_5(\theta_2+\theta_6)^3} - \frac{2{\theta_1}^2\theta_3{\theta_4}^2{\theta_6}^2}{\theta_5(\theta_2+\theta_6)^3} + \frac{{\theta_1}^3\theta_4{\theta_6}^3}{(\theta_2+\theta_6)^3} + \frac{3{\theta_1}^2\theta_3{\theta_4}^2\theta_6}{\theta_5(\theta_2+\theta_6)^2} - \\ &\frac{3{\theta_1}^2\theta_3\theta_4{\theta_6}^2}{(\theta_2+\theta_6)^2} + \frac{3\theta_1{\theta_3}^2\theta_4\theta_6}{\theta_2+\theta_6} \end{aligned}$$

$$\begin{aligned} y^{(4)}(0^+) = &{\theta_3}^4\theta_4 + \frac{15{\theta_1}^4{\theta_4}^4{\theta_6}^4}{{\theta_5}^3(\theta_2+\theta_6)^7} - \frac{4\theta_1{\theta_3}^3\theta_4\theta_6}{\theta_2+\theta_6} + \frac{-11{\theta_1}^2{\theta_3}^2{\theta_4}^2\theta_6 + 6{\theta_1}^2{\theta_3}^2\theta_4\theta_5{\theta_6}^2}{\theta_5(\theta_2+\theta_6)^2} + \\ &\frac{-7{\theta_1}^3\theta_3{\theta_4}^3\theta_6 + 22{\theta_1}^3\theta_3{\theta_4}^2\theta_5{\theta_6}^2 + 11{\theta_1}^2{\theta_3}^2{\theta_4}^2\theta_5{\theta_6}^2 - 4{\theta_1}^3\theta_3\theta_4{\theta_5}^2{\theta_6}^3}{{\theta_5}^2(\theta_2+\theta_6)^3} \\ &+\frac{-25{\theta_1}^4{\theta_4}^4{\theta_6}^3 + 25{\theta_1}^4{\theta_4}^3\theta_5{\theta_6}^4}{{\theta_5}^3(\theta_2+\theta_6)^6} + \\ &\frac{11{\theta_1}^4{\theta_4}^4{\theta_6}^2 - 36{\theta_1}^4{\theta_4}^3\theta_5{\theta_6}^3 - 21{\theta_1}^3\theta_3{\theta_4}^3\theta_5{\theta_6}^3 + 11{\theta_1}^4{\theta_4}^2{\theta_5}^2{\theta_6}^4}{{\theta_5}^3(\theta_2+\theta_6)^5} + \\ &\frac{-\left({\theta_1}^4{\theta_4}^4\theta_6\right) + 11{\theta_1}^4{\theta_4}^3\theta_5{\theta_6}^2 + 28{\theta_1}^3\theta_3{\theta_4}^3\theta_5{\theta_6}^2}{{\theta_5}^3(\theta_2+\theta_6)^4} + \\ &\frac{-11{\theta_1}^4{\theta_4}^2{\theta_5}^2{\theta_6}^3 - 22{\theta_1}^3\theta_3{\theta_4}^2{\theta_5}^2{\theta_6}^3 + {\theta_1}^4\theta_4\theta_5{\theta_6}^3{\theta_6}^4}{{\theta_5}^3(\theta_2+\theta_6)^4} \end{aligned}$$

Now for some $\theta^0 \in \Omega_p$, consider the Jacobian matrix of derivatives of the Taylor series coefficients of y with respect to the parameter vector $\theta=(\theta_1,\theta_2,\theta_3,\theta_4,\theta_5,\theta_6)$. The coefficients of the Jacobian matrix are obtained using MATHEMATICA as

the expressions involved are very large, the coefficients are listed in Appendix A.3. Using MATHEMATICA it can be shown by a process of row reduction that the matrix reduces to,

$$G'\left(\theta^0\right) = \begin{bmatrix} 1 & 0 & 0 & 0 & 0 & 0 \\ 0 & 1 & 0 & 0 & 0 & -\frac{\theta_2}{\theta_6} \\ 0 & 0 & 1 & 0 & 0 & 0 \\ 0 & 0 & 0 & 1 & 0 & 0 \\ 0 & 0 & 0 & 0 & 1 & \frac{\theta_5}{\theta_6} \end{bmatrix} \tag{4.71}$$

Hence Rank $G(\theta^0) = 5$.

In [50] Chappell and Godfrey have shown that this model is unidentifiable and hence the rank of the infinite Jacobian matrix must be less than 6. Using this result and the previous calculations the infinite Jacobian must have rank 5 almost always which implies that $q = 5$. Using Theorem 2 there is 1 $(p - q)$ redundant parameters and there exists a reparameterisation of the system in terms of just 5 parameters which is locally identifiable.

Reparameterisation of the System

For the Jacobian matrix $G(\theta^0)$ the nullspace is spanned by the vector,

$$\underline{n} = \left[0,\ \frac{\theta_2}{\theta_6},\ 0,\ 0,\ -\frac{\theta_5}{\theta_6},\ 1\right] \tag{4.72}$$

To solve for functions ϕ whose images are identifiable combinations of the parameters consider,

$$< \left[\frac{\partial\phi}{\partial\theta_1},\ \frac{\partial\phi}{\partial\theta_2},\ \frac{\partial\phi}{\partial\theta_3},\ \frac{\partial\phi}{\partial\theta_4},\ \frac{\partial\phi}{\partial\theta_5},\ \frac{\partial\phi}{\partial\theta_6}\right], \left[0,\ \frac{\theta_2}{\theta_6},\ 0,\ 0,\ -\frac{\theta_5}{\theta_6},\ 1\right] > = 0 \tag{4.73}$$

Hence the following partial differential equation in ϕ is obtained,

$$\frac{\theta_2}{\theta_6}\frac{\partial\phi}{\partial\theta_2} - \frac{\theta_5}{\theta_6}\frac{\partial\phi}{\partial\theta_5} + \frac{\partial\phi}{\partial\theta_6} = 0 \tag{4.74}$$

Some possible solutions for ϕ are,

$$\begin{array}{rcl} \phi_1(\theta_1,\theta_2,\theta_3,\theta_4,\theta_5,\theta_6) & = & \theta_1 \\ \phi_2(\theta_1,\theta_2,\theta_3,\theta_4,\theta_5,\theta_6) & = & \frac{\theta_2}{\theta_6} \\ \phi_3(\theta_1,\theta_2,\theta_3,\theta_4,\theta_5,\theta_6) & = & \theta_3 \\ \phi_4(\theta_1,\theta_2,\theta_3,\theta_4,\theta_5,\theta_6) & = & \theta_4\theta_5 \\ \phi_5(\theta_1,\theta_2,\theta_3,\theta_4,\theta_5,\theta_6) & = & \theta_5\theta_6 \end{array} \tag{4.75}$$

where $\Phi = \{\phi_1, \phi_2, \phi_3, \phi_4, \phi_5\}$ and rank $D\Phi = 5$.

The original system (4.70) may now be rearranged to include just these five parameter groupings and hence may be reparameterised in terms of them. Let $x_2(t)^* = \frac{x_2(t)}{\theta_6}$.

Substituting into the original pair of equations yields,

$$\frac{dx_1(t)}{dt} = \frac{\theta_1\theta_6 x_1(t)x_2(t)^*}{\theta_2 + \theta_6 x_2(t)^*} - \theta_3 x_1(t) + \theta_4\delta(t)$$

$$\theta_6\frac{dx_2(t)^*}{dt} = -\frac{\theta_1\theta_6 x_1(t)x_2(t)^*}{\theta_5\left(\theta_2 + \theta_6 x_2(t)^*\right)} + \theta_6\delta(t) \tag{4.76}$$

or after rearrangement,

$$\frac{dx_1(t)}{dt} = \frac{\theta_1 x_1(t)x_2(t)^*}{\frac{\theta_2}{\theta_6} + x_2(t)^*} - \theta_3 x_1(t) + \theta_4\delta(t)$$

$$\frac{dx_2(t)^*}{dt} = -\frac{\theta_1 x_1(t)x_2(t)^*}{\theta_2\theta_5 + \theta_5\theta_6 x_2(t)^*} + \delta(t) \tag{4.77}$$

This system then simplifies to,

$$\frac{dx_1(t)}{dt} = \frac{\theta_1 x_1(t)x_2(t)^*}{\frac{\theta_2}{\theta_6} + x_2(t)^*} - \theta_3 x_1(t) + \theta_4\delta(t)$$

$$\frac{dx_2(t)^*}{dt} = -\frac{\theta_1 x_1(t)x_2(t)^*}{\theta_5\theta_6\left(\frac{\theta_2}{\theta_6} + x_2(t)^*\right)} + \delta(t) \tag{4.78}$$

giving the following locally identifiable system,

$$\frac{dx_1(t)}{dt} = \frac{\phi_1 x_1(t) x_2(t)^*}{\phi_2 + x_2(t)^*} - \phi_3 x_1(t) + \phi_4 \delta(t)$$

$$\frac{dx_2(t)^*}{dt} = -\frac{\phi_1 x_1(t) x_2(t)^*}{\phi_5 (\phi_2 + x_2(t)^*)} + \delta(t)$$

$$\begin{aligned} y(t) &= x_1(t) \\ x_1(0) &= 0 \\ x_2(0)^* &= 0 \end{aligned} \tag{4.79}$$

where $\phi_1 = \theta_1, \phi_2 = \frac{\theta_2}{\theta_6}, \phi_3 = \theta_3, \phi_4 = \theta_4$, and $\phi_5 = \theta_5\theta_6$ are locally identifiable. Note that the reparameterisation is not unique and that the parameterisation of the system has been reduced from p $(= 6)$ to q $(= 5)$ parameters.

4.7 Discussion

A method has been provided for reparameterising unidentifiable systems. Theorem 2 presented here states that the rank of the appropriate Jacobian matrix determines the number of locally identifiable parameters. Theorem 3 gives the necessary and sufficient conditions for a set of parameters to provide a reparameterisation. A simple method for determining identifiable parameter groupings based on the nullspace of the Jacobian matrix has been presented. A reparameterisation of the system is obtained by performing a state space transformation which converts the system into a form in which only identifiable parameter groupings occur. It is then a relatively straightforward procedure to reparameterise the system. As the method is based on the Taylor series approach it is applicable to linear and nonlinear systems and also to systems with specified inputs. In order

to calculate the minimal form of the system it is necessary to know the rank of the infinite Jacobian matrix. To determine if the rank of the infinite Jacobian matrix is rank deficient by (at least) 1 this is accomplished in two parallel steps: 1) the system is shown to be unidentifiable (e.g. by employing, say, the Similarity transform approach). Hence the Jacobian matrix must be rank deficient by at least 1 (by Pohjanpalo's rank test). 2) a subset of the infinite Jacobian matrix is shown to be rank deficient by 1 . Hence the infinite Jacobian matrix is rank deficient by 1. In cases where the rank of the Jacobian is further deficient it may only be possible to get a lower bound on the rank of this matrix. The difficulty arises from the fact that there is no theoretical bound on the number of Taylor series coefficients which need to be considered in order that the Jacobian matrix has maximal rank. Other constraints, such as Vajda's result [63], for linear systems, may also prove useful in determining the rank of the Jacobian matrix. To reparameterise the system, identifiable parameter combinations are established via examination of the nullspace of the Jacobian. Then a state space transformation is searched for such that the resulting system's parameters only occur in identifiable groupings. It should be stressed that the reparameterisation obtained is not unique. Although a state space transformation is usually required this is not always the case, as in Example 2. By performing the reparameterisation a more valid model is obtained for the experiment considered. The reparameterised model is locally identifiable, by the theory given, and in addition may be globally identifiable.

Chapter 5

Modelling of Labelled Tracer Metabolites in Plasma

5.0.1 Overview

This chapter investigates the metabolism of two ligands used in PET brain scanning to measure receptor binding; [^{11}C]diprenorphine and [^{11}C]flumazenil are markers for the opiate receptor and benzodiazepine site, respectively. Changes in density or affinity of these receptor systems may be important for the study of addiction, neurological and psychiatric disorders [88] [89] [90]. Both these compounds produce radiolabelled metabolites, which being polar contribute to the total blood but not the cerebral radioactivity as they do not cross the blood brain barrier. Two different approaches for the correction of signal from tracer metabolism are considered. The first involves defining an arbitrary functional form that describes the fraction of labelled metabolite in plasma and the second approach employs a compartmental description of the underlying metabolism.

5.0.2 Introduction

Quantification of parent drug in a tissue of interest requires correction for metabolites. The majority of PET tracers produce labelled metabolites in the body, thus accurate methods for metabolite correction are required. Two situations are

observed:-

1. Only the blood data contain a signal due to labelled metabolites, as in Figure (5.1). Typical examples of this situation are [^{11}C]flumazenil and [^{11}C]diprenorphine brain studies, in which the metabolites are too polar to cross the blood brain barrier at a significant rate and the tissue signal is dominated by the parent drug.

2. Both the tissue data and blood data contain labelled metabolites, a typical example being [^{11}C]thymidine uptake in tumours. This case is considered in Chapter 9. (Figure 5.1).

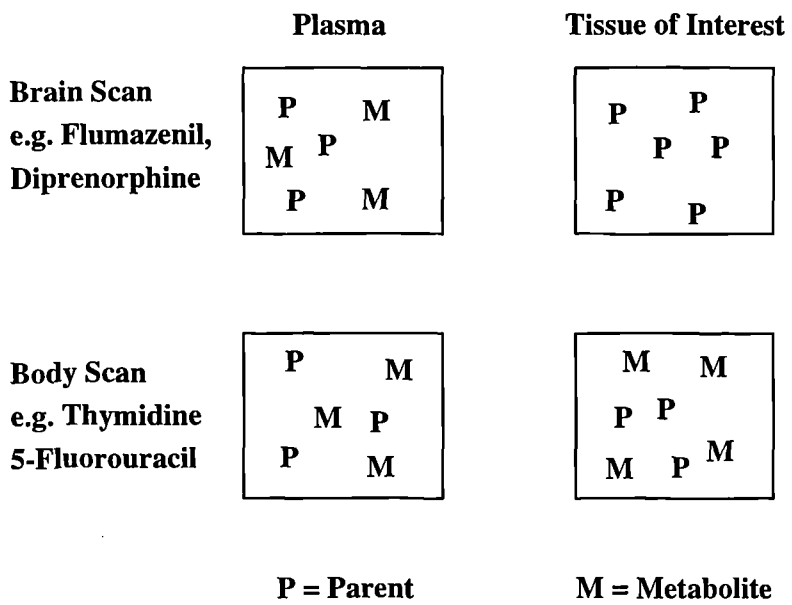

Figure 5.1: Metabolite distribution

It is known that both [^{11}C]diprenorphine and [^{11}C]flumazenil fall into the first category. Sadée et al [91] have shown that 1 hour after the injection of [^{11}C]diprenorphine at least 90 % of the label in brain is attributable to the parent compound. Similarly the metabolites of [^{11}C]flumazenil make a negligible contribution to the total label signal in the brain [92] [93].

5.0.3 [^{11}C]Diprenorphine

[^{11}C]Diprenorphine is a PET ligand that binds to μ-, δ-, and κ-opiate receptor subtypes with similar affinities for each [94]. One way to quantify the parameters specific to the binding of [^{11}C]diprenorphine in brain requires a metabolite-corrected plasma [^{11}C]diprenorphine input function. However two radiolabelled metabolites that can be detected in plasma using solid phase extraction followed by HPLC [24] are produced by the liver. Previous methods of correcting [^{11}C]diprenorphine plasma time courses have involved fitting an arbitrary functional form to the metabolite data, and then to interpolate and extrapolate the fitted metabolite fraction to correct the plasma input function for metabolites over the whole time course of the scan [95].

5.0.4 [^{11}C]Flumazenil

Quantitative analysis of the volume of distribution of the central benzodiazepine receptor *in vivo* also requires the determination of the unmetabolised radioligand in plasma[86]. Liver metabolism [96] [97] of [N-methyl-^{11}C]flumazenil however leads to the formation of the free acid, Ro 15-3890, and the alcohol, Ro 15-4965 [98] [99]. Indeed HPLC analysis of plasma samples indicates the presence of three metabolic products, two of which are expected to be the alcohol and the free acid. All the peaks are more hydrophyllic than the parent compound. Previous methods for correcting [^{11}C]flumazenil plasma time courses for the presence of metabolites have involved the fitting of an exponential functional form [83] [48] [100].

5.0.5 Plasma Metabolite-Corrected Input Functions

The main processes involved in calculating a plasma metabolite corrected input function are shown in Figure (5.2). This modelling scheme also indicates that the blood data are combined with the tissue data to calculate tissue specific functional

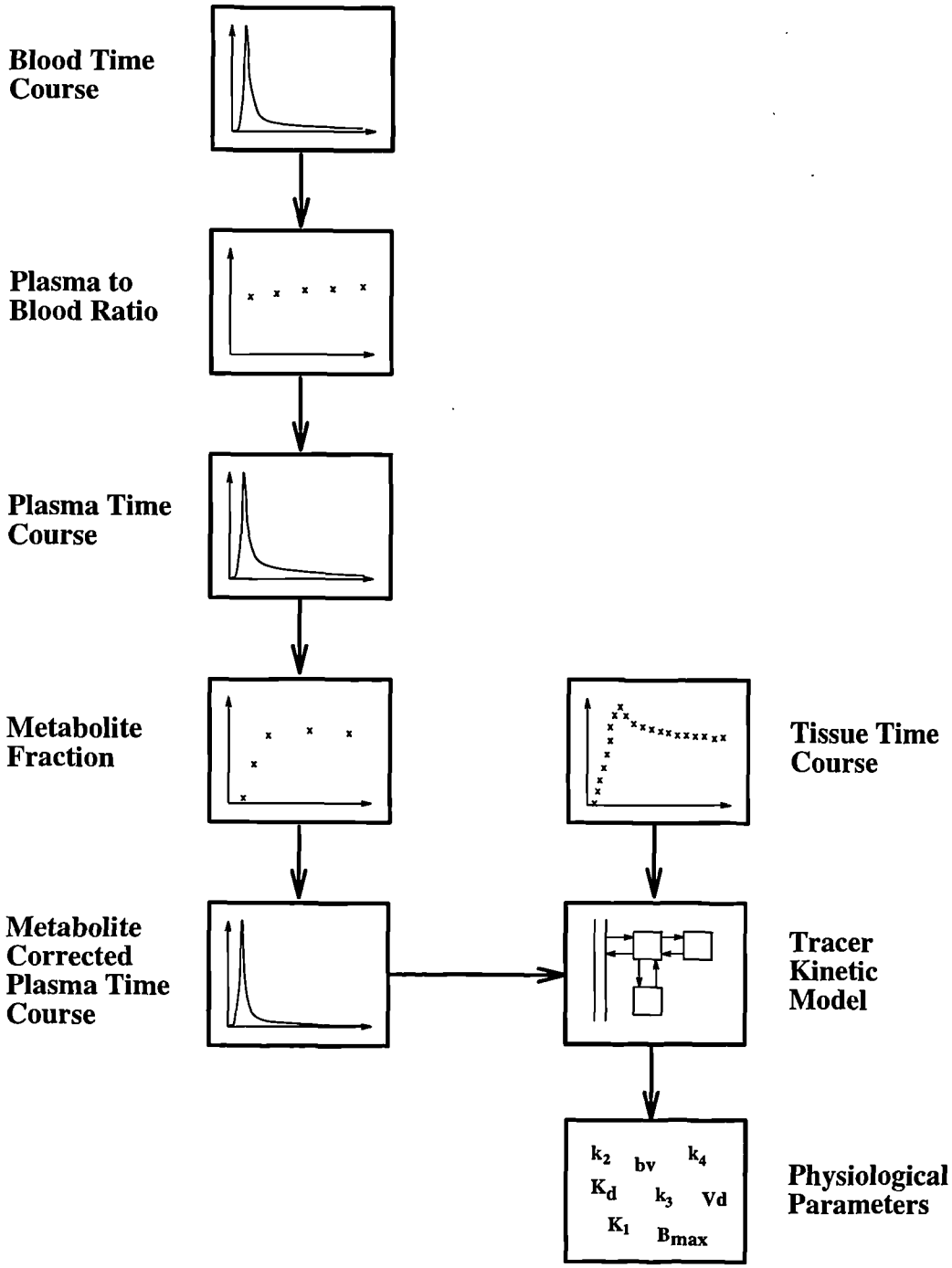

Figure 5.2: Modelling scheme

parameters. The modelling of the blood data can be split into two parts;

- Obtain a continuous time course for the concentration of total label in plasma.
- Obtain a continuous time course for the parent compound in plasma.

The temporally sparse metabolite data are a major problem in the creation of an accurate metabolite-corrected plasma input function. This is one of the weakest links in the overall modelling of PET data, see Figure (5.2) since the fraction of labelled metabolites in a plasma sample is normally measured only at 5 or 6 time points for a ligand scan usually lasting 60-120 minutes. Metabolite data are limited by the length of time required for HPLC analysis since the concentrations are very small and an accurate sensitive measure is thus required. To overcome the sparsity of the metabolite data, some form of model is required to interpolate and extrapolate the data and provide a continuous measure of the fraction of metabolites in plasma.

5.1 Methods

An on-line measuring system which allows for the collection of discrete blood samples was used to record the concentration of label in blood [22]. Measurements of the counts in whole blood were taken over one second intervals. This temporal resolution is especially important at the start of the scan to enable the delineation of the rapidly changing arterial blood curve. Separate analysis of the discrete blood samples was also carried out to calibrate the radioactive counts (n=5), to measure the relative amounts of parent and metabolite (n=5) compounds in the plasma and the distribution of counts between plasma and red cells (n=5). The technique of HPLC was utilised to give chemical resolution of these discrete plasma

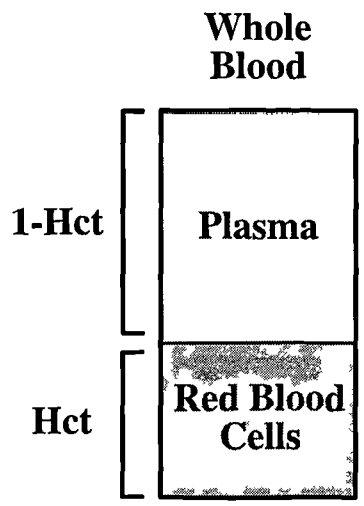

Figure 5.3: Whole blood constituents

samples (for details see Luthra et al. [24]). Hence, the measurements obtained were:

- A second by second measurement of the total arterial blood radioactivity collected on-line from the subject under investigation calibrated separately in a well counter. (μCi/ml Blood)
- A measurement of the distribution of counts between plasma (obtained by centrifugation) and whole blood taken at various time points during scanning.
- A measurement of the metabolite fraction in plasma, obtained by HPLC analysis of discrete blood samples taken at various time points during scanning.

In addition the haematocrit, Hct , was measured in some cases, (the fraction of the blood which is made up from red cells, see Figure (5.3)). The haematocrit as measured will be a slight over-estimation due to entrapped plasma. The presence of white cells is ignored since their volumetric component is less than 1 percent.

These assays allow the conversion of whole blood activity to plasma activity using the following equation,

$$Plasma\,(t) = pbr(t)WB(t) \tag{5.1}$$

where,

$Plasma(t)$	:	concentration of tracer in plasma
$WB(t)$	:	concentration of tracer in whole blood
$pbr(t)$	:	Ratio of counts in 1 ml of plasma to counts in 1 ml of whole blood

To create a continuous function for the ratio of counts in plasma to whole blood a function was fitted to the discrete data obtaining a least sum of squares solution. Normally the plasma to blood ratio, $pbr(t)$, can be represented by a straight line or an exponential function [95] [101] (cited in [44]). Examples for the ligands diprenorphine and flumazenil can be seen in Figures (5.5) and (5.6), respectively.

5.1.1 Preliminary Processing of Blood Data

The whole blood arterial time course was corrected for flushing periods, which occur when the arterial line is flushed with saline, and background radioactivity. These processes are independent of the ligand used.

Removal of Flushing Periods

Every 15-20 minutes the continuous counting of blood data is stopped while the tubing which connects the radial artery to the BGO detection system is flushed with heparinised (an anticoagulent) saline to prevent clotting in the system. This results in the loss of data for approximately 15-30 seconds. The data for these periods is extrapolated by manually selecting the beginning and end of each flushing period on the continuous blood radioactivity counts plot. A straight line was then fitted through a small portion of the data prior to and post flushing (normally about 15 seconds each side) by means of linear regression (see Figure 5.4).

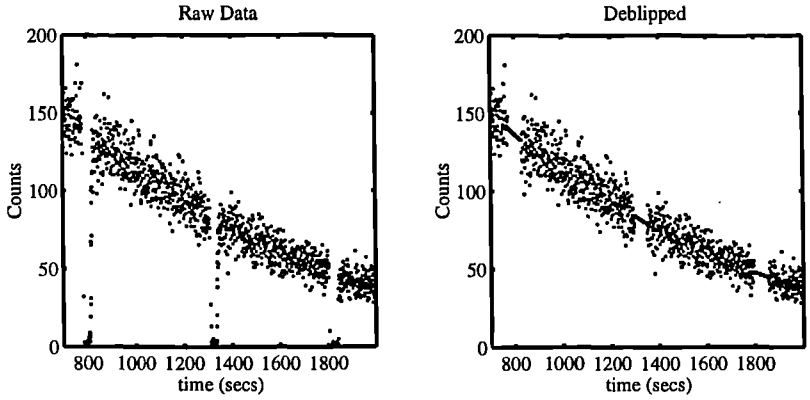

Figure 5.4: Section of whole blood curve

Background Correction

Background may be removed from the blood curve by subtracting the mean of the pre-injection value of the blood curve. The background correction must be done before any decay correction, otherwise the resulting blood curve is incorrect. This method of background subtraction provides a reasonable correction and effective lead shielding of the blood counter reduces this problem. However, the true background is a function of time and will depend on the activity distribution in the subject. If this correction is inaccurate the tail of the curve for long scans (~2hrs) will start rising when decay correction has been applied, although this was not observed for the studies corrected in this way.

Calibration

The on-line blood detection system was cross-calibrated using discrete blood samples taken from the arterial line and counted in a sodium iodide well counter, which is regularly calibrated with germanium sources of known activity

Interpolation and Extrapolation of the Plasma to Blood Ratio

Plasma to blood ratios from for all the [^{11}C]diprenorphine scans are illustrated in Figure (5.5). A linear fit (equation (5.2)) was found to produce a better fit to the

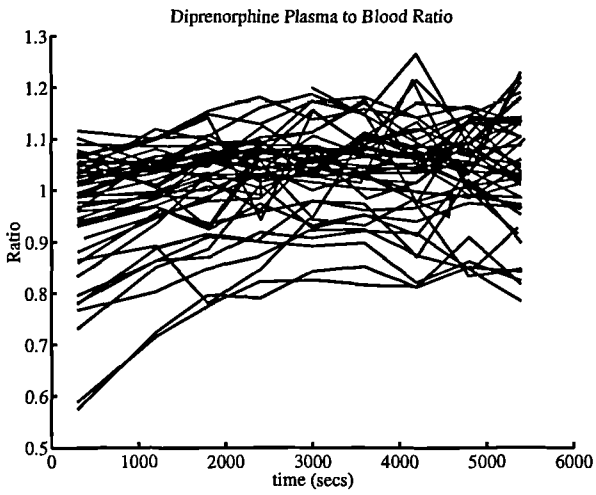

Figure 5.5: Plasma to blood ratio for the cohort of [^{11}C]diprenorphine scans

data than an exponential approach to a constant.

$$pbr(t) = \alpha + \beta t \tag{5.2}$$

The mean and standard deviation for the parameters in (5.2), calculated over all available studies, was $\alpha = 0.990 \pm 0.112$, and $\beta = 1.27e - 05 \pm 1.79e - 05$. Plasma to blood ratios from the set of [^{11}C]flumazenil scans are shown in Figure (5.6). The plasma to blood ratio was fitted with an exponential function $pbr(t)$,

$$pbr(t) = \alpha\left(1 - e^{-\beta t}\right) + 1 \tag{5.3}$$

The exponential function produced a better fit to the data than the linear fit. The mean and standard deviation for the parameters in (5.3), calculated over all available studies, was $\alpha = 0.434 \pm 0.0778$, and $\beta = 0.00290 \pm 0.000780$.

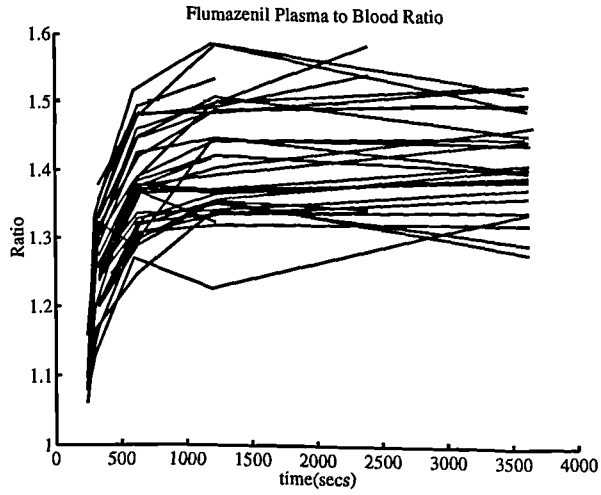

Figure 5.6: Plasma to blood ratio for the cohort of [^{11}C]flumazenil scans

5.2 Results

5.2.1 [^{11}C]Diprenorphine

A cohort of 72 [^{11}C]diprenorphine data sets was used to examine the accuracy of the different methods of metabolite correction. The mean metabolite fraction for the cohort ($\pm$ 1 s.d.) is shown in Figure (5.7).

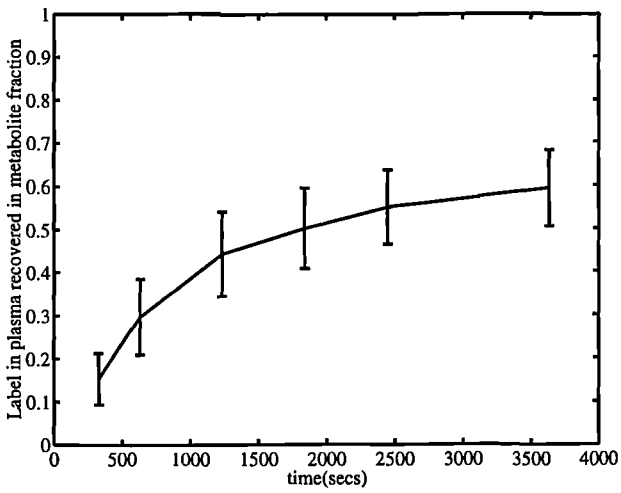

Figure 5.7: Metabolite data for the cohort of [^{11}C]diprenorphine scans

Functional Forms

Observation of the metabolite measurements shows that a saturating function is required to describe the metabolite fraction as a function of time. A number of saturating functions were applied to investigate which describes most accurately the measured metabolite fraction (see Table (5.1)). Characteristics of each of these functions can be visualised in Figure (5.8).

Model 1	Exponential	$\alpha\left(1-e^{-\beta t}\right)$
Model 2	Rectangular Hyperbola	$\frac{\gamma t}{\delta+t}$
Model 3	Sigmoid	$\frac{t^{\phi}}{(\theta+t)^{\phi}}$

Table 5.1: Functional forms for the metabolite fraction

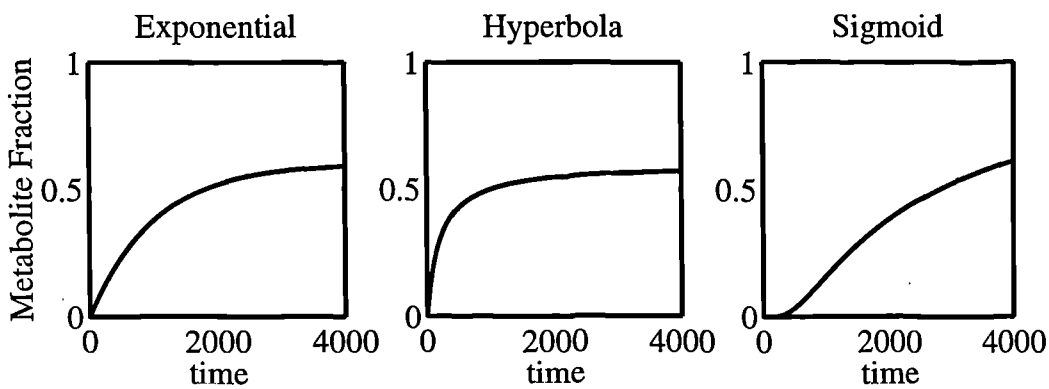

Figure 5.8: Functional forms for the metabolite fraction

The exponential model has been used previously to correct for the presence of labelled metabolites in plasma [95] [102] [83] [48] [100].

The functions were fitted to the available metabolite data (equal weighting was employed) by a simplex optimiser that attained the least sum of squares solution [103]. The results are given in Tables (5.3-5.6).

To determine which of the models provides the best segmentation of the plasma input function, the residual sum of squares was considered. This is sufficient because all models have the same number of degrees of freedom. It was decided

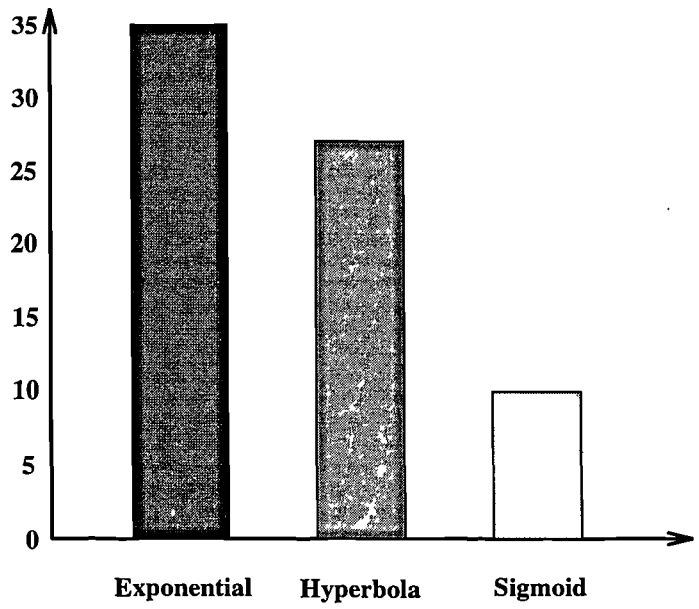

Figure 5.9: Number of studies producing best fit for [^{11}C]diprenorphine

that the best model would be the one which produced the smallest sum of squares most consistently. Figure (5.9) shows for each function the number of studies for which it produced the best fit. The exponential form for the metabolite fraction produced the best results followed closely by the hyperbolic function, with the sigmoid function giving the least satisfactory results.

Since a simple exponential function best described the metabolite data, this suggested that a simple compartmental structure could be used to describe the metabolism process.

Compartmental Metabolism Model

The simplest compartmental model for describing the metabolism of a compound is illustrated in Figure (5.10). This is a simplification of the body's complex metabolic system but it describes the important factors; the metabolite is created at a rate proportional to the concentration of the parent in plasma and the metabolite is eliminated from the plasma at a rate proportional to the concentra-

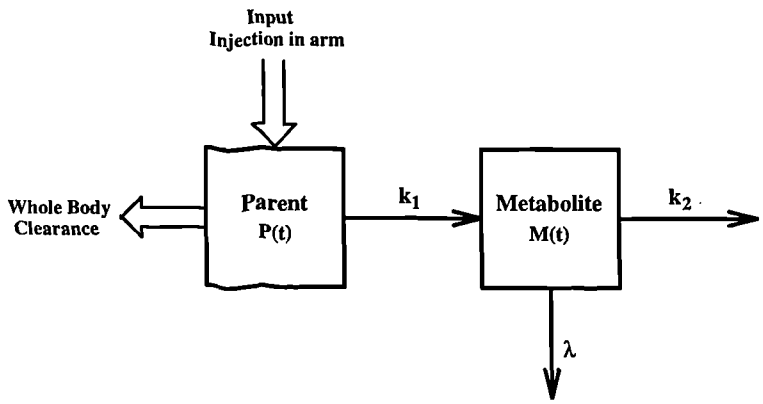

Figure 5.10: [^{11}C]Diprenorphine metabolism model

tion of metabolite in plasma. The model illustrated in Figure (5.10) is described by the following differential equation,

$$\frac{dM(t)}{dt} = k_1 P(t) - (k_2 + \lambda) M(t) \tag{5.4}$$

The system variables are defined by,

$T(t)$	-	Total plasma concentration
$P(t)$	-	Parent plasma concentration
$M(t)$	-	Metabolite plasma concentration
$Mf(t)$	-	Metabolite fraction in plasma

The parameter λ represents the decay of the radioisotope and is a known parameter. The model as postulated does not restrict the metabolism to occur in the plasma; the metabolism will also occur in the body's metabolising tissues (principally liver). The effective transfer rate between the tissue compartment and plasma is assumed to be fast and this allows a tissue compartment to be neglected.

Equation (5.4) is solved to give the metabolite concentration as a function of the parent concentration,

$$M(t) = k_1 e^{-(k_2+\lambda)t} \otimes P(t) \tag{5.5}$$

where $\otimes$ represents the convolution operator. The following are deduced from the variable definitions.

$$T(t) = P(t) + M(t), \tag{5.6}$$

$$Mf(t) = \frac{M(t)}{T(t)}. \tag{5.7}$$

Equation (5.5) can be transformed to give the metabolite fraction $Mf(t)$ in terms of the total plasma concentration $T(t)$. Eliminating $P(t)$ from equation (5.5) gives,

$$M(t) = k_1 e^{-(k_2+\lambda)t} \otimes (T(t) - M(t)) \tag{5.8}$$

Taking Laplace transforms yields

$$\tilde{M} = \frac{k_1}{s + k_2 + \lambda}\tilde{T} - \frac{k_1}{s + k_2 + \lambda}\tilde{M}, \tag{5.9}$$

which, after rearrangement, gives

$$\tilde{M}\left(1 + \frac{k_1}{s + k_2 + \lambda}\right) = \frac{k_1}{s + k_2 + \lambda}\tilde{T} \tag{5.10}$$

or

$$\tilde{M} = \left(\frac{s + k_2 + \lambda}{s + k_1 + k_2 + \lambda}\right)\left(\frac{k_1}{s + k_2 + \lambda}\right)\tilde{T}. \tag{5.11}$$

Hence

$$\tilde{M} = \left(\frac{k_1}{s + k_1 + k_2 + \lambda}\right)\tilde{T}. \tag{5.12}$$

and taking inverse Laplace transforms gives,

$$M(t) = k_1 e^{-(k_1+k_2+\lambda)t} \otimes T(t), \tag{5.13}$$

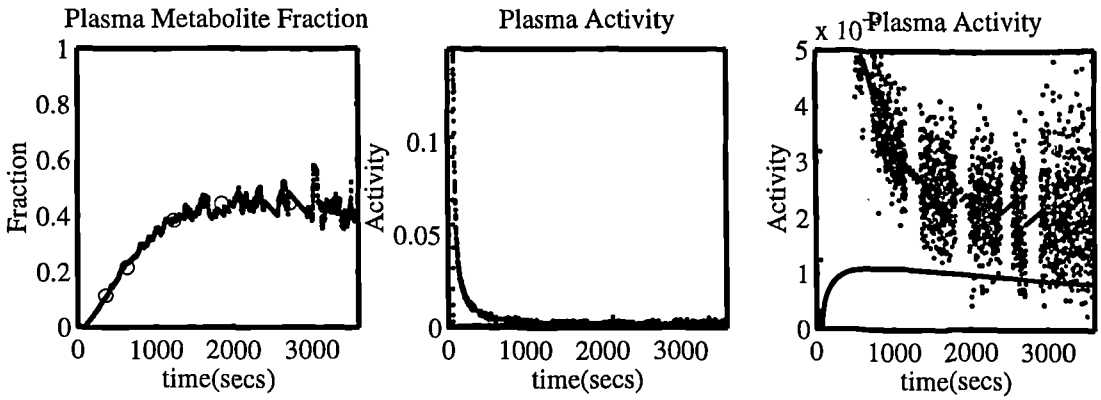

Figure 5.11: Fit and metabolite contribution for p02447 ([^{11}C]diprenorphine)

Thus the metabolite fraction $Mf(t)$ is given by

$$Mf(t) = \frac{k_1 e^{-(k_1+k_2+\lambda)t} \otimes T(t)}{T(t)}. \tag{5.14}$$

Examination of equation (5.12) reveals that both k_1 and k_2 are uniquely (globally) identifiable (via the Laplace transform approach). The fitting procedure involves obtaining 2 parameter values from 5 observations. Figure (5.11) illustrates a typical fit to the metabolite fraction, the second and third graph showing the total plasma activity and the metabolite contribution. The plasma metabolite-corrected input function is simply obtained by subtracting the metabolite component from the total plasma activity. This technique of manipulating the equations allows the metabolite component to be described as a function of the known total plasma activity. This approach has been used by Huang et al. [104] to describe the conversion of the injected tracer to its metabolites for [^{18}F]fluoro-L-dopa and $^{15}O_2$. Tables (5.3-5.6) list the parameter values and residual sums of squares for the different models. The fitting of the compartmental model is robust and little correlation between the two parameters is observed (correlation coefficient : mean 0.8770 $\pm$ 0.0539sd) (ranging from .625 to .965). Thus this demonstrates that the model parameters are numerically identifiable. The distribution of the parameter

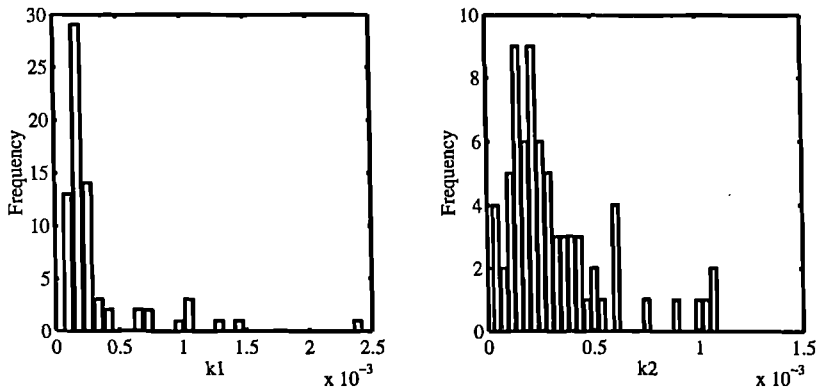

Figure 5.12: Histograms of parameter values for all studies

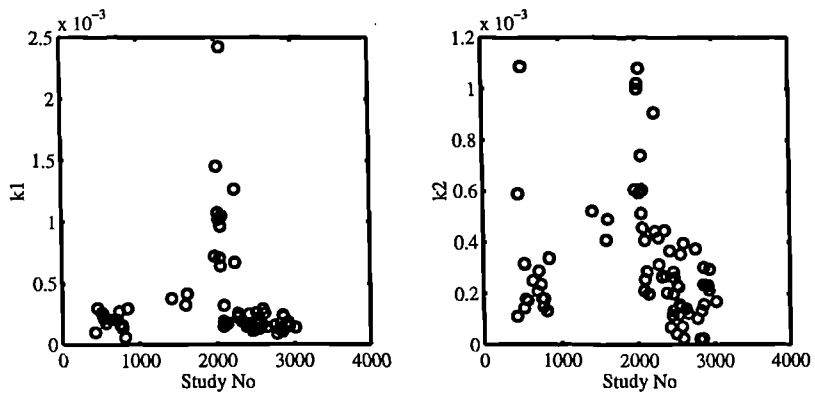

Figure 5.13: Plot of parameter values against scan number

values k_1 and k_2 obtained for all the studies is displayed in Figure (5.12). Both parameters appear to be approximately normally distributed apart from a group of outliers. After further investigation of various factors (patient age, weight, condition, clinician, study no.) the outliers were found to correspond to a particular period in time. This was indicated by the study number which lists the scans in chronological order ($\sim$ no. 2000).

The parameter values are plotted against study number in Figure (5.13). It is likely that an error had occurred in one of the measuring systems. One possible explanation is that a faulty column was installed on the HPLC system. Once the scans around this period have been removed the parameter distributions appear

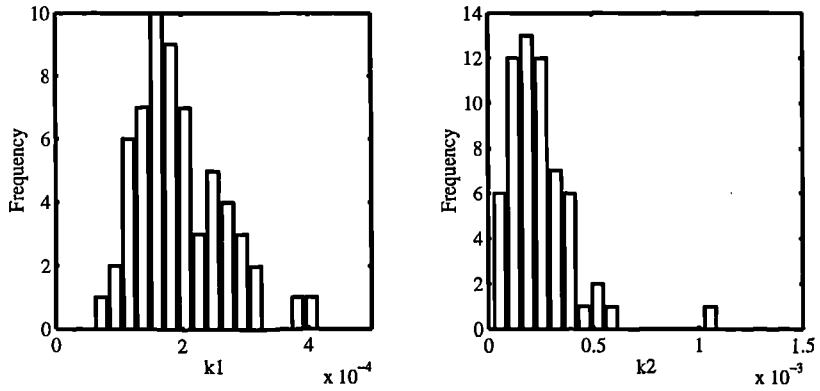

Figure 5.14: Histograms of parameter values for reduced set of studies

to be approximated by a normal distribution, see Figure (5.14).

5.2.2 Discussion

An important feature of these models is the ability to extrapolate the data well after the final data point, especially for the case where no late metabolite data exists. This fact is implicit in the functional forms which are all saturating functions, and effect an asymptote which is determined reasonably accurately from just the early time points (up to 1800 seconds). The compartmental model also handles the extrapolation effectively with the model tending towards an equilibrium in which the distribution between parent and metabolite is a constant factor which is determined by $(\frac{k_1}{k_1+k_2})$, and these values can be seen in Tables (5.5-5.6). The advantage of using the compartmental approach is its flexibility in dealing with different forms of input and its parameter values having a more physiological interpretation. When the injection does not approximate a bolus the compartmental approach is more applicable, relying on an underlying physiological model rather than the arbitrary functional forms. In conclusion the metabolism of $[^{11}C]$diprenorphine can be adequately accommodated in terms of a simple precursor product relationship. This is not the case for the next example.

5.2.3 [^{11}C]Flumazenil

The blood curves obtained from [^{11}C]flumazenil scans suggests the presence of metabolite by exhibiting a non-monotonic decrease from the peak plasma radioactivity , see Figure (5.15). It was hypothesised that this bump may give important

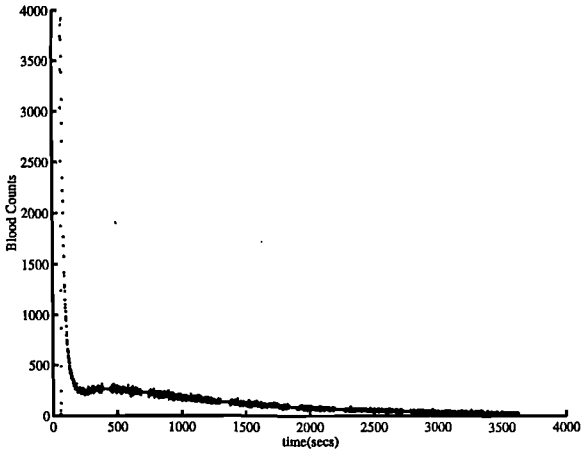

Figure 5.15: Typical [^{11}C]flumazenil whole blood time activity curve

information about the metabolism in the system. Inspection of the metabolite fraction indicated a delay in the production of metabolites (see Figure(5.16)). This delay being the key factor which causes a bump to appear in the blood

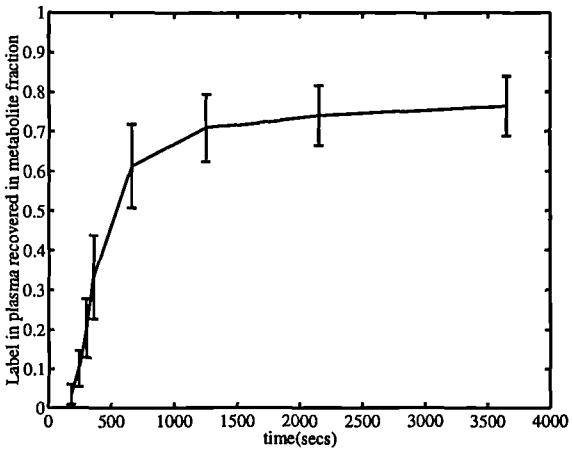

Figure 5.16: Metabolite data for the cohort of [^{11}C]flumazenil scans

curve. The inherent delay implies an apparently more complex model than the one used for [^{11}C]diprenorphine. The delay was approximately 90 seconds and this was established by inspection of metabolite time course data obtained from plasma samples. A cohort of 32 [^{11}C]flumazenil studies was considered to evaluate the effectiveness of a series of postulated models for metabolite correction. The mean metabolite fraction for the cohort ($\pm$ 1 s.d.) is shown in Figure (5.16). Initially the metabolite data were fitted to the functional forms used previously, (5.1), with the addition of a delay term. The results of fitting the functional forms are listed in Tables (5.7-5.8). The exponential function again proved to be the most successful approach and this is demonstrated in Figure (5.17).

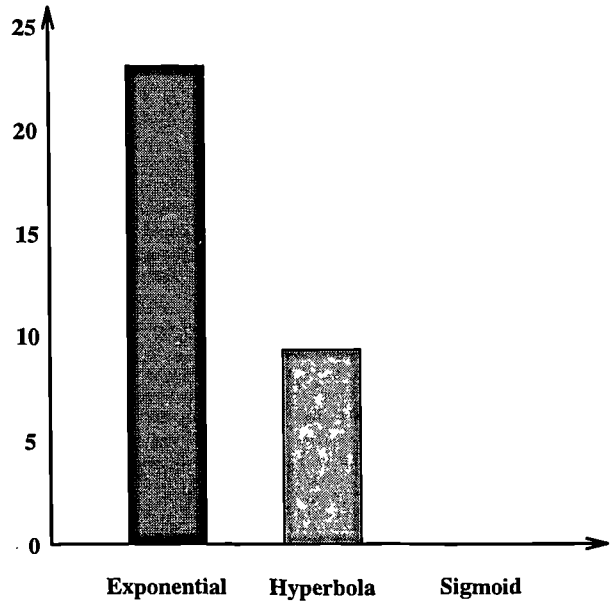

Figure 5.17: Number of studies producing best fit for [^{11}C]flumazenil

Compartmental Metabolism Model

System identification of an appropriate metabolism model is more readily achieved by examining the metabolite as a function of parent. Examination of possible models was initially investigated by segmenting the plasma curve into parent and

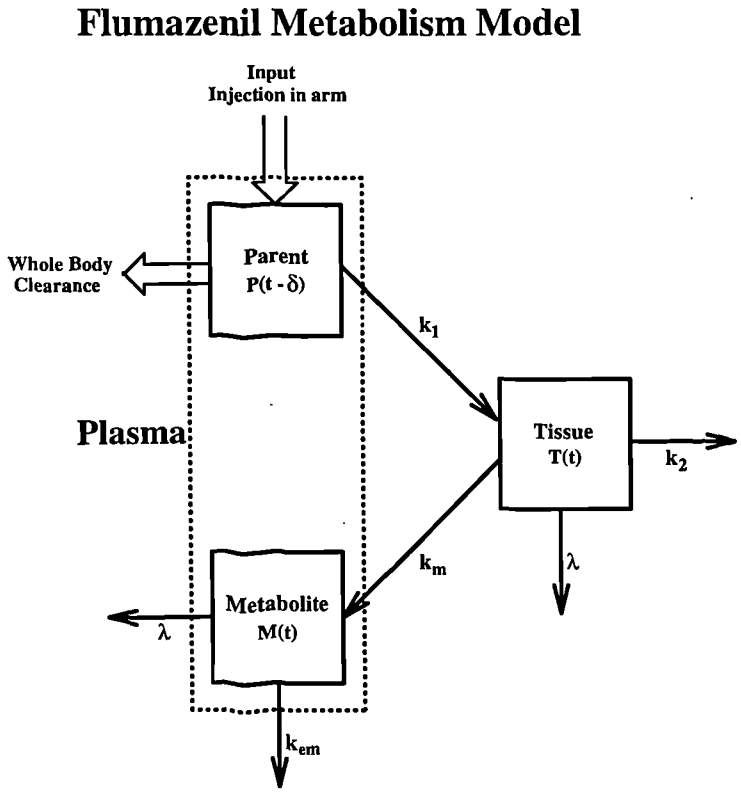

Figure 5.18: [^{11}C]Flumazenil metabolism model

metabolite time courses (using the exponential functional form). It was discovered that the simple model used previously was insufficient to describe the metabolism of [^{11}C]flumazenil. A more comprehensive metabolism model, including the addition of a tissue compartment for metabolism, was thus chosen (Figure (5.18)). The observed delay in the formation of metabolite also necessitated the introduction of a delay term in the model.

Segmentation of the plasma time activity curve produces a parent in plasma time activity curve $P(t)$ and a metabolite in plasma time activity curve $M(t)$. These two functions were fitted to the equations derived from the compartmental model illustrated in Figure (5.18). This model describes the exchange of parent drug between plasma and the body's metabolising tissues (principally liver), the elimination of compound from this tissue and the transfer of metabolite from the

metabolising tissue back into plasma. The model includes a delay ,δ, and λ represents the decay of the isotope, with a known value. The following set of ordinary differential equations describes the system,

$$\begin{aligned}\frac{dT(t)}{dt} &= k_1 P(t-\delta) - (k_2 + k_m + \lambda)T(t) \\ \frac{dM(t)}{dt} &= k_m T(t) - (k_{em} + \lambda)M(t)\end{aligned} \tag{5.15}$$

where

$P(t)$	-	Parent plasma concentration
$T(t)$	-	Metabolising tissue concentration
$M(t)$	-	Metabolite plasma concentration
k_1	-	Rate constant for transfer of parent from plasma to metabolising tissue
k_2	-	Rate constant for transfer of parent from metabolising tissue to plasma
k_m	-	Rate constant for transfer of metabolite from metabolising tissue to plasma
k_{em}	-	Rate constant for elimination of metabolite from plasma
λ	-	Decay constant (0.0005663 sec^{-1})

Identifiability and Reparameterisation

Identifiability analysis and a subsequent reparameterisation was performed on the system (5.15) using the methods presented in the previous chapter. The identifiability analysis was performed using the Taylor series method. Without loss of generality, λ is set to 0 for the identifiability analysis and the reparameterisation, and it is readily reintroduced at the end. The first 3 Taylor series coefficients of the observation evaluated about δ are given by;

$$\begin{aligned}y^{(1)}\left(\delta^+\right) &= k_1 k_m \\ y^{(2)}\left(\delta^+\right) &= -k_1 k_m (k_{em} + k_2 + k_m)\end{aligned}$$

$$y^{(3)}\left(\delta^{+}\right) = k_1 k_m (k_2^2 + 2k_2 k_m + k_m^2 + k_{em}^2 + k_2 k_{em} + k_m k_{em}) \tag{5.16}$$

The Jacobian matrix defined by the partial derivatives of the Taylor series coefficients with respect to the parameters is,

$$G(\theta^0) = \begin{bmatrix} k_m & 0 & k_1 & 0 \\ -k_m\left(k_2 + k_{em} + k_m\right) & -k_1 k_m & -k_1\left(k_2 + k_{em} + 2k_m\right) & -k_1 k_m \\ C_1 & C_2 & C_3 & C_4 \end{bmatrix} \tag{5.17}$$

where

$$\begin{aligned} C_1 &= k_m\left(k_2 + k_m\right)^2 + k_{em} k_m\left(k_2 + k_{em} + k_m\right) \\ C_2 &= k_1 k_m\left(2k_2 + k_{em} + 2k_m\right) \\ C_3 &= k_1\left(k_2^2 + k_2 k_{em} + k_{em}^2 + 4k_2 k_m + 2k_{em} k_m + 3k_m^2\right) \\ C_4 &= k_1 k_m\left(k_2 + 2k_{em} + k_m\right). \end{aligned} \tag{5.18}$$

The infinite Jacobian matrix, $G(\theta^0)$, can be shown to have rank less than or equal to 3 by considering the transfer function for M when Laplace transforms are applied to (5.15) yielding,

$$\tilde{M} = \frac{k_1 k_m}{(s + k_{em})(s + k_2 + k_m)}\tilde{P} \tag{5.19}$$

It can readily be seen that the 4 parameters k_1, k_2, k_m, k_{em} are combined together in just three coefficients in the transfer function. Therefore $G(\theta^0)$ can have, at most, rank 3. By considering the rank of (5.17) this implies that $G(\theta^0)$ has rank

equal to 3.

To calculate the identifiable parameter groupings it is necessary to consider the nullspace of the Jacobian matrix (5.17). The nullspace is spanned by,

$$n = \{-\frac{k_l}{k_m}, -1, 1, 0\} \tag{5.20}$$

Applying Theorems 2 and 3 enables the calculation of identifiable parameter groupings from

$$< D\Phi(\theta^0), n > = 0. \tag{5.21}$$

The simplest identifiable parameter groupings are ;

$$\{k_{em}, k_2 + k_m, k_1 k_m\}$$

N.B. It should be noted that these identifiable parameter groupings are also readily established from the transfer function defined in (5.19). A suitable state space transformation can be obtained by making the following substitution for the state variable T in equation (5.15),

$$T^* = k_m T. \tag{5.22}$$

This yields the following state space transformation for the system which provides a locally identifiable reparameterisation.

$$\begin{aligned} \dot{T^*} &= \phi_1 P - \phi_2 T^* \\ \dot{M} &= T^* - \phi_3 M \end{aligned} \tag{5.23}$$

where $\phi_1 = k_1 k_m, \phi_2 = k_2 + k_m$, and $\phi_3 = k_{em}$. The parameter λ may readily be reintroduced to obtain the true reparameterisation of system (5.15), given by

$$\begin{aligned} \dot{T}^* &= \phi_1 P - \phi_2 T^* \\ \dot{M} &= T^* - \phi_3 M \end{aligned} \tag{5.24}$$

where $\phi_1 = k_1 k_m, \phi_2 = k_2 + k_m + \lambda$, and $\phi_3 = k_{em} + \lambda$. This system is then solved using the method of Laplace transforms, i.e. taking transforms of (5.24) gives

$$\begin{aligned} s\tilde{T}^* &= \phi_1 \tilde{P} - \phi_2 \tilde{T}^* \\ s\tilde{M} &= T^* - \phi_3 \tilde{M}, \end{aligned} \tag{5.25}$$

whereby

$$\begin{aligned} \tilde{M} &= \frac{\tilde{T}^*}{s + \phi_3} \\ \tilde{T}^* &= \frac{\phi_1 \tilde{P}}{s + \phi_2} \end{aligned} \tag{5.26}$$

and solving for $\tilde{M}$ gives

$$\tilde{M} = \frac{\phi_1 \tilde{P}}{(s + \phi_3)(s + \phi_2)}. \tag{5.27}$$

By employing the inverse Laplace transformation,

$$M(t) = \begin{cases} 0 & t < \delta \\ \frac{\phi_1}{\phi_3 - \phi_2}(e^{-\phi_2 t} - e^{-\phi_3 t}) \otimes P(t - \delta) & t \geq \delta \end{cases} \tag{5.28}$$

The data were then fitted to this equation using a simplex optimiser to obtain the least sum of squares fit, data being weighted as the reciprocal of the dependent variable.

Fitting of Model to Metabolite Data

The next step was to rearrange this model in terms of the total plasma activity. There is no explicit solution for the metabolite fraction in terms of the total plasma activity because of the delay in the model, thus a novel fitting procedure was proposed.

Iterative Method

The delay in the production of the metabolites averages approximately 90 seconds and so the initial part of the plasma curve is simply parent drug. This measure of the initial amount of parent compound allows the employment of an iterative procedure to calculate the full time courses of parent and metabolite. Given a set of parameter values and numerically convolving the initial parent concentration with the metabolism model provides the initial, delayed, metabolite signal. This metabolite signal is then subtracted from the subsequent total plasma concentration to give the second segment of parent concentration. This procedure is repeated, calculating the parent and metabolite concentrations in segments whose lengths are equal to the delay. The parameters for the metabolite model are optimised using a simplex method until the metabolite fraction best represents the measured fraction, in a least sum of squares sense. Each data point is weighted equally. The iterative scheme was found to be robust for delays that occur with [^{11}C]flumazenil's metabolites (50 - 200 seconds).

It was necessary to fit for the delay in formation of the metabolite. This process could not be included easily in the parameter fitting routine because the total plasma curve is sampled every second and this would mean that the total plasma curve would have to be resampled every iteration. This problem was eliminated by employing a golden ratio search [105], on top of the simplex fitting routine to find the delay that minimised the residual sum of squares. A typical fit is shown

in Figure (5.19) and the results are listed in Tables (5.7 and 5.9).

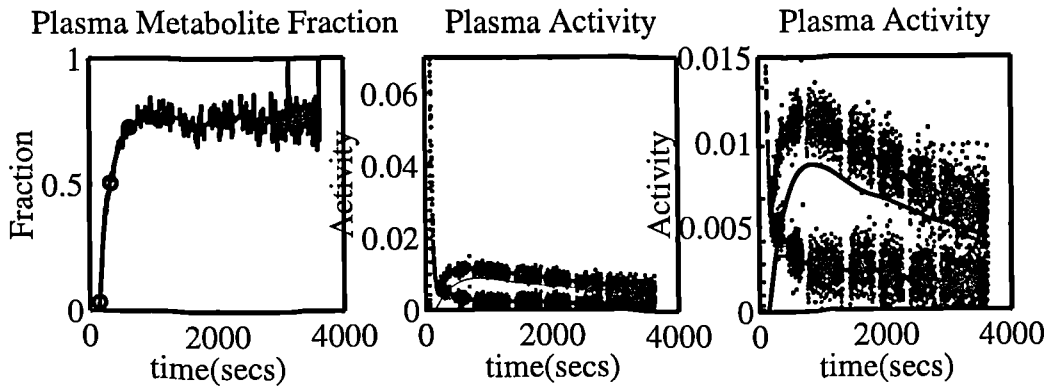

Figure 5.19: Fit and segmentation for n00296 ([^{11}C]flumazenil)

5.2.4 Discussion

Prediction of the metabolite component from the non-monotonicity in the curve is very difficult because to fit to solely the total plasma time course, a functional form for the parent is required. Any functional form for the parent requires many parameters [106], and coupling this with the four parameters in the metabolism model, any subsequent fitting becomes unfeasible.

5.2.5 Partition Coefficient Model

Inspection of the plasma to blood ratio revealed that there was a simple relationship with the metabolite fraction, see Figure (5.20). This indicated that the parent and metabolite components had significantly different partition coefficients between red cells and plasma. The correlation coefficient for the metabolite fraction and the blood to plasma ratio was significant at the 5% level for 21 of the 32 studies, see Figure (5.21). For the studies in which this correlation was not significant the plasma to blood ratio measured at the late time point ($\sim$ 5000 secs) was different from the equilibrating trends of the previous points. This suggested that

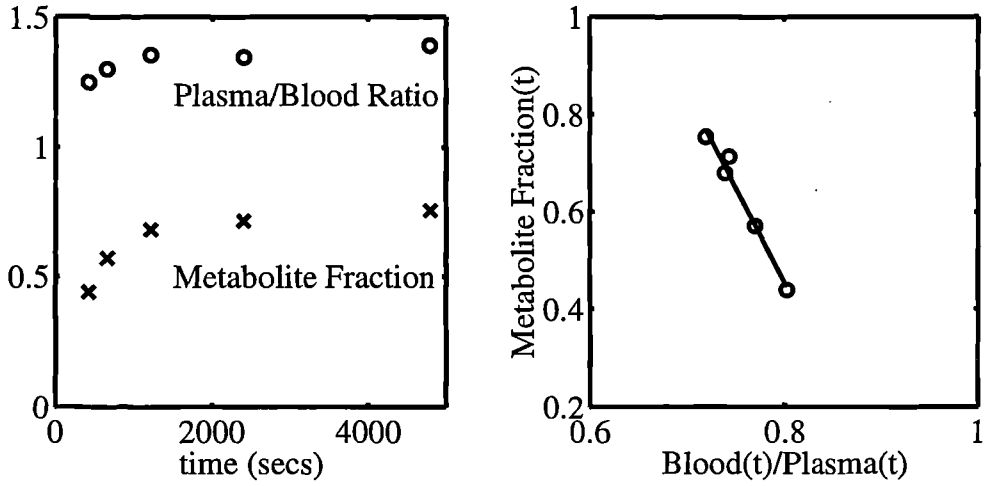

Figure 5.20: Plot of blood/plasma partition and metabolite fraction

the assay of the blood samples at later times was inaccurate, and that the samples should have been counted for a longer period (see Discussion that follows).

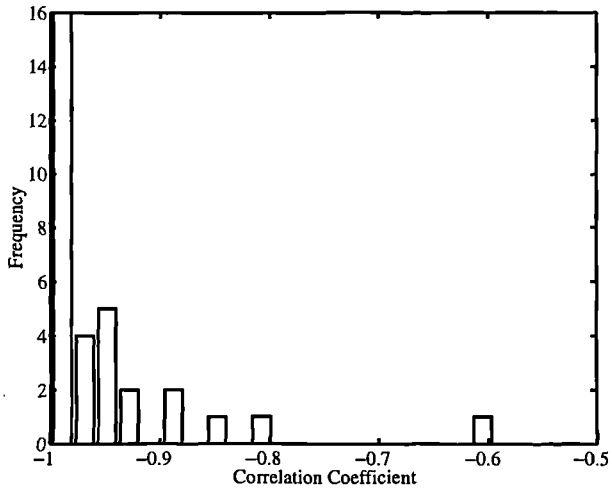

Figure 5.21: Correlation coefficients for a cohort of 32 scans (blood/plasma vs metabolite fraction)

Model

A linear relationship as seen in Figure (5.20) was therefore predicted. At equilibrium, the partition of parent [^{11}C]flumazenil and its labelled metabolites between

plasma and red cells can be considered to be:

$$
\begin{aligned}
Pl\_Par(t)\alpha &= Rc\_Par(t) \\
Pl\_Met(t)\beta &= Rc\_Met(t)
\end{aligned}
\tag{5.29}
$$

Concentration of label in plasma	$Pl(t)$
Concentration of label in red cells	$Rc(t)$
Concentration of label in blood	$Wb(t)$
Fraction of metabolite in plasma	$Mf(t)$
Haematocrit	h
Concentration of parent in plasma	$Pl\_Par(t)$
Concentration of metabolite in plasma	$Pl\_Met(t)$
Concentration of parent in plasma	$Rc\_Par(t)$
Concentration of metabolite in plasma	$Rc\_Met(t)$
Partition coefficient for flumazenil	α
Partition coefficient for metabolites	β

Table 5.2: Parameters for partition coefficient model

The variables used in the model postulated are given Table (5.2). The metabolite fraction, the concentration in plasma and the concentration in red cells are defined by

$$
\begin{aligned}
Mf(t) &= \frac{Pl\_Met(t)}{Pl(t)} \\
Pl(t) &= Pl\_Par(t) + Pl\_Met(t) \\
Rc(t) &= Rc\_Par(t) + Rc\_Met(t)
\end{aligned}
\tag{5.30}
$$

Given these definitions one can proceed to derive a linear relationship between the metabolite fraction and the whole blood to plasma ratio.

Since

$$Wb(t) = hRc(t) + (1-h)Pl(t) \tag{5.31}$$

using (5.30) this gives

$$\begin{aligned} Wb(t) &= h(Rc\_Par(t) + Rc\_Met(t)) + (1-h)(Pl\_Par(t) + Pl\_Met(t)) \\ &= h(\alpha Pl\_Par(t) + \beta Pl\_Met(t)) + (1-h)(Pl\_Par(t) + Pl\_Met(t)) \\ &= Pl(t)(1-h+\alpha h) + h(\beta-\alpha)Pl\_Met(t) \end{aligned} \tag{5.32}$$

Dividing through by $Pl(t)$ yields

$$\frac{Wb(t)}{Pl(t)} = (1-h+\alpha h) + h(\beta-\alpha)Mf(t) \tag{5.33}$$

or

$$Mf(t) = \frac{Wb(t)}{Pl(t)}\frac{1}{h(\beta-\alpha)} - \frac{1-h+\alpha h}{h(\beta-\alpha)} \tag{5.34}$$

Model Results

For the (32) data sets considered, time points were chosen which comprised both a whole blood to plasma ratio and a metabolite fraction, producing data sets containing between 3 and 5 data points. These data sets were fitted to equation (5.34) using a measured haematocrit value (1 to 17) and a standard hameatocrit of 0.4 when no haematocrit was measured (18 to 32). The parameter values obtained for the partition coefficients α and β are listed in Table (5.10) and histograms of the parameters are illustrated in Figure (5.22).

Examination of the histograms reveals that the partition coefficients α and β are approximately normally distributed with mean values of 0.84 and 0.036 respectively. The significance of this result is the distribution of the metabolite, which is predominantly in the plasma (96% of metabolite in plasma).

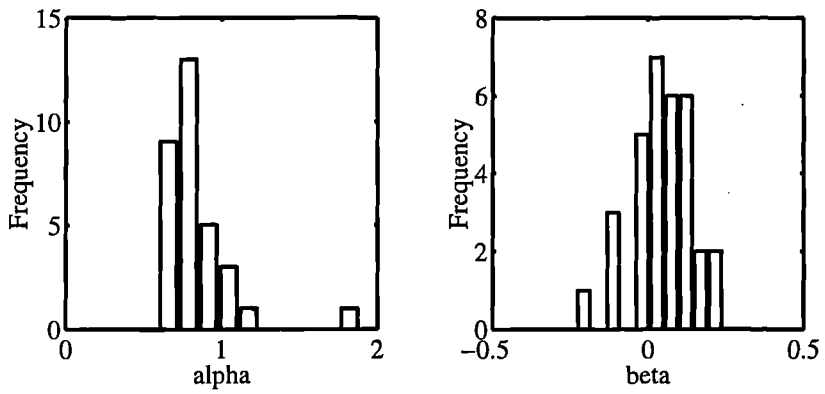

Figure 5.22: Histograms of calculated partition coefficients

At first a number of the fitted values for β were negative, which is physiologically impossible, hence the model was refitted fixing β and allowing α and h to vary. This process was repeated, varying β each time, until the fitted values for h most closely matched the measured h in a least squares sense. This process was carried out for data sets in which the haematocrit had been measured. A value of $\beta = .036$ minimised the difference between the haematocrits, see Table (5.11). The correlation between the two haematocrits can be seen in Figure (5.24) and the correlation coefficient was 0.77. A histogram of the α and h values for all the studies with $\beta = .036$ is shown in Figure (5.23).

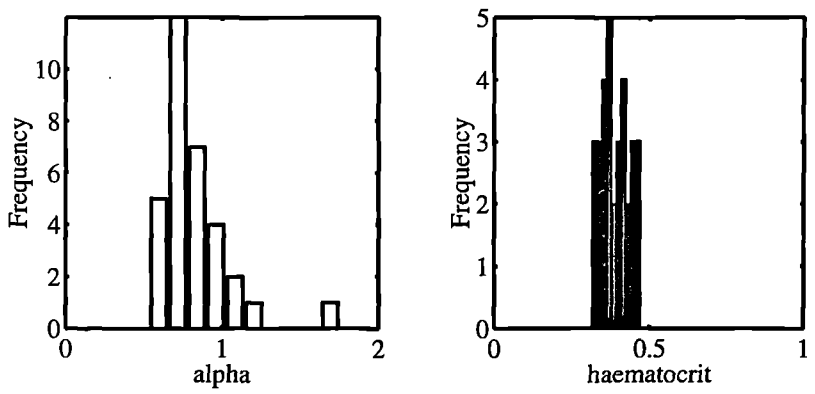

Figure 5.23: Histograms of flumazenil partition coefficients and haematocrits

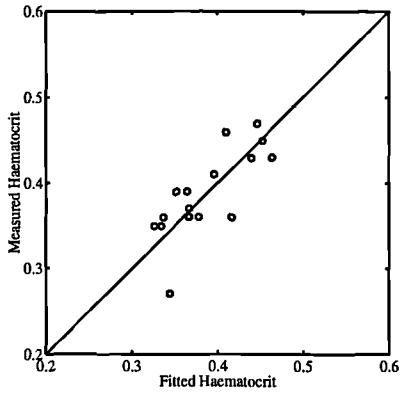

Figure 5.24: Correspondence between measured and calculated haematocrit

5.2.6 Prediction of Metabolite Data

The data sets were investigated to see if early metabolite and plasma to blood ratio data could be used to predict the late metabolite points simply from the plasma to blood ratio. A typical example can be seen in Figure(5.25) where the predicted values are 0.5% and 5.4% different from the measured values. This prediction was applied to all the studies and the percentage error was calculated for the final data point. It was found that 62.5% of the studies were within 10% error at this time point. Inspection of the data again emphasised the need for more accurate measurement of blood data towards the end of the scan.

5.2.7 Discussion

To summarise, two results have been obtained. Firstly, the accurate correction of the [^{11}C]flumazenil blood input function for metabolites has been achieved using a compartmental model. Secondly, a partition model has been applied to the plasma/blood data to produce additional metabolite measurements. A novel proposal for the accurate creation of a metabolite corrected plasma input function for [^{11}C]flumazenil is summarised by Figure (5.26). The proposed scheme involves collecting more plasma to blood partition data later in the scan and counting the

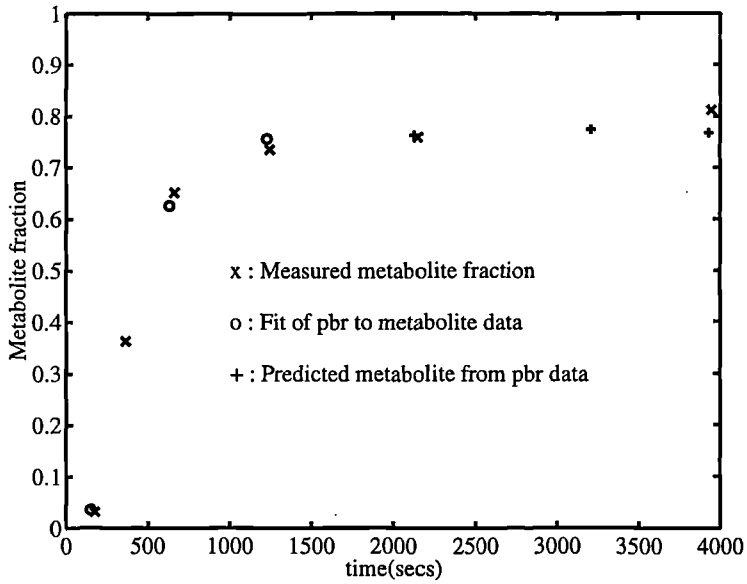

Figure 5.25: Prediction of late metabolite data using blood/plasma data and partition model

samples for a much longer period to increase accuracy. This data in conjunction with the partition model will then allow for the creation of accurate metabolite data later in the scan. This process is less complicated than the HPLC procedure and it is predicted that it will be more accurate at these late time where the HPLC method is inaccurate due to the very small concentrations of parent and metabolites. The plasma to blood ratio is interpolated with an exponential function and multiplied with the continuous blood radioactivity time course to create a total plasma radioactivity time course. Finally the compartmental model, shown earlier, is applied to the composite metabolite data to create a metabolite corrected plasma input function. This proposal would involve no increase in complexity of the blood analysis, the metabolite analysis being the most laborious step, and it is hypothesised that a more accurate metabolite correction would be obtained.

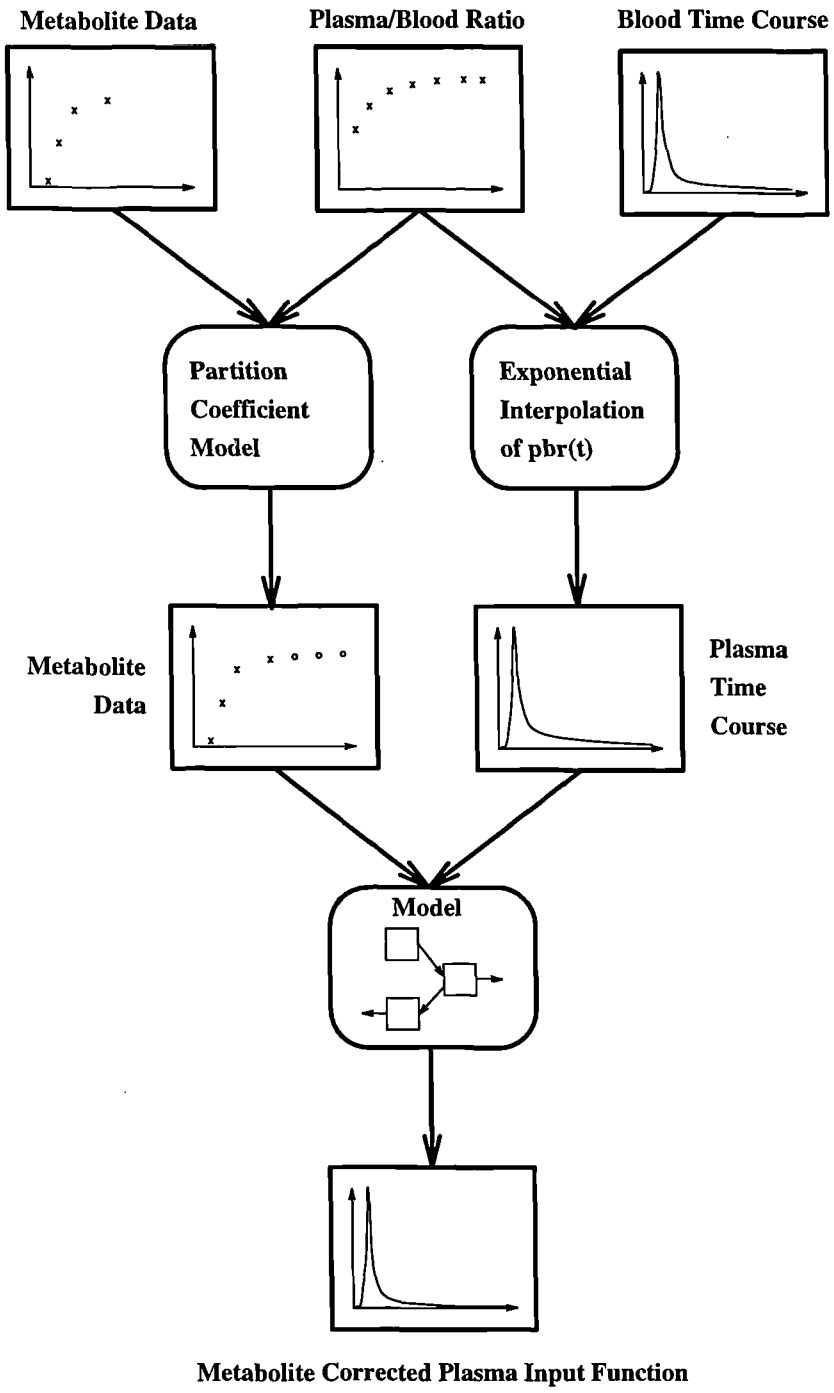

Figure 5.26: Proposed method for metabolite correction of [^{11}C]flumazenil blood data

Study	Negative Exp	Hyperbola	Sigmoid	Compartmental
n00694	4.9e-03	1.1e-03	1.8e-03	1.4e-02
n00706	2.9e-03	1.9e-03	5.4e-03	2.4e-03
n00749	2.8e-04	6.6e-04	5.0e-03	1.3e-03
n00771	1.1e-03	2.4e-04	3.2e-03	1.1e-02
n00779	1.2e-03	8.7e-04	3.4e-03	6.5e-03
n00814	5.1e-04	8.4e-04	2.2e-03	3.4e-04
n00845	1.5e-03	2.0e-03	6.1e-03	8.2e-03
p01414	1.4e-03	2.5e-04	2.3e-03	8.4e-03
p01597	8.8e-04	3.1e-03	9.0e-03	4.9e-03
p01614	9.1e-04	2.7e-04	2.2e-03	9.8e-03
p01971	1.5e-03	4.5e-03	8.9e-03	9.9e-03
p02055	4.7e-03	8.1e-04	5.3e-04	2.7e-02
p02065	1.8e-03	6.7e-04	1.7e-03	2.9e-02
p02068	4.1e-04	1.1e-03	2.4e-03	7.2e-03
p02084	1.4e-03	9.3e-04	2.1e-03	1.5e-03
p02091	2.4e-03	4.1e-03	6.1e-03	1.3e-03
p02230	4.7e-03	4.2e-03	6.1e-03	1.7e-02
p02238	1.6e-03	3.8e-03	8.8e-03	1.8e-03
p02277	1.3e-03	1.3e-03	2.0e-03	6.8e-03
p02353	3.7e-04	7.6e-04	3.0e-03	7.1e-04
p02370	2.3e-04	9.3e-04	2.8e-03	2.8e-03
p02376	1.2e-03	3.3e-04	8.5e-04	3.0e-03
p02417	4.8e-03	3.6e-03	5.8e-03	8.9e-03
p02447	4.4e-03	6.3e-03	8.5e-03	4.9e-04
p02467	3.4e-03	5.1e-03	7.6e-03	1.2e-03
p02501	6.6e-04	4.6e-04	6.6e-04	2.5e-03
p02512	3.2e-03	1.9e-03	2.9e-03	9.8e-03
p02526	4.3e-03	2.9e-03	3.8e-03	6.4e-03
p02531	1.6e-02	9.8e-03	5.6e-03	3.0e-02
p02540	4.4e-03	5.8e-03	6.2e-03	4.0e-04
p02653	2.5e-03	3.6e-03	5.7e-03	2.2e-03
p02755	5.1e-04	1.7e-04	9.4e-04	2.8e-03
p02774	2.0e-03	2.8e-03	4.0e-03	5.3e-04
p02810	3.8e-03	3.9e-03	3.1e-03	6.4e-03
p02826	6.5e-03	9.1e-03	1.0e-02	4.5e-03
p02845	5.8e-03	6.6e-03	5.5e-03	3.6e-03

Table 5.3: Diprenorphine metabolism model results

Study	Negative Exp	Hyperbola	Sigmoid	Compartmental
p02854	3.5e-03	6.6e-03	5.8e-03	2.3e-03
p02862	1.8e-03	2.7e-03	3.8e-03	2.0e-03
p02864	1.2e-04	1.5e-03	5.4e-03	8.5e-03
p02915	8.9e-04	2.7e-03	6.2e-03	1.3e-03
p02925	1.4e-03	2.7e-03	1.2e-03	3.5e-04
p02936	2.8e-03	3.9e-03	3.2e-03	1.7e-03
p03020	3.6e-03	5.8e-03	6.3e-03	7.7e-04
p02010	1.6e-03	2.3e-03	5.9e-03	1.8e-02
p02018	1.3e-05	9.6e-04	3.2e-03	1.2e-03
p02029	8.7e-04	1.9e-03	6.1e-03	6.3e-03
p02037	1.5e-03	9.7e-04	8.1e-04	4.3e-02
p02049	2.7e-03	1.7e-03	3.3e-03	1.1e-02
p02098	1.9e-03	3.5e-03	6.0e-03	4.3e-03
p02122	4.0e-03	3.1e-03	4.0e-03	1.1e-02
p02139	7.1e-03	5.3e-03	5.1e-03	5.7e-03
p02271	9.1e-03	1.2e-02	1.8e-02	5.8e-03
p02315	6.7e-04	5.9e-04	1.8e-03	1.6e-03
p02424	7.0e-03	9.7e-03	8.6e-03	2.9e-03
p02456	6.1e-03	7.8e-03	1.0e-02	1.8e-03
p02464	4.2e-04	8.0e-04	2.2e-03	2.0e-04
p02472	1.2e-03	5.3e-04	5.9e-04	3.5e-03
n00427	9.4e-04	2.3e-03	1.0e-02	4.3e-03
n00457	2.8e-03	1.4e-03	5.6e-03	2.1e-01
p02557	1.8e-03	6.7e-04	5.9e-04	9.7e-03
p02559	6.8e-04	8.3e-04	1.6e-03	4.9e-03
n00512	6.7e-03	3.4e-03	3.9e-03	3.3e-01
p02572	4.2e-03	5.7e-03	3.2e-03	8.5e-04
n00522	4.1e-03	2.3e-03	6.2e-03	2.0e-02
n00529	8.1e-04	8.0e-04	3.8e-03	5.9e-03
p02591	1.8e-03	1.5e-03	3.4e-03	4.2e-04
p02597	3.0e-03	2.3e-03	3.8e-03	4.9e-03
n00542	2.3e-03	9.1e-04	1.5e-03	4.8e-03
p02621	3.5e-03	5.4e-03	3.4e-04	2.7e-03
n00569	1.9e-03	8.2e-04	3.1e-03	1.1e-02
n00630	1.2e-02	1.9e-02	2.6e-02	5.5e-03
n00737	1.2e-03	6.9e-03	1.8e-02	4.0e-03
Mean	2.9e-03	3.2e-03	4.9e-03	1.4e-02
Std	2.8e-03	3.2e-03	4.3e-03	4.5e-02

Table 5.4: Diprenorphine metabolism model results

Study	α	β	γ	δ	ϕ	θ	k_1	k_2	$\frac{k_1}{k_1+k2}$
n00694	6.0e-01	2.0e-03	6.9e-01	4.0e+02	-1.0e+02	3.2e-01	2.1e-04	2.1e-04	5.0e-01
n00706	6.1e-01	1.5e-03	7.3e-01	6.0e+02	-7.8e+01	4.4e-01	2.1e-04	2.9e-04	4.2e-01
n00749	5.5e-01	1.4e-03	6.6e-01	6.4e+02	9.5e+01	4.2e-01	1.7e-04	1.8e-04	4.8e-01
n00771	5.9e-01	1.5e-03	7.1e-01	5.9e+02	-8.5e+01	4.1e-01	1.6e-04	1.5e-04	5.2e-01
n00779	5.6e-01	1.1e-03	7.1e-01	9.3e+02	7.7e+01	5.5e-01	1.4e-04	1.8e-04	4.3e-01
n00814	4.6e-01	6.4e-04	6.6e-01	2.0e+03	8.7e+01	7.3e-01	6.0e-05	1.3e-04	3.1e-01
n00845	6.8e-01	1.6e-03	8.0e-01	5.2e+02	6.0e+01	4.5e-01	2.9e-04	3.4e-04	4.6e-01
p01414	5.8e-01	2.3e-03	6.8e-01	3.5e+02	1.0e+02	3.1e-01	3.8e-04	5.2e-04	4.2e-01
p01597	6.0e-01	2.1e-03	7.1e-01	4.3e+02	7.7e+01	3.8e-01	3.3e-04	4.1e-04	4.5e-01
p01614	6.7e-01	1.9e-03	7.9e-01	4.6e+02	5.8e+01	4.4e-01	4.2e-04	4.9e-04	4.6e-01
p01971	7.5e-01	2.4e-03	8.7e-01	3.4e+02	4.1e+01	4.6e-01	7.2e-04	6.1e-04	5.4e-01
p02055	7.3e-01	3.1e-03	8.1e-01	2.2e+02	7.1e+01	2.5e-01	9.7e-04	7.4e-04	5.7e-01
p02065	8.5e-01	3.3e-03	9.4e-01	2.0e+02	2.9e+01	4.2e-01	1.0e-03	4.6e-04	7.0e-01
p02068	9.2e-01	5.3e-03	9.6e-01	7.9e+01	2.9e+01	2.0e-01	2.4e-03	6.0e-04	8.0e-01
p02084	4.5e-01	1.4e-03	5.8e-01	7.4e+02	1.0e+02	4.7e-01	1.5e-04	2.1e-04	4.1e-01
p02091	6.0e-01	1.0e-03	8.3e-01	1.2e+03	5.0e+01	8.1e-01	1.9e-04	2.6e-04	4.3e-01
p02230	7.5e-01	2.2e-03	8.9e-01	4.0e+02	3.8e+01	5.3e-01	6.7e-04	4.4e-04	6.0e-01
p02238	7.0e-01	2.6e-03	8.0e-01	3.0e+02	6.4e+01	3.2e-01	1.3e-03	9.1e-04	5.8e-01
p02277	6.0e-01	1.3e-03	7.7e-01	8.4e+02	6.0e+01	5.9e-01	2.6e-04	3.1e-04	4.5e-01
p02353	4.6e-01	1.5e-03	5.8e-01	7.0e+02	1.1e+02	4.5e-01	1.9e-04	4.4e-04	3.0e-01
p02370	5.4e-01	1.2e-03	7.2e-01	9.7e+02	6.8e+01	6.1e-01	1.8e-04	2.7e-04	4.0e-01
p02376	5.0e-01	1.5e-03	6.3e-01	6.4e+02	9.7e+01	4.3e-01	1.5e-04	2.0e-04	4.2e-01
p02417	6.6e-01	2.2e-03	7.8e-01	4.0e+02	6.5e+01	3.7e-01	2.6e-04	3.7e-04	4.1e-01
p02447	5.5e-01	9.3e-04	7.9e-01	1.4e+03	5.3e+01	8.6e-01	1.3e-04	1.2e-04	5.3e-01
p02467	5.1e-01	9.5e-04	7.2e-01	1.4e+03	6.4e+01	7.6e-01	1.2e-04	2.8e-04	3.0e-01
p02501	6.4e-01	9.4e-04	8.9e-01	1.3e+03	4.8e+01	8.2e-01	1.4e-04	4.3e-05	7.6e-01
p02512	6.5e-01	1.6e-03	8.1e-01	6.4e+02	5.3e+01	5.5e-01	2.7e-04	2.3e-04	5.3e-01
p02526	6.0e-01	1.5e-03	7.6e-01	7.0e+02	6.2e+01	5.3e-01	2.1e-04	2.3e-04	4.9e-01
p02531	6.3e-01	1.5e-03	7.8e-01	6.1e+02	6.6e+01	4.6e-01	2.2e-04	1.2e-04	6.5e-01
p02540	6.1e-01	8.0e-04	8.9e-01	1.7e+03	4.4e+01	1.1e+00	1.3e-04	1.6e-04	4.5e-01
p02653	6.1e-01	1.1e-03	8.2e-01	1.0e+03	4.9e+01	7.6e-01	1.5e-04	1.2e-04	5.5e-01
p02755	4.6e-01	1.3e-03	5.9e-01	7.8e+02	1.0e+02	4.8e-01	1.6e-04	3.7e-04	3.1e-01
p02774	5.0e-01	7.6e-04	7.4e-01	1.8e+03	6.3e+01	8.6e-01	8.8e-05	1.0e-04	4.6e-01
p02810	7.4e-01	7.0e-04	1.1e+00	2.0e+03	3.3e+01	1.3e+00	1.3e-04	2.2e-05	8.5e-01
p02826	6.5e-01	1.1e-03	8.8e-01	1.1e+03	4.0e+01	9.4e-01	1.8e-04	1.3e-04	5.7e-01
p02845	6.6e-01	6.2e-04	1.0e+00	2.4e+03	3.9e+01	1.3e+00	1.1e-04	2.4e-05	8.2e-01
p02854	7.1e-01	1.1e-03	9.8e-01	1.1e+03	2.8e+01	1.3e+00	2.4e-04	1.6e-04	6.1e-01

Table 5.5: Diprenorphine metabolism model results

Study	α	β	γ	δ	ϕ	θ	k_1	k_2	$\frac{k_1}{k_1+k2}$
p02862	5.6e-01	8.9e-04	8.1e-01	1.5e+03	5.4e+01	8.5e-01	1.2e-04	2.3e-04	3.4e-01
p02864	6.0e-01	1.7e-03	7.4e-01	5.5e+02	6.5e+01	4.7e-01	2.4e-04	3.0e-04	4.4e-01
p02915	5.5e-01	1.3e-03	7.2e-01	8.6e+02	6.4e+01	6.1e-01	1.5e-04	2.3e-04	4.0e-01
p02925	7.5e-01	8.5e-04	1.1e+00	1.5e+03	2.8e+01	1.5e+00	1.9e-04	2.1e-04	4.7e-01
p02936	6.7e-01	7.0e-04	1.0e+00	2.0e+03	3.8e+01	1.3e+00	1.5e-04	2.9e-04	3.4e-01
p03020	6.4e-01	9.3e-04	9.1e-01	1.4e+03	3.9e+01	1.1e+00	1.4e-04	1.7e-04	4.6e-01
p02010	7.2e-01	3.9e-03	7.8e-01	1.5e+02	1.1e+02	1.6e-01	1.5e-03	1.0e-03	5.9e-01
p02018	6.8e-01	3.7e-03	7.6e-01	1.8e+02	8.4e+01	2.2e-01	1.1e-03	1.0e-03	5.1e-01
p02029	7.5e-01	3.4e-03	8.3e-01	1.9e+02	6.6e+01	2.3e-01	1.0e-03	5.9e-04	6.3e-01
p02037	5.6e-01	7.0e-03	5.8e-01	4.7e+01	7.0e+03	5.7e-02	7.1e-04	1.1e-03	4.0e-01
p02049	7.5e-01	2.2e-03	8.8e-01	3.8e+02	4.0e+01	4.9e-01	6.4e-04	5.1e-04	5.6e-01
p02098	6.6e-01	1.4e-03	8.4e-01	7.7e+02	4.5e+01	7.0e-01	3.2e-04	4.1e-04	4.4e-01
p02122	5.4e-01	1.2e-03	7.1e-01	9.3e+02	6.9e+01	5.9e-01	1.7e-04	2.9e-04	3.7e-01
p02139	6.9e-01	9.6e-04	9.4e-01	1.2e+03	4.2e+01	8.6e-01	1.8e-04	2.0e-04	4.7e-01
p02271	5.1e-01	1.4e-03	6.7e-01	7.8e+02	7.2e+01	5.7e-01	2.2e-04	4.2e-04	3.5e-01
p02315	6.1e-01	1.2e-03	8.0e-01	9.4e+02	5.4e+01	6.7e-01	1.9e-04	2.6e-04	4.2e-01
p02424	7.0e-01	9.1e-04	9.9e-01	1.4e+03	3.1e+01	1.3e+00	1.4e-04	6.8e-05	6.7e-01
p02456	5.3e-01	9.6e-04	7.5e-01	1.3e+03	5.7e+01	8.2e-01	1.1e-04	2.0e-04	3.6e-01
p02464	4.0e-01	9.4e-04	5.6e-01	1.3e+03	9.7e+01	6.3e-01	1.1e-04	1.3e-04	4.6e-01
p02472	4.6e-01	1.2e-03	6.0e-01	8.7e+02	9.7e+01	5.0e-01	1.7e-04	2.6e-04	3.9e-01
n00427	4.6e-01	1.1e-03	5.6e-01	8.2e+02	1.5e+02	3.9e-01	1.0e-04	1.1e-04	4.8e-01
n00457	7.2e-01	1.1e-03	8.6e-01	7.9e+02	-5.1e+01	6.0e-01	3.0e-04	5.9e-04	3.4e-01
p02557	4.9e-01	1.3e-03	6.3e-01	7.8e+02	9.2e+01	4.9e-01	2.1e-04	3.5e-04	3.7e-01
p02559	6.8e-01	1.2e-03	8.9e-01	9.3e+02	4.2e+01	7.9e-01	1.8e-04	1.5e-04	5.5e-01
n00512	6.1e-01	1.7e-03	6.9e-01	4.9e+02	-1.2e+02	3.2e-01	2.6e-04	1.1e-03	2.0e-01
p02572	7.6e-01	8.5e-04	1.1e+00	1.6e+03	2.4e+01	1.8e+00	1.6e-04	7.0e-05	7.0e-01
n00522	6.6e-01	1.8e-03	7.7e-01	4.7e+02	7.2e+01	3.8e-01	2.4e-04	1.4e-04	6.3e-01
n00529	5.7e-01	1.8e-03	7.0e-01	5.2e+02	7.8e+01	4.2e-01	2.5e-04	3.2e-04	4.4e-01
p02591	9.5e-01	5.9e-04	1.5e+00	2.5e+03	2.1e+01	2.1e+00	1.7e-04	2.5e-05	8.7e-01
p02597	5.6e-01	1.9e-03	6.9e-01	5.0e+02	8.0e+01	4.1e-01	2.9e-04	4.0e-04	4.3e-01
n00542	7.4e-01	1.3e-03	9.1e-01	7.3e+02	-4.1e+01	6.8e-01	2.1e-04	1.8e-04	5.4e-01
p02621	8.7e-01	9.8e-04	1.2e+00	1.3e+03	8.2e+00	8.9e+00	2.6e-04	1.4e-04	6.5e-01
n00569	6.0e-01	1.2e-03	7.4e-01	8.0e+02	-7.1e+01	5.2e-01	1.8e-04	1.7e-04	5.0e-01
n00630	6.6e-01	1.3e-03	8.3e-01	8.0e+02	4.3e+01	8.0e-01	2.1e-04	2.5e-04	4.5e-01
n00737	6.7e-01	2.0e-03	7.8e-01	4.2e+02	6.7e+01	3.9e-01	2.7e-04	2.4e-04	5.3e-01
Mean	6.3e-01	1.6e-03	8.0e-01	8.9e+02	1.4e+02	7.6e-01	3.3e-04	3.2e-04	5.0e-01
Std	1.1e-01	1.1e-03	1.6e-01	5.5e+02	8.1e+02	1.0e+00	3.8e-04	2.5e-04	1.4e-01

Table 5.6: Diprenorphine metabolism model results

Study	Negative Exp	Hyperbola	Sigmoid	Compartmental
n00153	1.3e-03	1.9e-03	1.1e-02	1.4e-05
n00215	2.1e-04	3.1e-05	2.4e-04	4.1e-04
n00222	2.8e-03	1.0e-03	8.0e-03	2.4e-05
n00224	1.1e-04	5.9e-03	2.9e-02	2.1e-05
n00232	1.9e-03	2.5e-03	6.1e-03	5.4e-03
n00234	4.4e-03	2.2e-04	1.9e-03	4.3e-03
n00257	6.8e-04	4.9e-03	1.8e-02	2.4e-03
n00258	9.0e-03	7.4e-03	1.5e-02	1.4e-03
n00296	5.9e-05	4.4e-03	1.7e-02	7.4e-05
n00298	7.4e-04	7.5e-04	4.2e-03	1.5e-03
n00304	6.0e-03	5.7e-04	2.1e-03	7.0e-05
n00331	4.5e-04	1.3e-03	3.3e-03	4.4e-03
n00333	2.9e-03	7.7e-05	4.1e-03	2.5e-04
n00339	1.9e-04	2.7e-03	1.4e-02	2.5e-03
n00341	2.2e-03	7.8e-04	8.7e-03	5.7e-04
n00344	9.4e-04	4.7e-03	1.8e-02	8.0e-04
n00346	1.0e-03	1.4e-03	1.2e-02	5.0e-04
n00361	2.5e-03	1.0e-02	2.9e-02	1.2e-03
n00365	7.5e-04	2.6e-03	1.5e-02	7.8e-05
n00372	1.8e-03	1.9e-03	1.1e-02	2.5e-04
n00375	1.3e-03	5.0e-03	2.0e-02	4.5e-05
n00389	5.9e-03	3.5e-03	8.7e-03	1.9e-03
n00392	7.5e-04	6.5e-03	2.3e-02	4.5e-04
n00399	1.1e-04	4.0e-03	1.6e-02	1.8e-03
n00401	4.9e-03	7.7e-03	1.6e-02	3.0e-04
n00459	1.6e-03	7.0e-03	2.3e-02	4.0e-04
n00471	1.5e-03	2.0e-03	5.2e-03	1.3e-02
n00472	1.7e-03	3.7e-04	3.4e-03	3.2e-02
n00682	4.3e-03	1.1e-02	2.2e-02	1.3e-03
n00687	5.1e-03	9.3e-03	2.3e-02	5.0e-04
n00693	6.8e-03	1.2e-02	1.4e-02	2.4e-04
n00696	3.9e-03	1.3e-02	3.2e-02	9.0e-05
Mean	2.4e-03	4.3e-02	1.4e-02	2.4e-03
Std	2.3e-03	3.8e-03	8.6e-03	5.9e-03

Table 5.7: Flumazenil metabolism model results

Study	α	β	*delay*	γ	δ	*delay*	ϕ	θ	*delay*
n00153	7.2e-01	4.9e-03	1.8e+02	5.6e+01	2.8e-01	1.9e+02	8.0e-01	1.4e+02	1.8e+02
n00215	8.1e-01	4.4e-03	1.1e+02	1.8e+02	7.0e-02	3.0e+02	8.4e-01	6.5e+01	2.2e+02
n00222	7.2e-01	3.2e-03	1.4e+02	1.0e+02	2.0e-01	1.9e+02	7.9e-01	2.1e+02	1.4e+02
n00224	7.3e-01	3.2e-03	1.5e+02	5.8e+01	3.2e-01	1.5e+02	8.0e-01	2.2e+02	1.5e+02
n00232	8.2e-01	7.7e-03	1.3e+02	1.3e+02	8.3e-02	1.5e+02	8.5e-01	5.6e+01	1.4e+02
n00234	8.5e-01	7.3e-03	1.4e+02	5.6e+01	1.4e-01	1.5e+02	9.0e-01	7.1e+01	1.5e+02
n00257	6.9e-01	4.7e-03	1.5e+02	1.3e+02	1.7e-01	4.0e+02	7.4e-01	1.4e+02	1.5e+02
n00258	7.5e-01	3.2e-03	1.5e+02	4.5e+01	3.8e-01	3.1e+02	8.5e-01	2.4e+02	1.5e+02
n00296	7.7e-01	5.8e-03	1.4e+02	1.1e+02	1.3e-01	1.5e+02	8.1e-01	9.5e+01	1.5e+02
n00298	8.1e-01	5.7e-03	1.4e+02	3.7e+01	2.7e-01	1.5e+02	8.9e-01	1.1e+02	1.5e+02
n00304	7.1e-01	6.0e-03	1.4e+02	1.4e+02	1.4e-01	1.5e+02	7.6e-01	9.9e+01	1.5e+02
n00331	8.1e-01	3.5e-03	1.2e+02	2.4e+01	5.8e-01	1.4e+02	9.3e-01	2.1e+02	1.3e+02
n00333	7.8e-01	7.2e-03	2.1e+02	4.2e+01	2.5e-01	2.1e+02	8.6e-01	9.4e+01	2.1e+02
n00339	7.5e-01	6.1e-03	1.4e+02	1.4e+02	1.2e-01	5.2e+02	8.0e-01	8.8e+01	1.5e+02
n00341	7.5e-01	4.3e-03	1.4e+02	7.1e+01	2.2e-01	1.5e+02	8.2e-01	1.5e+02	1.5e+02
n00344	6.4e-01	3.9e-03	1.5e+02	1.3e+02	2.0e-01	2.5e+02	7.0e-01	1.8e+02	1.5e+02
n00346	6.5e-01	3.0e-03	1.4e+02	8.9e+01	2.7e-01	3.7e+02	7.3e-01	2.4e+02	1.4e+02
n00361	7.0e-01	3.0e-03	1.5e+02	5.7e+01	3.6e-01	1.7e+02	7.9e-01	2.6e+02	1.5e+02
n00365	7.0e-01	4.0e-03	1.5e+02	9.0e+01	2.2e-01	1.5e+02	7.7e-01	1.7e+02	1.5e+02
n00372	7.2e-01	3.0e-03	1.4e+02	5.5e+01	3.4e-01	1.5e+02	8.2e-01	2.5e+02	1.5e+02
n00375	6.8e-01	3.3e-03	1.5e+02	7.3e+01	2.9e-01	1.8e+02	7.7e-01	2.3e+02	1.5e+02
n00389	7.4e-01	4.1e-03	1.3e+02	7.4e+01	2.2e-01	1.5e+02	8.1e-01	1.7e+02	1.4e+02
n00392	7.0e-01	3.6e-03	1.4e+02	7.6e+01	2.5e-01	1.6e+02	7.8e-01	2.0e+02	1.5e+02
n00399	7.7e-01	5.5e-03	1.5e+02	8.4e+01	1.6e-01	1.5e+02	8.3e-01	1.1e+02	1.5e+02
n00401	8.3e-01	5.6e-03	1.5e+02	5.0e+01	2.0e-01	2.0e+02	8.9e-01	1.1e+02	1.5e+02
n00459	6.8e-01	3.2e-03	1.4e+02	7.3e+01	3.0e-01	1.5e+02	7.6e-01	2.4e+02	1.5e+02
n00471	8.7e-01	8.2e-03	1.3e+02	7.8e+01	8.9e-02	1.5e+02	9.0e-01	5.2e+01	1.4e+02
n00472	8.8e-01	5.8e-03	1.1e+02	3.8e+01	1.8e-01	1.5e+02	9.3e-01	8.2e+01	1.3e+02
n00682	7.5e-01	2.3e-03	1.4e+02	3.0e+01	7.5e-01	1.4e+02	8.7e-01	3.6e+02	1.5e+02
n00687	7.3e-01	2.9e-03	1.5e+02	4.0e+01	4.9e-01	1.5e+02	8.4e-01	2.9e+02	1.5e+02
n00693	7.5e-01	2.6e-03	1.6e+02	1.5e+01	1.9e+00	1.2e+02	9.2e-01	3.9e+02	1.5e+02
n00696	7.0e-01	2.7e-03	1.6e+02	4.5e+01	4.9e-01	2.4e+02	8.1e-01	3.1e+02	1.5e+02
Mean	7.5e-01	4.5e-03	1.4e+02	6.6e+01	3.1e-01	2.0e+02	8.2e-01	1.8e+02	1.5e+02
Std	6.1e-02	1.6e-03	1.7e+01	5.5e+01	3.2e-01	9.0e+01	5.9e-02	9.0e+01	1.9e+01

Table 5.8: Flumazenil metabolism model results

Study	$\frac{\phi_1}{\phi_3-\phi_2}$	ϕ_2	ϕ_3	δ
n00153	2.1e-03	1.2e-03	4.8e-03	1.2e+02
n00215	1.9e-03	7.7e-04	2.5e-02	1.7e+02
n00222	2.5e-03	1.1e-03	3.2e-03	7.0e+01
n00224	3.8e-03	1.4e-03	2.8e-03	8.3e+01
n00232	8.8e-03	1.7e-03	3.0e-03	8.1e+01
n00234	2.9e-03	9.7e-04	2.2e-02	1.6e+02
n00257	1.4e-03	1.2e-03	2.9e-02	1.9e+02
n00258	1.6e-03	1.1e-03	3.4e-02	1.9e+02
n00296	5.8e-03	1.6e-03	4.5e-03	5.1e+01
n00298	2.4e-03	8.7e-04	2.7e-02	1.8e+02
n00304	1.9e-03	1.0e-03	6.4e-03	5.5e+01
n00331	2.1e-03	8.0e-04	7.3e-03	1.4e+02
n00333	3.0e-03	1.1e-03	6.8e-03	1.3e+02
n00339	2.2e-03	1.2e-03	3.8e-02	1.9e+02
n00341	1.7e-03	1.1e-03	3.9e-02	1.8e+02
n00344	1.5e-03	1.2e-03	2.5e-02	1.9e+02
n00346	1.1e-03	9.6e-04	1.6e-02	1.6e+02
n00361	1.4e-03	8.8e-04	1.9e-02	2.0e+02
n00365	1.3e-03	1.1e-03	4.0e-02	1.9e+02
n00372	1.5e-03	8.4e-04	9.6e-03	1.6e+02
n00375	1.3e-03	8.2e-04	1.5e-02	1.8e+02
n00389	2.1e-03	1.2e-03	1.1e-02	1.4e+02
n00392	1.8e-03	1.1e-03	1.5e-02	1.8e+02
n00399	1.7e-03	8.9e-04	2.6e-02	1.9e+02
n00401	1.7e-01	2.5e-03	2.5e-03	9.6e+01
n00459	1.8e-03	1.1e-03	6.0e-03	1.3e+02
n00471	2.8e-03	9.9e-04	1.7e-02	1.5e+02
n00472	3.2e-03	1.1e-03	1.4e-02	1.5e+02
n00682	1.5e-03	7.6e-04	5.2e-03	1.6e+02
n00687	1.2e-03	8.0e-04	3.9e-02	1.9e+02
n00693	2.1e-03	1.1e-03	4.5e-03	1.2e+02
n00696	1.8e-03	1.2e-03	5.0e-03	1.4e+02
Mean	7.7e-03	1.1e-03	1.6e-02	1.5e+02
Std	3.0e-02	3.3e-04	1.2e-02	4.3e+01

Table 5.9: Flumazenil compartmental model parameter values

Study	α	β
n00153	0.8239	-0.0398
n00215	0.7042	-0.1146
n00222	0.7897	0.1519
n00224	0.9057	0.0178
n00232	1.8835	-0.1302
n00234	1.0833	0.1640
n00257	0.7259	0.1036
n00258	0.7827	0.1293
n00296	1.0943	-0.0087
n00298	0.9815	-0.2297
n00304	0.8506	-0.1045
n00331	0.7548	0.0301
n00333	0.6926	-0.0322
n00339	0.9292	0.0137
n00341	0.7765	0.0488
n00344	0.7507	-0.0320
n00346	0.7526	0.0993
n00361	0.6340	0.2401
n00365	0.7704	0.0789
n00372	0.6502	0.1363
n00375	0.6726	0.0201
n00389	0.6602	0.2217
n00392	0.8051	0.0982
n00399	0.8012	0.0760
n00401	0.8954	0.0442
n00459	0.8356	-0.0120
n00471	0.9135	0.0524
n00472	1.1586	0.0166
n00682	0.8573	0.1019
n00687	0.5946	0.0840
n00693	0.7087	0.0686
n00696	0.5961	0.1399
Mean	0.8386	0.0448
Std	0.2359	0.1014

Table 5.10: Calculated partition coefficients for [^{11}C]flumazenil and metabolites

Study	α	h (fitted)	h (measured)	mean ssq
n00153	0.8368	0.4638	0.4300	0.0130
n00215	0.7441	0.4162	0.3600	0.0019
n00222	0.7610	0.3519	0.4000	0.0018
n00224	0.9075	0.3668	0.3600	0.0145
n00232	1.7536	0.4690	0.4000	0.0165
n00234	1.0960	0.3469	0.4000	0.0029
n00257	0.7053	0.3720	0.4000	0.0011
n00258	0.7593	0.3522	0.3900	0.0029
n00296	1.0901	0.4185	0.4000	0.0044
n00298	0.9855	0.3444	0.2700	0.0107
n00304	0.8696	0.4583	0.4000	0.0027
n00331	0.7563	0.4528	0.4500	0.0006
n00333	0.7129	0.4283	0.4000	0.0001
n00339	0.9308	0.4399	0.4300	0.0019
n00341	0.7735	0.3947	0.4000	0.0020
n00344	0.7671	0.4282	0.4000	0.0018
n00346	0.7353	0.3644	0.3900	0.0066
n00361	0.5357	0.3153	0.4000	0.0429
n00365	0.7598	0.3344	0.3500	0.0017
n00372	0.6096	0.3584	0.4000	0.0041
n00375	0.6779	0.3660	0.3600	0.0055
n00389	0.5791	0.3230	0.4000	0.0006
n00392	0.7917	0.3368	0.3600	0.0200
n00399	0.7925	0.3834	0.4000	0.0056
n00401	0.8945	0.3668	0.3700	0.0015
n00459	0.8434	0.3779	0.3600	0.0005
n00471	0.9120	0.3932	0.4000	0.0001
n00472	1.1555	0.4081	0.4000	0.0006
n00682	0.8468	0.3261	0.3500	0.0439
n00687	0.5733	0.4466	0.4700	0.0258
n00693	0.6986	0.3961	0.4100	0.0006
n00696	0.5473	0.4104	0.4600	0.0134
Mean	0.8251	0.3878	0.3928	0.0079
Std	0.2279	0.0446	0.0369	0.0113

Table 5.11: Calculated partition coefficient for [^{11}C]flumazenil and haematocrit

Chapter 6

Spectral Analysis

6.1 Overview

This chapter contains an introduction to spectral analysis and its implementation. A novel proof is presented that shows that the problem is well defined. This proof may also be interpreted in an identifiability framework and, as such, gives a sufficient condition for a uniquely (globally) identifiable solution. To understand the solution of the problem more fully, the nonnegative least squares algorithm is considered in conjunction with the Kuhn Tucker theorem [107]. Novel extensions of the basic method involving different basis functions and multiple inputs are investigated. These methods of spectral analysis are applied to the tracer kinetics of carbon dioxide and thymidine in Chapters 8 and 9.

6.2 Introduction and Background

Spectral analysis is a kinetic modelling technique that lies between the strictly data-led and highly structured methods. It is based on the *a priori* definition of a relatively large set of basis functions which are used in the fitting of PET data, the fit consisting of a small subset of these. Spectral analysis is the least structured technique to employ an input function (see Figure 3.2 in Chapter 3) and gives

quantitative measures of physiological parameters, e.g. K_1, VD etc. The method is based on a constrained linear optimisation problem and is a further development of an approach used by Tobler and Engel [108], who used a set of hyperbolic basis functions to investigate *in vitro* binding data. Cunningham and Jones [34] chose a set of exponential functions convolved with the plasma input function to form a set of basis functions facilitating the analysis of PET tissue data. The choice of exponential basis functions stemmed from the theory of first order tracer kinetics. Most linear compartmental structures used for the analysis of PET data produce a series of first order differential equations whose solution is a sum of positive exponentials. (Note that the original assumption by Cunningham and Jones [34] that all first order tracer kinetic models satisfy a nonnegative sum of exponentials is incorrect. Cases exist which have negative coefficients and others with repeated eigenvalues). Components are obtained by fitting a large set of these basis functions to the tissue time activity curves with suitable system parameter constraints. The linear optimisation problem is however highly underdetermined and a constraint is essential to construct a robust framework, see Figure (6.1).
The technique employs a nonnegativity constraint that makes the problem well defined (see section 6.4). This chapter considers why constraints are required and how they ensure that the problem is well defined. Spectral analysis can be considered as a constrained deconvolution technique that avoids the problems that many direct deconvolution techniques encounter in the presence of noisy data. By deconvolving the input from the observed tissue signals, variations due to different types of injections and plasma characteristics are removed and the resulting function becomes a plasma independent measure of the tissue's behaviour. Since the deconvolution process is badly determined, the method of spectral analysis produces a more robust deconvolution by restricting the possible deconvolution to a nonnegative sum of exponentials. This, by definition, forces the impulse

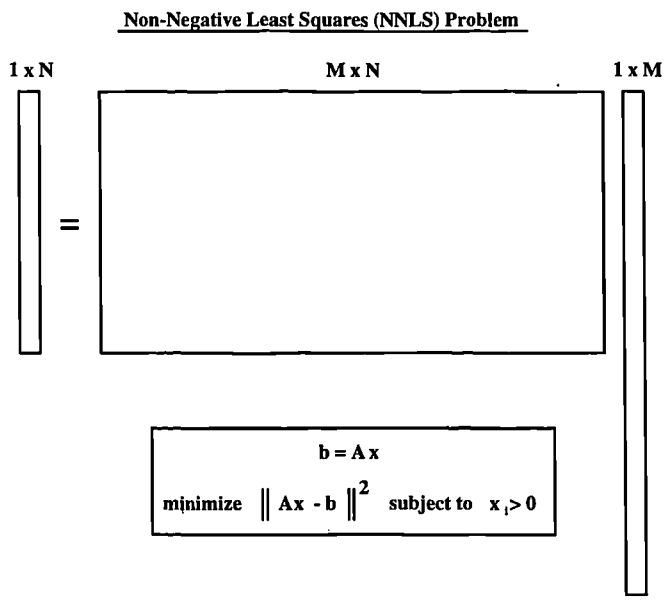

Figure 6.1: The matrix problem

response of the system to be a monotonically decreasing function. The basis functions are chosen so that they span all possible dynamics from fast blood effects to irreversible binding.

Once a solution has been obtained from the spectral analysis process the spectrum of chosen exponentials may give important kinetic information about the system (Figure (6.2)). The various components can be interpreted to give an understanding of the physiological, pharmacological and biochemical processes involved. Fast kinetics with a large β value correspond to blood effects, intermediate kinetics to reversible kinetics, and slow kinetics to irreversible kinetics of the tracer.

Lack of structure restriction by the method results in the obtained spectra having a number of possible interpretations. This refers to the problem of indistinguishability of models. For example, the method will not distinguish between two parallel or catenary compartments, both of which contain an indistinguishable sum of positive exponentials. However since both systems have an equal volume of distribution determined by the area under the tissue response function extrap-

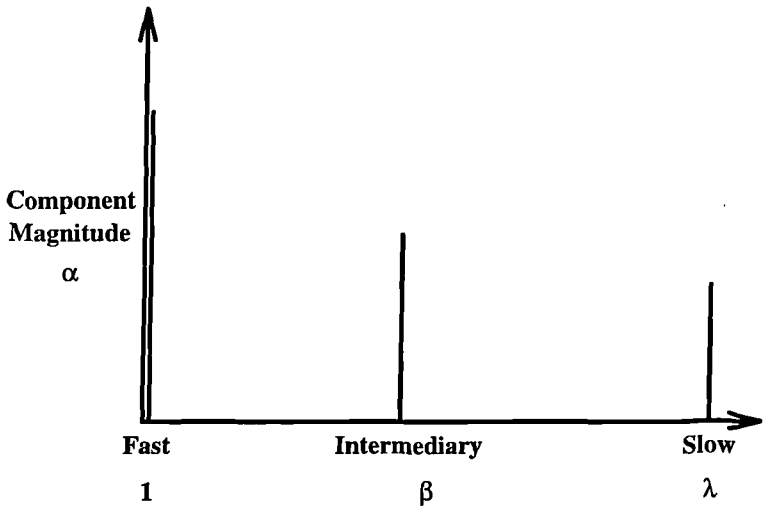

Figure 6.2: Spectrum interpretation

olated to infinity, VD is a robust parameter estimate independent of structural interpretation. The method is a good process for investigating appropriate model order.

Spectral analysis has been applied successfully to PET data [34] [35], although there is a problem as to whether the solution obtained is unique. A condition for uniqueness is presented in section 6.4 . The non-negative least squares algorithm used to solve the problem is presented and discussed in the context of the Kuhn Tucker Theorem which guarantees that a local minimum is obtained on termination of the algorithm.

6.3 Methods

The method of spectral analysis involves finding a solution to the problem (as in Figure(6.3)),

$$PETobs(t_k) = Input(t) \otimes \sum_{i=1}^{n} \alpha_i e^{-\beta_i t_k} \tag{6.1}$$

given $k \in \{1, 2, ..., N\}$ and the non-negativity constraint $\alpha_i \geq 0, \alpha_i \in \Re$

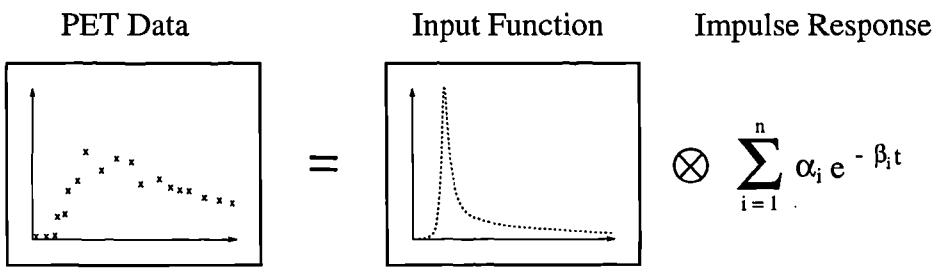

Figure 6.3: Spectral analysis

The β_i's are chosen in a logarithmic range and $n > N$. In practice $n = 100$ is found to be an acceptable number providing a good kinetic resolution. The values for β are normally chosen in a logarithmic range so that the linear dependence between the basis functions is similar.

6.3.1 Functional Parameters

Key characteristics of a system can be obtained by various manipulations of the impulse response function. The delivery rate constant, K_1, of the compound corresponds to the intercept of the impulse response at $t = 0$ in the absence of blood volume and dispersion. The area under the impulse response function extrapolated to infinity equals the volume of distribution in the tissue of interest. Often, the most important measure is the volume of distribution, VD, that quantifies the ratio of concentration of compound in tissue to the concentration of compound in plasma which would pertain at equilibrium. The mean residence time of the compound in tissue can be calculated as the ratio of the VD over the delivery K_1. In ligand studies it is possible to show that the volume of distribution is proportional to the number of available binding sites [109].

6.3.2 Non-Negative Least Squares Algorithm (NNLS)

Before considering the algorithm for NNLS [110], the method is presented graphically for the case where three data points exist. This simplification of the method

allows us to visualise it in three dimensions, Figure (6.4). In the diagram the vectors are the basis functions ranging from fast to slow dynamics. The circle represents a noisy data set generated from a single exponential. If there was no noise in this data set the circle would lie on the surface defined by the basis vectors. The solution to the NNLS problem is obtained by minimising the distance between the data point and a point in the volume defined by a non-negative span of the basis vectors. In this case the solution is a single basis function whose magnitude is given by the distance along the vector on which the data point projects orthogonally.

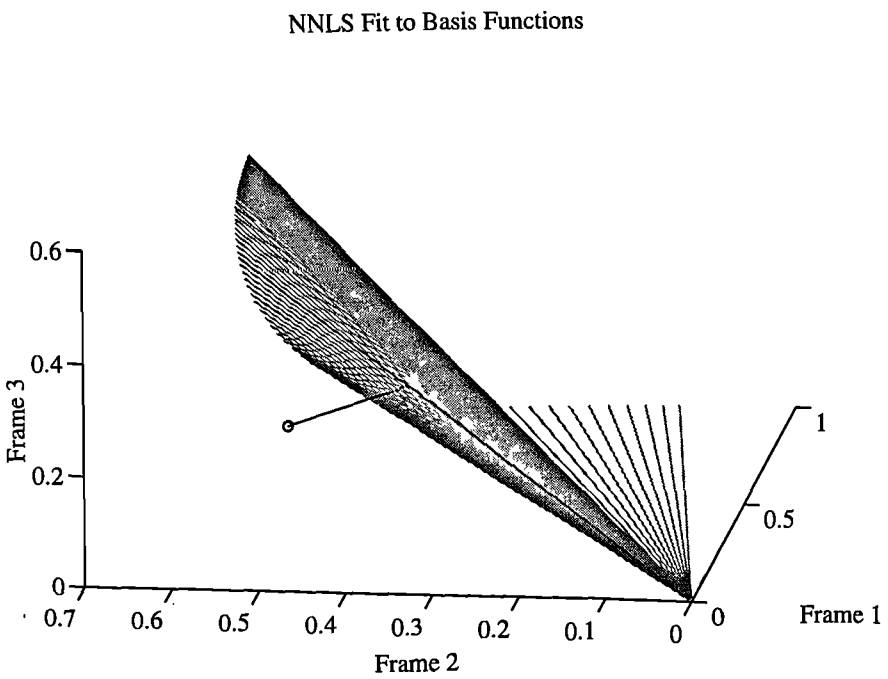

Figure 6.4: Solution to NNLS problem

The nonnegative least squares algorithm [110] determines the least sum of squares solution given the nonnegativity constraint on the parameter vector. The algorithm proceeds by maximising the dual problem which corresponds to a minimisation of the primal problem [110], these are given by

$$\begin{array}{llll} Primal & J = (Ax-b)^T(Ax-b), x > 0 & minimise & J \\ Dual & w = -\frac{\partial J}{\partial x} = -2A^T(Ax-b), w \leq 0 & maximise & w \end{array} \tag{6.2}$$

The dual gives the derivative of the sum of squares with respect to the introduction of each component. The algorithm proceeds by calculating the dual vector, w, and introducing a component whose dual value is a maximum. The problem is then solved for just this component and the dual is recalculated. A new component is then introduced in the same manner. However, if at any stage the introduction of any components causes the regular least squares fit to produce negative coefficients, these components are eliminated such that the positivity constraint is upheld. This process continues until the introduction or deletion of any component can only increase the residual sum of squares. At this point the algorithm stops and a local minimum has been found. The following algorithm is taken from Lawson and Hanson [110].

NNLS(A,m,n,b,x,w,z,P,Z) [110]

1 *Set* $P = \phi$, $Z = \{1, 2, \ldots, n\}$, *and* $x = 0$.
2 *Compute the* $n-$ *vector* $w = A^T(b - Ax)$.
3 *If the set* Z *is empty or if* $w_j \leq 0$ *for all* $j \in Z$, *go to Step* 12.
4 *Find an index* $t \in Z$ *such that* $w_t = max\{w_j : j \in Z\}$.
5 *Move the index* $t \in Z$ *from set* Z *to set* P.
6 *Let* A_p *denote the* $m \times n$ *matrix defined by*
$$Column\ j\ of\ A_p = \begin{cases} column\ j\ of\ A & if\ j \in P \\ 0 & if\ j \in Z \end{cases}$$
Compute the $n-$ *vector* z *as a solution of the least squares problem* $A_p z \cong b$.
Note that only the components z_j, $j \in P$, *are determined by this problem.*
Define $z_j = 0$ *for* $j \in Z$.
7 *If* $z_j > 0$ *for all* $j \in P$, *set* $x = z$ *and go to step* 2.
8 *Find an index* $q \in P$ *such that* $\frac{x_q}{x_q - z_q} = min\{\frac{x_j}{x_j - z_j} : z_j \leq 0, j \in P\}$.
9 *Set* $\alpha = \frac{x_q}{x_q - z_q}$.
10 *Set* $x = x + \alpha(z - x)$.
11 *Move from set* P *to set* Z *all indices* $j \in P$ *for which* $x_j = 0$. *Go to step* 6.
12 *Computation Complete.*

6.3.3 Kuhn Tucker Conditions

The NNLS algorithm terminates with a solution vector x which satisfies

$$x_j > 0, \ j \in P \tag{6.3}$$

$$x_j = 0, \ j \in Z \tag{6.4}$$

and x solves the least squares problem

$$A_p x \cong b \tag{6.5}$$

The dual vector w satisfies

$$w_j = 0, \ j \in P \tag{6.6}$$

$$w_j \leq 0, \ j \in Z \tag{6.7}$$

and

$$w = A^T (b - Ax) \tag{6.8}$$

Equations (6.3,6.4,6.6,6.7, and 6.8) constitute the Kuhn Tucker conditions [110]. The essential point is that the dual is the (negative of the) gradient vector of the residual sum of squares, and, given that this is less than or equal to zero no component can be introduced without increasing the residual sum of squares. Hence in parameter space any perturbation of the solution x causes an inferior fit and therefore x is a local minimum (for proof see [110], pg 160).

6.4 A Well Defined Problem

A problem exists concerning whether the solution obtained is unique due to the underdetermination of the system (see Figure (6.1)). This section provides a proof to show that the problem is well defined. The proof is based on an identifiability framework and considers whether a given spectrum obtained from the described form of spectral analysis is a unique solution to the problem.

Spectral analysis concerns the solution of an underdetermined system of linear equations. If no constraints are employed the method yields a solution which is unidentifiable (as the number of equations is less than the number of unknowns) and infinitely many solutions exist. However this is not the case with the introduction of a non-negativity constraint. This section gives conditions such that the problem postulated is well defined, and yields a unique solution.

To establish a condition for uniqueness the system is considered for a bolus input and perfect input-output data. This gives rise to a problem whereby a non-negative sum of exponentials is to be fitted to the system's impulse response function.

$$ImpulseResponse(t_k) = \sum_{i=1}^{n} \alpha_i e^{-\beta_i t_k} \tag{6.9}$$

given $k \in \{1, 2, ..., N\}$ for some $N \in \mathbf{N}$ subject to the non-negativity constraint

$$\alpha_i \geq 0$$

6.4.1 Uniqueness of the Solution

The problem is constructed in an identifiability context and is examined for the case where perfect data is available. The proof considers a spectrum that has been obtained from the algorithm and determines whether this solution is uniquely (globally) identifiable.

Brief Overview of Proof

- Lemma 1. Show that for rational β's any β can be constructed as the product of a natural number and a chosen constant. The proof's restriction to rational values for β is consistent with a computer implementation.

- Lemma 2. Show that number of positive real roots of a polynomial is conditional on the number of sign changes in the polynomial (Descartes Rule

of Signs).

- Theorem 4. Show that a sum of exponentials can be mapped onto a polynomial and deduce that no positive sum of exponentials can be made up from any other under appropriate conditions. The theorem considers the maximum number of time points for which two different positive sums of exponentials can be equal.

The following two results will be required.

Lemma 1 *Given* $B = \{\beta_i : \beta_i \in \mathbf{Q}$ *for* $i = 1, \ldots, N\}$, *then there exists*

$$\varepsilon \in \Re^+ and\, n_i \in \mathbf{N}\ such\ that \beta_i = n_i \varepsilon\ for\ i = 1, \ldots, N.$$

Proof *Choose* $\varepsilon \in \Re^+$ *to be the greatest common divisor (GCD) for all* $\beta \in B$.

$$\varepsilon = GCD(\beta)$$

Hence $\beta_i = n_i \varepsilon$ *for all* i.

Lemma 2 Descarte's Rule of Signs [111]
Given a polynomial of the form,

$$a_n \lambda^n + a_{n-1} \lambda^{n-1} + \ldots + a_1 \lambda + a_0 = 0 \tag{6.10}$$

Let S be the number of sign changes in the sequence of coefficients $\{a_n, a_{n-1}, \ldots, a_1, a_0\}$ *ignoring any which are zero. Then there are at most S roots of (6.10) which are real and positive. Furthermore there are either S,S-2,S-4,... positive real roots of the polynomial.*

Theorem 4 *Given that the impulse response is a realisation for some* $m < \frac{N}{2}$,

$$\sum_{i=1}^{m} \alpha_i e^{-\beta_i t_k} \tag{6.11}$$

then

$$\sum_{i=1}^{m} \alpha_i e^{-\beta_i t_k} \neq \sum_{j=1}^{n} \gamma_j e^{-\delta_j t_k} \tag{6.12}$$

for any given $k \in \{1, 2, ..., N\}$, *and subject to the non-negativity constraint* $\alpha_i, \beta_i, \gamma_j, \delta j > 0$, *except the degenerate solution* $m = n, \alpha_i = \gamma_j, \beta_i = \gamma_j$ *for all* i, j.

Proof *To prove the Theorem by contradiction, let us assume there exists an* $m < \frac{N}{2}$ *such that,*

$$\sum_{i=1}^{m} \alpha_i e^{-\beta_i t_k} = \sum_{j=1}^{n} \gamma_j e^{-\delta_j t_k}. \tag{6.13}$$

Define $f(t_k)$ *by*

$$f(t_k) = \sum_{i=1}^{m} \alpha_i e^{-\beta_i t_k} - \sum_{j=1}^{n} \gamma_j e^{-\delta_j t_k} = 0 \tag{6.14}$$

Using Lemma 1, define $\varepsilon \in \mathbf{Q}$ *such that*

$$0 < \varepsilon = GCD\,(\beta, \delta)$$

and such that for all i, j

$$\beta_i = n_i \varepsilon \quad for \;\; some\, n_i \in \mathbf{N}$$

and

$$\delta_j = n_j \varepsilon \quad for \;\; some\, n_j \in \mathbf{N}.$$

Let

$$\lambda(t_k) = e^{-\varepsilon t_k}$$

which implies that

$$e^{-\beta_i t_k} = \lambda(t_k)^{n_i} \tag{6.15}$$

$$e^{-\delta_j t_k} = \lambda(t_k)^{n_j}. \tag{6.16}$$

Substitution of equations (6.16) and (6.16) into equation (6.14) yields

$$f(t_k) = g(\lambda) = \sum_{i=1}^{m} \alpha_i \lambda(t_k)^{n_i} - \sum_{j=1}^{n} \gamma_j \lambda(t_k)^{n_j} = 0 \tag{6.17}$$

such that for each $i, j, n_i, n_j \in \mathbf{N}$ *and so equation (6.17) is a polynomial in* λ. *Using Lemma 2, the polynomial* $g(\lambda) = 0$ *has at most* $2m$ *changes of sign, which implies* $g(\lambda) = 0$ *has at most* $2m$ *positive real roots of the form*

$$\lambda(t_k) = e^{-\epsilon t_k}$$

This implies that

$$\lambda(t_k) \in \Re^+ \ if \ and \ only \ if \ t_k \in \Re$$

and

$$\lambda(t_k) \notin \Re^+ \ if \ and \ only \ if \ t_k \notin \Re$$

Hence $f(t_k) = 0$ *is satisfied for at most* $2m$ *distinct values of* t_k.
Therefore if $m < \frac{N}{2}$ *then*

$$\sum_{i=1}^{m} \alpha_i e^{-\beta_i t_k} \neq \sum_{j=1}^{n} \gamma_j e^{-\delta_j t_k} \tag{6.18}$$

except for the degenerate case $m = n, \alpha_i = \gamma_j, \beta_I = \gamma_j$ *for all* i, j.

Remark : This Theorem guarantees that, if a solution to the spectral analysis problem with N data points has m components and $m < \frac{N}{2}$ then the solution is unique.

6.4.2 Example

Flumazenil is a ^{11}C-labelled PET radioligand for the study of the central benzodiazepine site (CBZR) in humans and primates [48] [85]. In PET studies, as carried out in the MRC Cyclotron Unit, Hammersmith Hospital, the drug is intravenously injected for a short period (approximately 20 seconds), and during the scan the arterial blood is sampled once a second. The arterial blood curve is converted into a plasma activity curve and corrected for plasma metabolites (see Chapter 5) to give the input function for the tracer kinetic analysis (Figure (6.5)). The scan contains 28 time frames of data, these frames becoming longer as the scan progresses due to the slowing of the dynamics in the data and the loss of counts as a result of the isotope's decay. A region of interest (ROI) is then applied to the dynamic tissue data to obtain a time activity curve for the particular region. The ROI used in this particular example contains 36 pixels and the ROI covers $1.45cm^2$ $(36(2.006)^2mm^2)$. This gives us a time activity curve containing 28 data points, i.e. $N = 28$.

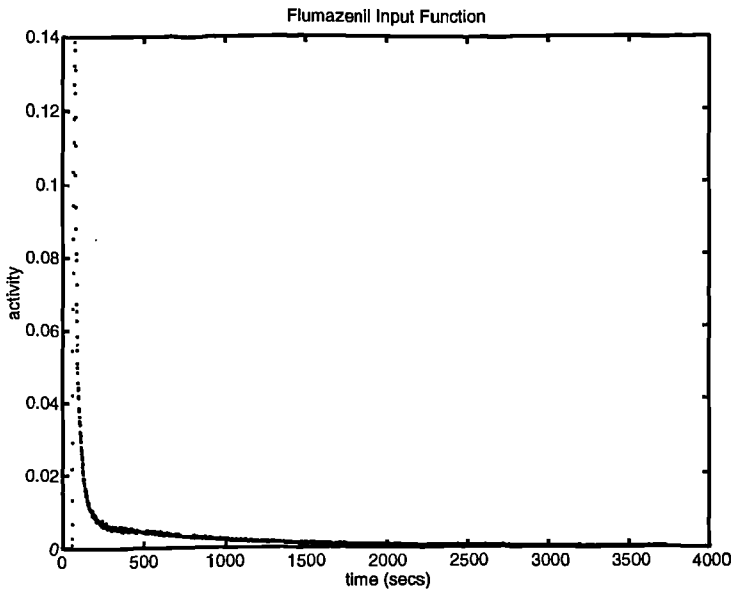

Figure 6.5: Flumazenil metabolite corrected plasma input function

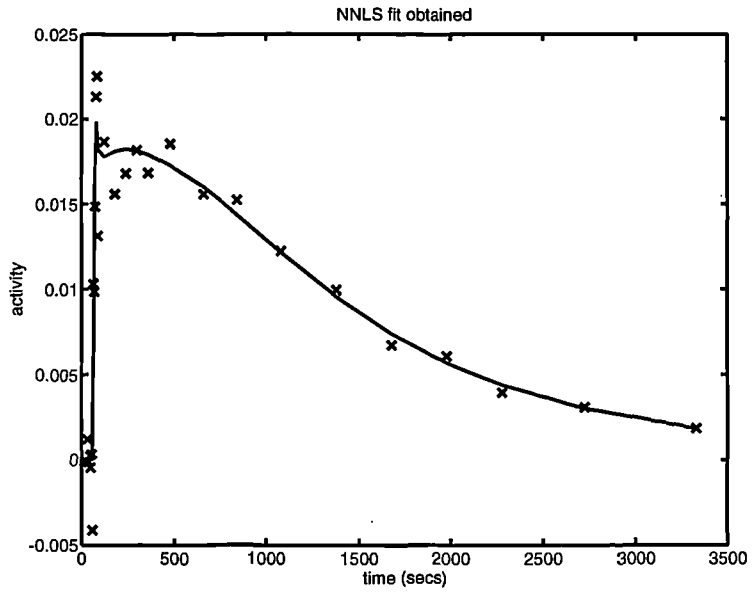

Figure 6.6: PET data (x) and spectral analysis solution (-)

Figure (6.6) shows the spectral analysis solution to the measured tissue data and Figure (6.7) gives the spectrum of kinetics obtained. The fitting procedure pulls out 5 components for the impulse response function. This is effectively three exponentials because two pairs are observed for adjacent β values, which is the result of the algorithm trying to pick an exponential in between the discretised values.

The data consists of 28 points (N) and the solution has 5 components (m), so the inequality $m < \frac{N}{2}$ is satisfied and hence, by the Theorem, the solution is unique. The spectrum obtained can be interpreted as a two compartment model with a blood volume component. This is consistent with the known kinetics of flumazenil in the brain [109].

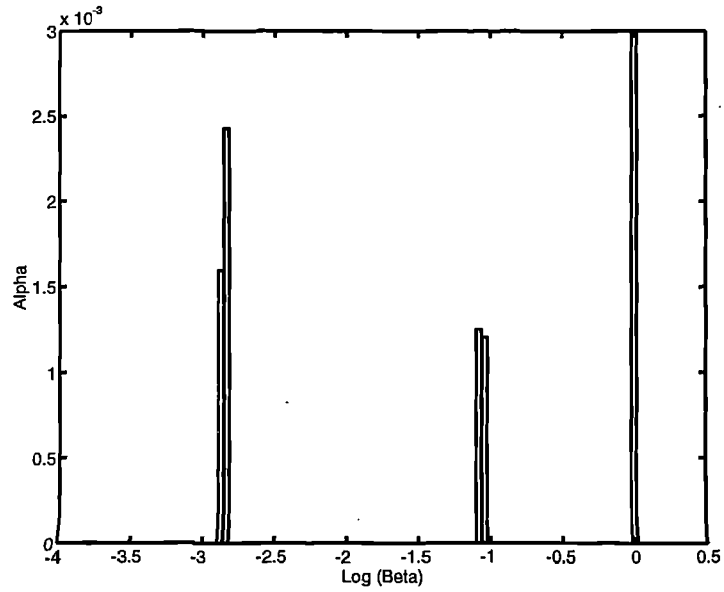

Figure 6.7: Spectrum defined by the solution to the NNLS fit

6.5 Extensions of Spectral Analysis

6.5.1 Basis Functions for Displacement Studies

Flumazenil is a ligand which binds to benzodiazepine receptors in the brain and this binding can be reduced by introducing a competing non-radioactive ligand into the system [83]. The endogenous or exogenous ligand competes for the same receptor type lowering the permissible binding of the radiolabelled PET ligand and causes a decrease in the tracer's signal.

Experiments were performed using an adapted whole body gamma counter [112]. Two detectors were wired in coincidence above and below the patient's head allowing for the acquisition of a whole head tissue time course. Due to the sensitivity of the large gamma detectors and the lack of tomographic information, counts thus being summed from the whole volume of interest (head), it was possible to obtain highly accurate time courses for very low doses of administered radioactivity ($\sim$ 80μCi). The system has a very high temporal resolution and the spatial resolu-

tion is limited to the number of detectors [113]. High temporal resolution results from the trade-off in spatial resolution. The head curve data is acquired every 5 seconds. Initially labelled flumazenil is administered and, after 30 minutes, an exogenous dose of cold flumazenil is injected to displace the signal.

Method

A representative ^{11}[C]flumazenil input function was calculated from a population of (n=32) plasma metabolite corrected input functions (no increase in plasma concentration was observed after displacement in similar PET studies with arterial sampling). Flumazenil's kinetics in the brain can be approximated by a single compartment with specifically bound, non-specifically bound and free ligand compartments all equilibrating quickly [109]. The system characteristics are allowed to change at the time of displacement and the problem is analysed by constructing a set of displaced basis functions, given by

$$BF = \begin{cases} \sum_{i=1}^{n} e^{-k_{2_i} t_k} & if\ t_k < t_d \\ \sum_{i=1}^{n} e^{-k_{2_i} t_d} e^{-k_{2_i} DF(t_k - t_d)} & otherwise \end{cases} \tag{6.19}$$

where $i = 1, \ldots, 100$ and k_{2_i} is chosen in a logarithmic range between the fastest and slowest possible dynamics $1 > k_{2_i} > .0005663$. In this system DF is a displacement factor which accounts for the change in the system characteristics and t_d is the time of displacement. If $DF = 1$ there is no displacement and the basis set corresponds to using a set of exponentials as described earlier in this Chapter. When $DF > 1$ the basis set describes a displaced system.

The system corresponds to generating a model of heterogeneous single compartments, Figure (6.8). The model makes the assumption that all compartments are displaced by the same fraction. This may not always be the case, however the model approximates the overall behaviour of the system.

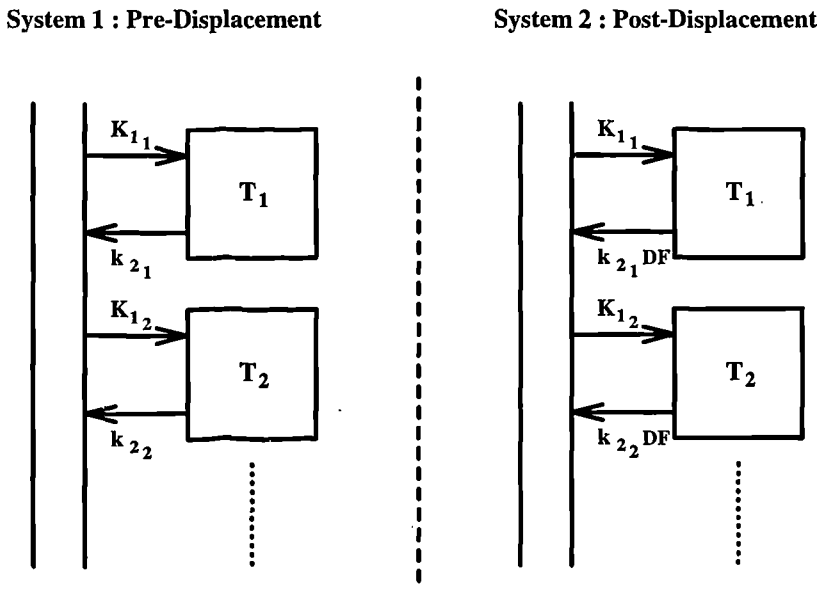

Figure 6.8: Displaced system structure

where

T_i	-	the i th tissue compartment
K_{1_i}	-	the delivery rate constant for compartment i
k_{2_i}	-	the efflux rate constant for compartment i

The volume of distribution of system 1 is given by,

$$VD_1 = \sum_{i=1}^{n} \frac{K_{1_i}}{k_{2_i}} \tag{6.20}$$

and the volume of distribution of the second system is defined by,

$$VD_2 = \sum_{i=1}^{n} \frac{K_{1_i}}{DFk_{2_i}} \tag{6.21}$$

and hence the following relation is obtained,

$$\frac{VD_1}{VD_2} = DF. \tag{6.22}$$

Using the approximate change in Volume of Distribution, an index of occupancy can be obtained. The occupancy represents the fraction of sites which are filled by the exogenous dose of cold flumazenil. The occupancy index is calculated as,

$$Occ = \frac{VD_1 - VD_2}{VD_1} = 1 - \frac{1}{DF} \tag{6.23}$$

Interpreted in a compartmental framework the system corresponds to a sum of n single compartments with influx rates K_{1_i} and efflux rates k_{2_i}. At the time of displacement the system's characteristics change; the influx remains constant but the efflux changes by a factor equal to DF. When $DF > 1$ the basis functions possess a "kink" and allow for the description of a displaced system. Figure (6.9) illustrates a set of basis functions with a displacement factor $DF = 2$.

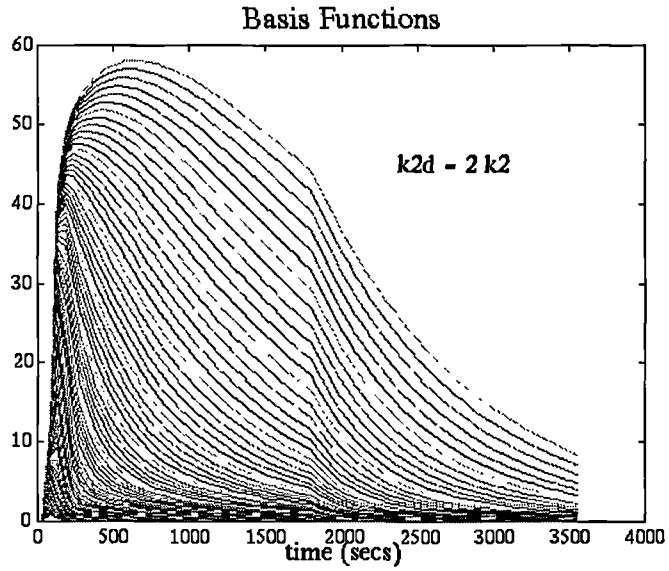

Figure 6.9: Basis functions for displacement study

A golden ratio search [105] is employed to find the value of DF which minimises the least sum of squares fit to the data. The approach optimises DF within the range $1 \leq DF \leq 10$. An example of a fit obtained to a particular data set is shown in Figure (6.10). The data is integrated over time intervals of 50 seconds to reduce the size of the basis function matrix without a significant effect on the solution.

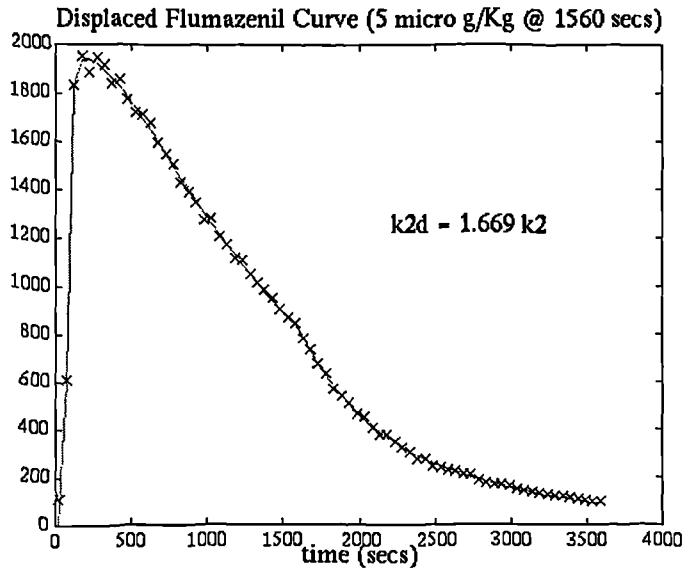

Figure 6.10: Typical fit (-) to displaced head curve data (x)

Results

A cohort of 12 patients was considered with 8 patients each receiving a different dose of cold flumazenil, $\{2.5, 5, 7, 10, 12.5, 15, 20, 30\mu g/kg\}$, at 20-30 mins after the injection of the radiotracer. Four studies with no displacement were used to calculate a baseline value for the occupancy index ($Occ = .039 \pm .011(1sd)$). Figure (6.11) illustrates the occupancy indices obtained from the eight doses of cold flumazenil. The index of occupancy is plotted against the normalised dose illustrating a saturation effect. It is evident that not all the signal can be displaced and this is because some of the signal represents non-specifically bound ligand.

6.5.2 Discussion

This chapter has presented two novel additions to spectral analysis. The first, a theoretical consideration, is a proof which gives conditions under which a unique solution is guaranteed. The second, an application, extends the original technique of Cunningham and Jones [34] to take account of systems involving displacement

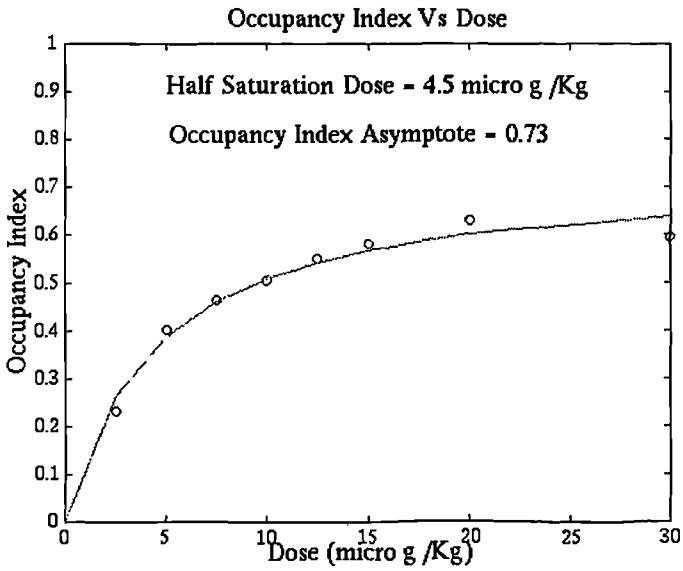

Figure 6.11: Plot of dose against occupancy index for [^{11}C]flumazenil displaced with cold flumazenil

of the labelled compound. Another basis set with useful properties is $te^{-\beta t}$, this basis set allows for a different range of kinetic behaviour for our system response which the traditional set of exponentials prohibits. It allows for impulse response functions whose initial values are zero. The method of spectral analysis may also be extended to consider the case of two input functions. In this case both the inputs are convolved with a set of exponentials and then fitted to the data. The scheme of this approach as might be applied to a system involving metabolites is shown in Figure (6.12). This novel approach is applied to ^{11}[C]thymidine in Chapter 9 to try and predict the parent and metabolite contributions to the tissue signal.

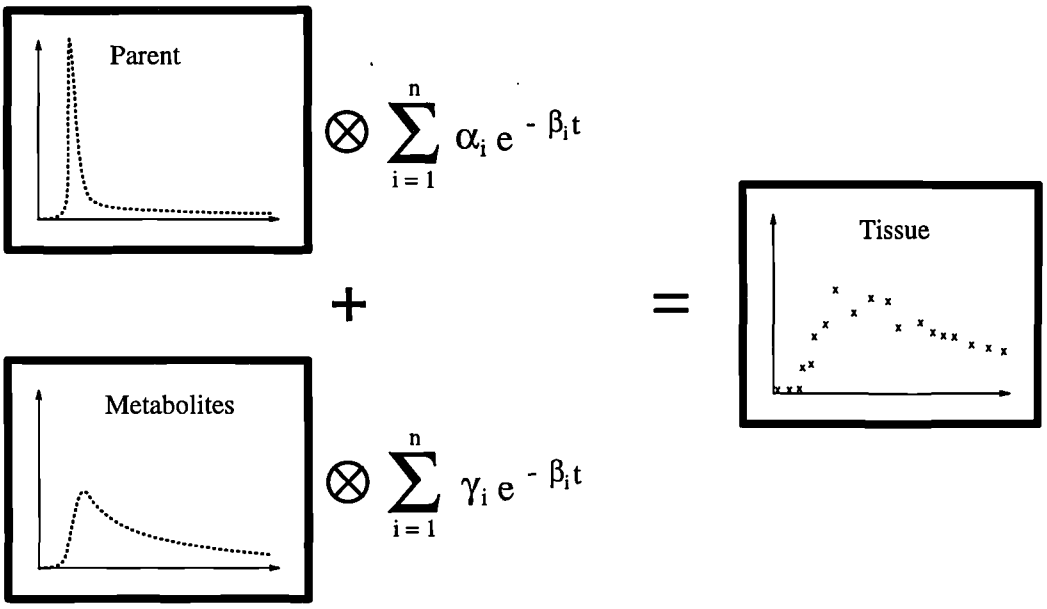

Figure 6.12: Multiple input spectral analysis applied to a system with labelled metabolites in plasma and tissue

Chapter 7

[^{11}C]Thymidine

7.1 Overview

In this chapter, observations of data derived from clinical [^{11}C]thymidine studies are presented. The behaviour of the tracer is investigated in tumours and it is seen that some encouraging results are obtained. Metabolic breakdown of [^{11}C]thymidine in plasma and tissue during the course of the study contributes to the PET signal and as a result these metabolites must be defined to allow adequate interpretation of the data. This is studied in detail in the two subsequent Chapters.

7.2 Introduction

[^{11}C]Thymidine is currently under investigation as an *in vivo* marker of cell proliferation in tumours [114] [115] [116] [117] [118]. It is proposed that the tracer [^{11}C]thymidine is taken up into proliferative tissues and incorporated into DNA, providing a measure of DNA synthesis from which cell proliferation can be inferred. To date the assessment of anti-cancer therapies rely on crude clinical response markers. The ability to measure cell proliferation in vivo would provide clinicians with a more sensitive marker of response to therapy which may

be achievable at a preclinical level. Thus allowing great individualisation of the therapeutic regime. These measures would enable the monitoring of tumours with respect to radiotherapy, anti-cancer drugs, etc.

7.3 Methods

Nine patients were scanned with [^{11}C]thymidine and an independent *ex vivo* measure of tumour proliferation was obtained. Each 1 hour thymidine scan consisted of 30 dynamic frames and the frame durations are given in Table (7.1). Following each of these thymidine scans, the tumour was removed and stained with a molecular immunology borstal 1 antibody (MIB 1) to produce a histological measure of cell proliferation [119] [120] [121]. In this case the MIB 1 index was expressed as the number of labelled cells out of a total of 2000 tumour cells counted. The MIB 1 values are shown in Table (7.2).

10	x	30	secs
5	x	60	secs
5	x	120	secs
5	x	180	secs
5	x	300	secs

Table 7.1: Frame lengths for thymidine scans

Study	p03059	p03206	p03494	p03726	p03737	p03766	p03847	p03898	p03946
MIB	839	926	167	346	1278	1503	1297	838	831

Table 7.2: MIB 1 antibody staining results from nine patients scanned with [^{11}C]thymidine

The 2-D dynamic data sets were reconstructed using filtered back-projection (Hanning filter : cut-off 0.5xNyquist frequency) and a measured attenuation correction

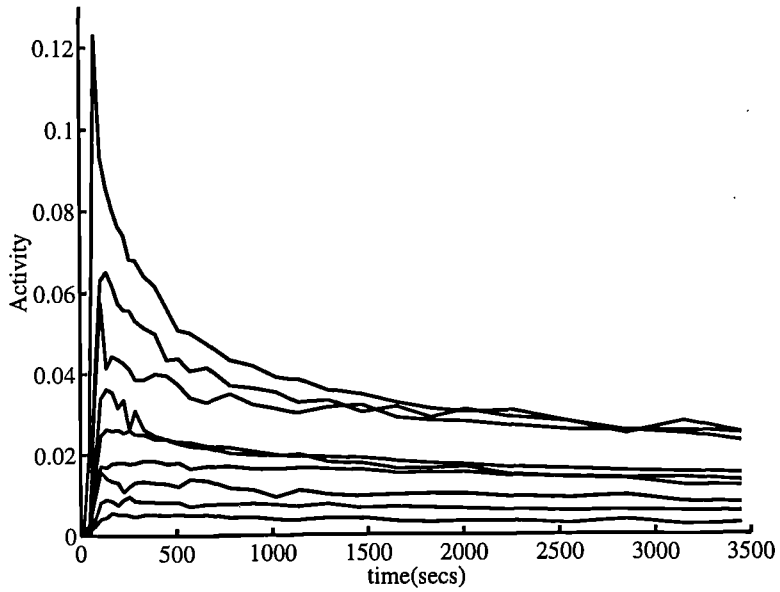

Figure 7.1: Decay-corrected tumour time activity curves from the nine [^{11}C]thymidine scans

was applied. ROI's were drawn around tumour rims on an "add" image (0-60 mins) from each of the [^{11}C]thymidine studies. These regions were then applied to the dynamic data sets and tumour time activity curves obtained. The tumour time activity curves were corrected for the decay of the isotope and are illustrated in Figure (7.1).

7.4 Results and Discussion

The terminal half-life in tissue was calculated by fitting an exponential to the tail of the tumour time activity curves (between 1800 and 3600 seconds), i.e.

$$TAC_{1800-3600}(t) = \alpha e^{-\beta t} \tag{7.1}$$

from which,

$$t_{\frac{1}{2}} = \frac{\log(2)}{\beta} \tag{7.2}$$

where $t_{\frac{1}{2}}$ is the terminal half-life of label in the tissue. The terminal tissue half-life was calculated for the nine patients and the results are tabulated in Table (7.3).

Study	β	$t_{\frac{1}{2}}$ (secs)
p03059	1.23e-04	5.62e+03
p03206	8.38e-05	8.27e+03
p03494	2.24e-04	3.09e+03
p03726	1.70e-04	4.09e+03
p03737	7.73e-05	8.96e+03
p03766	9.59e-05	7.22e+03
p03847	1.17e-04	5.91e+03
p03898	1.58e-04	4.37e+03
p03946	1.55e-04	4.46e+03

Table 7.3: Terminal tissue half-life of label in tumour for the nine patients

If, as hypothesised, [^{11}C]thymidine is retained by proliferative tissues, then the terminal tissue half-life of label may correlate with the degree of proliferation. By plotting the terminal tissue half-life of the total tumour radioactivity, it becomes apparent that the half-life of label in tissue is indeed correlated to the independent measure of cell proliferation, as shown in Figure (7.2). The correlation coefficient, 0.754, was significant ($p < 0.02$ for $n = 9$).

This result suggests increased retention of the label in highly proliferative tissues. This may reflect either increased incorporation into DNA or slower turnover of label due to higher intracellular concentrations of endogenous thymidine in highly proliferative tissues. These results illustrate the potential of [^{11}C]thymidine as a marker of cell proliferation. However, in the set of studies presented, only the behaviour of total label in tissue was analysed. To obtain a more comprehensive understanding of the mechanisms involved it is necessary to take account of the contribution of labelled metabolites to the signal. The metabolism of [^{11}C]thymidine, of which the major labelled metabolite produced is $^{11}CO_2$ is con-

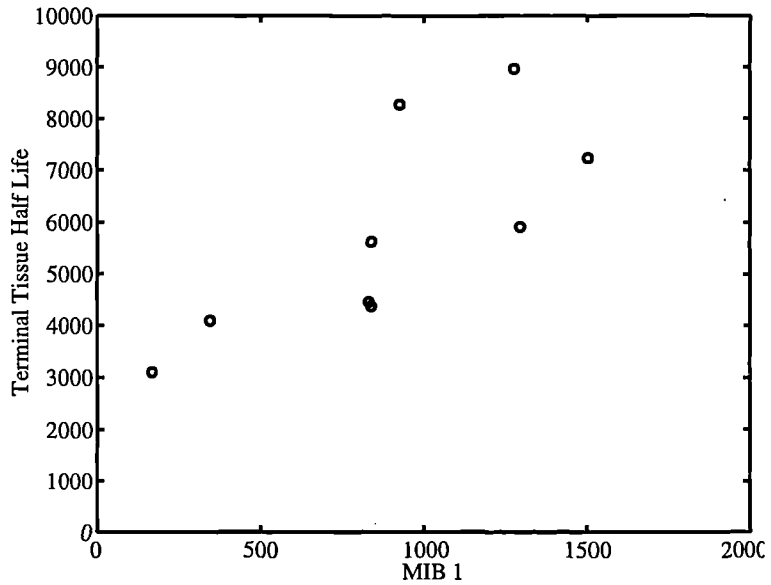

Figure 7.2: Correlation between MIB 1 and terminal tissue half-life

sidered in Chapter 9. A series of bicarbonate studies was therefore proposed in order to investigate the behaviour of carbon dioxide and enable clarification of the [^{11}C]thymidine signal. Before returning to modelling of [^{11}C]thymidine the measurement and modelling of labelled carbon dioxide is dealt with in the next chapter.

Chapter 8

Carbon Dioxide

8.1 Overview

$^{11}CO_2$ is the predominant metabolite for many ^{11}C labelled PET tracers [122]. [^{11}C]Thymidine is a typical example and is studied in detail in the next chapter. To assess the contribution of labelled carbon dioxide in the thymidine scans, a series of bicarbonate studies were proposed. These studies were to be performed in conjunction with [^{11}C]thymidine scans to enable characterisation of the carbon dioxide system and subsequent $^{11}CO_2$ correction of the thymidine data. Extra information was obtained by monitoring the expired $^{11}CO_2$ activity during these studies. In this present chapter the analysis of the CO_2 data in both the expired air and blood is described along with the calculation of tissue impulse response functions. In this chapter $^{11}CO_2$ refers to either $^{11}CO_2$ in expired air or $^{11}CO_2/H^{11}CO_3^-$ in blood (bicarbonate equilibrates rapidly with CO_2 in blood, see chemical reaction scheme (8.1)).

$$H_2O + CO_2 \rightleftharpoons H^+ + HCO_3^- \tag{8.1}$$

8.2 Methods

8.2.1 Monitoring of Exhaled Activity

A sensitive monitoring system which allows the continuous monitoring of the levels of expired $^{11}CO_2$ and CO_2 during a PET scan was developed in response to problems identified with the tracer [^{11}C]thymidine (Ranicar et al., in preparation). The expired air is sampled via a pair of soft plastic nasal prongs which are inserted into the nostrils of the patient prior to scanning. As a result a proportion of the expired air was drawn through a β^+ plastic detection chamber to monitor labelled $^{11}CO_2$ and subsequently through a capnograph to monitor the stable CO_2. Both time courses are sampled at 10 Hz providing a good characterisation of each breath.

8.2.2 Bicarbonate Scans

The data analysed here were taken from an ongoing programme of bicarbonate studies. $^{11}CO_2$ was injected intravenously as [^{11}C]bicarbonate solution over a 30 second period. The time course of $^{11}CO_2$ in the subject was monitored in expired air, blood and tissues of interest for the duration of the scan (1 hour). Tissue data were collected according to the protocol of frame lengths given in Table (8.1). A high temporal sampling rate was used initially to characterise the delivery and distribution stages, followed by longer frames to characterise the tracer uptake.

8.3 Results

8.3.1 Exhaled Activity as a Measure of Blood and Plasma Activity

Typical examples of the time courses of exhaled $^{11}CO_2$ and CO_2 are shown in Figures (8.1) and (8.2), respectively. These data were collected following intra-

1	x	30	secs
6	x	5	secs
6	x	10	secs
6	x	20	secs
6	x	30	secs
3	x	300	secs
4	x	600	secs

Table 8.1: Frame lengths for bicarbonate scans

venous administration of [^{11}C]thymidine (see Chapter 9). $^{11}CO_2$ was detected in the breath almost immediately, reflecting the rapid whole body catabolism of the parent tracer. Inspection of this type of data suggested that the "envelope" may provide a suitable description and measure of the underlying time course of $^{11}CO_2$ in the blood.

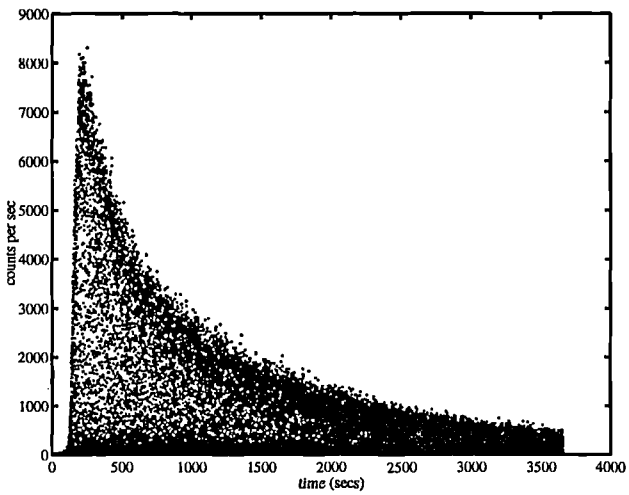

Figure 8.1: Exhaled $^{11}CO_2$ data

A magnified version of the exhaled $^{11}CO_2$ data is shown in Figure(8.3). The respiratory oscillations in the raw data are clearly defined. The raw data were characterised by examining it's power spectral density, as calculated by the Welch method [123]. The corresponding power spectral density of the exhaled $^{11}CO_2$

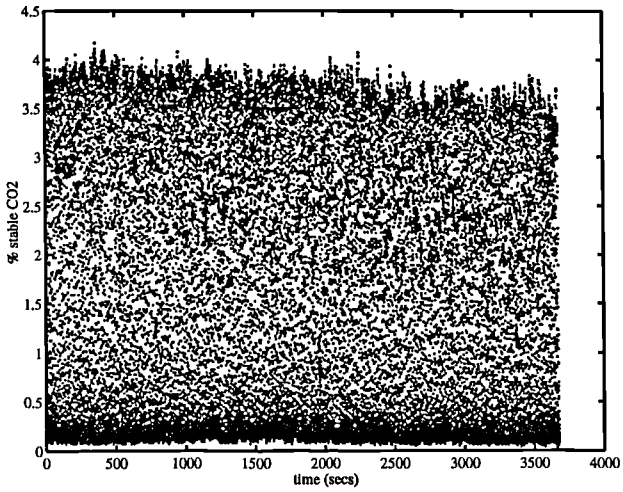

Figure 8.2: Exhaled CO_2 data

data is shown in Figure (8.4). A power spectrum defines the power of the signal at each frequency. The method provides a more robust spectral estimate than a Fourier transform of the autocorrelation function by averaging across adjacent records. The Welch method has the advantage that the variance of the power spectral density estimate tends to zero with increasing signal length. The process may be summarised as follows;

- Separate the sequence into sections of length 256.
- Multiply each section by the Hanning window (window length 256).
- Take Fourier transform of the sections.
- Accumulate results for all sections and then normalise.

The power spectrum yields two important pieces of information. Firstly, in the example shown it can be seen that the power of the signal decreases above 2 Hz, and secondly, the maximum energy of the signal occurs at a frequency of 0.186 Hz. This suggested that the raw data could be smoothed with a low pass filter with a cut-off frequency of 2 Hz. A 4th order Butterworth filter was applied and

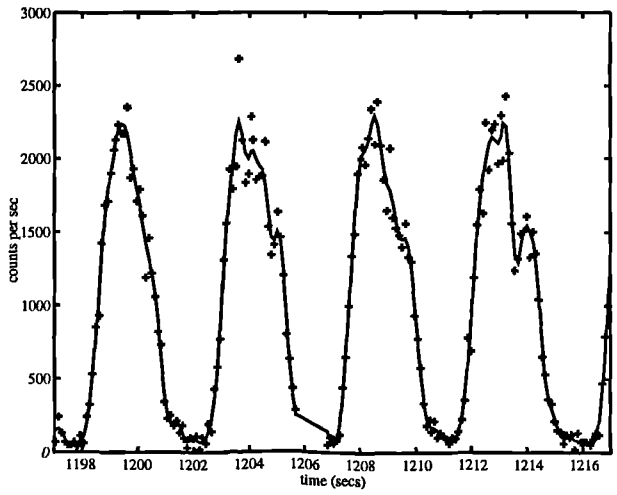

Figure 8.3: Exhaled $^{11}CO_2$ data (+) together with low pass filtered signal (-)

the smoothed time course is shown as a solid line in Figure (8.3). This allows the peak value of each breath to be used as a more robust measure of the envelope.

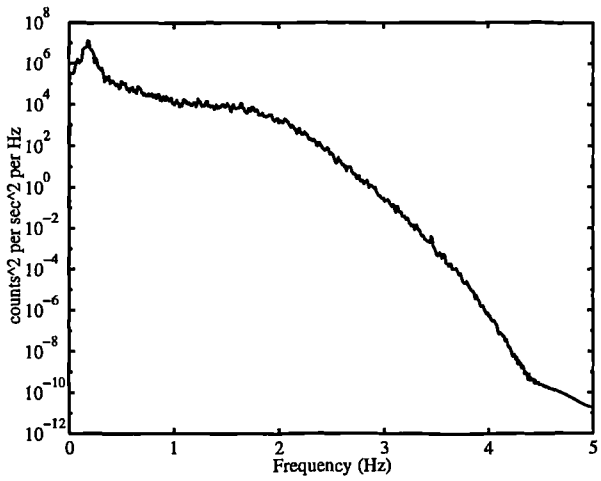

Figure 8.4: Power spectral density of labelled CO_2 data

The power spectral density may also be used to obtain the frequency for which the signal has maximal energy. This corresponds to the average respiration rate of the subject. The maximum energy of the signal has a frequency of 0.186 Hz which corresponds to a respiratory cycle of 5.40 seconds, see Figure (8.4). Having

determined the average period of the respiratory cycle, (rc), this length was used as a window with which to search the filtered $^{11}CO_2$ data for maximum. Once a maximum has been found at t the next maximum is obtained in the interval $[t+\frac{rc}{2}, t+\frac{3rc}{2}]$. This procedure may then be carried out for the whole curve to yield a peak exhaled $^{11}CO_2$ curve, see Figure (8.5). The same procedure of filtering and

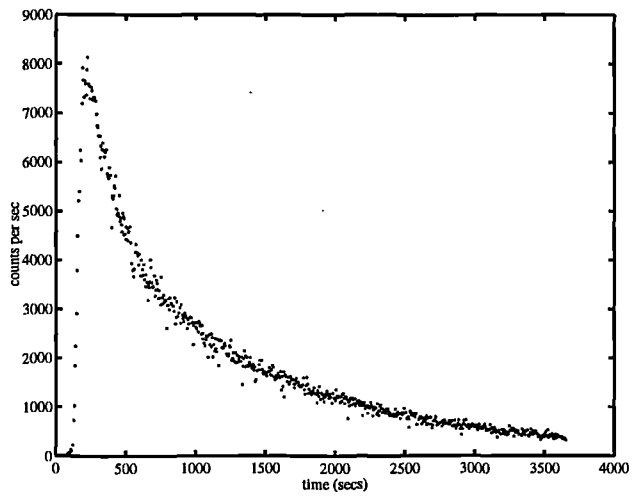

Figure 8.5: Peak exhaled $^{11}CO_2$ data

peak finding was applied to the stable CO_2 to produce a peak exhaled CO_2 curve, Figure (8.6). A point by point ratio of the two curves was then obtained. The stable CO_2 curve was used to normalise for varying breath volumes, see example in Figure (8.7), and by inspection this is a smoother curve than the labelled CO_2 (see example in Figure (8.5)).

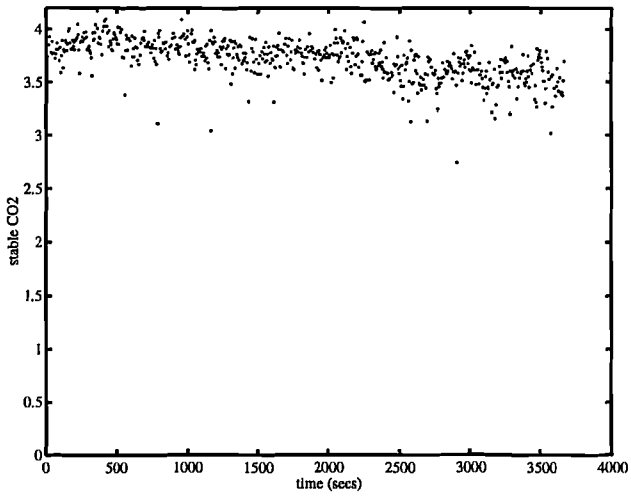

Figure 8.6: Peak exhaled CO_2 data

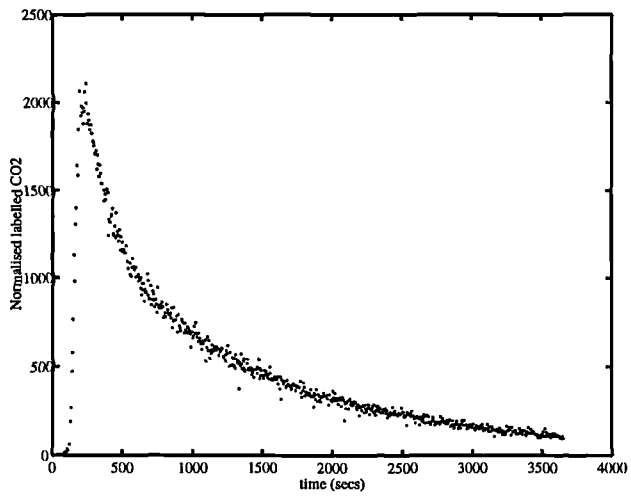

Figure 8.7: Normalised exhaled $^{11}CO_2$ data

Blood CO_2 Time Course

The next stage was to establish a relationship between the normalised exhaled $^{11}CO_2$ (e.g. Figure (8.7)) and the time course of $^{11}CO_2$ activity in blood. Experiments were therefore carried out in which the subjects received $^{11}CO_2$ alone, as an intravenous injection of ^{11}C bicarbonate. These experiments were carried out in conjunction with [^{11}C]thymidine scans as described in the next chapter.

Bicarbonate solution was intravenously injected over a 30 sec period and the time course of $^{11}CO_2$ was continuously monitored in breath, as described previously. Total radioactivity was also assayed on-line in blood, and discrete blood samples were assayed for the fraction of $^{11}CO_2$. The results for a typical scan are shown in Table (8.2).

Time (secs)	% HCO_3^-
0	100
100	99.19
309	97.81
640	97.30
1817	95.68
3614	92.32
4708	89.96

Table 8.2: Fraction of blood activity due to HCO_3^- for p4161 bicarbonate study

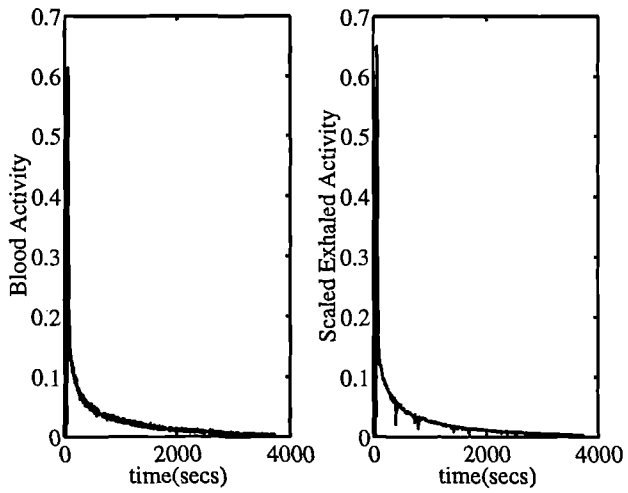

Figure 8.8: Blood activity and exhaled activity from bicarbonate scan (p4161)

The discrete measurements of the fraction of $^{11}CO_2$ in the blood allowed the creation of an $^{11}CO_2$ blood input function. A linear interpolation of the discrete measurements was employed to fit a gradual decrease in the percentage of $^{11}CO_2$

(to approximately 90% at 1 hour). The $^{11}CO_2$ blood and $^{11}CO_2$ exhaled curves were matched allowing for a time delay ($\sim$ 30 secs) between them and a simple scaling factor based on the total collected counts. The result for one example is shown in Figure (8.8). This shows that the two measurements are indeed very similar and by plotting these two measures against each other the relationship is more clearly defined, as shown in Figure (8.9). The two measures are very well matched except for small differences around the initial part of the curves. These differences may be due to a small amount of dispersion of the two measures.

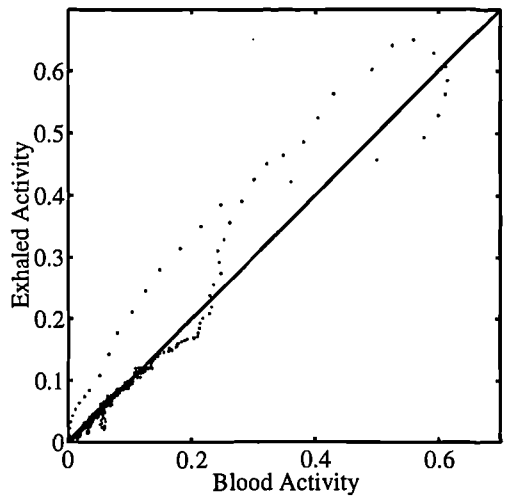

Figure 8.9: Correspondence plot of blood $^{11}CO_2$ activity against exhaled $^{11}CO_2$ activity (Line of identity is also shown)

Plasma CO_2 Time Course

Figure (8.10) shows that the relationship between total label in plasma and that in whole blood for the $^{11}CO_2$ scans was linear. Hence, a plasma $^{11}CO_2$ input function was created by multiplying the blood $^{11}CO_2$ time course by a factor of 1.62. Analysis of this equilibration in terms of a partition model and an average haematocrit of 0.4 ,as described in Chapter 5, suggests that 96% of the label was present in the plasma.

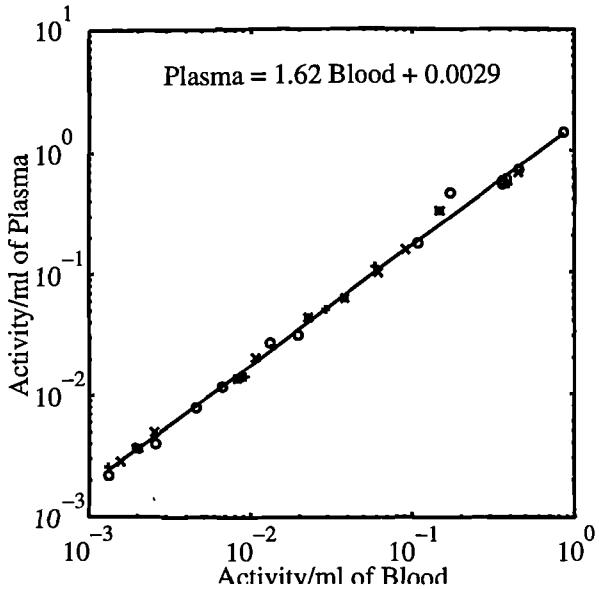

Figure 8.10: Plot of $^{11}CO_2$ activity in 1 ml of whole blood versus $^{11}CO_2$ activity in 1ml of plasma for four studies (Different symbols represent separate scans)

8.3.2 Tissue Kinetics of $^{11}CO_2$

The second purpose of the ^{11}C bicarbonate scans was to determine the unit impulse response functions of various tissues to the $^{11}CO_2$ in plasma, with a view to subsequent correction of tissue data for the presence of $^{11}CO_2$ in plasma, deriving from whole body metabolism of parent tracers such as [^{11}C]thymidine as described in chapter 9. Analysis of the plasma to tissue dynamics of CO_2 was examined using spectral analysis. An impulse response function $IRF_{CO_2}(t)$ was obtained such that,

$$Tumour_{CO_2}(t) = IRF_{CO_2}(t) \otimes Plasma_{CO_2}(t) \tag{8.2}$$

The CO_2 plasma input function was convolved with a series of exponentials and these functions, considered as basis functions, were subsequently fitted to the tissue time activity curves as described in Chapter 6. A fit obtained to a typical tumour time activity curve is illustrated in Figure (8.11). Results obtained for

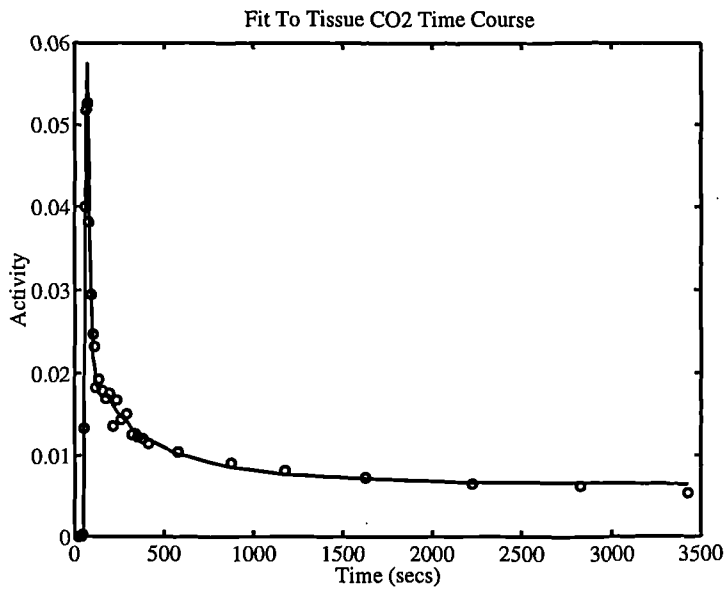

Figure 8.11: Spectral analysis fit (-) to tumour time activity curve (o) for bicarbonate data (p4161)

the four bicarbonate scans are given in Table (8.3) and the impulse responses are shown in Figure (8.12). Analysis of the spectra obtained revealed three key kinetics components. A blood volume component, a flow component and a small amount of trapping. The impulse responses returned for the tumours in either study show different behaviour. These initial results indicate the variability of the system response in tumour which may reflect differing pH of the tumours [124] [125].

8.4 Summary

The measured exhaled $^{11}CO_2$ can be transformed to give a continuous measure of $^{11}CO_2$ in blood or plasma. The application of the tumour impulse response functions will be discussed in the next chapter.

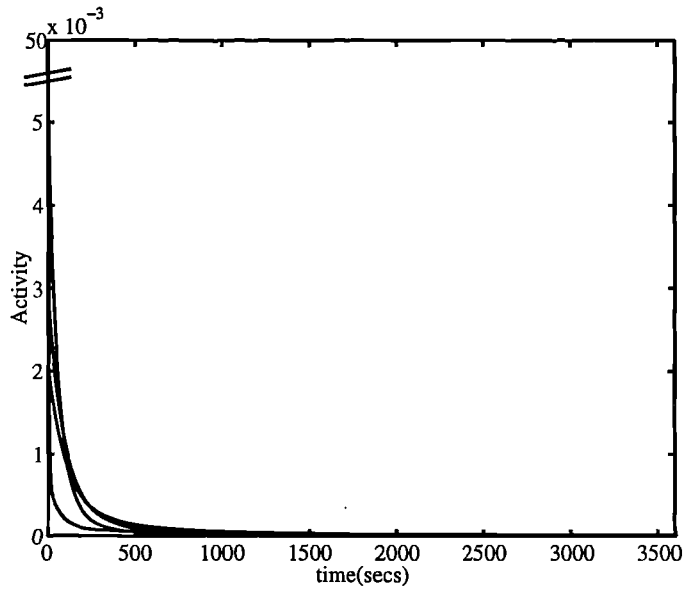

Figure 8.12: CO_2 impulse responses in tumours obtained from spectral analysis of bicarbonate data (for all four studies)

Study no.	$\beta(s^{-1})$	$\alpha(s^{-1})$
p4060	1.01e-3	4.53e-5
	2.36e-3	4.46e-5
	1.67e-2	5.85e-4
	3.94e-1	2.98e-2
p4161	5.75e-4	1.09e-5
	3.97e-3	4.56e-4
	1.22e-2	2.51e-3
p4132	5.75e-4	1.31e-5
	2.65e-3	3.26e-4
	1.09e-2	1.79e-3
	1.00	1.08e-1
p4213	5.75e-4	1.13e-5
	4.75e-3	3.14e-4
	1.76e-2	4.44e-3
	3.12e-2	2.31e-4
	1.00	7.92e-2

Table 8.3: Spectral analysis of tumour data from four bicarbonate scans

Chapter 9

Modelling of [^{11}C]Thymidine in Plasma and in Tissue

9.1 Overview

This chapter considers [2-^{11}C]thymidine as a PET tracer, its degradation pathway, modelling of plasma metabolites, and methods for analysis of the time course of label in tissues of interest. CO_2 is identified as the major metabolite in plasma and a method for correcting the tissue signal for $^{11}CO_2$ deriving from plasma is presented. This method involves a $^{11}CO_2$/[^{11}C]thymidine two scan protocol. A dual input spectral analysis was also considered.

9.2 Introduction

The principal problem inherent in the use of radiolabelled thymidine as a PET tracer in tumour studies is the contamination of signal due to labelled metabolites, not only in plasma but also in the tissues in the field of view. This contrasts with the radiolabelled ligands discussed previously, such as diprenorphine and flumazenil, whose metabolites would not be expected to cross the blood brain barrier and the tissue signal is not contaminated by metabolites [91] [92].

[^{3}H]Thymidine has been used *in vitro* and in animal work [126], [127] to investigate

tumour proliferation. On administration thymidine is either directly incorporated into DNA or rapidly metabolised. However initial studies using tritiated thymidine in mouse, rat and dog tumour models demonstrated a high tumour to tissue uptake ratio with prolonged retention in tumour [126] [128]. In mouse tumour models a significant correlation has been shown between [^{3}H]thymidine uptake and tumour grade [126]. Absolute quantification of thymidine incorporation into DNA might not be possible simply by using a plasma born tracer, because of endogenous tissue synthesis of thymidine and reutilisation of thymidine from dying cells. However it may prove of great value as a quantitative index of tumour status as suggested by the results presented in Chapter 7.

9.2.1 Labelling of Thymidine

Thymidine has been labelled with ^{11}C in two different ring positions, [2-^{11}C] [129] and [methyl-^{11}C] [130]. With thymidine labelled in the C-2, position the label follows a catenary metabolic path through thymine, dihydrothymine, N-Carbamoylisobutyrate (intermediary metabolites) before the label is lost in the form of CO_2 [122] [131], as shown in Figure (9.1). Advantages gained in labelling thymidine in the C-2 position are the presence of fewer labelled metabolites and a larger proportion of labelled DNA in tumour [114]. Further advantages include the major labelled metabolic component being $^{11}CO_2$; extra $^{11}CO_2$ measurements can be obtained via the measurement of expired labelled $^{11}CO_2$, as has been described in the previous chapter. When [^{11}C]thymidine is labelled in the methyl position more labelled metabolites are produced creating a more complex system and the proportion of labelled DNA in tumour is significantly smaller [114]. Vander Borght et al. [132] have demonstrated the advantages of using [2-^{14}C]thymidine as a potential index for liver regeneration, they also concluded that the 2-C label was preferable (no accumulation of labelled metabolites) to the methyl label (labelled

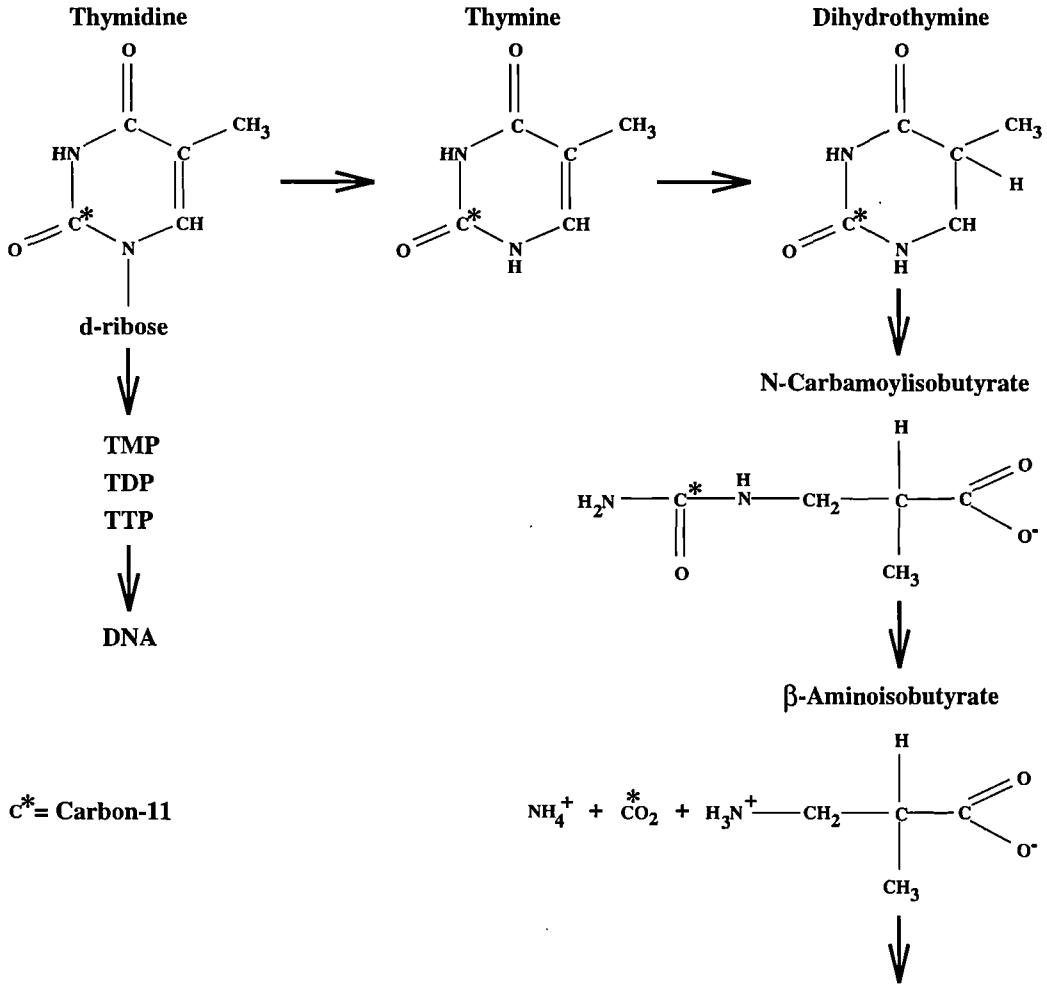

Figure 9.1: Catenary metabolism of [2-^{11}C]thymidine

metabolites in tissue). For thymidine to become a useful PET tracer it is necessary to quantify the behaviour of its metabolites in both plasma and tissue. The studies analysed in this thesis consider thymidine labelled in the 2-C position.

9.3 Modelling

$^{11}CO_2$ is the major labelled metabolite of [^{11}C]thymidine and an accurate description of its time course in tissue and plasma is essential for the quantification of the behaviour of thymidine in tumour and tissue. The purpose of this chapter is to

describe models which attempt to take into account the contribution of labelled metabolites to the plasma and tissue signals following intravenous injection of [^{11}C]thymidine. The availability of discrete measurements of the metabolites in plasma allows for correction of the plasma time course. In tissue the correction is more complicated as no chemical resolution is possible. Methods for correction must rely on the actual kinetics of thymidine and its metabolites being identifiable from the total label time course, or the performance of additional experiments. An approach to the modelling of [^{11}C]thymidine kinetics has been presented by Mankoff [133] which extends the method of graphical (or Patlak) analysis to consider systems containing labelled metabolites. This method applies if the tracer [^{11}C]thymidine is irreversibly trapped in tissue but the labelled metabolites are not.

9.4 Methods

Four [^{11}C]thymidine scans (paired with [^{11}C]bicarbonate scans) were performed. The [^{11}C]thymidine scans were initiated 10-20 minutes after the end of the bicarbonate scans (described in Chapter 8). The tracer was injected intravenously as a smooth bolus over 30 seconds. Dynamic data sets were acquired and reconstructed as described previously (section 7.3). A simultaneous measure of the expired radioactive and stable CO_2 was collected together with a continuous measure of the whole blood activity. Discrete samples of blood were removed during the scan for three purposes; namely calibration, calculation of the fraction of label in the blood due to HCO_3^- (Blood samples were divided into two. The first sample was added to NaOH to trap the $^{11}CO_2$ and this test tube was rapidly capped to avoid any loss of $^{11}CO_2$. The second sample was added to isopropanol followed by HCl to release $^{11}CO_2$. Nitrogen gas was then bubbled through each sample to help this process before both samples were assayed for radioactivity [122] [131]) and calculation of

the fraction of label due to thymidine after the removal of $^{11}CO_2$ in plasma (Blood was centrifuged and a plasma sample obtained was added to methanol to precipitate proteins. The thymidine and metabolite components were then obtained in the methanol which was injected into the HPLC system for analysis).

9.5 Results

9.5.1 Plasma Time Courses

The time course of radioactivity in blood was segmented to give time courses of [^{11}C]thymidine, [^{11}C]intermediary metabolites and $^{11}CO_2$ in plasma. A diagrammatic representation of this process is shown in Figure (9.2). A plasma $^{11}CO_2$ time course was generated using the exhaled $^{11}CO_2$ activity, the continuous measure of whole blood activity and discrete measures of the fraction of total label in blood as HCO_3^- (see section 8.3.1). A typical example of an $^{11}CO_2$ time course and fit to the discrete blood measurements is illustrated in Figure (9.3). This measure was scaled by a factor of 1.62 to give a plasma $^{11}CO_2$ time course (see section 8.3.1). The whole blood time course was converted into a plasma time course using a linear interpolation and extrapolation of the plasma to blood ratio. The $^{11}CO_2$ plasma time course was subtracted from this measure to leave just labelled thymidine and intermediary metabolites. The remaining segmentation of the plasma curve was achieved by fitting a functional form to the measured fraction of thymidine in plasma (CO_2 had been removed from the plasma samples). The functional form used was,

$$Thymidine\ Fraction(t) = \begin{cases} 1 & t < \delta \\ 1 - \frac{t-\delta}{(t-\delta)+\alpha} & t \geq \delta \end{cases} \tag{9.1}$$

This function was fitted to the metabolite data and a typical fit can be seen in Figure (9.4). This function was used as it extrapolates the thymidine fraction to zero and also fitted better than an exponential approach to a constant. This gave

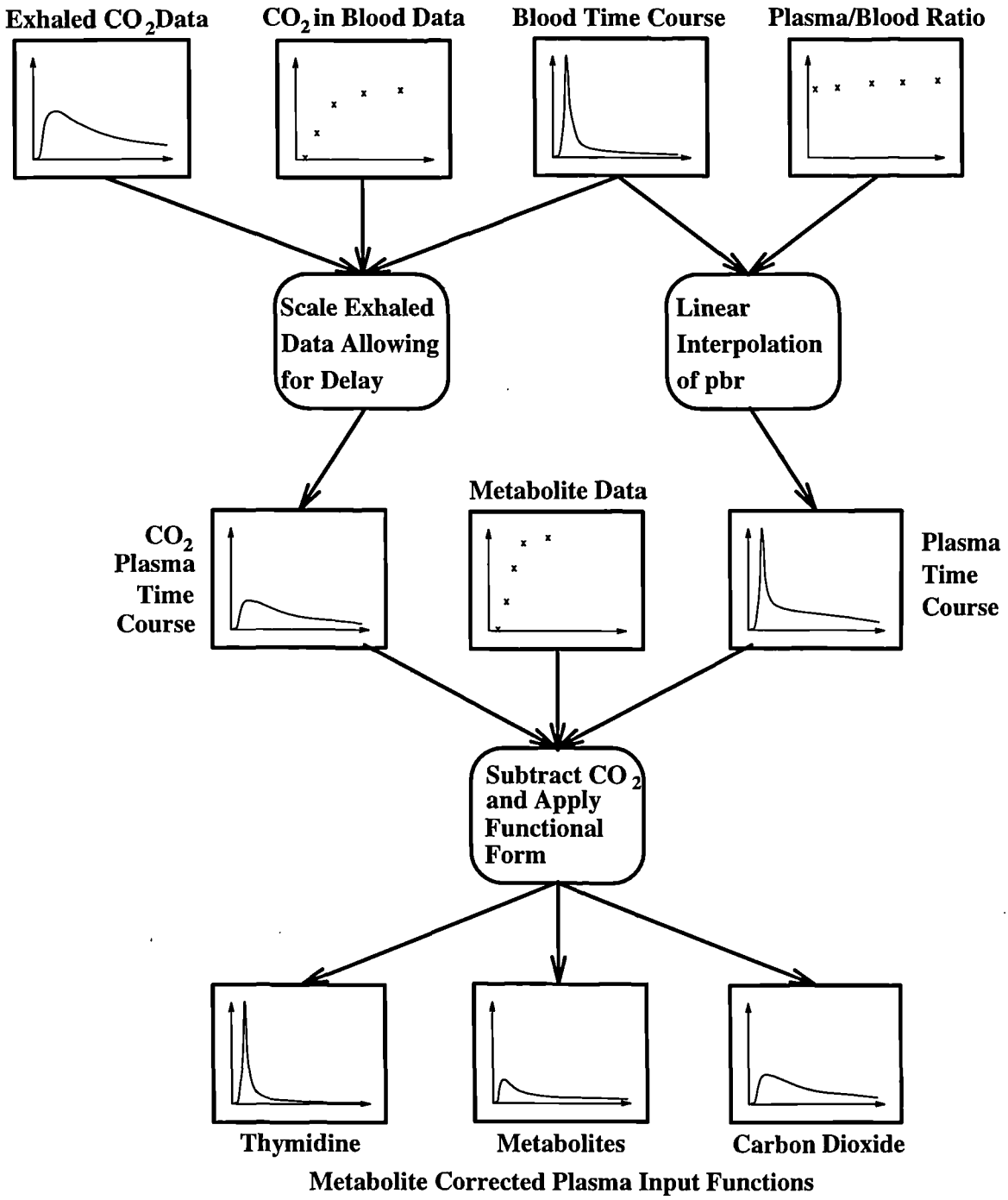

Figure 9.2: Scheme of plasma input function generation

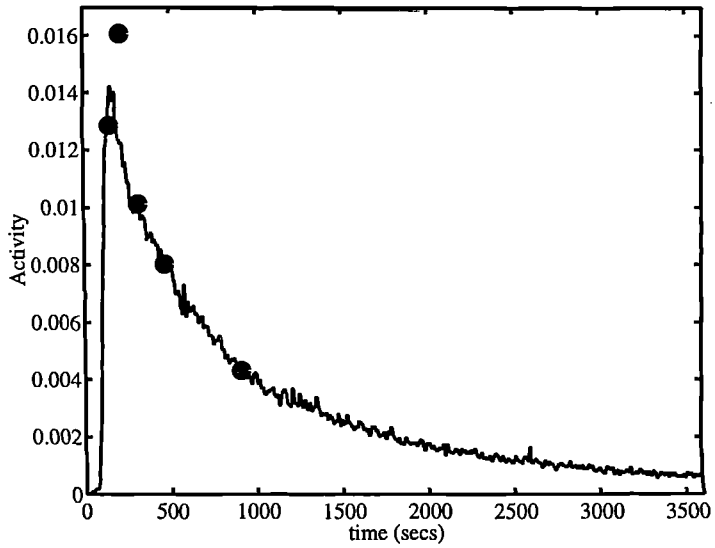

Figure 9.3: Calibration of exhaled $^{11}CO_2$ using direct blood assays

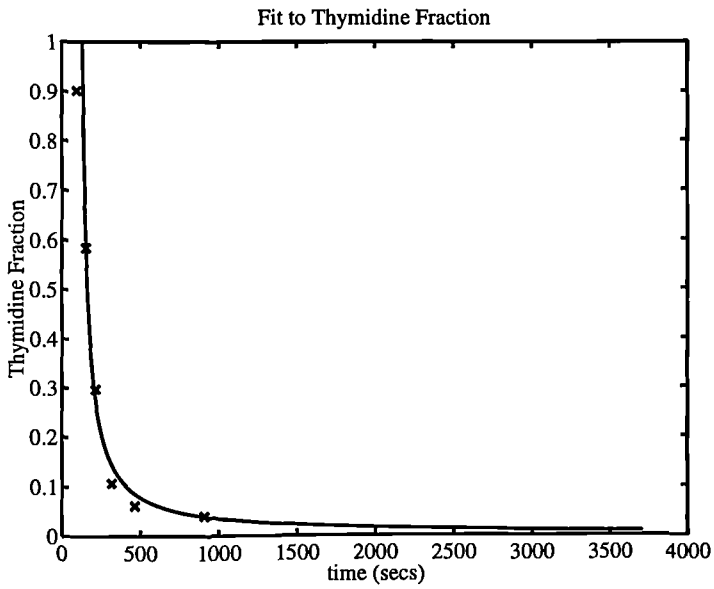

Figure 9.4: Fit to thymidine fraction in plasma (excluding CO_2) using functional form

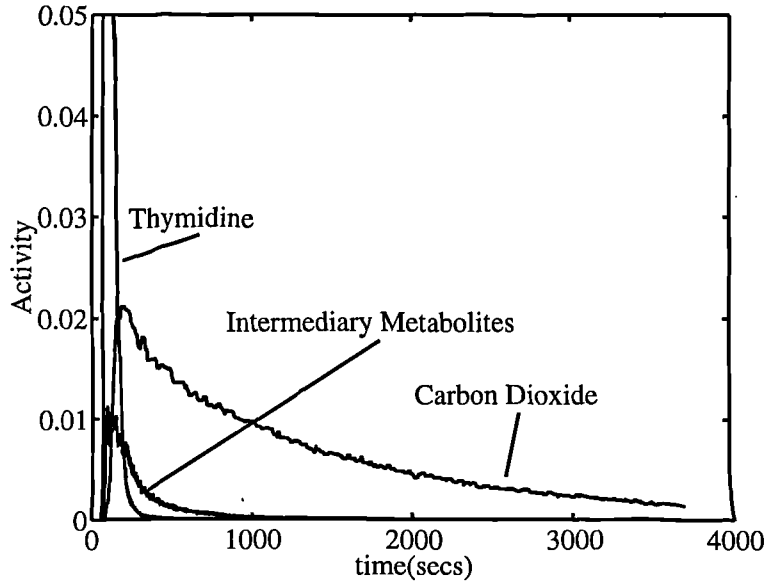

Figure 9.5: Distribution of label in plasma (p4161)

three plasma input functions; [^{11}C]thymidine, [^{11}C]intermediary metabolites and $^{11}CO_2$. Typical time courses for these plasma time courses are shown in Figure (9.5). It is obvious from these data that thymidine disappears very quickly from the plasma. After approximately 15 minutes the thymidine level in plasma is so small it is difficult to measure.

Initial investigations were carried out in an attempt to derive a compartmental relationship between [^{11}C]thymidine, $^{11}CO_2$ and [^{11}C]intermediary metabolites, the latter being considered as a single compartment. This was performed with a view to obtaining a function describing the [^{11}C]thymidine and $^{11}CO_2$ fractions in terms of the total label time course. Unfortunately, it was found that models describing such a relationship were numerically unidentifiable with a high degree of parameterisation required. However it is interesting to consider the relationship between labelled [^{11}C]thymidine and the major metabolite, labelled $^{11}CO_2$, in plasma.

9.5.2 [^{11}C]Thymidine and $^{11}CO_2$ in Plasma

To investigate the metabolism of [^{11}C]thymidine further, the plasma $^{11}CO_2$ concentration was examined as a function of the plasma [^{11}C]thymidine concentration using the method of spectral analysis. The $^{11}CO_2$ plasma time course was fitted as a linear combination of a set of basis functions, which comprised different exponentials convolved with the plasma thymidine input function. A typical fit is shown in Figure (9.6), and the components chosen by the NNLS method are presented in Table (9.1).

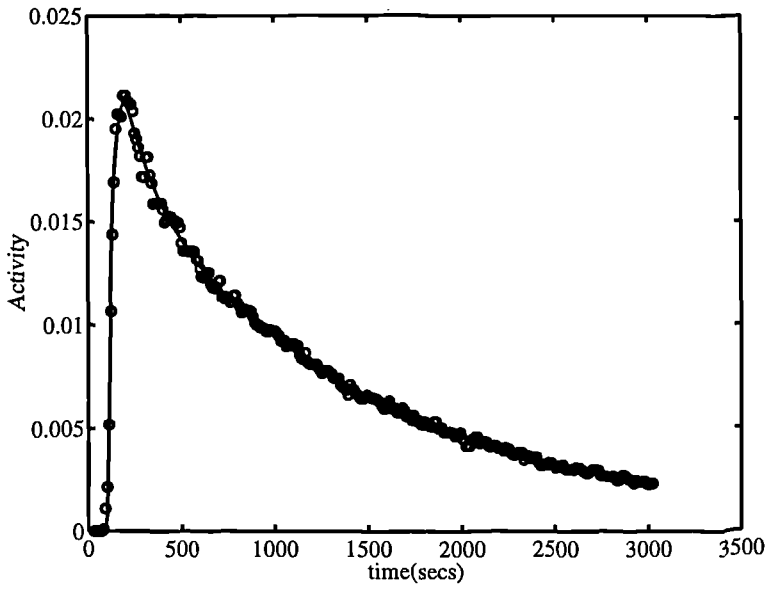

Figure 9.6: Spectral analysis fit (-) to exhaled $^{11}CO_2$ data (o) (p4161)

p4161	$\beta(s^{-1})$	$\alpha(s^{-1})$
Exhaled	6.08e-04	9.22e-04
$^{11}CO_2$	2.21e-03	1.98e-03
	1.80e-02	2.24e-03
	1.00	9.43e-03

Table 9.1: Spectral analysis of exhaled $^{11}CO_2$ as a function of plasma thymidine

The presence of fast components in the spectrum indicates that the metabolism of [^{11}C]thymidine to $^{11}CO_2$ is very rapid and this is reflected by the concentration time course of $^{11}CO_2$ in plasma.

Summary

A method has been presented for the correction of the contribution of labelled metabolites to the plasma signal. It is now necessary to consider techniques for similarly correcting the tissue signal.

9.5.3 Correction for [^{11}C]Carbon Dioxide in Tissue

The problem of identifying the tissue kinetics of [^{11}C]thymidine is complicated by the presence of the confounding metabolite signal in the tissue of interest. Resolution of the tissue signal requires kinetic models or additional experiments to be performed. To obtain additional information on the behaviour of CO_2 in tissue a set of $^{11}CO_2$ scans in conjunction with [^{11}C]thymidine scans was proposed. The scheme is shown in Figure (9.7). The bicarbonate scans allowed for plasma to tissue dynamics of CO_2 to be identified. This information was then used in conjunction with the [^{11}C]thymidine scan to remove the contribution of $^{11}CO_2$ in tissue originating from the plasma. The carry over of radioactivity from the [^{11}C]bicarbonate scans to the [^{11}C]thymdine scans was monitored using a background frame and was negligible.

Removal of CO_2 Tissue Contribution using Paired Scans

The four bicarbonate scans were analysed with spectral analysis, as described in the previous chapter, creating impulse response functions ($IRF_{CO_2}(t)$) for CO_2 in the tumours (see Figure (8.12)).

Plasma input functions were obtained for the [^{11}C]thymidine scans using the methods presented in section (9.5.1). The $^{11}CO_2$ plasma input function was convolved

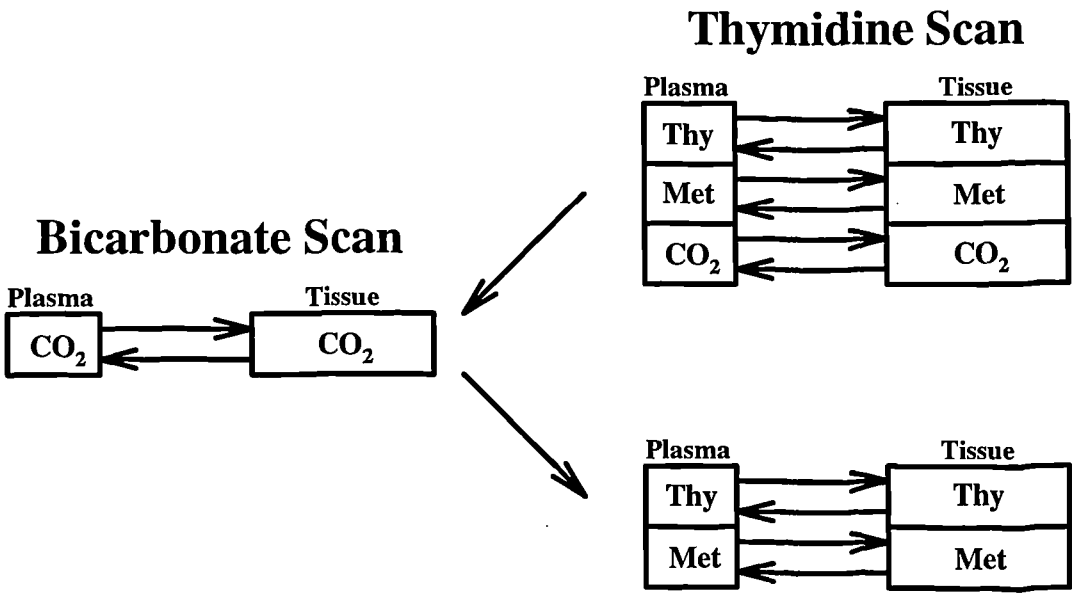

Figure 9.7: Dual scan method enabling correction of CO_2 in tissue

with the CO_2 impulse response for the system, producing the component of $^{11}CO_2$ in tissue due to the exchange of $^{11}CO_2$ between plasma and tissue. This $^{11}CO_2$ component may then be removed from the total label time course by subtraction, i.e.

$$Tumour_{CO_2Corrected}(t) = Tumour_{Label}(t) - IRF_{CO_2}(t) \otimes Plasma_{CO_2}(t) \quad (9.2)$$

The time courses of total label in tumour and the appropriate $^{11}CO_2$ corrections for the four studies are shown in Figures (9.8 - 9.11).

It is evident that the contribution of carbon dioxide to the signal is significant. The percentage contribution of carbon dioxide at 1 hour is given in Table (9.2). These results are consistent with work performed by Shields et al. in animals who found that 80% of label in animal tumours one hour post injection was accounted for by labelled DNA [114]. They also found that methyl labelled thymidine gave only 40% as labelled DNA at one hour, again demonstrating the advantages of

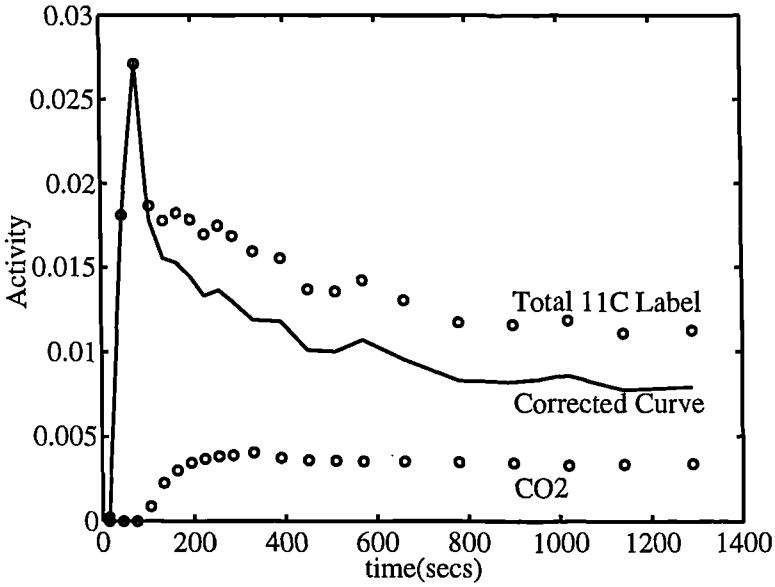

Figure 9.8: Correction of tumour time course for the presence of $^{11}CO_2$ (p4060)

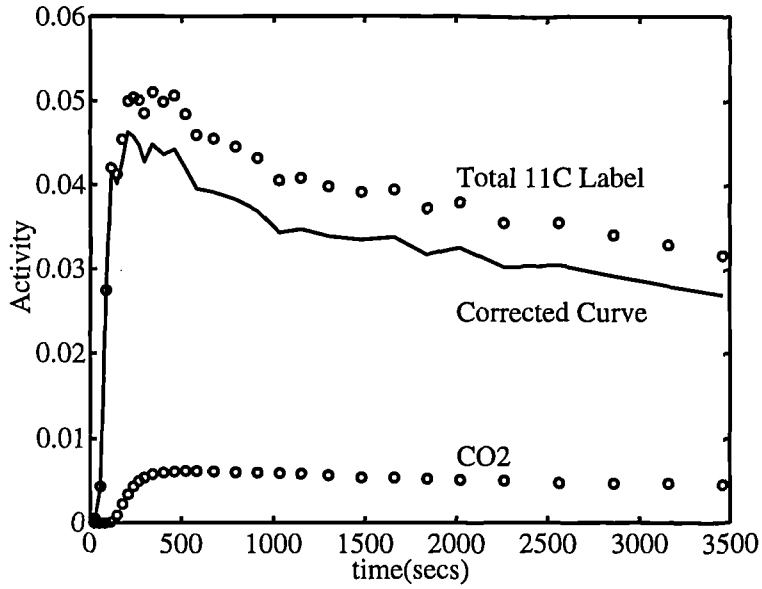

Figure 9.9: Correction of tumour time course for the presence of $^{11}CO_2$ (p4161)

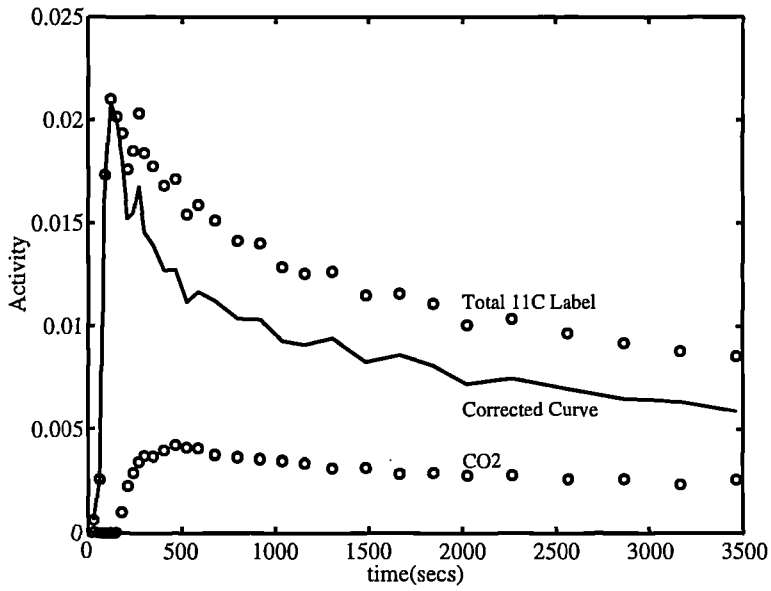

Figure 9.10: Correction of tumour time course for the presence of $^{11}CO_2$ (p4132)

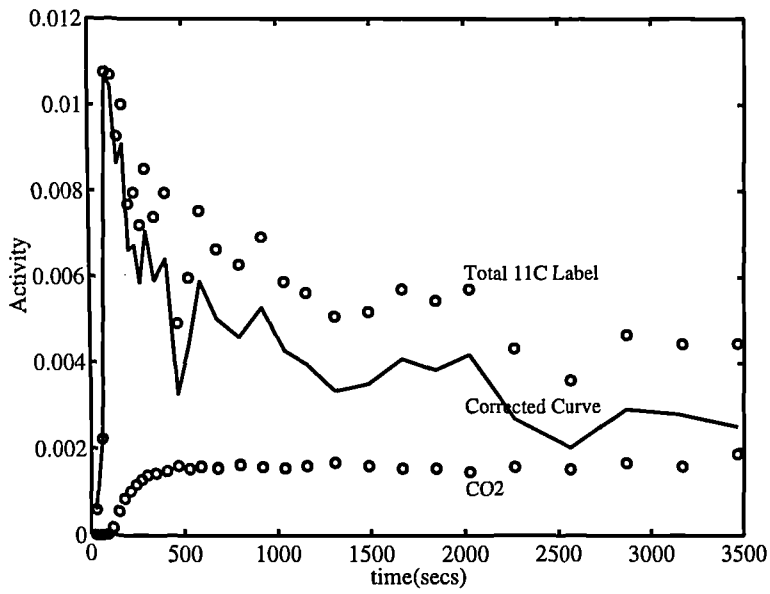

Figure 9.11: Correction of tumour time course for the presence of $^{11}CO_2$ (p4213)

Study	% CO_2 at 60 mins
p4060	30.3^+
p4161	14.4
p4132	28.7
p4213	37.2

Table 9.2: Contribution of carbon dioxide in tumour at 60 minutes ($^+$extrapolated, see Figure (8.8))

using the [2-^{11}C] label. Under the assumption that the animal results can be extrapolated to human studies it would suggest that there is little or no contribution from the intermediary metabolites in tumour.

Initial results suggest that a standard correction for carbon dioxide may be difficult to apply due to the variability in impulse responses. However, the dynamics of carbon dioxide are very fast and a model could approximate the contribution simply as a plasma or blood volume term in any modelling procedure.

9.5.4 Dual Input Spectral Analysis

To assess whether the kinetics of [^{11}C]thymidine and $^{11}CO_2$ could be distinguished implicitly from the tumour time activity curves, the method of dual spectral analysis was implemented and applied. This technique is an extension of the standard spectral analysis technique involving just a single input function (see Chapter 6). The problem is considered such that the tissue constitutes labelled thymidine and carbon dioxide. Plasma input functions were identified for these two compounds as described previously. The tumour time activity curves were then fitted to a composite function of possible thymidine and carbon dioxide behaviour. This is described mathematically by,

$$PET_{tumour}(t) = Plasma_{thymidine}(t) \otimes \sum_{i=1}^{100} \alpha_i e^{-\beta_i t} + Plasma_{CO_2}(t) \otimes \sum_{i=1}^{100} \gamma_i e^{-\beta_i t} \quad (9.3)$$

subject to the non-negativity constraint $\alpha_i, \gamma_i \geq 0$.

This equation was applied to the tumour time activity curves utilising the NNLS algorithm described in Chapter 6. This was applied to all four studies and the predicted components (Spectral analysis approach) are compared with the measured components (two scan approach) in Figures (9.12 - 9.15).

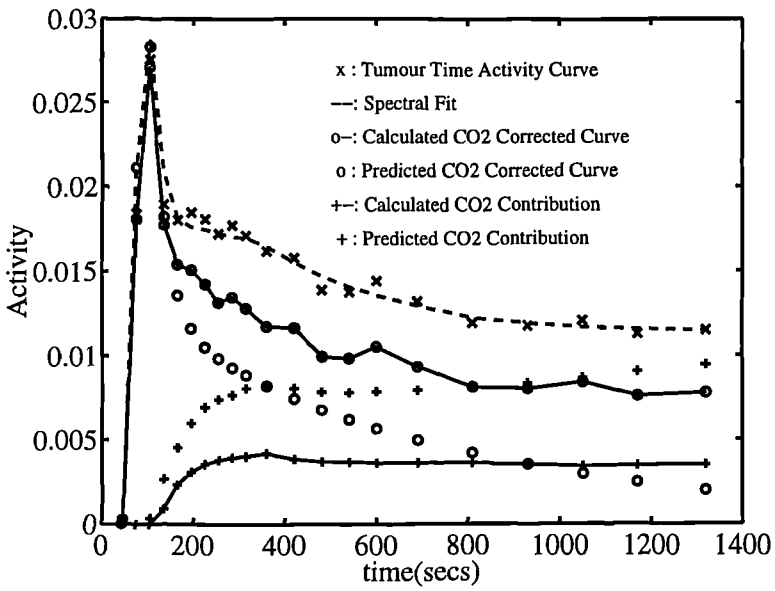

Figure 9.12: Prediction of carbon dioxide contribution in tumour using spectral analysis (p4060)

Unfortunately the spectral analysis fails to characterise the different kinetics. However, the shapes of the curves are correct and if further constraints could be applied it might be possible to predict the curves (i.e. if the $^{11}CO_2$ fraction in tissue was known at 60 mins).

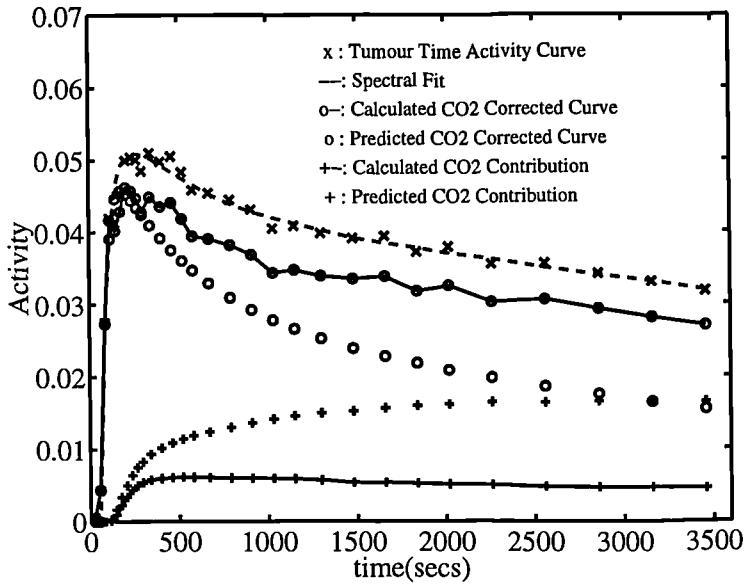

Figure 9.13: Prediction of carbon dioxide contribution in tumour using spectral analysis (p4161)

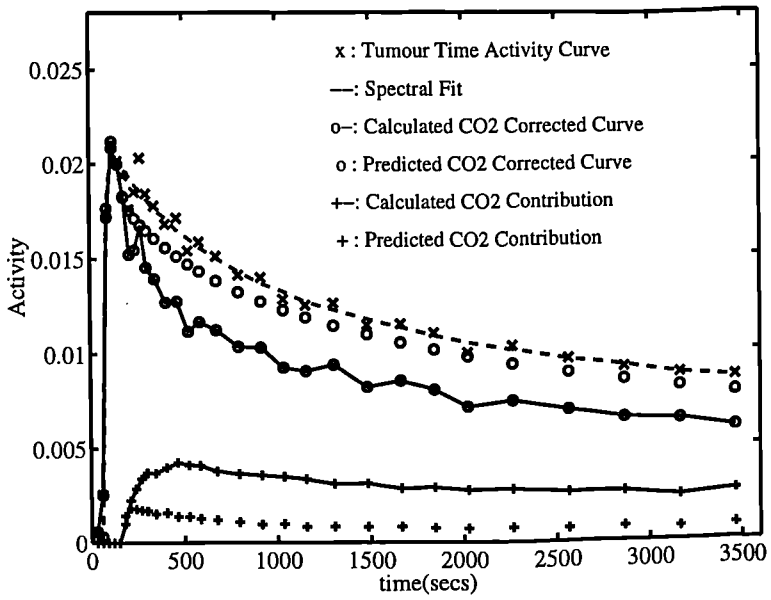

Figure 9.14: Prediction of carbon dioxide contribution in tumour using spectral analysis (p4132)

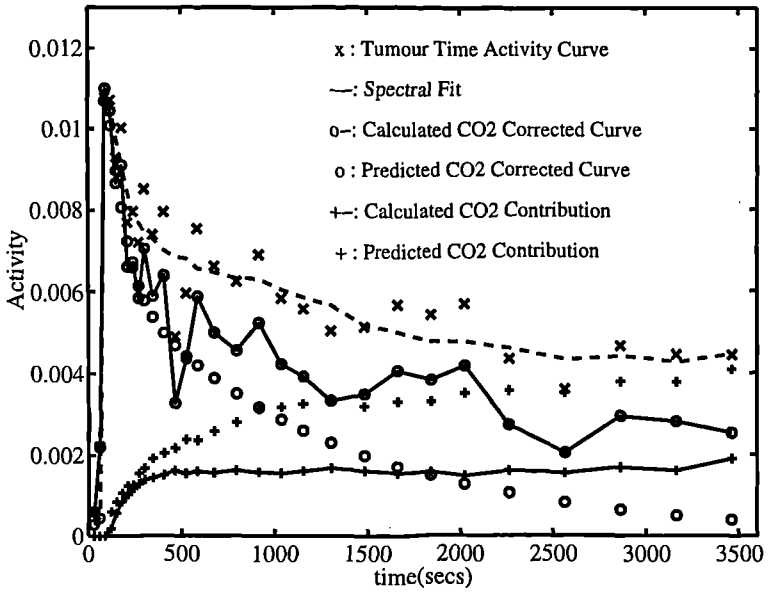

Figure 9.15: Prediction of carbon dioxide contribution in tumour using spectral analysis (p4213)

Parametric Images

The correction of [^{11}C]thymidine scans using a [^{11}C]bicarbonate scan and equation (9.2) may be applied at a single "pixel" level. This method was applied to create a $^{11}CO_2$-corrected dynamic data set. Spectral analysis was then applied to both the uncorrected and corrected data sets using a [^{11}C]thymidine plasma input function and the impulse response functions were derived at 60 minutes. These images are representative of the retention of the total uncorrected and corrected tracer signal. A transaxial slice through the abdomen is shown in Figure (9.16). It is clear from the images that the $^{11}CO_2$ correction removes a large part of the diffuse $^{11}CO_2$ signal thus enabling the production of more accurate functional images of thymidine retention.

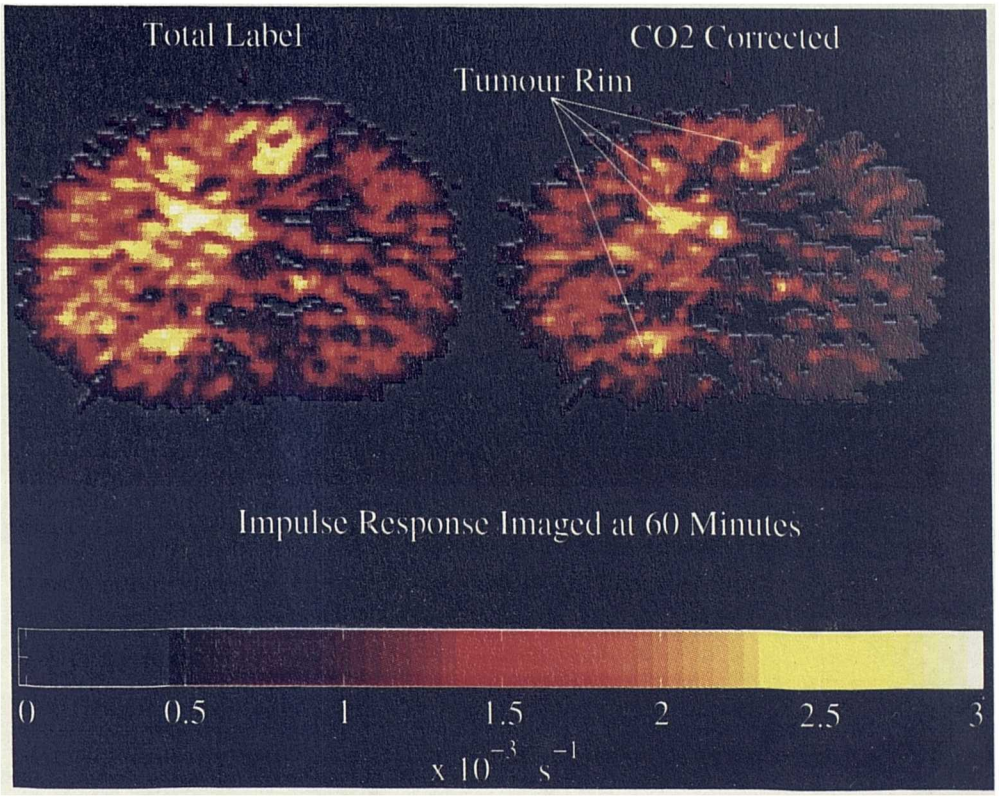

Figure 9.16: Thymidine impulse response functions imaged at 60 minutes with and without correction for the contribution of carbon dioxide in tissue

9.6 Discussion

The first clinical application of [^{11}C]thymidine uptake in tumours using PET was described by Martiat et al. [134] using thymidine labelled in the methyl position. In this work a relatively simple compartmental model was employed and it was argued that the signal due to labelled metabolites was unimportant. They showed a correlation between the uptake of [^{11}C]thymidine in lymphoma and histological grade. The advantages of thymidine labelled in the 2-C position was first proposed by Vander Borght [129] and its application to PET was studied further by Shields [114] who drew attention to the need to take the contribution of metabolites into account in any subsequent analysis. A plausible compartmental model for the analysis of the behaviour of [^{11}C]thymidine and its labelled metabolites was

also proposed by Shields [114]. However, as the author commented the model is over-parameterised and numerically unidentifiable from the PET data. More recently Mankoff et al. [133] from the same group have suggested a graphical Patlak approach. The technique assumes that none of the metabolites involve an irreversible step, such an assumption would be invalidated by any fixation of CO_2. Although Mankoff et al. do consider the case where there is a "small" amount of metabolite trapping, they agree that it is difficult to mathematically separate the contribution of [^{11}C]thymidine and its labelled metabolites in this case. In this thesis I have demonstrated that the determination of the relative contributions of [^{11}C]thymidine and metabolite components, simply from the total label in tissue, is non trivial with the application of dual input spectral analysis. Both this technique and that of Mankoff et al. stem from basically the same model and are therefore likely to suffer from similar inherent problems.

The approach used in the present work has been to address the metabolite problem directly, and to conduct an additional scan aimed at characterising the behaviour of the principal labelled metabolite, namely $^{11}CO_2$. The advantages of this approach are simply that it allows for the removal of $^{11}CO_2$ from the tissue signal, enabling subsequent modelling techniques to be simplified. A disadvantage arises from the need for an additional scan. For example, it may also be necessary in some cases to combine the thymidine scans with an $H_2^{15}O$ blood flow scan to investigate delivery. However, the consecutive acquisition of all three studies would rarely be feasible. The work presented in this chapter has been based on four paired scans. These preliminary data are insufficient to examine whether population data could be used to correct for the $^{11}CO_2$ contribution in tissue in the general case. On the basis of the present analyses further paired scans are therefore being carried out in the Unit.

The present analyses were carried out as part of a programme investigating the

potential use of [^{11}C]thymidine in PET as a marker of tumour cell proliferation. In this context the present work establishes an experimental approach to the removal of the confounding signal from the major metabolite. The next steps will involve the investigation of the corrected signal to see if it provides a more robust index of cell proliferation. Clearly this presents a difficult exercise in validation - a possible approach however is suggested by the results presented in Chapter 7 on MIB 1. With the benefit of hind sight it may be profitable to repeat these studies coupled with the two scan approach presented here.

Chapter 10

Conclusions and Future Work

10.1 Conclusions

This thesis has considered three main themes; identifiability analysis, tracer kinetic modelling and contamination of the data by labelled metabolites. After an introduction to PET, modelling and identifiability analysis (Chapters 2 and 3) the thesis considered unidentfiable systems in Chapter 4. A new method has been presented which allows for the reparameterisation of unidentifiable systems. The method was based on the Taylor series approach to identifiability analysis and enables the original unidentifiable system to be reduced to a locally identifiable system. Furthermore this reparameterisation may be globally identifiable. Theorems have been presented, firstly to give conditions for the existence of a reparameterisation of an unidentifiable model and secondly to dictate how a reparameterisation must be constructed. This reparameterisation method was then applied to a metabolism model in Chapter 5 which considered methods for the correction of the plasma input function due to labelled metabolites. Chapter 5 has considered using compartmental models for the description of metabolite formation and two models were presented for the metabolism of [^{11}C]diprenorphine and [^{11}C]flumazenil. A partition coefficient model was applied to [^{11}C]flumazenil blood data which allowed for the creation of metabolite data solely from the distribution

of label between plasma and red cells. These findings spawned a proposal for a future blood sampling protocol involving fewer metabolite samples. This would enable metabolite correction of the plasma curve using the compartmental and partition coefficient models.

Chapter 6 considered a tracer kinetic modelling technique (spectral analysis) with reference to the problem of the uniqueness of the solution. A Theorem was presented which gives a sufficient condition for a unique solution to the spectral analysis problem. This condition is normally satisfied in practice. The method of spectral analysis was extended to consider systems involving displacement of the tracer signal. This method was applied to a set of head displacement data, from a whole body counter, utilising a novel set of basis functions. This allowed for the change in occupancy to be inferred.

Chapter 7 investigated [^{11}C]thymidine, a possible tracer for the (*in-vivo*) measure of tumour cell proliferation. PET derived indices of tumour cell proliferation were found to correlate with an *ex-vivo* histological measure. The PET tracer [^{11}C]thymidine suffers from the metabolism of the injected compound, the major metabolite being $^{11}CO_2$. Therefore dual experiments were proposed and performed using both $^{11}CO_2$ and [^{11}C]thymidine. This novel dual scan approach allowed for the removal of the contaminating $^{11}CO_2$ contribution to the tissue data. This correction was performed using spectral analysis to characterise the carbon dioxide tissue dynamics and then convolution with the carbon dioxide plasma time course to establish the contribution to the tissue signal. The $^{11}CO_2$ plasma time course was obtained using a novel breath sampling and analytical technique for characterising expired radioactivity. The applicability of a dual input spectral analysis method was investigated as a kinetic modelling technique to distinguish between the [^{11}C]thymidine and $^{11}CO_2$ signals in tissue. Unfortunately this failed to resolve the two time courses.

10.2 Future Work

It is anticipated that the following work will be carried out in the future.

A revision of the [^{11}C]flumazenil protocol will be implemented as proposed at the end of Chapter 5. This will utilise the partition coefficient model to enable accurate estimation of metabolite data at late time points.

The method of spectral analysis for displacement studies will be extended to consider data on a tomographic scale. The technique will necessitate statistical considerations at this resolution, and a proposed method involving an F-test of displaced and undisplaced spectral methods will be investigated to determine whether individual pixels contain a displaced signal.

[^{11}C]Thymidine experiments will be carried out as proposed at the end of Chapter 9, further examining the possibility of a standard $^{11}CO_2$ correction. $^{11}CO_2$ correction of the [^{11}C]thymidine data will allow for a more comprehensive investigation of [^{11}C]thymidine kinetics. Experiments involving [^{11}C]thymidine, [^{11}C]bicarbonate and MIB 1 measures are being planned to validate the use of [^{11}C]thymidine as an *in vivo* marker of cell proliferation.

Bibliography

[1] *J Nucl Med*, 32:559–752, 1991.

[2] R. S. J. Frackowiak and K. J. Friston. Functional neuroanatomy of the human brain : positron emission tomography - a new neuroanatomical technique. *J Anat*, 184:211–225, 1994.

[3] R. A. Weeks and D. J. Brooks. Positron emission tomography and central neurotransmitter systems in movement disorders. *Fundam Clin Pharmacol*, 8:503–517, 1994.

[4] R. E. Butler, D. C. Costa, and C. L. E. Katona. PET and SPECT imaging in the dementias. In I. P. C. Murray and P. J. Ell, editors, *Nuclear medicine in clinical diagnosis and treatment*, pages 613–627. Churchill Livingstone, 1994.

[5] R. de Silva and P. G. Camici. Assessment of myocardial perfusion, metabolism and pharmacology using positron emission tomography. *Cardioscience*, 3(4):205–216, 1992.

[6] V.J. Cunningham, S.D. Rosen, H. Boyd, S. Osman, R.J. Davenport, R.N. Gunn, V.W. Pike, and P.G. Camici. Uptake of [N-methyl-C11] propionyl-L-carnitine in human myocardium. *J Pharm Exp Therap*, 227(1):511–517, 1996.

[7] R. L. Wahl. Positron emission tomography : applications in oncology. In I. P. C. Murray and P. J. Ell, editors, *Nuclear medicine in clinical diagnosis and treatment*, pages 801–820. Churchill Livingstone, 1994.

[8] D. W. O. Tilsley, R. J. A. Harte, Jones. T., F. Brady, S. K. Luthra, G. Brown, and P. M. Price. New techniques in the pharmacokinetic analysis of cancer drugs IV positron emission tomography. *Cancer Surveys*, 17:425–442, 1993.

[9] P. Wells, R. J. A. Harte, and P. Price. Positron emission tomography : a new investigational area for cancer research. *Clin Onc*, 8:7–14, 1996.

[10] P. F. Liddle, K. J. Friston, C. D. Frith, S. R. Hirsch, T. Jones, and R. S. J. Frackowiak. Patterns of cerebral blood flow in schizophrenia. *Br J Psychiatry*, 160:179–186, 1992.

[11] E. J. Hoffman and M. E. Phelps. Positron emission tomography : principles and quantitation. In M. E. Phelps, J. C. Mazziotta, and H. R. Schelbert, editors, *Positron emission tomography and autoradiography : principles and applications for the brain and heart*, pages 237–286. Raven Press, 1986.

[12] J. S. Flower and A. P. Wolf. Positron emitter-labeled compounds : priorities and problems. In M. E. Phelps, J. C. Mazziotta, and H. R. Schelbert, editors, *Positron emission tomography and autoradiography : principles and applications for the brain and heart*, pages 391–450. Raven Press, 1986.

[13] R. Myers, T. J. Spinks, S. K. Luthra, and D. J. Brooks. Positron emission tomography. In M. G. Stewart, editor, *Quantitative methods in neuroanatomy*, pages 117–161. John Wiley and Sons, 1992.

[14] S. R. Meikle and M. Dahlbon. Positron emission tomography. In I. P. C. Murray and P. J. Ell, editors, *Nuclear medicine in clinical diagnosis and treatment*, pages 613–627. Churchill Livingstone, 1994.

[15] T. J. Spinks, T. Jones, M-C. Gilardi, and J. D. Heather. Physical performance of the latest generation of commercial positron scanner. *IEEE Trans Nucl Sci*, 35:721–725, 1988.

[16] T. J. Spinks, T. Jones, D. L. Bailey, D. W. Townsend, S. Grootoonk, P. M. Bloomfield, M-C. Gilardi, M. E. Casey, B. Sipe, and J. Reed. Physical performance of a positron tomograph for brain imaging with retractable septa. *Phys Med Biol*, 37:1637–1655, 1992.

[17] T. F. Budinger, G. T. Gullberg, and Huesman R. H. Image reconstruction from projections. In G. T. Herman, editor, *Emission computed tomography*, pages 147–245. Springer-Verlag, 1979.

[18] Y. Vardi, A. Shepp, and L. Kaufman. A statistical model for positron emission tomography. *J American Statistical Association*, 80:8–37, 1985.

[19] M. Bergström, L. Eriksson, C. Bohm, G. Blomqvist, and J. Litton. Correction for scattered radiation in a ring detector positron camera by integral transformation of the projections. *J Comput Assist Tomogr*, 7(1):42–50, 1983.

[20] S. Grootoonk, T. J. Spinks, T. Jones, C. Michel, and A. Bol. Correction for scatter using a dual energy window technique with a tomograph operated without septa. In *IEEE Nuclear Science Symposium and Medical Imaging Conference*, volume 3, pages 1569–1573, 1991.

[21] D. W. Townsend, A. Geissbühler, M. Defrise, E. J. Hoffman, T. J. Spinks, D. L. Bailey, M-C. Gilardi, and T. Jones. Fully three-dimensional recon-

struction for a PET camera with retractable septa. *IEEE Trans Med Imaging*, 10:505–512, 1991.

[22] A. S. O. Ranicar, C. W. Williams, L. Schnorr, J. C. Clark, C. G. Rhodes, P. M. Bloomfield, and T. Jones. The on-line monitoring of continuously withdrawn arterial blood during PET studies using a single BGO photomultiplier assembly and non-stick tubing. *Med Proc Tech*, 17:259–264, 1991.

[23] B. Mazière, R. Cantineau, H. H. Coenen, M. Guillaume, C. Halldin, A. Luxen, C. Loc'h, and S. K. Luthra. PET radiopharmaceutical metabolism - plasma metabolite analysis. In G. Stöcklin and V. W. Pike, editors, *Radiopharmaceuticals for positron emission tomography : methodological aspects*, pages 151–178. Kluwer Academic Publishers, 1993.

[24] S. K. Luthra, S. Osman, D. R. Turton, V. Vaja, K. Dowsett, and F. Brady. An automated system on solid phase extraction and HPLC for the routine determination in plasma of unchanged [^{11}C]-L-deprenyl, [^{11}C]diprenorphine, [^{11}C]flumazenil, [^{11}C]raclopride and [^{11}C]scherring 23390. *J Labelled Compd Radiopharm*, 32:518–520, 1993.

[25] S. C. Huang and M. E. Phelps. Principles of tracer kinetic modelling in positron emission tomography and autoradiography. In M. E. Phelps, J. C. Mazziotta, and H. R. Schelbert, editors, *Positron emission tomography and autoradiography : principles and applications for the brain and heart*, pages 287–346. Raven Press, 1986.

[26] S. C. Huang, D. G. Feng, and M. E. Phelps. Model dependency and estimation reliability in measurement of cerebral oxygen utilization rate with oxygen-15 and dynamic positron emission tomography. *J Cereb Blood Flow Metab*, 6(1):105–119, 1986.

[27] J. Delforge, A. Syrota, and B. M. Mazoyer. Experimental design optimisation : theory and application to estimation of receptor model parameters using dynamic positron emission tomography. *Phys Med Biol*, 34(4):419–435, 1989.

[28] I. T. Joliffe. *Principal components analysis.* Springer-Verlag, 1986.

[29] M. Samal, M. Karny, H. Surova, P. Penicka, E. Marikova, and Z. Diensbier. Rotation to simple structure in factor analysis of dynamic radionuclide studies. *Phys Med Biol*, 32(3):371–382, 1987.

[30] J. T. Yap, M. Cooper, C. T. Chen, and V. J. Cunningham. Generation of parametric images using factor analysis of dynamic PET data. In R. Myers, V. J. Cunningham, D. L. Bailey, and T. Jones, editors, *Quantification of brain function using PET*, pages 292–296. Academic Press, 1996.

[31] F. Hermansen and A. A. Lammertsma. Linear dimesion reduction of sequences of medical images : I. optimal inner products. *Phys Med Biol*, 40:1909–1920, 1995.

[32] F. Hermansen, P. M. Bloomfield, J. Ashburner, P. G. Camici, and A. A. Lammertsma. Linear dimesion reduction of sequences of medical images : II. direct sum decomposition. *Phys Med Biol*, 40:1921–1941, 1995.

[33] F. O'Sullivan, M. Muzi, M. M. Graham, and A. Spence. Parametric imaging by mixture analysis in 3D validation for dual-tracer glucose studies. In R. Myers, V. J. Cunningham, D. L. Bailey, and T. Jones, editors, *Quantification of brain function using PET*, pages 297–300. Academic Press, 1996.

[34] V.J. Cunningham and T. Jones. Spectral analysis of dynamic PET studies. *J Cereb Blood Flow Metab*, 13:15–23, 1993.

[35] M. Tadoroko, A. K. P. Jones, V. J. Cunningham, D. Sashin, S. Grootoonk, J. Ashburner, and T. Jones. Parametric images of ^{11}C-diprenorphine binding using spectral analysis of dynamic PET images acquired in 3D. In K. Uemura, N. A. Lassen, T. Jones, and I. Kanno, editors, *Quantification of brain function : tracer kinetic and image analysis in brain PET*, pages 289–294. Elsevier Science Publishers, 1993.

[36] V. J. Cunningham, J. Ashburner, H. Byrne, and T. Jones. Use of spectral analysis to obtain parametric images from dynamic PET studies. In K. Uemura, N. A. Lassen, T. Jones, and I. Kanno, editors, *Quantification of brain function : tracer kinetic and image analysis in brain PET*, pages 101–111. Elsevier Science Publishers, 1993.

[37] C. S. Patlak, R. G. Blasberg, and J. D. Fenstermacher. Graphical evaluation of blood-to-brain transfer constants from multiple-time uptake data. *J Cereb Blood Flow Metab*, 3:1–7, 1983.

[38] A. Gjedde. High- and low-affinity transport of d-glucose from blood to brain. *J Neurochem*, 36:1463–1471, 1981.

[39] J. Logan, J. S. Fowler, N. D. Volkow, A. P. Wolf, S. L. Dewey, D. J. Schyler, R. R. MacGregor, R. Hitzemann, B. Bendriem, S. J. Gatley, and D. R. Christman. Graphical analysis of reversible radioligand binding from time-activity measurements applied to [N-^{11}C-methyl]-(-)-cocaine PET studies in human subjects. *J Cereb Blood Flow Metab*, 10:740–747, 1990.

[40] M. D. Rutland. A single injection technique for subtraction of blood background in ^{131}I-hippuran renograms. *Br J Radiol*, 52:134–137, 1979.

[41] S-C Huang, R. E. Carson, and M. E. J. Phelps. Measurement of local blood flow and distribution volume with short-lived isotopes : a general input technique. *J Cereb Blood Flow Metab*, 2:99–108, 1982.

[42] N. M. Alpert, L. Eriksson, J. Y. Chang, M. Bergström, J. E. Litton, J. A. Correia, C. Bohm, R. H. Ackerman, and J. M. Taveras. Strategy for the measurement of regional cerebral blood flow using short-lived tracers and emission tomography. *J Cereb Blood Flow Metab*, 4:28–34, 1984.

[43] H. Iida, P. M. Bloomfield, S. Miura, I. Kanno, M. Murakami, K. Uemura, M. Amano, K. Tanaka, Y. Hirose, and S. Yamamoto. Effect of real-time weighted integration system for rapid calculation of functional images in clinical positron emission tomography. *IEEE Trans Med Imaging*, 14:116–121, 1995.

[44] N. A. Lassen, P. A. Bartenstein, A. A. Lammertsma, M. C. Prevett, D. R. Turton, S. K. Luthra, S. Osman, P. M. Bloomfield, T. Jones, P. N. Patsalos, M. T. O'Connell, J. S. Duncan, and J. Vanggaard Andersen. Benzodiazepine receptor quantification in vivo in humans using [^{11}C]flumazenil and PET: application of the steady-state principle. *J Cereb Blood Flow Metab*, 15:152–165, 1995.

[45] P. Doucet and P. B. Sloep. *Mathematical modelling in the life sciences.* Ellis Horwood, 1992.

[46] J. A. Jacquez. *Compartmental Analysis in Biology and Medicine.* University Press, Ann Arbor, Michigan, second edition, 1985.

[47] D. A. Sanchez, R. C. Allen, and W. T. Kyner. *Differential equations.* Addison Wesley Publishing Company, second edition, 1988.

[48] J. C. Price, H. S. Mayberg, R. F. Dannals, A. A. Wilson, H. T. Ravert, B. Sadzot, Z. Rattner, A. Kimball, M. A. Feldman, and J. J. Frost. Measurement of benzodiazepine receptor number and affinity using tracer kinetic modelling, positron emission tomography, and [^{11}C]flumazenil. *J Cereb Blood Flow Metab*, 13:656–667, 1993.

[49] M. J. Chappell. Structural identifiability of compartmental models characterising saturable binding: comparison between pseudo-steady state and non-pseudo steady state model formulations. *Math Biosci*, 133(1):1–20, 1996.

[50] M. J. Chappell and K. R. Godfrey. Structural identifiability of the parameters of a nonlinear batch reactor model. *Math Biosci*, 108:241–251, 1992.

[51] K. R. Godfrey and III DiStefano, J. J. Identifiability of model parameters. In E. Walter, editor, *Identifiability of Parametric Models*, pages 1–20. Pergamon Press, 1987.

[52] S. Vajda, K. R. Godfrey, and H. Rabitz. Similarity transformation approach to structural identifiability of nonlinear models. *Math Biosci*, 93:217–248, 1989.

[53] H. Pohjanpalo. System identifiability based on the power series expansion of the solution. *Math Biosci*, 41:21–33, 1978.

[54] S. Vajda, H. Rabitz, E. Walter, and Y. Lecourtier. Qualitative and quantitative identifiability analysis of nonlinear chemical kinetic models. *Chem Eng Comm*, 83:191–219, 1989.

[55] R. Bellman and K. J. Åström. On structural identifiability. *Math Biosci*, 7:329–339, 1970.

[56] J. Delforge, A. Syrota, and Mazoyer B. M. Experimental design optimisation: theory and application to estimation of receptor model parameters using dynamic positron emission tomography. *Phys Med Biol*, 34:419–435, 1989.

[57] A. Raksanyi, Y. Lecourtier, E. Walter, and A. Venot. Identifiability and distinguishability testing via computer algebra. *Math Biosci*, 77:245–266, 1985.

[58] S. M. Skinner, R. E. Clark, N. Baker, and R. A. Shipley. Complete solution of the three compartmental model in steady-state after single injection of radioactive tracer. *Amer J Physiol*, 196:238–244, 1959.

[59] J. J. DiStefano, K. C. Wilson, M. Jang, and P. H. Mak. Identification of the dynamics of thyroid metabolism. *Automatica*, 11:149–159, 1975.

[60] M. Milanese and G. P. Molino. Structural identifiability of compartmental models and pathophysiological information from the kinetics of drugs. *Math Biosci*, 26:175–190, 1975.

[61] J.P. Norton. Sources of nonuniqueness in deterministic identfiability. *Math Biosci*, 60:89–108, 1982.

[62] K. R. Godfrey. *Compartmental Models and their Applications.* Academic Press, New York and London, 1983.

[63] S. Vajda. Structural identifiability of linear, bilinear, polynomial and rational systems. In *9th IFAC World Congress, Budapest, Hungary*, 1982.

[64] M. J. Chappell, K. R. Godfrey, and S. Vajda. Global identifiability of the parameters of nonlinear systems with specified inputs: a comparison of methods. *Math Biosci*, 102:41–73, 1990.

[65] E. Walter and Y. Lecourtier. Global approaches to identifiability testing for linear and nonlinear state space models. *Math and Comput in Simulation*, 24:472–482, 1982.

[66] M. Chapman and K. R. Godfrey. Some extensions to the exhaustive-modelling approach to structural identifiability. *Math Biosci*, 77:305–323, 1985.

[67] Y. Lecourtier, F. Lamnabhi-Lagarrigue, and E Walter. Volterrra and generating power series approaches to identifiability testing. In E. Walter, editor, *Identifiability of Parametric Models*, pages 50–66. Pergamon Press, 1987.

[68] L. Ljung and T. Glad. On global identifiability for arbitrary model parametrizations. *Automatica*, 30(2):265–276, 1994.

[69] M. Berman. A postulate to aid in model building. *J Theoret Biol*, 4:229–236, 1962.

[70] K. Glover and J. C. Willems. Parameterization of linear dynamical systems: canonical forms and identifiability. *IEEE Trans Automatic Control*, AC-19(6):640–645, 1974.

[71] M. Milanese and N. Sorrentino. Decomposition methods for the identifiability analysis of large systems. *International Journal of Control*, 1:71–79, 1978.

[72] T. J. Rothenburg. Identification in parametric models. *Econometrica*, 39(3):577–591, 1971.

[73] C. Cobelli and G. Toffolo. Theoretical aspects and practical strategies for the identification of unidentifiable compartmental systems. In E. Walter,

editor, *Identifiability of Parametric Models*, pages 85–91. Pergamon Press, 1987.

[74] E. Walter and Y. Lecourtier. Unidentifiable compartmental models: what to do ? *Math Biosci*, 56:1–25, 1981.

[75] H. Pohjanpalo. Identifiability of deterministic differential models in state space. Technical report, Technical Research Centre of Finland, 1982.

[76] J. E. Marsden and M. J. Hoffman. *Elementary Classical Analysis.* W. H. Freeman and Company, second edition, 1993.

[77] V. J. Cunningham, S. P. Hume, G. R. Price, R. G. Ahier, J. E. Cremer, and A. K. P. Jones. Compartmental analysis of diprenorphine binding to opiate receptors in the rat in vivo and its comparison with equilibrium data in vitro. *J Cereb Blood Flow Metab*, 11:1–9, 1991.

[78] S. Pappata, Y. Samson, C. Chavoix, C. Prenant, M. Mazière, and J. C. Baron. Regional specific binding of [^{11}C]RO 15 1788 to central type benzodiazepine receptors in human brain : quantitative evaluation by PET. *J Cereb Blood Flow Metab*, 8(3):304–313, 1988.

[79] P. Abadie and J. C. Baron. In vivo studies of the central benzodiazepine receptors in the human brain with positron emission tomography. In M. Diksic and R. C. Reba, editors, *Radiopharmaceuticals and Brain Pathology Studied with PET and SPECT*, pages 357–379. CRC Press, 1991.

[80] M. A. Mintun, M. E. Raichle, M. R. Kilbourn, G. F. Wooten, and M. J. Welch. A quantitative model for the in vivo assessment of drug binding sites with positron emission tomography. *Ann Neurol*, 15:217–227, 1984.

[81] A. J. Clark. *The mode of action of drugs on cells.* Edward Arnold, 1933.

[82] R. W. Kerwin and Pilowsky L. S. Traditional receptor theory and its application to neuroreceptor measurements in functional imaging. *Eur J Nucl Med*, 22(7):699–709, 1995.

[83] J. Delforge, S. Pappata, P. Millet, Y. Samson, B. Bendriem, A. Jobert, C. Crouzel, and A. Syrota. Quantification of benzodiazepine receptors in human brain using PET, [^{11}C]flumazenil, and a single experiment protocol. *J Cereb Blood Flow Metab*, 15:284–300, 1995.

[84] J. Delforge, A. Syrota, and Mazoyer B. M. Identifiability analysis and parameter identification of an in vivo ligand-receptor model from PET data. *IEEE Trans Biomed Eng*, 37:653–662, 1990.

[85] N. Lassen. Neuroreceptor quantitation in vivo by the steady-state principle using constant infusion or bolus injection of radioactive tracers. *J Cereb Blood Flow Metab*, 12:709–716, 1993.

[86] G. Blomqvist, S. Pauli, L. Farde, L. Ericksson, A. Person, and C. Halldin. Dynamic models of reversible ligand binding. In C. Beckers, A. Goffinet, and A. Bol, editors, *Clinical Research and Clinical Diagnosis*, pages 35–44. Kluwer Academic Publishers, 1989.

[87] A. Holmberg. On the practical identifiability of microbial growth models incorporating michaelis-menten type nonlinearities. *Math Biosci*, 62:23–43, 1982.

[88] D. J. Nutt. Addiction : brain mechanisms and their treatment application. *Lancet*, 347:31–36, 1996.

[89] A. L. Malizia and M. P. Richardson. Benzodiazepine receptors and positron emission tomography : ten years experience. a new beginning? *J Psychopharmacol*, 9(4):355–368, 1995.

[90] P. A. Bartenstein, J. S. Duncan, M. C. Prevett, Cunningham V. J., D. R. Fish, A. K. Jones, S. K. Luthra, G. V. Sawle, and D. J. Brooks. Investigation of opiod system in absence seizures with positron emission tomography. *J Neurol Neurosurg Psychiatry*, 56:1295–1302, 1993.

[91] W. Sadée, D. C. Perry, J. S. Rosenbaum, and A Herz. [^{3}H]diprenorphine receptor binding in vivo and in vitro. *Eur J Pharmacol*, 81:431–440, 1982.

[92] D. Inoue, Y. Akimoto, K. Hashimoto, and T. Yamasaki. Alterations in biodistribution of [^{3}H]RO 15-1788 in mice by acute stress: possible changes in in vivo binding availability of brain benzodiazepine receptor. *Int J Nucl Med Biol*, 12:369–374, 1985.

[93] A. Persson, S. Pauli, C. G. Swahn, C. Halldin, and G. Sedvall. Cerebral uptake of ^{11}C-RO 15-1788 and its acid metabolite ^{11}C-RO 15-3890; PET study in healthy volunteers. *Human Psychopharmacology*, 4:215–220, 1989.

[94] A. K. P. Jones, S. K. Luthra, B. Mazière, V. W. Pike, C. Loc'h, C. Crouzel, A. Syrota, and T. Jones. Regional cerebral opioid receptor studies with [^{11}C]diprenorphine in normal volunteers. *J Neurosci Methods*, 23:121–129, 1988.

[95] A. K. P. Jones, V. J. Cunningham, S. Ha-Kawa, T. Fujiwara, Q. Liyii, S. K. Luthra, S. Osman, and T. Jones. Quantitation of [^{11}C]diprenorphine cerebral kinetics in man acquired by PET using presaturation, pulse-chase and tracer-only protocols. *J Neurosci Methods*, 51:123–134, 1994.

[96] U. Klotz, G. Ziegler, and I. W. Reimnan. Pharmacokinetics of the selective benzodiazepine antagonist RO 15-1788 in man. *Eur J Clin Pharmacol*, 27:115–117, 1984.

[97] G. Pommier-layrargues, J. F. Giguere, J. Lavere, B. Willems, and R. F. Butterworth. Pharmacokinetics of benzodiazepine antagonist RO 15-1788 in cirrhotic patients with moderate or severe liver dysfunction. *Hepatology*, 10:969–972, 1989.

[98] C. Halldin, S. Stone-Elander, J. O. Thorell, A. Persson, and G. Sedvall. ^{11}C labelling of RO 15-3890, for PET studies of benzodiazepine receptors. *Appl Radiat Isot*, 39:993, 1988.

[99] L. Barre, D. Debruyne, P. Abadie, M. Moulin, and J. C. Baron. A comparison of methods for the separation of [^{11}C]RO 15-1788 (flumazenil) from its metabolites in the blood of rabbits, baboons and humans. *Appl Radiat Isot*, 42:435–439, 1990.

[100] D. Debruyne, P. Abadie, L. Barre, F. Alberssard, M. Moulin, E. Zarifian, and J. C. Baron. Plasma pharmacokinetics and metabolism of the benzodiazepine antagonist ^{11}C RO 15-1788 (flumazenil) in baboon and human during positron emission tomography studies. *Eur J Drug Metabol Pharmacol*, 16:141–152, 1991.

[101] A. A. Lammertsma, C. J. Bench, G. W. Price, J. E. Cremer, S. K. Luthra, D. Turton, N. D. Wood, and R. S. J. Frackowiak. Measurement of cerebral monamine oxidase B activity using L-[^{11}C]deprenyl and dynamic positron emission tomography. *J Cereb Blood Flow Metab*, 11:545–556, 1991.

[102] C-Y. Shiue, L-Q. Bai, R-R. Teng, C. D. Arnett, S. L. Dewey, A. P. Wolf, D. W. Mcpherson, J. S. Fowler, J. Logan, M. J. Holland, and E. J. Simon. A comparison of the brain uptake of N-(cyclopropyl[^{11}C]methylnorbuprenorphine ([^{11}C]buprenorphine) and N-

(cyclopropyl[^{11}C]methylnordiprenorphine ([^{11}C]diprenorphine) in baboon using PET. *Nucl Med Biol*, 18(3):281–288, 1991.

[103] J. A. Nelder and R. Mead. A simplex method for function minimization. *Comput J*, 7:308–313, 1965.

[104] S. C. Huang, J. R. Barrio, D. C. Yu, B. Chen, S. Grafton, W. P. Melega, J. M. Hoffman, N. Satyamurthy, J. C. Mazziotta, and M. E. Phelps. Modelling approach for separating blood time-activity curves in positron emission tomographic studies. *Phys Med Biol*, 36(6):749–761, 1991.

[105] W. H. Press, B. P. Flannery, S. A. Teukolsky, and W. T. Vetterling. *Numerical Recipes : The Art of Scientific Computing.* Cambridge University Press, 1989.

[106] D. G. Feng, S. C. Huang, and X. Wang. Models for computer simulation studies of input functions for tracer kinetic modeling with positron emission tomography. *Int J Biomed Comput*, 32:95–110, 1993.

[107] D. G. Luenberger. *Optimisation by Vector Space Methods.* Wiley, 1969.

[108] H.J. Tobler and G. Engel. Affinity spectra : a novel way for the evaluation of equilibrium binding experiments. *Arch Pharmacol*, 322:183–192, 1983.

[109] R. A. Koeppe, V. A. Holthoff, K. A. Frey, M. R. Kilbourn, and D. E. Kuhl. Compartmental analysis of [^{11}C]flumazenil kinetics for the estimation of ligand transport rate and receptor distribution using positron emission tomography. *J Cereb Blood Flow Metab*, 11:735–744, 1991.

[110] C. L. Lawson and R. J. Hanson. *Solving least squares problems.* Prentice-Hall, 1974.

[111] J.D. Murray. *Mathematical Biology.* Springer-Verlag, second edition, 1990.

[112] A. Malizia, G. Forse, R. N. Gunn, L. Schnorr, S. Rajeswaran, K. Poole, D. Nutt, and T. Jones. The MOC counter : a pharmacological tool for the *in vivo* measurement of ligand occupancy indices in the human brain. In R. Myers, V. J. Cunningham, D. L. Bailey, and T. Jones, editors, *Quantification of brain function using PET*, pages 20–25. Academic Press, 1996.

[113] A. Malizia, G. Forse, A. Haida, R. Gunn, J. Melichar, K. Poole, D. Bateman, D. Fahy, L. Schnorr, D. Brown, C. Rhodes, D. J. Nutt, and T. Jones. A new human (psycho)pharmacology tool : the multiple organs coincidences counter (MOCC). *J Psychopharmacol*, 9(4):294–306, 1995.

[114] A. F. Shields. Measurement of tumour proliferation using [C-11]thymidine and PET. In *Clinical PET in Oncology, Proc. Of the 2nd Int'l Symp. on PET in Oncology, Sendai, Japan*, volume 2, pages 41–45, 1993.

[115] A. F. Shields, D. V. Coonrod, R. C. Quackenbush, and J. J. Crowley. Cellular sources of thymidine nucleotides : studies for PET. *J Nucl Med*, 28(9):1435–1440, 1987.

[116] H. Thierens, M. Van Eijkeren, and P. Goethals. Biokinetics and dosimetry for [methyl-^{11}C]thymidine. *Br J Radiol*, 67:292–295, 1994.

[117] A. F. Shields, S. M. Larson, Z. Grunbaum, and M. M. Graham. Short-term uptake in normal and neoplastic tissues : studies for PET. *J Nucl Med*, 25:759–764, 1984.

[118] R. N. Gunn, P. Wells, V. J. Cunningham, T. Jones, and P. Price. An investigation into the use of [2-C^{11}]thymidine as a noninvasive index of cell proliferation in tumours in human subjects using PET. In A. M. J. Paans, J. Pruim, E. J. F. Franssen, and W. Vaalburg, editors, *Metabolic imaging of cancer*, pages 123–125. PET-Centrum AZG, 1996.

[119] G. Cattoretti, M. H. G. Becker, G. Key, M. Duchrow, C. Schluter, J. Galle, and J. Gerdes. Monoclonal antibodies against recombinant parts of the Ki-67 antigen (MIB 1 and MIB 3) detect proliferating cells in microwave-processed formalin-fixed paraffin sections. *J Pathol*, 168:357–363, 1992.

[120] J. Gerdes, M. H. Becker, G. Key, and G. Cattoretti. Immunohistological detection of tumour growth fraction (Ki-67 antigen) in formalin-fixed and routinely processed tissues. *J Pathol*, 168(1):85–86, 1992.

[121] M. Alison, Z. Chaudry, J. Baker, I. Lauder, and H. Pringle. Liver regeneration : a comparison of in situ hybridization for histone mRNA with bromodeoxyuridine labelling for detection of S-phase cells. *J Histochem Cytochem*, 42(12):1603–1608, 1994.

[122] A. F. Shields, M. M. Graham, S. M. Kozawa, L. B. Kozell, J. M. Link, E. R. Swenson, A. M. Spence, J. B. Bassingthwaighte, and K. A. Krohn. Contribution of labeled carbon dioxide to PET imaging of carbon-11-labeled compounds. *J Nucl Med*, 33(4):581–584, 1992.

[123] A. V. Oppenheim and R. W. Schafer. *Digital Signal Processing.* Prentice-Hall, 1975.

[124] B. B. Buxton, N. M. Alpert, V. Babikian, S. Weise, J. A. Correia, and R. H. Ackerman. Evaluation of the $^{11}co_2$ positron emission tomographic method for measuring brain pH. I. pH changes measured in states of altered PCO_2. *J Cereb Blood Flow Metab*, 7:709–719, 1987.

[125] D. J. Brooks, R. P. Beaney, D. G. T. Thomas, J. Marshall, and T. Jones. Studies on regional cerebral pH in patients with cerebral tumours using continuous inhalation of $^{11}CO_2$ and positron emission tomography. *J Cereb Blood Flow Metab*, 6:529–535, 1986.

[126] S. M. Larson, P. L. Weiden, Z. Grunbaum, J. S. Rasey, H. Kaplan, M. M. Graham, G. D. Harp, G. E. Sale, and D. L. Williams. Positron imaging feasibility studies. I : characteristics of [^{3}h]thymidine uptake in rodent and canine neoplasms : concise communication. *J Nucl Med*, 22:869–874, 1981.

[127] S. M. Larson, Z. Grunbaum, and J. S. Rasey. Positron imaging feasibility study : selective tumor concentration of ^{3}H-thymidine, ^{3}H-uridine, and ^{14}C-2-deoxyglucose. *Radiol*, 134:771–773, 1980.

[128] A. F. Shields, S. M. Larson, Z. Grunbaum, and M. M. Graham. Short-term thymidine uptake in normal and neoplastic tissues : studies for PET. *J Nucl Med*, 25:759–764, 1984.

[129] V. Vander Borght, D. Labar, S. Pauwels, and L. Lambotte. Production of [2-^{11}C]thymidine for quantification of cellular proliferation with PET. *Int J Rad Appl Instrum A*, 42(1):103–104, 1991.

[130] B. M. Sundoro-Wu, B. Schmall, P. S. Conti, J. R. Dahl, P. Drumm, and J. K. Jacobsen. Selective alkylation of pyrimidyldianions : synthesis and purification of ^{11}C labeled thymidine for tumor visualization using positron emission tomography. *Int J Appl Radiat Isot*, 35(8):705–708, 1984.

[131] A. F. Shields, D. Mankoff, M. M. Graham, M. Zheng, S. M. Kozawa, J. M. Link, and K. A. Krohn. Analysis of 2-carbon-11-thymidine blood metabolites in PET imaging. *J Nucl Med*, 37(2):290–296, 1996.

[132] T. M. Vander Borght, L. E. Lambotte, S. A. Pauwels, and C. C. Dive. Uptake of thymidine labeled on the carbon 2 : a potential index of liver regeneration by positron emission tomography. *Hepatology*, 12(1):113–118, 1990.

[133] D. A. Mankoff, M. M. Graham, and A. F. Shields. A graphical method of determining tracer influx constants in the presence of labelled metabolites. In R. Myers, V. J. Cunningham, D. L. Bailey, and T. Jones, editors, *Quantification of brain function using PET*, pages 312–316. Academic Press, 1996.

[134] P. Martiat, A. Ferrant, D. Labar, M. Cogneau, A. Bol, C. Michel, J. L. Michaux, and G. Sokal. In vivo measurement of carbon-11 thymidine uptake in non-hodgkin's lymphoma using positron emission tomography. *J Nucl Med*, 29(10):1633–1637, 1988.

Appendix A

Jacobian Coefficients

A.1 Example 2 : Nonlinear Saturable Ligand Binding Model

The jacobian matrix is defined by,

$$G(\alpha) = \begin{bmatrix} G_{11} & G_{12} & G_{13} & G_{14} & G_{15} & G_{16} \\ G_{21} & G_{22} & G_{23} & G_{24} & G_{25} & G_{26} \\ G_{31} & G_{32} & G_{33} & G_{34} & G_{35} & G_{36} \\ G_{41} & G_{42} & G_{43} & G_{44} & G_{45} & G_{46} \\ G_{51} & G_{52} & G_{53} & G_{54} & G_{55} & G_{56} \end{bmatrix} \tag{A.1}$$

The following output was generated using MATHEMATICA, a mod- ern symbolic manipulation package.

$G_{11} = 1$

$G_{12} = 0$

$G_{13} = 0$

$G_{14} = 0$

$G_{15} = 0$

$G_{16} = 0$

$G_{21} = -k_2$

$G_{22} = -K_1$

$G_{23} = 0$

$G_{24} = 0$

$G_{25} = 0$

$$G_{26} = 0$$

$$G_{31} = {k_2}^2 + \frac{k_2 k_{on} B_{max}}{V_r}$$

$$G_{32} = 2K_1 k_2 + \frac{K_1 k_{on} B_{max}}{V_r}$$

$$G_{33} = \frac{K_1 k_2 B_{max}}{V_r}$$

$$G_{34} = -\frac{K_1 k_2 k_{on} B_{max}}{{V_r}^2}$$

$$G_{35} = \frac{K_1 k_2 k_{on}}{V_r}$$

$$G_{36} = 0$$

$$G_{41} = -\frac{k_2 \left({k_2}^2 {V_r}^2 + 2K_1 {k_{on}}^2 B_{max} + 2k_2 k_{on} V_r B_{max} + {k_{on}}^2 {B_{max}}^2 + k_{on} V_r B_{max} k_{off}\right)}{{V_r}^2}$$

$$G_{42} = -\frac{K_1 \left(3{k_2}^2 {V_r}^2 + K_1 {k_{on}}^2 B_{max} + 4k_2 k_{on} V_r B_{max} + {k_{on}}^2 {B_{max}}^2 + k_{on} V_r B_{max} k_{off}\right)}{{V_r}^2}$$

$$G_{43} = -\frac{K_1 k_2 B_{max} \left(2K_1 k_{on} + 2k_2 V_r + 2k_{on} B_{max} + V_r k_{off}\right)}{{V_r}^2}$$

$$G_{44} = \frac{K_1 k_2 k_{on} B_{max} \left(2K_1 k_{on} + 2k_2 V_r + 2k_{on} B_{max} + V_r k_{off}\right)}{{V_r}^3}$$

$$G_{45} = -\frac{K_1 k_2 k_{on} \left(K_1 k_{on} + 2k_2 V_r + 2k_{on} B_{max} + V_r k_{off}\right)}{{V_r}^2}$$

$$G_{46} = -\frac{K_1 k_2 k_{on} B_{max}}{V_r}$$

$$G_{51} = \frac{k_2 \left({k_2}^3 {V_r}^3 + 3{K_1}^2 {k_{on}}^3 B_{max} + 8K_1 k_2 {k_{on}}^2 V_r B_{max} + 3{k_2}^2 k_{on} {V_r}^2 B_{max}\right.}{{V_r}^3}$$

$$\frac{+8K_1 {k_{on}}^3 {B_{max}}^2 + 3k_2 {k_{on}}^2 V_r {B_{max}}^2 + {k_{on}}^3 {B_{max}}^3 + 4K_1 {k_{on}}^2 V_r B_{max} k_{off} + 2k_2 k_{on} {V_r}^2 B_{ma}}{{V_r}^3}$$

$$\frac{\left.+2{k_{on}}^2 V_r {B_{max}}^2 k_{off} + k_{on} {V_r}^2 B_{max} {k_{off}}^2\right)}{{V_r}^3}$$

$$G_{52} = \frac{K_1 \left(4{k_2}^3 {V_r}^3 + {K_1}^2 {k_{on}}^3 B_{max} + 8K_1 k_2 {k_{on}}^2 V_r B_{max} + 9{k_2}^2 k_{on} {V_r}^2 B_{max}\right.}{{V_r}^3}$$

$$\frac{+4K_1 {k_{on}}^3 {B_{max}}^2 + 6k_2 {k_{on}}^2 V_r {B_{max}}^2 + {k_{on}}^3 {B_{max}}^3 + 2K_1 {k_{on}}^2 V_r B_{max} k_{off} + 4k_2 k_{on} {V_r}^2 B_{ma}}{{V_r}^3}$$

$$\frac{\left.+2{k_{on}}^2 V_r {B_{max}}^2 k_{off} + k_{on} {V_r}^2 B_{max} {k_{off}}^2\right)}{{V_r}^3}$$

$$G_{53} = \frac{K_1 k_2 B_{max} \left(3K_1{}^2 k_{on}{}^2 + 8K_1 k_2 k_{on} V_r + 3k_2{}^2 V_r{}^2 + 12K_1 k_{on}{}^2 B_{max} + 6k_2 k_{on} V_r B_{max}\right.}{V_r{}^3}$$

$$\frac{\left. +3k_{on}{}^2 B_{max}{}^2 + 4K_1 k_{on} V_r k_{off} + 2k_2 V_r{}^2 k_{off} + 4k_{on} V_r B_{max} k_{off} + V_r{}^2 k_{off}{}^2\right)}{V_r{}^3}$$

$$G_{54} = -\frac{K_1 k_2 k_{on} B_{max} \left(3K_1{}^2 k_{on}{}^2 + 8K_1 k_2 k_{on} V_r + 3k_2{}^2 V_r{}^2 + 12K_1 k_{on}{}^2 B_{max}\right.}{V_r{}^4}$$

$$\frac{+6k_2 k_{on} V_r B_{max} + 3k_{on}{}^2 B_{max}{}^2 + 4K_1 k_{on} V_r k_{off} + 2k_2 V_r{}^2 k_{off} + 4k_{on} V_r B_{max} k_{off} + V_r{}^2 k_{o.}}{V_r{}^4}$$

$$G_{55} = \frac{K_1 k_2 k_{on} \left(K_1{}^2 k_{on}{}^2 + 4K_1 k_2 k_{on} V_r + 3k_2{}^2 V_r{}^2 + 8K_1 k_{on}{}^2 B_{max} + 6k_2 k_{on} V_r B_{max}\right.}{V_r{}^3}$$

$$\frac{\left. +3k_{on}{}^2 B_{max}{}^2 + 2K_1 k_{on} V_r k_{off} + 2k_2 V_r{}^2 k_{off} + 4k_{on} V_r B_{max} k_{off} + V_r{}^2 k_{off}{}^2\right)}{V_r{}^3}$$

$$G_{56} = \frac{2K_1 k_2 k_{on} B_{max} \left(K_1 k_{on} + k_2 V_r + k_{on} B_{max} + V_r k_{off}\right)}{V_r{}^2}$$

A.2 Example 3 : Reference Region Model

The jacobian matrix is defined by,

$$G(\alpha) = \begin{bmatrix} G_{11} & G_{12} & G_{13} & G_{14} & G_{15} & G_{16} \\ G_{21} & G_{22} & G_{23} & G_{24} & G_{25} & G_{26} \\ G_{31} & G_{32} & G_{33} & G_{34} & G_{35} & G_{36} \\ G_{41} & G_{42} & G_{43} & G_{44} & G_{45} & G_{46} \\ G_{51} & G_{52} & G_{53} & G_{54} & G_{55} & G_{56} \end{bmatrix} \tag{A.2}$$

The following output was generated using MATHEMATICA,

$$G_{11} = \frac{1}{K_5}$$

$$G_{12} = 0$$

$$G_{13} = 0$$

$$G_{14} = 0$$

$$G_{15} = -\frac{K_1}{{K_5}^2}$$

$$G_{16} = 0$$

$$G_{21} = \frac{-k_2 + k_6}{K_5}$$

$$G_{22} = -\frac{K_1}{K_5}$$

$$G_{23} = 0$$

$$G_{24} = 0$$

$$G_{25} = \frac{K_1 (k_2 - k_6)}{{K_5}^2}$$

$$G_{26} = \frac{K_1}{K_5}$$

$$G_{31} = \frac{k_2 (k_2 + k_3 - k_6)}{K_5}$$

$$G_{32} = \frac{K_1 (2k_2 + k_3 - k_6)}{K_5}$$

$$G_{33} = \frac{K_1 k_2}{K_5}$$

$$G_{34} = 0$$

$$G_{35} = -\frac{K_1 k_2 (k_2 + k_3 - k_6)}{{K_5}^2}$$

$$G_{36} = -\frac{K_1 k_2}{K_5}$$

$$G_{41} = -\frac{k_2\left({k_2}^2 + 2k_2k_3 + {k_3}^2 + k_3k_4 - k_2k_6 - k_3k_6\right)}{K_5}$$

$$G_{42} = -\frac{K_1\left(3{k_2}^2 + 4k_2k_3 + {k_3}^2 + k_3k_4 - 2k_2k_6 - k_3k_6\right)}{K_5}$$

$$G_{43} = -\frac{K_1k_2\left(2k_2 + 2k_3 + k_4 - k_6\right)}{K_5}$$

$$G_{44} = -\frac{K_1k_2k_3}{K_5}$$

$$G_{45} = \frac{K_1k_2\left({k_2}^2 + 2k_2k_3 + {k_3}^2 + k_3k_4 - k_2k_6 - k_3k_6\right)}{{K_5}^2}$$

$$G_{46} = \frac{K_1k_2\left(k_2 + k_3\right)}{K_5}$$

$$G_{51} = \frac{k_2\left({k_2}^3 + 3{k_2}^2k_3 + 3k_2{k_3}^2 + {k_3}^3 + 2k_2k_3k_4 + 2{k_3}^2k_4 + k_3{k_4}^2 - {k_2}^2k_6 - 2k_2k_3k_6\right.}{K_5}$$

$$\frac{\left.-{k_3}^2k_6 - k_3k_4k_6\right)}{K_5}$$

$$G_{52} = \frac{K_1\left(4{k_2}^3 + 9{k_2}^2k_3 + 6k_2{k_3}^2 + {k_3}^3 + 4k_2k_3k_4 + 2{k_3}^2k_4 + k_3{k_4}^2 - 3{k_2}^2k_6 - 4k_2k_3k_6\right.}{K_5}$$

$$\frac{\left.-{k_3}^2k_6 - k_3k_4k_6\right)}{K_5}$$

$$G_{53} = \frac{K_1k_2\left(3{k_2}^2 + 6k_2k_3 + 3{k_3}^2 + 2k_2k_4 + 4k_3k_4 + {k_4}^2 - 2k_2k_6 - 2k_3k_6 - k_4k_6\right)}{K_5}$$

$$G_{54} = \frac{K_1k_2k_3\left(2k_2 + 2k_3 + 2k_4 - k_6\right)}{K_5}$$

$$G_{55} = -\frac{K_1k_2\left({k_2}^3 + 3{k_2}^2k_3 + 3k_2{k_3}^2 + {k_3}^3 + 2k_2k_3k_4 + 2{k_3}^2k_4 + k_3{k_4}^2 - {k_2}^2k_6 - 2k_2k_3k_6\right.}{{K_5}^2}$$

$$\frac{\left.-{k_3}^2k_6 - k_3k_4k_6\right)}{{K_5}^2}$$

$$G_{56} = -\frac{K_1k_2\left({k_2}^2 + 2k_2k_3 + {k_3}^2 + k_3k_4\right)}{K_5}$$

A.3 Example 4 : Batch Reactor Model

The jacobian matrix is defined by,

$$G(\alpha) = \begin{bmatrix} G_{11} & G_{12} & G_{13} & G_{14} & G_{15} & G_{16} \\ G_{21} & G_{22} & G_{23} & G_{24} & G_{25} & G_{26} \\ G_{31} & G_{32} & G_{33} & G_{34} & G_{35} & G_{36} \\ G_{41} & G_{42} & G_{43} & G_{44} & G_{45} & G_{46} \\ G_{51} & G_{52} & G_{53} & G_{54} & G_{55} & G_{56} \end{bmatrix} \tag{A.3}$$

The following output was generated using MATHEMATICA,

$$G_{11} = 0$$

$$G_{12} = 0$$

$$G_{13} = 0$$

$$G_{14} = 1$$

$$G_{15} = 0$$

$$G_{16} = 0$$

$$G_{21} = \frac{\theta_4\theta_6}{\theta_2 + \theta_6}$$

$$G_{22} = -\frac{\theta_1\theta_4\theta_6}{(\theta_2 + \theta_6)^2}$$

$$G_{23} = -\theta_4$$

$$G_{24} = -\theta_3 + \frac{\theta_1\theta_6}{\theta_2 + \theta_6}$$

$$G_{25} = 0$$

$$G_{26} = \frac{\theta_1\theta_2\theta_4}{(\theta_2 + \theta_6)^2}$$

$$G_{31} = \frac{2\theta_4\theta_6\left(-(\theta_1\theta_2\theta_4) - {\theta_2}^2\theta_3\theta_5 + \theta_1\theta_2\theta_5\theta_6 - 2\theta_2\theta_3\theta_5\theta_6 + \theta_1\theta_5{\theta_6}^2 - \theta_3\theta_5{\theta_6}^2\right)}{\theta_5(\theta_2 + \theta_6)^3}$$

$$G_{32} = -\frac{\theta_1\theta_4\theta_6\left(-2\theta_1\theta_2\theta_4 - 2{\theta_2}^2\theta_3\theta_5 + \theta_1\theta_4\theta_6 + 2\theta_1\theta_2\theta_5\theta_6 - 4\theta_2\theta_3\theta_5\theta_6 + 2\theta_1\theta_5{\theta_6}^2 - 2\theta_3\theta_5{\theta_6}^2\right)}{\theta_5(\theta_2 + \theta_6)^4}$$

$$G_{33} = 2\theta_3\theta_4 - \frac{2\theta_1\theta_4\theta_6}{\theta_2 + \theta_6}$$

$$G_{34} = {\theta_3}^2 + \frac{2{\theta_1}^2\theta_4{\theta_6}^2}{\theta_5(\theta_2 + \theta_6)^3} - \frac{2{\theta_1}^2\theta_4\theta_6}{\theta_5(\theta_2 + \theta_6)^2} + \frac{{\theta_1}^2{\theta_6}^2}{(\theta_2 + \theta_6)^2} - \frac{2\theta_1\theta_3\theta_6}{\theta_2 + \theta_6}$$

$$G_{35} = \frac{{\theta_1}^2\theta_2{\theta_4}^2\theta_6}{{\theta_5}^2(\theta_2 + \theta_6)^3}$$

$$G_{36} = -\frac{\theta_1\theta_2\theta_4\left(\theta_1\theta_2\theta_4 + 2\theta_2{}^2\theta_3\theta_5 - 2\theta_1\theta_4\theta_6 - 2\theta_1\theta_2\theta_5\theta_6 + 4\theta_2\theta_3\theta_5\theta_6 - 2\theta_1\theta_5\theta_6{}^2 + 2\theta_3\theta_5\theta_6{}^2\right)}{\theta_5(\theta_2+\theta_6)^4}$$

$$G_{41} = \theta_4\theta_6\left(3\theta_1{}^2\theta_2{}^2\theta_4{}^2 + 8\theta_1\theta_2{}^3\theta_3\theta_4\theta_5 + 3\theta_2{}^4\theta_3{}^2\theta_5{}^2 - 6\theta_1{}^2\theta_2\theta_4{}^2\theta_6 - 12\theta_1{}^2\theta_2{}^2\theta_4\theta_5\theta_6 + \right.$$

$$16\theta_1\theta_2{}^2\theta_3\theta_4\theta_5\theta_6 - 6\theta_1\theta_2{}^3\theta_3\theta_5{}^2\theta_6 + 12\theta_2{}^3\theta_3{}^2\theta_5{}^2\theta_6 - 12\theta_1{}^2\theta_2\theta_4\theta_5\theta_6{}^2 + 8\theta_1\theta_2\theta_3\theta_4\theta_5\theta_6{}^2 +$$

$$3\theta_1{}^2\theta_2{}^2\theta_5{}^2\theta_6{}^2 - 18\theta_1\theta_2{}^2\theta_3\theta_5{}^2\theta_6{}^2 + 18\theta_2{}^2\theta_3{}^2\theta_5{}^2\theta_6{}^2 + 6\theta_1{}^2\theta_2\theta_5{}^2\theta_6{}^3 - 18\theta_1\theta_2\theta_3\theta_5{}^2\theta_6{}^3 +$$

$$\left.12\theta_2\theta_3{}^2\theta_5{}^2\theta_6{}^3 + 3\theta_1{}^2\theta_5{}^2\theta_6{}^4 - 6\theta_1\theta_3\theta_5{}^2\theta_6{}^4 + 3\theta_3{}^2\theta_5{}^2\theta_6{}^4\right) / \left(\theta_5{}^2(\theta_2+\theta_6)^5\right)$$

$$G_{42} = -\theta_1\theta_4\theta_6\left(3\theta_1{}^2\theta_2{}^2\theta_4{}^2 + 8\theta_1\theta_2{}^3\theta_3\theta_4\theta_5 + 3\theta_2{}^4\theta_3{}^2\theta_5{}^2 - 10\theta_1{}^2\theta_2\theta_4{}^2\theta_6 - 12\theta_1{}^2\theta_2{}^2\theta_4\theta_5\theta_6 + \right.$$

$$12\theta_1\theta_2{}^2\theta_3\theta_4\theta_5\theta_6 - 6\theta_1\theta_2{}^3\theta_3\theta_5{}^2\theta_6 + 12\theta_2{}^3\theta_3{}^2\theta_5{}^2\theta_6 + 2\theta_1{}^2\theta_4{}^2\theta_6{}^2 - 8\theta_1{}^2\theta_2\theta_4\theta_5\theta_6{}^2 +$$

$$3\theta_1{}^2\theta_2{}^2\theta_5{}^2\theta_6{}^2 - 18\theta_1\theta_2{}^2\theta_3\theta_5{}^2\theta_6{}^2 + 18\theta_2{}^2\theta_3{}^2\theta_5{}^2\theta_6{}^2 + 4\theta_1{}^2\theta_4\theta_5\theta_6{}^3 - 4\theta_1\theta_3\theta_4\theta_5\theta_6{}^3 +$$

$$6\theta_1{}^2\theta_2\theta_5{}^2\theta_6{}^3 - 18\theta_1\theta_2\theta_3\theta_5{}^2\theta_6{}^3 + 12\theta_2\theta_3{}^2\theta_5{}^2\theta_6{}^3 + 3\theta_1{}^2\theta_5{}^2\theta_6{}^4 - 6\theta_1\theta_3\theta_5{}^2\theta_6{}^4 +$$

$$\left.3\theta_3{}^2\theta_5{}^2\theta_6{}^4\right) / \theta_5{}^2(\theta_2+\theta_6)^6$$

$$G_{43} = -\theta_4\left(3\theta_2{}^3\theta_3{}^2\theta_5 - 4\theta_1{}^2\theta_2\theta_4\theta_6 - 6\theta_1\theta_2{}^2\theta_3\theta_5\theta_6 + 9\theta_2{}^2\theta_3{}^2\theta_5\theta_6 + 3\theta_1{}^2\theta_2\theta_5\theta_6{}^2 - 12\theta_1\theta_2\theta_3\theta_5\theta_6{}^2\right.$$

$$9\ \theta_2\theta_3{}^2\theta_5\theta_6{}^2 + 3\theta_1{}^2\theta_5\theta_6{}^3 - 6\theta_1\theta_3\theta_5\theta_6{}^3 + 3\theta_3{}^2\theta_5\theta_6{}^3\Big)/\theta_5(\theta_2+\theta_6)^3$$

$$G_{44} = -\theta_3{}^3 - \frac{3\theta_1{}^3\theta_2\theta_4{}^2\theta_6{}^2}{\theta_5{}^2(\theta_2+\theta_6)^5} + \frac{6\theta_1{}^3\theta_4{}^2\theta_6{}^3}{\theta_5{}^2(\theta_2+\theta_6)^5} + \frac{2\theta_1{}^3\theta_2\theta_4\theta_6{}^3}{\theta_5(\theta_2+\theta_6)^5} + \frac{2\theta_1{}^3\theta_4\theta_6{}^4}{\theta_5(\theta_2+\theta_6)^5} + \frac{3\theta_1{}^3\theta_2\theta_4{}^2\theta_6}{\theta_5{}^2(\theta_2+\theta_6)^4} -$$

$$\frac{6\theta_1{}^3\theta_4{}^2\theta_6{}^2}{\theta_5{}^2(\theta_2+\theta_6)^4} - \frac{2\theta_1{}^3\theta_2\theta_4\theta_6{}^2}{\theta_5(\theta_2+\theta_6)^4} - \frac{2\theta_1{}^2\theta_2\theta_3\theta_4\theta_6{}^2}{\theta_5(\theta_2+\theta_6)^4} + \frac{4\theta_1{}^3\theta_4\theta_6{}^3}{\theta_5(\theta_2+\theta_6)^4} - \frac{2\theta_1{}^2\theta_3\theta_4\theta_6{}^3}{\theta_5(\theta_2+\theta_6)^4} +$$

$$\frac{2\theta_1{}^2\theta_2\theta_3\theta_4\theta_6}{\theta_5(\theta_2+\theta_6)^3} - \frac{6\theta_1{}^3\theta_4\theta_6{}^2}{\theta_5(\theta_2+\theta_6)^3} - \frac{4\theta_1{}^2\theta_3\theta_4\theta_6{}^2}{\theta_5(\theta_2+\theta_6)^3} + \frac{\theta_1{}^3\theta_6{}^3}{(\theta_2+\theta_6)^3} + \frac{6\theta_1{}^2\theta_3\theta_4\theta_6}{\theta_5(\theta_2+\theta_6)^2} -$$

$$\frac{3\theta_1{}^2\theta_3\theta_6{}^2}{(\theta_2+\theta_6)^2} + \frac{3\theta_1\theta_3{}^2\theta_6}{\theta_2+\theta_6}$$

$$G_{45} = -2\theta_1{}^2\theta_2\theta_4{}^2\theta_6\Big(\theta_1\theta_2\theta_4 + 2\theta_2{}^2\theta_3\theta_5 - 2\theta_1\theta_4\theta_6 - 2\theta_1\theta_2\theta_5\theta_6 + 4\theta_2\theta_3\theta_5\theta_6 - 2\theta_1\theta_5\theta_6{}^2 +$$

$$2\theta_3\theta_5\theta_6{}^2\Big)/\theta_5{}^3(\theta_2+\theta_6)^5$$

$$G_{46} = \theta_1\theta_2\theta_4\Big(\theta_1{}^2\theta_2{}^2\theta_4{}^2 + 4\theta_1\theta_2{}^3\theta_3\theta_4\theta_5 + 3\theta_2{}^4\theta_3{}^2\theta_5{}^2 - 8\theta_1{}^2\theta_2\theta_4{}^2\theta_6 - 8\theta_1{}^2\theta_2{}^2\theta_4\theta_5\theta_6 -$$

$$6\theta_1\theta_2{}^3\theta_3\theta_5{}^2\theta_6 + 12\theta_2{}^3\theta_3{}^2\theta_5{}^2\theta_6 + 6\theta_1{}^2\theta_4{}^2\theta_6{}^2 - 12\theta_1\theta_2\theta_3\theta_4\theta_5\theta_6{}^2 + 3\theta_1{}^2\theta_2{}^2\theta_5{}^2\theta_6{}^2 -$$

$$18\theta_1\theta_2{}^2\theta_3\theta_5{}^2\theta_6{}^2 + 18\theta_2{}^2\theta_3{}^2\theta_5{}^2\theta_6{}^2 + 8\theta_1{}^2\theta_4\theta_5\theta_6{}^3 - 8\theta_1\theta_3\theta_4\theta_5\theta_6{}^3 + 6\theta_1{}^2\theta_2\theta_5{}^2\theta_6{}^3 -$$

$$18\theta_1\theta_2\theta_3\theta_5{}^2\theta_6{}^3 + 12\theta_2\theta_3{}^2\theta_5{}^2\theta_6{}^3 + 3\theta_1{}^2\theta_5{}^2\theta_6{}^4 - 6\theta_1\theta_3\theta_5{}^2\theta_6{}^4 + 3\theta_3{}^2\theta_5{}^2\theta_6{}^4\Big)/\theta_5{}^2(\theta_2+\theta_6)^6$$

$$G_{51} = \theta_4\theta_6\Big(-4\theta_1{}^3\theta_2{}^3\theta_4{}^3 - 21\theta_1{}^2\theta_2{}^4\theta_3\theta_4{}^2\theta_5 - 22\theta_1\theta_2{}^5\theta_3{}^2\theta_4\theta_5{}^2 - 4\theta_2{}^6\theta_3{}^3\theta_5{}^3 + 32\theta_1{}^3\theta_2{}^2\theta_4{}^3\theta_6 +$$

$$44\theta_1{}^3\theta_2{}^3\theta_4{}^2\theta_5\theta_6 + 66\theta_1{}^2\theta_2{}^4\theta_3\theta_4\theta_5{}^2\theta_6 - 88\theta_1\theta_2{}^4\theta_3{}^2\theta_4\theta_5{}^2\theta_6 + 12\theta_1\theta_2{}^5\theta_3{}^2\theta_5{}^3\theta_6 -$$

$$24\theta_2{}^5\theta_3{}^3\theta_5{}^3\theta_6 - 24\theta_1{}^3\theta_2\theta_4{}^3\theta_6{}^2 - 12\theta_1{}^3\theta_2{}^2\theta_4{}^2\theta_5\theta_6{}^2 + 63\theta_1{}^2\theta_2{}^2\theta_3\theta_4{}^2\theta_5\theta_6{}^2 -$$

$$44\theta_1{}^3\theta_2{}^3\theta_4\theta_5{}^2\theta_6{}^2 + 198\theta_1{}^2\theta_2{}^3\theta_3\theta_4\theta_5{}^2\theta_6{}^2 - 132\theta_1\theta_2{}^3\theta_3{}^2\theta_4\theta_5{}^2\theta_6{}^2 - 12\theta_1{}^2\theta_2{}^4\theta_3\theta_5{}^3\theta_6{}^2 +$$

$$60\theta_1\theta_2{}^4\theta_3{}^2\theta_5{}^3\theta_6{}^2 - 60\theta_2{}^4\theta_3{}^3\theta_5{}^3\theta_6{}^2 - 56\theta_1{}^3\theta_2\theta_4{}^2\theta_5\theta_6{}^3 + 42\theta_1{}^2\theta_2\theta_3\theta_4{}^2\theta_5\theta_6{}^3 -$$

$$88\theta_1{}^3\theta_2{}^2\theta_4\theta_5{}^2\theta_6{}^3 + 198\theta_1{}^2\theta_2{}^2\theta_3\theta_4\theta_5{}^2\theta_6{}^3 - 88\theta_1\theta_2{}^2\theta_3{}^2\theta_4\theta_5{}^2\theta_6{}^3 + 4\theta_1{}^3\theta_2{}^3\theta_5{}^3\theta_6{}^3 -$$

$$48\theta_1{}^2\theta_2{}^3\theta_3\theta_5{}^3\theta_6{}^3 + 120\theta_1\theta_2{}^3\theta_3{}^2\theta_5{}^3\theta_6{}^3 - 80\theta_2{}^3\theta_3{}^3\theta_5{}^3\theta_6{}^3 - 44\theta_1{}^3\theta_2\theta_4\theta_5{}^2\theta_6{}^4 +$$

$$66\theta_1{}^2\theta_2\theta_3\theta_4\theta_5{}^2\theta_6{}^4 - 22\theta_1\theta_2\theta_3{}^2\theta_4\theta_5{}^2\theta_6{}^4 + 12\theta_1{}^3\theta_2{}^2\theta_5{}^3\theta_6{}^4 - 72\theta_1{}^2\theta_2{}^2\theta_3\theta_5{}^3\theta_6{}^4 +$$

$$120\theta_1\theta_2{}^2\theta_3{}^2\theta_5{}^3\theta_6{}^4 - 60\theta_2{}^2\theta_3{}^3\theta_5{}^3\theta_6{}^4 + 12\theta_1{}^3\theta_2\theta_5{}^3\theta_6{}^5 - 48\theta_1{}^2\theta_2\theta_3\theta_5{}^3\theta_6{}^5 +$$

$$60\theta_1\theta_2\theta_3{}^2\theta_5{}^3\theta_6{}^5 - 24\theta_2\theta_3{}^3\theta_5{}^3\theta_6{}^5 + 4\theta_1{}^3\theta_5{}^3\theta_6{}^6 - 12\theta_1{}^2\theta_3\theta_5{}^3\theta_6{}^6 + 12\theta_1\theta_3{}^2\theta_5{}^3\theta_6{}^6 -$$

$$4\theta_3{}^3\theta_5{}^3\theta_6{}^6\Big)/\theta_5{}^3(\theta_2+\theta_6)^7$$

$$G_{52} = -\theta_1\theta_4\theta_6\Big(-4\theta_1{}^3\theta_2{}^3\theta_4{}^3 - 21\theta_1{}^2\theta_2{}^4\theta_3\theta_4{}^2\theta_5 - 22\theta_1\theta_2{}^5\theta_3{}^2\theta_4\theta_5{}^2 - 4\theta_2{}^6\theta_3{}^3\theta_5{}^3 +$$

$$43\theta_1{}^3\theta_2{}^2\theta_4{}^3\theta_6 + 44\theta_1{}^3\theta_2{}^3\theta_4{}^2\theta_5\theta_6 + 28\theta_1{}^2\theta_2{}^3\theta_3\theta_4{}^2\theta_5\theta_6 + 66\theta_1{}^2\theta_2{}^4\theta_3\theta_4\theta_5{}^2\theta_6 -$$

$$77\theta_1\theta_2{}^4\theta_3{}^2\theta_4\theta_5{}^2\theta_6 + 12\theta_1\theta_2{}^5\theta_3{}^2\theta_5{}^3\theta_6 - 24\theta_2{}^5\theta_3{}^3\theta_5{}^3\theta_6 - 52\theta_1{}^3\theta_2\theta_4{}^3\theta_6{}^2 -$$

$$48\theta_1{}^3\theta_2{}^2\theta_4{}^2\theta_5\theta_6{}^2 + 105\theta_1{}^2\theta_2{}^2\theta_3\theta_4{}^2\theta_5\theta_6{}^2 - 44\theta_1{}^3\theta_2{}^3\theta_4\theta_5{}^2\theta_6{}^2 + 176\theta_1{}^2\theta_2{}^3\theta_3\theta_4\theta_5{}^2\theta_6{}^2 -$$

$$88\theta_1\theta_2{}^3\theta_3{}^2\theta_4\theta_5{}^2\theta_6{}^2 - 12\theta_1{}^2\theta_2{}^4\theta_3\theta_5{}^3\theta_6{}^2 + 60\theta_1\theta_2{}^4\theta_3{}^2\theta_5{}^3\theta_6{}^2 - 60\theta_2{}^4\theta_3{}^3\theta_5{}^3\theta_6{}^2 +$$

$$6\theta_1{}^3\theta_4{}^3\theta_6{}^3 - 78\theta_1{}^3\theta_2\theta_4{}^2\theta_5\theta_6{}^3 + 42\theta_1{}^2\theta_2\theta_3\theta_4{}^2\theta_5\theta_6{}^3 - 77\theta_1{}^3\theta_2{}^2\theta_4\theta_5{}^2\theta_6{}^3 +$$

$$132\theta_1{}^2\theta_2{}^2\theta_3\theta_4\theta_5{}^2\theta_6{}^3 - 22\theta_1\theta_2{}^2\theta_3{}^2\theta_4\theta_5{}^2\theta_6{}^3 + 4\theta_1{}^3\theta_2{}^3\theta_5{}^3\theta_6{}^3 - 48\theta_1{}^2\theta_2{}^3\theta_3\theta_5{}^3\theta_6{}^3 +$$

$$120\theta_1\theta_2{}^3\theta_3{}^2\theta_5{}^3\theta_6{}^3 - 80\theta_2{}^3\theta_3{}^3\theta_5{}^3\theta_6{}^3 + 14\theta_1{}^3\theta_4{}^2\theta_5\theta_6{}^4 - 14\theta_1{}^2\theta_3\theta_4{}^2\theta_5\theta_6{}^4 -$$

$$22\theta_1{}^3\theta_2\theta_4\theta_5{}^2\theta_6{}^4 + 22\theta_1\theta_2\theta_3{}^2\theta_4\theta_5{}^2\theta_6{}^4 + 12\theta_1{}^3\theta_2{}^2\theta_5{}^3\theta_6{}^4 - 72\theta_1{}^2\theta_2{}^2\theta_3\theta_5{}^3\theta_6{}^4 +$$

$$120\theta_1\theta_2{}^2\theta_3{}^2\theta_5{}^3\theta_6{}^4 - 60\theta_2{}^2\theta_3{}^3\theta_5{}^3\theta_6{}^4 + 11\theta_1{}^3\theta_4\theta_5{}^2\theta_6{}^5 - 22\theta_1{}^2\theta_3\theta_4\theta_5{}^2\theta_6{}^5 +$$

$$11\theta_1\theta_3{}^2\theta_4\theta_5{}^2\theta_6{}^5 + 12\theta_1{}^3\theta_2\theta_5{}^3\theta_6{}^5 - 48\theta_1{}^2\theta_2\theta_3\theta_5{}^3\theta_6{}^5 + 60\theta_1\theta_2\theta_3{}^2\theta_5{}^3\theta_6{}^5 -$$

$$24\theta_2\theta_3{}^3\theta_5{}^3\theta_6{}^5 + 4\theta_1{}^3\theta_5{}^3\theta_6{}^6 - 12\theta_1{}^2\theta_3\theta_5{}^3\theta_6{}^6 + 12\theta_1\theta_3{}^2\theta_5{}^3\theta_6{}^6 -$$

$$4\theta_3{}^3\theta_5{}^3\theta_6{}^6\Big)/\theta_5{}^3(\theta_2+\theta_6)^8$$

$$G_{53} = \theta_4\Big(4\theta_2{}^5\theta_3{}^3\theta_5{}^2 - 7\theta_1{}^3\theta_2{}^2\theta_4{}^2\theta_6 - 22\theta_1{}^2\theta_2{}^3\theta_3\theta_4\theta_5\theta_6 - 12\theta_1\theta_2{}^4\theta_3{}^2\theta_5{}^2\theta_6 +$$

$$20\theta_2{}^4\theta_3{}^3\theta_5{}^2\theta_6 + 14\theta_1{}^3\theta_2\theta_4{}^2\theta_6{}^2 + 22\theta_1{}^3\theta_2{}^2\theta_4\theta_5\theta_6{}^2 - 44\theta_1{}^2\theta_2{}^2\theta_3\theta_4\theta_5\theta_6{}^2 +$$

$$12\theta_1{}^2\theta_2{}^3\theta_3\theta_5{}^2\theta_6{}^2 - 48\theta_1\theta_2{}^3\theta_3{}^2\theta_5{}^2\theta_6{}^2 + 40\theta_2{}^3\theta_3{}^3\theta_5{}^2\theta_6{}^2 + 22\theta_1{}^3\theta_2\theta_4\theta_5\theta_6{}^3 -$$

$$22\theta_1{}^2\theta_2\theta_3\theta_4\theta_5\theta_6{}^3 - 4\theta_1{}^3\theta_2{}^2\theta_5{}^2\theta_6{}^3 + 36\theta_1{}^2\theta_2{}^2\theta_3\theta_5{}^2\theta_6{}^3 - 72\theta_1\theta_2{}^2\theta_3{}^2\theta_5{}^2\theta_6{}^3 +$$

$$40\theta_2{}^2\theta_3{}^3\theta_5{}^2\theta_6{}^3 - 8\theta_1{}^3\theta_2\theta_5{}^2\theta_6{}^4 + 36\theta_1{}^2\theta_2\theta_3\theta_5{}^2\theta_6{}^4 - 48\theta_1\theta_2\theta_3{}^2\theta_5{}^2\theta_6{}^4 +$$

$$20\theta_2\theta_3{}^3\theta_5{}^2\theta_6{}^4 - 4\theta_1{}^3\theta_5{}^2\theta_6{}^5 + 12\theta_1{}^2\theta_3\theta_5{}^2\theta_6{}^5 - 12\theta_1\theta_3{}^2\theta_5{}^2\theta_6{}^5 +$$

$$4\theta_3{}^3\theta_5{}^2\theta_6{}^5\Big)/\theta_5{}^2(\theta_2+\theta_6)^5$$

$$G_{54} = \Big(\theta_2{}^7\theta_3{}^4\theta_5{}^3 - 4\theta_1{}^4\theta_2{}^3\theta_4{}^3\theta_6 - 21\theta_1{}^3\theta_2{}^4\theta_3\theta_4{}^2\theta_5\theta_6 - 22\theta_1{}^2\theta_2{}^5\theta_3{}^2\theta_4\theta_5{}^2\theta_6 -$$

$$4\theta_1\theta_2{}^6\theta_3{}^3\theta_5{}^3\theta_6 + 7\theta_2{}^6\theta_3{}^4\theta_5{}^3\theta_6 + 32\theta_1{}^4\theta_2{}^2\theta_4{}^3\theta_6{}^2 + 33\theta_1{}^4\theta_2{}^3\theta_4{}^2\theta_5\theta_6{}^2 +$$

$$44\theta_1{}^3\theta_2{}^4\theta_3\theta_4\theta_5{}^2\theta_6{}^2 - 88\theta_1{}^2\theta_2{}^4\theta_3{}^2\theta_4\theta_5{}^2\theta_6{}^2 + 6\theta_1{}^2\theta_2{}^5\theta_3{}^2\theta_5{}^3\theta_6{}^2 -$$

$$24\theta_1\theta_2{}^5\theta_3{}^3\theta_5{}^3\theta_6{}^2 + 21\theta_2{}^5\theta_3{}^4\theta_5{}^3\theta_6{}^2 - 24\theta_1{}^4\theta_2\theta_4{}^3\theta_6{}^3 - 9\theta_1{}^4\theta_2{}^2\theta_4{}^2\theta_5\theta_6{}^3 +$$

$$63\theta_1{}^3\theta_2{}^2\theta_3\theta_4{}^2\theta_5\theta_6{}^3 - 22\theta_1{}^4\theta_2{}^3\theta_4\theta_5{}^2\theta_6{}^3 + 132\theta_1{}^3\theta_2{}^3\theta_3\theta_4\theta_5{}^2\theta_6{}^3 -$$

$$132\theta_1{}^2\theta_2{}^3\theta_3{}^2\theta_4\theta_5{}^2\theta_6{}^3 - 4\theta_1{}^3\theta_2{}^4\theta_3\theta_5{}^3\theta_6{}^3 + 30\theta_1{}^2\theta_2{}^4\theta_3{}^2\theta_5{}^3\theta_6{}^3 - 60\theta_1\theta_2{}^4\theta_3{}^3\theta_5{}^3\theta_6{}^3 +$$

$$35\theta_2{}^4\theta_3{}^4\theta_5{}^3\theta_6{}^3 - 42\theta_1{}^4\theta_2\theta_4{}^2\theta_5\theta_6{}^4 + 42\theta_1{}^3\theta_2\theta_3\theta_4{}^2\theta_5\theta_6{}^4 - 44\theta_1{}^4\theta_2{}^2\theta_4\theta_5{}^2\theta_6{}^4 +$$

$$132\theta_1{}^3\theta_2{}^2\theta_3\theta_4\theta_5{}^2\theta_6{}^4 - 88\theta_1{}^2\theta_2{}^2\theta_3{}^2\theta_4\theta_5{}^2\theta_6{}^4 + \theta_1{}^4\theta_2{}^3\theta_5{}^3\theta_6{}^4 - 16\theta_1{}^3\theta_2{}^3\theta_3\theta_5{}^3\theta_6{}^4 +$$

$$60\theta_1{}^2\theta_2{}^3\theta_3{}^2\theta_5{}^3\theta_6{}^4 - 80\theta_1\theta_2{}^3\theta_3{}^3\theta_5{}^3\theta_6{}^4 + 35\theta_2{}^3\theta_3{}^4\theta_5{}^3\theta_6{}^4 - 22\theta_1{}^4\theta_2\theta_4\theta_5{}^2\theta_6{}^5 +$$

$$44\theta_1{}^3\theta_2\theta_3\theta_4\theta_5{}^2\theta_6{}^5 - 22\theta_1{}^2\theta_2\theta_3{}^2\theta_4\theta_5{}^2\theta_6{}^5 + 3\theta_1{}^4\theta_2{}^2\theta_5{}^3\theta_6{}^5 - 24\theta_1{}^3\theta_2{}^2\theta_3\theta_5{}^3\theta_6{}^5 +$$

$$60\theta_1{}^2\theta_2{}^2\theta_3{}^2\theta_5{}^3\theta_6{}^5 - 60\theta_1\theta_2{}^2\theta_3{}^3\theta_5{}^3\theta_6{}^5 + 21\theta_2{}^2\theta_3{}^4\theta_5{}^3\theta_6{}^5 + 3\theta_1{}^4\theta_2\theta_5{}^3\theta_6{}^6 -$$

$$16\theta_1{}^3\theta_2\theta_3\theta_5{}^3\theta_6{}^6 + 30\theta_1{}^2\theta_2\theta_3{}^2\theta_5{}^3\theta_6{}^6 - 24\theta_1\theta_2\theta_3{}^3\theta_5{}^3\theta_6{}^6 + 7\theta_2\theta_3{}^4\theta_5{}^3\theta_6{}^6 + \theta_1{}^4\theta_5{}^3\theta_6{}^7 -$$

$$4\theta_1{}^3\theta_3\theta_5{}^3\theta_6{}^7 + 6\theta_1{}^2\theta_3{}^2\theta_5{}^3\theta_6{}^7 - 4\theta_1\theta_3{}^3\theta_5{}^3\theta_6{}^7 + \theta_3{}^4\theta_5{}^3\theta_6{}^7\Big) / \theta_5{}^3(\theta_2 + \theta_6)^7$$

$$G_{55} = \theta_1{}^2\theta_2\theta_4{}^2\theta_6 \Big(3\theta_1{}^2\theta_2{}^2\theta_4{}^2 + 14\theta_1\theta_2{}^3\theta_3\theta_4\theta_5 + 11\theta_2{}^4\theta_3{}^2\theta_5{}^2 - 24\theta_1{}^2\theta_2\theta_4{}^2\theta_6 -$$

$$22\theta_1{}^2\theta_2{}^2\theta_4\theta_5\theta_6 - 22\theta_1\theta_2{}^3\theta_3\theta_5{}^2\theta_6 + 44\theta_2{}^3\theta_3{}^2\theta_5{}^2\theta_6 + 18\theta_1{}^2\theta_4{}^2\theta_6{}^2 + 6\theta_1{}^2\theta_2\theta_4\theta_5\theta_6{}^2 -$$

$$42\theta_1\theta_2\theta_3\theta_4\theta_5\theta_6{}^2 + 11\theta_1{}^2\theta_2{}^2\theta_5{}^2\theta_6{}^2 - 66\theta_1\theta_2{}^2\theta_3\theta_5{}^2\theta_6{}^2 + 66\theta_2{}^2\theta_3{}^2\theta_5{}^2\theta_6{}^2 +$$

$$28\theta_1{}^2\theta_4\theta_5\theta_6{}^3 - 28\theta_1\theta_3\theta_4\theta_5\theta_6{}^3 + 22\theta_1{}^2\theta_2\theta_5{}^2\theta_6{}^3 - 66\theta_1\theta_2\theta_3\theta_5{}^2\theta_6{}^3 + 44\theta_2\theta_3{}^2\theta_5{}^2\theta_6{}^3 +$$

$$11\theta_1{}^2\theta_5{}^2\theta_6{}^4 - 22\theta_1\theta_3\theta_5{}^2\theta_6{}^4 + 11\theta_3{}^2\theta_5{}^2\theta_6{}^4\Big) / \theta_5{}^4(\theta_2 + \theta_6)^7$$

$$G_{56} = -\theta_1\theta_2\theta_4 \Big(\theta_1{}^3\theta_2{}^3\theta_4{}^3 + 7\theta_1{}^2\theta_2{}^4\theta_3\theta_4{}^2\theta_5 + 11\theta_1\theta_2{}^5\theta_3{}^2\theta_4\theta_5{}^2 + 4\theta_2{}^6\theta_3{}^3\theta_5{}^3 -$$

$$22\theta_1{}^3\theta_2{}^2\theta_4{}^3\theta_6 - 22\theta_1{}^3\theta_2{}^3\theta_4{}^2\theta_5\theta_6 - 42\theta_1{}^2\theta_2{}^3\theta_3\theta_4{}^2\theta_5\theta_6 - 44\theta_1{}^2\theta_2{}^4\theta_3\theta_4\theta_5{}^2\theta_6 +$$

$$22\theta_1\theta_2{}^4\theta_3{}^2\theta_4\theta_5{}^2\theta_6 - 12\theta_1\theta_2{}^5\theta_3{}^2\theta_5{}^3\theta_6 + 24\theta_2{}^5\theta_3{}^3\theta_5{}^3\theta_6 + 58\theta_1{}^3\theta_2\theta_4{}^3\theta_6{}^2 +$$

$$64\theta_1{}^3\theta_2{}^2\theta_4{}^2\theta_5\theta_6{}^2 - 63\theta_1{}^2\theta_2{}^2\theta_3\theta_4{}^2\theta_5\theta_6{}^2 + 33\theta_1{}^3\theta_2{}^3\theta_4\theta_5{}^2\theta_6{}^2 - 88\theta_1{}^2\theta_2{}^3\theta_3\theta_4\theta_5{}^2\theta_6{}^2 -$$

$$22\theta_1\theta_2{}^3\theta_3{}^2\theta_4\theta_5{}^2\theta_6{}^2 + 12\theta_1{}^2\theta_2{}^4\theta_3\theta_5{}^3\theta_6{}^2 - 60\theta_1\theta_2{}^4\theta_3{}^2\theta_5{}^3\theta_6{}^2 + 60\theta_2{}^4\theta_3{}^3\theta_5{}^3\theta_6{}^2 -$$

$$24\theta_1{}^3\theta_4{}^3\theta_6{}^3 + 44\theta_1{}^3\theta_2\theta_4{}^2\theta_5\theta_6{}^3 + 28\theta_1{}^2\theta_2\theta_3\theta_4{}^2\theta_5\theta_6{}^3 + 44\theta_1{}^3\theta_2{}^2\theta_4\theta_5{}^2\theta_6{}^3 -$$

$$88\theta_1\theta_2{}^2\theta_3{}^2\theta_4\theta_5{}^2\theta_6{}^3 - 4\theta_1{}^3\theta_2{}^3\theta_5{}^3\theta_6{}^3 + 48\theta_1{}^2\theta_2{}^3\theta_3\theta_5{}^3\theta_6{}^3 - 120\theta_1\theta_2{}^3\theta_3{}^2\theta_5{}^3\theta_6{}^3 +$$

$$80\theta_2{}^3\theta_3{}^3\theta_5{}^3\theta_6{}^3 - 42\theta_1{}^3\theta_4{}^2\theta_5\theta_6{}^4 + 42\theta_1{}^2\theta_3\theta_4{}^2\theta_5\theta_6{}^4 - 11\theta_1{}^3\theta_2\theta_4\theta_5{}^2\theta_6{}^4 +$$

$$88\theta_1{}^2\theta_2\theta_3\theta_4\theta_5{}^2\theta_6{}^4 - 77\theta_1\theta_2\theta_3{}^2\theta_4\theta_5{}^2\theta_6{}^4 - 12\theta_1{}^3\theta_2{}^2\theta_5{}^3\theta_6{}^4 + 72\theta_1{}^2\theta_2{}^2\theta_3\theta_5{}^3\theta_6{}^4 -$$

$$120\theta_1\theta_2{}^2\theta_3{}^2\theta_5{}^3\theta_6{}^4 + 60\theta_2{}^2\theta_3{}^3\theta_5{}^3\theta_6{}^4 - 22\theta_1{}^3\theta_4\theta_5{}^2\theta_6{}^5 + 44\theta_1{}^2\theta_3\theta_4\theta_5{}^2\theta_6{}^5 -$$

$$22\theta_1\theta_3{}^2\theta_4\theta_5{}^2\theta_6{}^5 - 12\theta_1{}^3\theta_2\theta_5{}^3\theta_6{}^5 + 48\theta_1{}^2\theta_2\theta_3\theta_5{}^3\theta_6{}^5 - 60\theta_1\theta_2\theta_3{}^2\theta_5{}^3\theta_6{}^5 +$$

$$24\theta_2\theta_3{}^3\theta_5{}^3\theta_6{}^5 - 4\theta_1{}^3\theta_5{}^3\theta_6{}^6 + 12\theta_1{}^2\theta_3\theta_5{}^3\theta_6{}^6 - 12\theta_1\theta_3{}^2\theta_5{}^3\theta_6{}^6 +$$

$$4\theta_3{}^3\theta_5{}^3\theta_6{}^6\Big)/\theta_5{}^3(\theta_2+\theta_6)^8$$